

# UC Irvine

## UC Irvine Electronic Theses and Dissertations

### Title

Tenocyte transcriptional diversity and responses to muscle contraction force

### Permalink

<https://escholarship.org/uc/item/476023w4>

### Author

Nayak, Pavan

### Publication Date

2023

### Copyright Information

This work is made available under the terms of a Creative Commons Attribution-NonCommercial-NoDerivatives License, available at

<https://creativecommons.org/licenses/by-nc-nd/4.0/>

Peer reviewed|Thesis/dissertation

UNIVERSITY OF CALIFORNIA,  
IRVINE

Tenocyte transcriptional diversity and responses to muscle contraction force

DISSERTATION

Submitted in partial satisfaction of the requirements  
for the degree of

DOCTOR OF PHILOSOPHY

In Mathematical, Computational and Systems Biology

by

Pavan Nayak

Dissertation Committee:  
Professor Thomas Schilling, Chair  
Professor Kavita Arora  
Professor Wenqi Wang  
Professor Ken Cho  
Professor Kathleen Treseder

2023



## TABLE OF CONTENTS

	<b>Page</b>
<b>List of Figures</b>	iv
<b>List of Tables</b>	vi
<b>Acknowledgements</b>	vii
<b>Vita</b>	viii
<b>Abstract of the Dissertation</b>	x
<b>Chapter I: Introduction and Background</b>	1
<b>Chapter II: An in vivo investigation of tenocyte transcriptional responses to muscle contraction force paradigms</b>	16
Introduction	16
Results	19
Discussion	32
Methods	37
<b>Chapter III: Cranial tenocyte diversity and roles for Wnt signaling in embryonic tendon patterning</b>	43
Introduction	43
Results	45
Discussion	78
Methods	87
<b>Chapter IV: Identification of novel protein-protein interactions with tenocyte fate regulator Scleraxis</b>	94
Introduction	94
Results	96
Discussion	99
Methods	101
<b>Chapter V: Conclusion and Future Directions</b>	103
<b>References</b>	110
<b>Appendix I: Supplementary Material: Chapter II</b>	141
<b>Appendix II: Supplementary Material: Chapter III</b>	148



## LIST OF FIGURES

	Page
<b>Chapter I</b>	
<b>Figure 1:</b> Schematic of generalized dynamic reciprocity in cell-ECM interactions	5
<b>Figure 2:</b> Schematic of the effects of force conditions on tenocyte-ECM dynamic reciprocity	9
<b>Chapter II</b>	
<b>Figure 1:</b> Genes differentially expressed in tendon progenitor cells upon onset of embryonic muscle contraction	20
<b>Figure 2:</b> Embryonic expression of novel tenocyte markers	23
<b>Figure 3:</b> Co-expression of <i>matn1</i> , <i>klf2a</i> and <i>mxra5b</i> with <i>scxa</i> in cranial and trunk tenocytes	24
<b>Figure 4:</b> Differential gene expression analyses under varied force conditions	25
<b>Figure 5:</b> Tenocyte subpopulation specific gene expression of <i>matn1</i> , <i>klf2a</i> , <i>mxra5b</i> , and phenotypic effects of <i>mxra5b</i> multiplex CRISPR knockout.	29
<b>Figure 6:</b> Proposed model for context-specific expression patterns of <i>matn1</i> , <i>klf2a</i> , and <i>mxra5b</i> across distinct tendon attachment regions.	32
<b>Chapter III</b>	
<b>Figure 1:</b> Analysis of generalized and tenocyte-specific gene expression responses to temperature associated cell dissociation stress	45
<b>Figure 2:</b> Unsupervised clustering and quality control of 72 hpf sorted mCherry+ cells from severed zebrafish heads	50
<b>Figure 3:</b> Co-expression of tenocyte markers <i>scxa</i> and <i>thbs4b</i> in 72 hpf cranial tendons	51
<b>Figure 4:</b> Co-expression of tenocyte markers <i>scxa</i> and <i>mkxa</i> in 72 hpf cranial tendons	52
<b>Figure 5:</b> Nebulosa expression overlap plots of <i>scxa</i> with individual cluster markers	53
<b>Figure 6:</b> isHCRs and colocalization of <i>scxa</i> , <i>sox9a</i> and <i>fndc1</i> expression	54
<b>Figure 7:</b> isHCRs and colocalization of <i>scxa</i> , <i>ehd2b</i> , <i>nr5a2</i> , <i>tbx1</i> , and <i>irx1b</i> expression	55
<b>Figure 8:</b> Labelling of spatially distinct tendon and cartilage regions on scRNAseq UMAP	56
<b>Figure 9:</b> UMAP regions of tenocytes from functionally distinct intra-tendinous zones	57
<b>Figure 10:</b> isHCRs <i>comp</i> and <i>klf2a</i> mark cranial MTJ and enthesis inter-tendon regions respectively	58

<b>Figure 11:</b> Modulescore plots of fibril collagens, basement membrane collagens, and laminins	59
<b>Figure 12:</b> Modulescore plots of FACIT and FACIT-like collagens and <i>loxa</i> expression	60
<b>Figure 13:</b> Identification of a novel population of tenocytes highly responsive to canonical Wnt signaling	61
<b>Figure 14:</b> Live imaging of heatshocked <i>Tg(scx:mCherry; hsp70l: dnTCF-GFP)</i> and <i>Tg(scx:mCherry; hsp70l:dkk1b-GFP)</i> embryos	64
<b>Figure 15:</b> Antibody staining and quantifications of control, (at 48 hpf) heatshocked <i>Tg(scx:mCherry; hsp70l: dnTCF-GFP)</i> and heatshocked <i>Tg(scx:mCherry; hsp70l:dkk1b-GFP)</i> 72 hpf embryos	65
<b>Figure 16:</b> Ectopic tenocytes and muscle attachments seen in heatshocked <i>Tg(scx:mCherry; hsp70l:dkk1b-GFP)</i> at 72 hpf	67
<b>Figure 17:</b> Antibody staining and quantifications of heatshocked (at 60 hpf) control, <i>Tg(scx:mCherry; hsp70l:dkk1b-GFP)</i> 72 hpf embryos	68
<b>Figure 18:</b> Thbs4b/MHC staining of <i>Tg(scx:mCherry; hsp70l:dkk1b-GFP)</i> and visualization of ectopic MTJ	69
<b>Figure 19:</b> Experimental strategy for Wnt antagonist/agonist treatments	70
<b>Figure 20:</b> Dose-dependent cranial muscle-attachment defects in Wnt antagonist (IWR-1 and XAV939) treated <i>Tg(scxa:mCherry; 7XTCF:GFP)</i> embryos	71
<b>Figure 21:</b> Quantification of selected concentrations of 24 hour Wnt antagonist treatments	72
<b>Figure 22:</b> Dose-dependent cranial muscle-attachment defects in Wnt agonist (BIO) treated <i>Tg(scxa:mCherry; 7XTCF:GFP)</i> embryos	73
<b>Figure 23:</b> Quantification of selected concentrations of 24 hour Wnt agonist treatments	74
<b>Figure 24:</b> Ligand-receptor analyses of Wnt signaling in 72 hpf cranial tenocyte scRNAseq using CellChat	75
<b>Figure 25:</b> Wnt receptors with high expression in CellChat ligand-receptor analysis	76
<b>Figure 26:</b> Wnt ligand-receptor interactions with high confidence in CellChat ligand-receptor analysis	77

## Chapter IV

<b>Figure 1:</b> Western blot of Co-immunoprecipitation of Myc-Scx and SFB-TCF3/4/12, SFB-COPB1, SFB-COPB2, and SFB-UBE20	97
<b>Figure 2:</b> Immunofluorescence of Myc-Scx with SFB-TCF3 and SFB-TCF4/12	98

## LIST OF TABLES

	<b>Page</b>
<b>Chapter IV</b>	
<b>Table 1:</b> PPIs detected from MS analysis of TAP human MKX transfected in HEK293 cells	96
<b>Table 2:</b> PPIs detected from MS analysis of TAP human SCX transfected in HEK293 cells	97

## ACKNOWLEDGEMENTS

I would like to take this opportunity to extend my deepest appreciation and gratitude to all those who have been an integral part of my academic journey and the completion of this thesis. First, I would like to thank my thesis advisor, Dr. Tom Schilling, whose mentorship guided me towards thinking and working as an independent researcher. Tom has always been open and available to discuss new ideas and explore alternative hypotheses when things don't go to plan. I am forever grateful for his mentorship, support, and receptiveness. I would also like to thank current and former members of the Schilling lab for their friendship, and roles in shaping and re-shaping how I think as a scientist. I have the utmost appreciation for Arul Subramanian for his friendship, his incredible technical mentorship, his wealth of knowledge in tendon biology, the breadth and depth of his expertise in molecular biology techniques, his cooking, and mostly, his infinite patience with me. He taught me that there is real joy in doing science for its own sake. Danny Dranow has been an amazing mentor, friend, and sounding board for all experiment ideas. Danny's sense of humor is a constant source of laughter, but his ability to pick apart every word and detail never fails to frustrate me. However, he has taught me to constantly think deeply before I speak. Lianna Fung has been a great mentor and friend as well. I have had enjoyable conversations and brainstorming sessions with her about everything from experiments to the latest stock market research. My time in the Schilling lab would not have been the same without David, Jessica, Praveer, Diego, Irene, Olga, Ines, Lauren, and our latest addition, Cameron. I thank friends from my MCSB cohort, especially Hamsi, Matt, and Neelakshi, for making my time in the program so enjoyable. I would also like to thank my committee members Dr. Ken Cho, Dr. Kathleen Treseder, Dr. Wenqi Wang, and Dr. Kavita Arora, for their valuable advice over the years. My gratitude goes to the NIH and NSF-Simons Center for Multiscale Cell Fate Research for funding my research work. Lastly, I'd like to thank my mom, dad, and brother, who believed in me even when I didn't believe in myself.

## VITA

**Pavan Nayak**

### **Education**

---

#### **University of California, Irvine**

Irvine, California

*Ph.D., Mathematical, Computational, and Systems Biology*

*Fall 2017-Summer 2023*

#### **University of California, Santa Cruz**

Santa Cruz, California

*B.S., Biology, Minor, Bioinformatics*

*Fall 2011-Spring 2015*

### **Research Experience**

---

#### **University of California, Irvine**

Irvine, California

*Mathematical, Computational, and Systems Biology (Thomas F. Schilling Lab), PhD Candidate*

*Summer 2018-Summer 2023*

#### **Tioga Research**

San Diego, California

*Research Associate*

*January 2016 – June 2017*

#### **Salk Institute**

La Jolla, California

*Asahina Lab, Research Associate*

*November 2015 – April 2016*

### **Publications and Presentations**

---

## Publications:

- Leng X., Wohl M., Ishii K., **Nayak P.**, Asahina K. Quantifying influence of human choice on the automated detection of *Drosophila* behavior by a supervised machine learning algorithm. *PLoS One*. 2020 Dec 16;15(12):e0241696. doi: 10.1371/journal.pone.0241696. PMID: 33326445; PMCID: PMC7743940.
- Nayak, P., Subramanian A., Schilling T. (2023) Transcriptome profiling of tendon fibroblasts at muscle contraction onset reveals novel force-responsive genes ***Manuscript in preparation***
- Nayak, P., Subramanian A., Dranow, D., Roberts R., Crump G., Schilling T. (2023) Cranial tenocyte diversity and roles for Wnt signaling in embryonic tendon patterning ***Manuscript in preparation***

## Presentations:

- Nayak, P., Subramanian A., Dranow D., Schilling T. (2023). Cranial tenocyte diversity and roles for Wnt signaling in embryonic tendon patterning. Poster Presentation. *Society for Developmental Biology Conference – Chicago IL*
- Nayak, P., Subramanian A., Schilling T. (2022) Deciphering spatio-temporal heterogeneity in cranial tenocytes using scRNAseq. Poster Presentation. *Center for Multiscale Cell Fate Symposium – Irvine CA*
- Nayak, P., Subramanian A., Schilling T. (2022) Transcriptome profiling of tendon fibroblasts at muscle contraction onset reveals novel force-responsive genes. Poster Presentation. *Orthopedic Research Society Conference – Philadelphia PA*
- Nayak, P., Subramanian A., Schilling T. (2021) Transcriptome profiling of tendon fibroblasts at muscle contraction onset reveals novel force-responsive genes. Research Talk. *West Coast Regional Society for Developmental Biology Conference – Virtual*
- Nayak, P., Subramanian A., Wang W., Schilling T. (2020) Deciphering the Gene Regulatory Network of Mechanotransduction in Vertebrate Tendon Development. Poster Presentation. *Orthopedic Research Society Conference – Phoenix AZ*
- Nayak, P., Subramanian A., Wang W., Schilling T. (2019) Deciphering the Gene Regulatory Network of Mechanotransduction in Vertebrate Tendon Development. Poster Presentation. *West Coast Regional Society for Developmental Biology Conference – Cambria CA*

## Academic Fellowships

---

- Member - Orthopedic Research Society (ORS) (2020, 2022)
- Member - Society for Developmental Biology (SDB) (2019, 2021, 2023)
- Graduate Fellow - NSF-Simons Center for Multiscale Cell Fate (CMCF) (2022-2023)

## **ABSTRACT OF THE DISSERTATION**

Tenocyte transcriptional diversity and responses to muscle contraction force

by

Pavan Nayak

Doctor of Philosophy in Mathematical, Computational and Systems Biology

University of California, Irvine, 2023

Professor Thomas F. Schilling, Chair

During vertebrate embryogenesis, tissue morphology and cell differentiation are constantly influenced by, and responding to, microenvironment cues such as physical forces and associated biochemical signaling processes. Few tissues exemplify the complex interplay of these coexisting processes better than tendons, the extracellular matrix (ECM) rich connective tissues which attach muscle to bone, cartilage, and soft tissues, and coordinate the optimal transfer of force from of muscle contraction to the skeleton. Though in recent years, much has been elucidated about gene regulatory networks coordinating tendon tissue morphogenesis and tendon fibroblast (tenocyte) fate specification/differentiation, very little is known about how heterogenous tenocyte populations sense and respond to muscle contraction forces and uniquely modify their ECM organization and composition in vivo. Current knowledge of tenocyte mechanotransduction has been primarily informed by studies in adult in vivo models, and generally in tendons restricted to mammalian limbs. Zebrafish embryonic tendons provide a particularly useful model to address these research questions, as heterogenous tenocyte populations inhabiting different tendons can easily be studied across developmental timepoints. In this thesis work, I leveraged next generation bulk and single-cell sequencing approaches combined with in vivo functional perturbations and protein binding assays to gain a more defined, holistic understanding of tenocyte-ECM functional interactions during vertebrate development.

I investigate tenocyte transcriptional responses to the onset of muscle contraction force during development by conducting RNA sequencing on sorted tenocytes from zebrafish embryos at developmental stages before and after the onset of muscle activity. I show that onset of muscle contractile forces leads to a specific transcriptional change in tenocytes, and using muscle-paralysis perturbation assays confirm that three novel tenocyte subpopulation markers, *matn1*, *klf2a*, and *mxra5b* are differentially expressed. Further, I show that variations in magnitude of muscle contractile force lead to unique transcriptional dynamics in specific tenocyte subpopulations in vivo, suggesting that tenocytes fine-tune ECM gene expression to adapt individual tendons to specific force conditions.

In vivo, tendon-like structures connect muscles not only to bone and cartilage, but to soft tissue such as eye sclera, and transmit varying intensity of forces from muscle contraction. Recent sequencing studies have begun to unravel distinct tenocyte subpopulations but have primarily looked at only gene regulatory networks of tenocytes inhabiting individual tendons or tendon subregions, prompting the question as to whether tenocyte populations are transcriptionally distinct within and between distinct tendons. To understand this tenocyte transcriptional heterogeneity at the level of both inter- and intra-tendon tissues, I conducted single-cell RNA sequencing (scRNAseq) on sorted cranial tenocytes from dissected zebrafish heads. I show for the first time that cranial tenocyte populations transcriptionally cluster into both spatially distinct tendons and functionally distinct intra-tendon regions, and that this clustering is driven not only by generalized patterning genes but also by specific ECM components. I further show that individual intra-tendon attachment zones have distinct ECM transcriptional signatures between tendons, suggesting that a combination of developmental programming and varying levels of force at attachment zones underlies tenocyte heterogeneity. Next, I identify a previously unknown population of Wnt-signaling responsive tenocytes populating multiple tendons in the cranium and show through independent Wnt signaling perturbation assays that a

proper balance of Wnt signaling is required for proper patterning of myotendinous junctions of the jaw. Through computational cell-communication inference software, I hypothesize that specific Wnt ligands and receptors are involved in this patterning process. These findings revealed a deeper layer of complexity to the understanding of tendon biology, demonstrating that transcriptional diversity of tenocytes is driven by the dual characteristics of specific attachment zone physiology and the load capacity of the tendon ECM.

Lastly, I investigate how tenocyte fate specification occurs at the level of transcriptional control by identifying putative binding partners to key tenocyte fate determining transcription factors Scleraxis and Mohawk. Through biochemical protein binding assays and immunofluorescence I show that Scleraxis binds a family of Class II helix-loop-helix transcription factor E-box proteins TCF3, TCF4, and TCF 12, and that these proteins are individually sufficient to drive Scleraxis translocation from the cytoplasm to the nucleus. This reveals a novel mechanism for initiation of Scleraxis transcription, which has sweeping implications for further understanding of tenocyte fate determination and maintenance. In this thesis, I have provided unique insights into novel roles for muscle-contraction force on tendon tissue remodeling, tenocyte transcriptional heterogeneity, and lineage specification.

## Chapter I

### Introduction and Background

A key question in developmental and cell biology is how biochemical signaling mechanisms at the cellular scale can coordinate broad changes at the tissue, organ, and organismal scale. While cell-cell signaling mechanisms have been broadly characterized across cell types since the early 1900s, studies of cell to extracellular matrix (ECM) signaling mechanisms begin advancing primarily in the 1970s (Borges & García, 2021). Judah Folkman, Anne Moscona, and Denis Gospodarowicz were among the first to recognize the influence of culture substrate thickness on cell shape, which in turn determined cell proliferation rates and growth factor sensitivity (Folkman & Moscona, 1978; Gospodarowicz et al., 1978). With the discovery of fibronectin, its integrin receptor, and the downstream signaling cascades leading to cell adhesion and cytoskeletal morphological changes, the understanding of cell-ECM signaling interactions and downstream cascades expanded (Hynes & Yamada, 1982; Schlaepfer et al., 1994). However, these studies usually perceived cell-ECM interactions from a unidirectional feed-forward perspective, in that they primarily studied only cell responses to the substrate microenvironment. How cells and local ECM bidirectionally influence each other to globally adapt tissues remained understudied. In the 1980s and 1990s the field of cell-ECM interactions began to flourish, and it became clear that one of the systems by which feedback loops, or bidirectional “dynamic reciprocity”, occurred was through mechanotransduction, the process in which cells sense and respond to mechanical stimuli from the ECM to modify their own behavior and that of the surrounding microenvironment and adapt tissue (and in turn, tissues re-adapt cells) to changing conditions (Bissell & Glennhall, 1982).

This bidirectional feedback mechanism became much more well studied in 2d culture assays in vitro, allowing for an understanding of cell-type agnostic and specific mechanotransduction signaling mechanisms, both from the perspective of cell sensing and response to ECM signals as well as subsequent cellular modification of surrounding ECM

(Discher et al., 2005; Vogel & Sheetz, 2006). As useful as these studies were for understanding individual signaling components, the geometry of 2d culture assays were found to differentially affect mechanotransduction responses as opposed to more modern 3d culture systems, likely due to lack of (more recently identified) cell mechanisms which sense 3d confinement (Saraswathibhatla et al., 2023). 3d culture models are likely to better simulate the force architecture of native tissue and provide a more realistic model for studying cell-type specific mechanotransduction responses than 2d cultures (Saraswathibhatla et al., 2023). They are especially useful for holding ECM microenvironment variables (e.g. stiffness, density, protein composition) relatively constant while modulating other parameters such as force direction, intensity, frequency, and duration to study subsequent feedback signaling mechanisms. However, though both 2d and 3d culture protocols continue to inform knowledge of cell-ECM interactions, the primary mechanosensitive signal transduction mechanisms under dynamic force conditions in vivo remains a key gap in knowledge. Fundamental questions remain regarding how functional heterogeneity of both ECM tissue and cell-types are mechanistically driven by the diverse force-laden environments of specific tissues in vivo, and across biological processes. A tissue model which optimally exemplifies the dynamicity of cell-ECM force-feedback mechanisms is that of tendons, ECM rich tissues that connect muscles to a range of other tissue types such as cartilage, soft tissue (e.g. eye sclera and muscle myosepta), and bone. The nature of tendons as connective tissue places a demand for optimized transference of muscle contraction force to the underlying structural tissue. Though the strength and adaptability of tendons are due to their rich ECM composition, the coordinators of these dynamic structures are the resident tendon fibroblasts, called tenocytes. These cells direct a huge variety of tissue-specific tasks, from ECM production and remodeling to sensing mechanical cues and adapting surrounding tissue throughout a range of diverse biological processes such as development, tissue homeostasis, and injury repair. Though in recent years the advancement of single-cell sequencing technologies has led to a better understanding of

tenocyte functional heterogeneity in vitro and within individual tendons, how spatially distinct tendons (and their resident tenocyte subpopulations) are functionally adapted to suit specific contraction force requirements remains unclear in vivo. In this thesis, I aim to explore tenocyte functional diversity, transcriptional responses to varied muscle contraction force across tenocyte populations, and protein interactors with key tenocyte fate-determining (TFs) to gain a holistic perspective of tenocyte differentiation during embryonic tendon tissue development. These findings will in turn better inform knowledge of how macro tissue-scale forces can drive both tenocyte-specific and generalizable dynamic reciprocity mechanisms in cell-ECM interactions which propel patterning, remodeling, and adaptation processes in healthy and diseased tissue systems.

### **Mechanotransduction across scales**

In 1982, Mina Bisell and Mary Helen Barcellos-Hoff postulated that the minimum required unit of function at the tissue level was a cell with its surrounding microenvironment ECM, and that the modified cytoskeletal morphology resulting from cell responses to substrate forces would further influence ECM gene expression and protein deposition from that cell, in a tissue-specific manner (Bisell & Barcellos-Hoff, 1987). Early mechanotransduction studies identified integrin signaling as a primary pathway connecting actin cytoskeletal elements to ECM mechanical stimuli to drive diverse cell behaviors but did not look at resultant ECM effects. Further studies demonstrated integrin signaling as a primary mechanotransductive pathway, for example, integrin receptor clustering responding to ECM mechanical stimuli can lead to downstream activation of Rho GTPases to stimulate actin remodeling and drive cell survival, or the activation of MAPK-ERK cascade which can drive behaviors like cell proliferation, differentiation, migration, and apoptosis during organogenesis and disease states by upregulating downstream TFs in the nucleus (Katsumi et al., 2004; Roovers & Assoian, 2003). Later, other individual mediators of mechanotransduction were identified spanning various

localizations both cell-intrinsic and extrinsic. These include membrane components such as membrane ion channels, surface receptors and various cilia, ECM components such as various collagen types (fibrillar, FACIT, basement membrane, etc...) and proteoglycans, and nucleus components such as nuclear ion channels, chromatin, and mechanoreceptive TFs (Barakat, 1999; Kolahi & Mofrad, 2010). It became clear that extensive diversity of these cell sensory mechanisms exists to optimally coordinate adaptive cell behavior to ever-changing microenvironment forces and conditions (**Fig. 1**). For example, in vitro mesenchymal stem cell (MSC) differentiation to either osteoblasts or adipocytes can be controlled by levels of retinoic acid regulated nuclear Lamin-A in combination with ECM stiffness (Swift et al., 2013). Another example is of MSC differentiation to osteoblasts at the cost of adipocyte differentiation which can be controlled via activation of mechanosensitive ion channel Piezo1 through application of constant hydrostatic pressure (Sugimoto et al., 2017). Mechanically driven cell behaviors can also serve to remodel ECM via cell interactions that lead to feedback loop systems (**Fig. 1**). These can present as, for example, locally aligned collagen 1 fibers resulting from actomyosin contractile force, which leads to higher ECM force generation thereby increasing cell stiffness in a mechanically dependent positive feedback loop (Hall et al., 2016). In vitro, cultured fibroblasts can additionally upregulate and secrete ECM proteins such as fibronectin and collagen to modify local ECM composition in response to substrate mechanosensing, leading to further downstream mechanotransduction signaling and altered cell behavior (Loebel et al., 2019).

The identification of individual mechanotransduction mediating proteins was informed by considerable research in 2d and newer 3d culture systems which allowed consistent control over experimental ECM environments (Saraswathibhatla et al., 2023). To gain a higher-level understanding, knowledge of individual components must be integrated to study processes

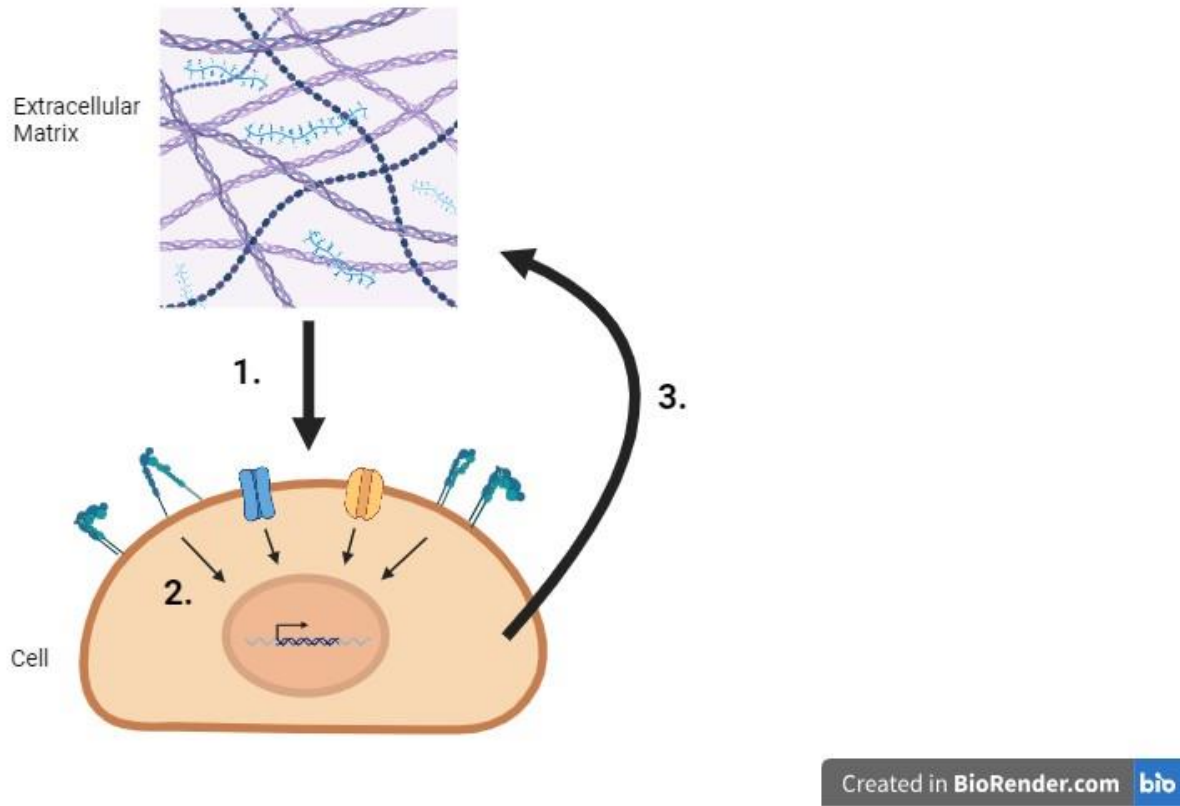


**Figure 1: Schematic of generalized dynamic reciprocity in cell-ECM interactions**

1) ECM forces are induced upon cells 2) Cells sense force-induced biochemical signals via integrin receptors, ion channels, cilia, and other protein components and activate signaling pathways to initiate transcriptional regulation 3) Proteins synthesized and cell behavior changes resulting from transcriptional and protein induction influence ECM protein composition and mechanical properties, and these changes further regulate cell behavior.

system-wide by understanding how variation in parameters of ECM forces can modulate cell-ECM interactions. These forces can be organized into two categories: passive forces, which includes effects of ECM physical properties such as stiffness, viscoelasticity, and geometry, and active forces, which includes variation of globally applied force direction, intensity, frequency, and duration. Passive force regulation examples include ECM stiffness and substrate

topography regulating subsequent secretion of inflammatory cytokines in endothelial cells (Jeon et al., 2015), generation of cartilage ECM proteins (such as collagen 2 and aggrecan) in MSCs cultured on surfaces with stiffnesses similar to native articular cartilage tissues (Olivares-Navarrete et al., 2017), and regulation of osteocyte gap junction formation and ECM mineralization, likely regulated by integrin/FAK (Focal Adhesion Kinase) /Beta-catenin signaling (Xie et al., 2018). These provide evidence that substrate passive forces most similar to native tissue mechanical qualities optimally preserve native cell-type transcriptional/protein expression signatures, triggering the cell to attempt to preserve tissue microenvironment quality to maintain homeostasis. Thus, when selecting in vitro models for studies of native tissue microenvironment, passive force characteristics must be optimized to the in vivo tissue context. Next, how do varied parameters of applied external force affect cell-ECM interaction in vitro? Responses are similarly context specific. Cultured fibroblasts showed applied cell-tractility based stretching forces upon the ECM over time, leading to unfolding of extracellular fibronectin, which could have downstream effects of exposing alternative binding motifs for protein interaction (Baneyx et al., 2002; Krammer et al., 2002; Smith et al., 2007; Vogel, 2006). In cultured cardiomyocytes, increases in both cyclical stretch amplitude and duration independently increased phosphorylation of FAK at residue Tyr-397, which caused changes in FAK subcellular localization and activation of an atrial natriuretic factor (ANF) promoter (detected via luciferase assay) (Torsoni et al., 2003). Increases in ANF expression are known to have antifibrotic and antihypertrophic effects in cardiac tissue and decrease arterial pressure by attenuating the renin-angiotensin-alderosterone system (Nakagawa et al., 2019). Changes in force amplitude can also cause cells to act in opposing manners, for example, fluid laminar shear stress can induce patterns of anti-inflammatory gene expression, whereas fluid oscillatory shear stress inhibits anti-inflammatory responses in endothelial cells, simulating healthy and atherosclerotic hemodynamic stressors respectively (Chappell et al., 1998; Davies, 2009). These provide examples of force-based positive feedback loops which further stimulate either

healthy or diseased tissue states. With the further understanding of mechanotransduction feedback systems in 2d and 3d in vitro models, we can begin to comprehend system-wide dynamic reciprocity of cell-ECM interactions in in vivo models across biological processes.

The comprehension of the mechanics of 3d cell and tissue movement in in vivo processes such as development, homeostasis, injury, regeneration, and disease demands models which connect systems between micro and macro scales. How tuning of mechanical properties at the tissue scales which arise as emergent properties of local ECM, cellular, and subcellular interactions to coordinate organ level morphological changes remains an ongoing field of study. In an in vivo study of skin wound healing, it was found that the tissue system undergoes a negative feedback loop dependent on dermal fibroblast ECM deposition driving repression of fibroblast proliferation shortly after wound invasion, to restore cell-ECM homeostasis post healing (Rognoni et al., 2018). The complexity of systemic interactions across scales increases when dealing with, for example, the process of embryonic development, where multiple organs are formed through comprehensive movement of tissues resulting from highly coordinated mechanical and signaling interactions between cell-ECM units. In *Xenopus laevis* development, for example, stiffening of head mesoderm (due to convergent extension of mesodermal cells) during gastrulation triggers neural crest cell epithelial-to-mesenchymal transition and subsequent migration behavior (and resultant downstream differentiation and tissue patterning) (Barriga et al., 2018). Bidirectional mechanotransduction cell-ECM feedback is, however, more easily observed in vertebrate tendon development, where muscle contraction force is required for proper cell morphology, ECM organization, and tissue structure (Subramanian et al., 2018; Subramanian & Schilling, 2015).

### **Tendon mechanobiology and development**

Early tendon force related studies, like those of other tissues, were primarily studied in vitro or ex vivo. These were primarily focused on gross ECM tissue mechanical properties and

were useful for gaining an understanding of the effects of force intensity across different tendons, and how tissue mechanical properties varied (Gomez et al., 1981; Viidik, 1969). However, tenocyte-specific mechanotransduction studies were not performed in vitro until the 1990s and early 2000s, which found applications of active force as a primary regulator of ECM synthesis, such as collagen 1 and 2 (which make up the bulk of the tendon ECM), and growth factor secretion, such as FGF, MAPK, and PDGF (Kim et al., 2002; Skutek et al., 2001). Cultured tenocytes also were found to reorganize collagen into aligned parallel fibrils, likely through cell-applied tension mediated by integrin receptors on the cell surface (Lamberti & Wezeman, 2002; G. M. Lee & Loeser, 1999). Further, application of static strain was shown to increase collagen fibril diameter which led to increases in mechanical strength of in vitro tissue constructs (Herchenhan et al., 2013). Similar to other cell types, tenocytes modulate their morphology in response to force in vitro, often elongating parallel to collagen fibers and the predominant axis of force transmission (Lamberti & Wezeman, 2002). Around this time, the first tenocyte fate specifying TF, a class B basic helix-loop-helix protein called Scleraxis (Scx), was identified and found to mark most tenocytes in the vertebrate head, limbs, trunk, and tail (Cserjesi et al., 1995; Schweitzer et al., 2001). Scx as a critical TF led to important mechanistic findings of tenocyte progenitor cell differentiation, such as Scx upstream regulation of tenocyte proliferation coordinator Tenomodulin (Tnmd) as well as *Col1a1* and *Col1a2* (Espira et al., 2009; Léjard et al., 2007). It was noticed that the morphological changes exhibited by tenocytes in vitro, an elongated high-aspect ratio shape, led to increased expression of these tenogenic marker genes and therefore ECM components, suggesting that feedback mechanisms of ECM/microenvironment tension and subsequent morphology maintain homeostasis of the tenocyte-ECM unit (Kishore et al., 2012; J. Zhu et al., 2010). Indeed, excess mechanical loading on cultured tenocytes led to damaged ECM, cell-death, and upregulation of inflammatory mediators, whereas loss of tenocyte mechanosensing via FAK inhibition even led to dedifferentiation, defined by decreased expression of tenogenic marker genes and morphology

disruption (T. Maeda et al., 2011b; J. H.-C. Wang et al., 2003; Xu et al., 2012). This provides a basic model by which external force conditions regulate the homeostasis of tenocyte-ECM dynamic reciprocity (**Fig. 2**). As research efforts evolved from in vitro studies of tenocyte mechanotransduction, the development of genetic tools, such as transgenic reporter lines for Scx across animal models, provided a means to bridge findings from cell culture experiments to investigate tendon biology in vivo at the tissue scale.

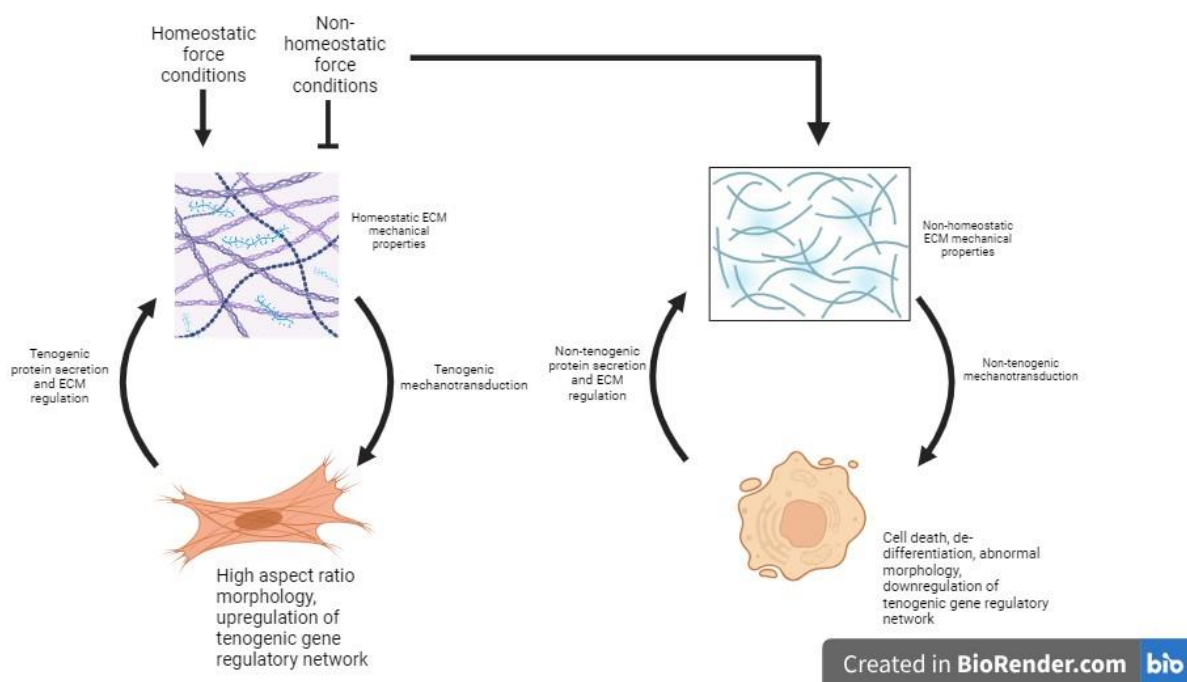


**Figure 2: Schematic of the effects of homeostatic force conditions on tenocyte-ECM dynamic reciprocity**

Proper force conditions are required to maintain homeostasis of the tenocyte-ECM functional unit, visualizable by tenocytes with high aspect ratio fibroblastic shape, which further maintains homeostatic ECM mechanical properties through upregulation of the tenogenic gene regulatory network. Non-homeostatic force conditions, i.e. chronic or acute excessive force through muscle contraction or loss of optimal force conditions, leads to abnormal morphology, upregulation of non-homeostatic ECM genes and inflammatory cytokines, which further alters local ECM mechanical properties to further degrade homeostatic ECM mechanical properties.

Soon, discovery of other TFs besides Scx, such as Mxk, Egr1, and Egr2, were shown to be sufficient to induce tenocyte fate specification in vitro, but in vivo knockouts showed that tenocyte progenitor cells still develop, suggesting that either 1) no single TF is necessary as a master regulator of tenocyte cell fate, unlike MyoD in muscle or Sox9 in skeletal lineages, or 2) such a master TF has yet to be identified (Guerquin et al., 2013; Kimura et al., 2011; Lejard et al., 2011). In vivo functional studies confirmed Transforming growth factor beta (TGF- $\beta$ ) signaling as a crucial regulator of tenocyte cell fate, and tendon ECM production, maintenance, and repair (Berthet et al., 2013; Havis et al., 2014; Pryce et al., 2009). Functional knockouts of *Tgf $\beta$ 2* and *Tgf $\beta$ 3* ligands, or receptor *Tgf $\beta$ r2* leads to a near total loss of differentiated tendons, and *ScxCre* conditional knockouts of *Tgf $\beta$ r2* lead to a de-differentiated transcriptional state, which can be rescued by viral *Tgf $\beta$ r2* reintroduction (Pryce et al., 2009; Tan et al., 2020). Further, TGF- $\beta$  regulates expression of TFs Scx and Mxk to dictate ECM production and tenocyte differentiation from tendon progenitor cells (TPC) (Berthet et al., 2013; Tan et al., 2020). TGF- $\beta$  signaling also presents an intriguing bridge between the developmental programming of tenocytes and their responsiveness to mechanical stimuli as it is thought to be a critical pathway by which tenocytes sense and respond to force to modulate the surrounding ECM. For example, gradual loss of mechanical loading on mouse achilles tendons causes TGF- $\beta$  mediated Scx downregulation. Muscle paralysis also induces TGF- $\beta$  dependent tenocyte morphological defects in zebrafish, which can be rescued by muscle contraction induced via electrical stimulation (T. Maeda et al., 2011b; Subramanian et al., 2018). However, how the mechanical force signal upon the ECM triggers TGF- $\beta$  signaling to act upon tenocytes is not fully clear. Currently, it is thought that TGF- $\beta$  ligand is bound in the ECM in an inactive state by latent TGF- $\beta$  binding proteins (LTBPs) and TGF- $\beta$  propeptide in a large latent TGF- $\beta$  complex (LLC) and regulated by fibrillin proteins (Rifkin, 2005). One possible mechanism by which TGF- $\beta$  becomes liberated from the LLC to bind cell surface receptors is through mechanical stress activation, as was shown in in vitro models of myofibroblast contractility (Wipff et al., 2007).

These findings hint at an in vivo model in which muscle-contraction acts as a primary mechanical mediator of TGF- $\beta$  signaling in tendon ECM, driving tenocyte fate determination, morphology, and subsequent ECM strengthening during development. TGF- $\beta$  signaling in tendon (and ligament) mechanotransduction has become more well studied in recent years, but other pathways are now being implicated using unique in vivo models. In a rat model of periodontal ligaments, Rho-cofilin signaling was found to be active in ECM remodeling downstream of mechanical strain (Meng et al., 2015). Hedgehog signaling has been implicated in regulation of *Mkx* to inhibit heterotopic ossification in mouse achilles tendon (H. Liu et al., 2019). Questions remain as to a holistic model of tendon formation and the role of mechanotransduction, especially due to muscle contraction, during development. Further, in vivo models for varied muscle contractile force are understudied, especially across different tendon tissues. Though modern genome-wide sequencing approaches have now become popular in both in vitro and in vivo studies of tenocytes under a variety of biological processes, in vivo mechanotransduction-induced expressional changes during vertebrate development remain largely unexplored. In chapter II of my thesis, I examine and implicate, using bulk RNA sequencing, a wide variety of genes and pathways involved in tenocyte mechanotransduction, and provide a putative force-responsive module of genes to provide a map for future research directions. Additionally, we implicate genes previously studied in mechanotransduction in other tissue types, postulating that mechanotransduction-induced expression of common genes may differ between tissues, and even between individual tendons, to account for variety in parameters of force dynamics. As sequencing and -omics technology has developed in recent years, the in-depth exploration of such individual tenocyte populations responses to varying force-related stimuli remains an exciting avenue of research.

### **Tenocyte diversity at single cell resolution**

Since the first RNA sequencing studies performed on tendon tissue in the earlier part of the last ten years, single-cell sequencing technology has allowed researchers to tease apart tenocyte populations to an ever-finer degree. For example, though tenocytes may originate from MSCs, a single cell studies have suggested that pericytes are progenitor cells of adult tenocytes, a finding that falls in line with questioning in recent years as to whether MSCs exist as separate populations from pericytes (Caplan, 2017; De Micheli et al., 2020). Even individual tenocyte stem cell populations have begun to be teased apart, providing an early map for both spatial localization and functional purpose (Z. Huang et al., 2021). One example is a *Tpp3+/Pdgfra+* stem cell population residing in the sheath surrounding the tendon and responding to injury by differentiating into new tenocytes and is present in tendon tissue from neonatal stages to adulthood (Harvey et al., 2019; Z. Huang et al., 2021). As tendons subregions have become described in terms of their protein structure and mechanical characteristics, such as the enthesis (tendon-bone/cartilage attachment interface), midsubstance (tendon proper), and myotendinous junction (MTJ, tendon-muscle attachment interface), the tenocyte diversity within an individual tendon subregion has begun to be elucidated. The enthesis, which was initially characterized as a mineralized fibrocartilage attachment zone containing a functional gradient of hybrid tendo-chondral ECM to distribute the force of muscle contraction optimally at the transition from soft to harder tissue, is known to experience forces up to four times greater than those of the tendon midsubstance (Lu & Thomopoulos, 2013; McGonagle et al., 2003). Studies of the enthesis have shown that it contains a unique population of cells which express both Scx and chondrocyte fate determining TF Sox9 with gene expression and chromatin accessibility resembling both tenocyte and chondrocytes, and that the ratio of gene expression of these TFs is controlled by the mechanical force of muscle contraction (Kult et al., 2021; Subramanian et al., 2023). Interestingly, a recent single cell analysis has even identified heterogeneity within the enthesis, along with an Gli1+ enthesis progenitor cell subpopulation which improves healing when administered to injured

mouse entheses (Fang et al., 2022). Heterogeneity of cells and ECM at the MTJ are also now being described, such as hybrid cells containing both myogenic and tendon fibroblastic transcriptional signatures fusing with myofibers at MTJ muscle tips to regulate muscle fiber anchorage (Yaseen et al., 2021). Proteomics analysis has identified unique MTJ ECM protein composition as well as distinct from that of the enthesis, suggesting the unique functional adaptation of this tendon subregion (Karlsen et al., 2022). These studies have primarily looked at tenocyte populations from the perspective of cell diversity within a single tendon, or even an intra-tendinous region. Decades of research, however, have shown 1) the huge influence of mechanical force on all aspects of tendon biology and 2) the vast differences in force intensity experienced in different tendons. These findings bring up questions of the effect of muscle contraction force in specific subpopulations of tenocytes in vivo and how the functional cell-ECM unit undergoes dynamic reciprocity to adapt the tissue level mechanical characteristics of a specific tendon to bear the unique forces specific to the attaching muscle (e.g. tendons of the eye versus those of the jaw and limb/trunk).

The use of mouse and chick models may be difficult for dissociation protocols to capture multiple tendon tissues within a single-cell sequencing experiment for comparative analysis while simultaneously avoiding batch effects associated with tissue dissociation. Usage of the zebrafish craniofacial tendons as a model provides an intriguing solution to performing comparative single-cell sequencing on tenocytes at multiple different tendons simultaneously as cranial tendons span a diversity of attachment regions such as tendon-soft tissue in the eye and tendon-cartilage in the jaw. Additionally, up to 50+ zebrafish embryo heads can be pooled together for dissociation to enrich for rare subpopulations that may be missed, which is particularly useful for modern single-cell library preparation protocols which can have lower cell capture rates. Though most cranial tenocyte populations arise from cranial neural crest (CNC) cells rather than mesoderm, as in trunk and limb tendons, they still express hallmark tenocyte

transcription factors such as *Scx* and *Tnmd*, and even have comparable morphologies to limb tendons, proving useful to translational outcomes beyond those restricted to craniofacial tendinopathies (Bobzin et al., 2021). In chapter III of my thesis, I aim to address knowledge gaps by understanding cranial tenocyte heterogeneity through the perspective of how anatomical locations and force-requirements of individual tendons influence tenocyte transcription at those tendon sub-regions.

### **Moving towards a functional understanding of tenocyte transcriptional regulation**

Though sequencing studies have increased the depth of understanding of tenocyte subpopulations, protein-interaction studies of key tenocyte regulators are much sparser. High throughput proteomic analyses of tendon tissue have begun to further dissect components of tendon substructure in vivo, however, functional analyses of interacting elements with key tenocyte TFs are being studied. TF Egr1, for example, can have variable functions based on specific protein modification and context. In protein kinase CKII dependent EGR1 phosphorylation, EGR1 DNA binding and transcription is inhibited in NIH 3T3 cells, whereas protein kinase C and tyrosine kinase phosphorylation of EGR1 in fibrosarcoma cells can induce suppression of proliferation via downregulating expression of Bcl-2 (R.-P. Huang et al., 1998; Jain et al., 1996). Protein-protein interaction studies have also identified APE/Ref-1, a DNA-repair enzyme, as binding with EGR1 in an osteoblast cell line, and that this transcriptional complex then further binds promoter regions of APE/Ref-1, forming an autoregulatory positive feedback loop. Though these interactions have been mapped in other cell types, a full understanding of Egr1 protein control in tenocytes is still unknown. Similarly, other critical tenocyte TF fate specifiers and maintainers such as *Scx* and *Mkx* have been described for years, but the proteins interacting with these TFs to carry out their function and the mechanisms involved in DNA binding and transcriptional control remain to be examined. Helix-loop-helix (HLH) transcription factors in the same family as *Scx*, such as *MyoD* (a regulator of muscle cell

fate) have been known to heterodimerize with HLH E-box proteins to drive DNA binding and transcriptional control of differentiation (L.-H. Wang & Baker, 2000). Conversely, HLH Id proteins seem to act as repressors, functionally opposing E-box proteins in differentiation, working mechanistically as a dominant negative HLH protein due to a missing critical binding domain (Massari & Murre, 2000). This system may work as a feedback inhibition on E-protein activation, to provide tight control of tissue-specific differentiation (Bhattacharya & Baker, 2011). Even less is known about protein-binding interactors of Mlx, though it is thought that proteins in the same family, termed TALE-homeodomain class cofactors, bind HOX proteins to increase context-specific DNA binding affinity (Merabet & Mann, 2016). Whether protein binding partners with tenocyte TFs, such as those described with similar proteins above, occur in the tenocyte differentiation process remains unknown. In chapter IV, I explore protein-protein interactions with Scx and Mlx using mass spectrometry, highlighting a mechanism for Scx to achieve subcellular localization to carry out its role as a TF. Understanding the binding partners of the tenocyte differentiation process downstream of mechanical force is necessary for mapping the transcriptional control mechanism by which feedback onto the surrounding ECM occurs. Overall, this thesis work furthers the understanding of force-induced dynamic reciprocity in tenocyte-ECM behavior from the scale of subcellular protein interactions to the tissue level across spatially distinct tendons.

## Chapter II

### **An in vivo investigation of tenocyte transcriptional responses to muscle contraction force paradigms**

#### **Introduction**

Cells experience mechanical forces from their environments such as adhesive interactions between adjacent epithelial cells or with the surrounding extracellular matrix (ECM). A key question is how cells adapt and respond to force through mechano-sensitive biochemical cell-signaling pathways and modify their local microenvironment in response, as well as how this modified microenvironment continues to influence cell behavior. Force-responsive cellular mechanisms have been implicated in many aspects of cell differentiation (D'Angelo et al., 2011), morphogenesis (Hamada, 2015; Keller et al., 2008), maintenance and repair (Riley et al., 2022.; Zhang et al., 2022). Despite their importance, these mechanisms remain understudied in vivo, particularly those that involve cell-ECM interactions. Dramatic examples of such interactions occur in tendons and ligaments of the vertebrate musculoskeletal system. Tendons experience a broad range of contractile forces from muscles, such as the extreme compressive forces on the human Achilles tendon during exercise, and constantly remodel themselves and their surrounding ECM to adapt (Subramanian & Schilling, 2015; J. H. C. Wang, 2006). Tendon injuries and atrophy with aging are very common and a better understanding of the roles played by force in tendon development will aid in developing effective treatments.

Tendons are ECM-rich structures that connect muscles to cartilages and bones. The highly coordinated events leading to the proper formation of these connections in vertebrates relies upon cell-ECM interactions (Schweitzer et al., 2010; Subramanian & Schilling, 2015). For example, in the early embryonic zebrafish trunk, myotendinous junctions (MTJs) develop via distinct tendon-independent and tendon-dependent stages of attachment. Differentiating myoblasts first secrete ECM proteins such as the integrin ligands Thrombospondin-4 (Tsp4) and Laminin-2 (Lama2) into the developing “pre-tendon” ECM, which establishes a rudimentary

attachment, after which tenocyte progenitor cells (TPC) migrate to the site leading to MTJ maturation (Subramanian & Schilling, 2015). Tenocytes also extend long microtubule-rich projections outwards into the surrounding ECM, with which they may respond to mechanical force to locally regulate ECM composition (Mcneilly et al., 1996; Pingel et al., 2014; Subramanian et al., 2018). The maturation of myoblasts and subsequent contractile forces acting on the MTJs activate Transforming Growth Factor  $\beta$  (TGF- $\beta$ ) coupled, phospho-SMAD (pSMAD)-dependent signaling in TPCs (Berthet et al., 2013; Pryce et al., 2009). Although TGF- $\beta$  is not necessary for TPC specification, it induces expression of the transcription factors Scleraxis (Scx) and Mohawk (Mkx), likely through Smad3 binding, which drive tenocyte fate by directly promoting transcription of tendon-specific ECM proteins, such as Collagen 1 (Col1a1, Col1a2), Col12a1 and Col14 as well as Matrix Metalloproteinases (MMPs) involved in ECM remodeling (Berthet et al., 2013; T. Maeda et al., 2011a; Rullman et al., 2009). TGF- $\beta$  signaling via Smad3 and/or Mkx also represses genes involved in myogenic and skeletogenic fates, such as *MyoD* (Chuang et al., 2014; D. Liu et al., 2001), *Sox6* (Anderson et al., 2012) and *Runx2* (Kang et al., 2005).

Cell type and matrix composition differ along the length of many tendons to aid in load bearing and force transmission. For example, the enthesis region where a tendon attaches to bone is structurally composed of a gradient of stiffer fibrocartilage closer to the attachment. This is thought to help transfer mechanical stress between the elastic tendon tissue and rigid bony matrix (Lu & Thomopoulos, 2013). Attachment cells along this fibrocartilage co-express Scx and Sox9, which likely contributes to the specialized enthesis ECM structure and the ratio of expression of these two TFs are regulated by muscle contraction force (Blitz et al., 2013; Subramanian et al., 2023; Zelzer et al., 2014). Further, dysregulation of force in tendons leads to changes in collagen fibril size and organization (Pingel et al., 2014), as well as levels of *COL1*, *COL3*, and *MMP3* mRNA (Ireland et al., 2001). Force-responsive tenocyte mRNA

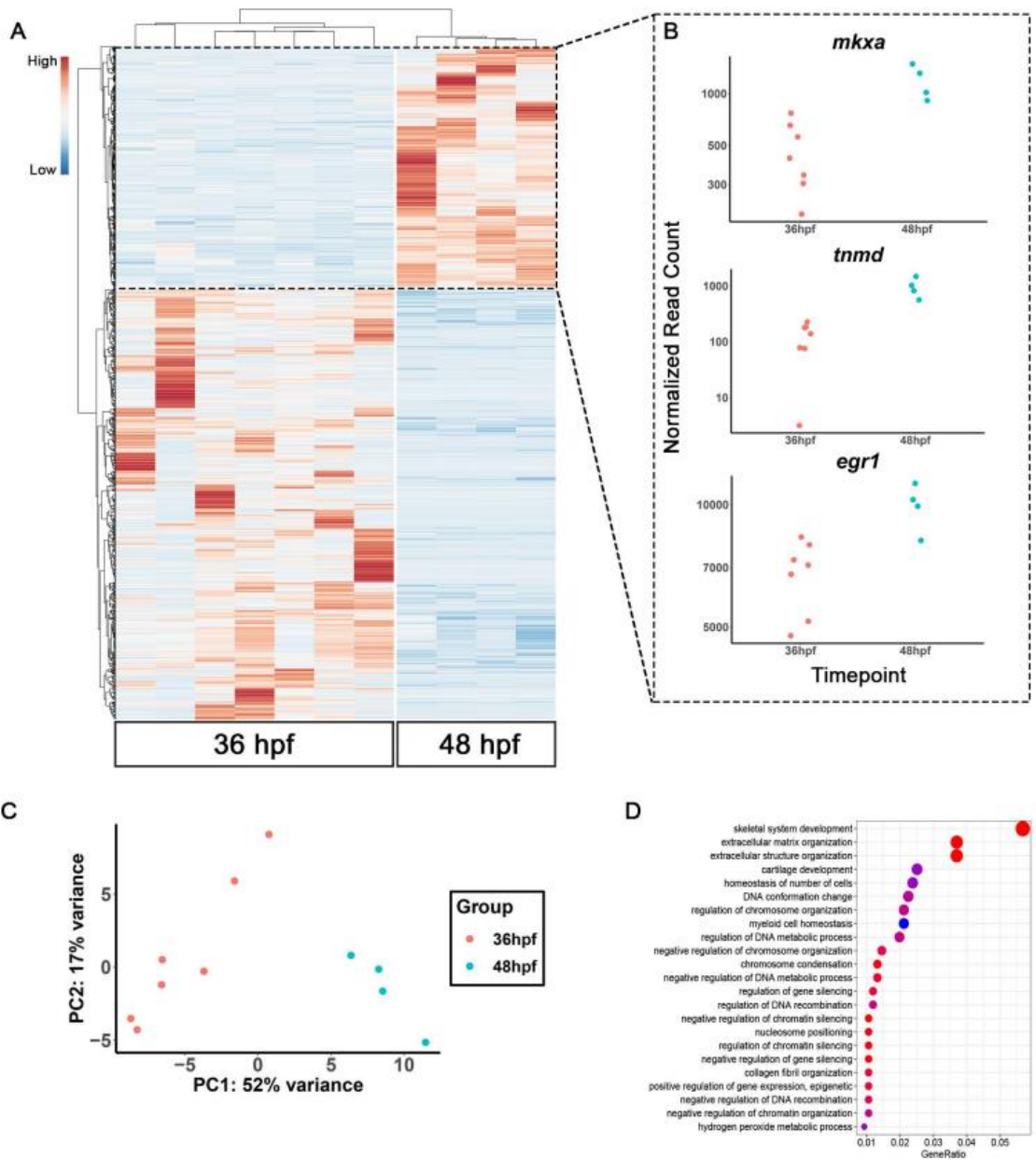
expression profiles have been examined in vitro and ex vivo following injury and during repair. However, while many studies have demonstrated effects of force on tenocyte transcription in vitro, there have been no comprehensive transcriptomic studies of tenocyte responses to force in vivo, especially during embryonic development and the onset of muscular contraction. We have previously shown that force resulting from the onset of embryonic muscular contraction is required for proper tendon maturation in zebrafish embryos, including tenocyte morphogenesis and ECM production (Subramanian et al. 2018).

Here we perform genome-wide bulk RNA-sequencing (RNA-seq) on FAC-sorted tenocytes of developing zebrafish embryos during the onset of active swimming and trunk muscle contraction. We identify several known tenocyte markers, expression of which is upregulated as tendons differentiate, as well as numerous other up- or downregulated genes about which relatively little is known in the context of tenocyte development or mechano-transduction. Using genetic and physiological perturbations of muscular force in vivo, we show force-responsiveness of several of these novel tenocyte-associated genes both in whole embryos and in sorted tenocytes. These include genes encoding two ECM proteins, Matrix Remodeling Associated 5b (*mxra5b*) and Matrilin 1 (*matn1*), as well as the transcription factor Kruppel-like factor 2a (*klf2a*). We further use quantitative in situ methods to confirm their tenocyte- and enthesis-specific expression as well as their force-responses and conduct multiplex CRISPR/Cas9 knockouts to understand gene function. These findings provide insights into force-dependent feedback mechanisms in tendons, which have important implications for improved treatments for tendon disease, injury and atrophy.

## Results

### Onset of active muscle contraction alters tenocyte gene expression

Previously, we showed that tenocytes in trunk muscle attachments undergo distinct morphological transformations coinciding with the onset of muscle contraction (Subramanian et al., 2018). Since these changes occur during the embryonic transition from twitching (36 hours post-fertilization, hpf) to free-swimming behavior (48 hpf), we hypothesized that force-induced transcriptional changes in tenocytes in addition to their maturation as they differentiate underlie these morphological changes. To test this and identify potential force-responsive factors, we conducted RNA-seq with FAC-sorted populations of *Tg(scxa:mCherry)*-positive tenocytes isolated from dissociated 36 or 48 hpf embryos. From 11 total biological replicates (7 replicates for 36 hpf, 4 replicates for 48 hpf after quality control (**see Methods**), 35 embryos per replicate) we obtained approximately 10,000 cells per sample replicate. Pair-wise comparisons of over 17,000 genes from bar-coded cDNA libraries revealed 2788 differentially expressed genes (DEGs) between 36 and 48 hpf with p-value < 0.05 (**Fig. 1A**). These included upregulation of known tenocyte markers such as *tnmd*, *mkxa*, and *egr1* (**Fig. 1B**), confirming that the sorted mCherry positive cells included mature tenocytes or progenitors in the process of differentiation. Principle Components (PCs) associated with biological replicates segregated according to experimental condition (36 versus 48 hpf), validating the library preparation protocol (**Fig. 1C**). GO analysis for Biological Process (BP) terms associated with the top DEGs showed significant enrichment for “skeletal system development” and “ECM organization” (**Fig 1D**), while Molecular Function (MF) and Cellular Component (CC) GO terms were similarly enriched for ECM-associated features (**Supplementary Fig. 1**). Surprisingly, among the DEGs were genes



typically associated with cartilage development and morphogenesis, including *matn1*, *col2a1a* and *col9a1a*, suggesting that tenocyte subpopulations, likely an early subset of *scxa*+ cells in embryonic tendons that have already adopted a fibrocartilage fate later associated with developing entheses. Indeed, recent research has confirmed dual expressing *scxa*/*sox9a*+ cells at patterning entheses of the zebrafish cranium at 48 hpf, suggesting that enthesis tenocyte subpopulation specification occurs before tendon, cartilage, and muscle tissue formation has

**Figure 1: Genes differentially expressed in tendon progenitor cells upon onset of embryonic muscle contraction**

**A)** Heatmap from bulk RNA-seq of FAC-sorted *scxa:mCherry+* tenocytes displaying top 1000 of 2788 genes differentially expressed between 36 hpf and 48 hpf.  $p < 0.05$ . **B)** Elevated expression of tenocyte marker genes *mkxa*, *tnmd*, and *egr1* in RNA-seq experiments at 48 hpf. Datapoints represent normalized read counts of single biological replicates for each color-coded timepoint (n=7 for 36 hpf, n=4 for 48 hpf). **C)** PCA of individual replicates showing separation of experimental conditions by timepoint. **D)** GO analysis using Biological Process (BP) terms of top 1,123 differentially expressed genes (DEGs) by adjusted p-value.

finalized, a finding in line with recent single-cell sequencing studies of enthesis subpopulation lineage trajectories in mice (Fang et al., 2022; Subramanian et al., 2023).

To identify cell signaling and cell adhesion pathways implicated in force-responses during embryonic tendon development, we analyzed our DEG list using two software suites, PANTHER (Mi & Thomas, 2009) (**Supplementary Table 1**) and DAVID (**Supplementary Table 2**), which utilize KEGG pathway annotations, for pathway analysis (D. W. Huang et al., 2008). We used both software suites in combination to maximize identification of novel pathways in our dataset, since DAVID covers multiple annotation categories including GO terms, KEGG pathway databases, and disease associations, whereas PANTHER focuses more deeply on pathway analysis by utilizing its own curated database for pathway annotations. PANTHER identified DEGs associated with 96 different pathways, including many genes implicated in Wnt, TGF- $\beta$ , Platelet Derived Growth Factor (PDGF), and Retinoic Acid (RA) signaling as well as Integrin (Itg) and Cadherin (Cdh) mediated adhesion (**Supplementary Table 1**). In contrast, DAVID identified DEGs involved in RA metabolism, an emerging pathway of interest in tendon development, and highlighted differential expression of genes encoding many ribosomal proteins. (**Supplementary Table 2**).

Our RNA-seq DEG datasets were obtained from TPCs and tenocytes during the onset of swimming, so we performed a targeted search for DEGs associated with mechanosensitive pathways, which might have been missed by pathway analysis software due to limitations in

annotation databases. Using a custom automated literature screening tool, (**see Methods**), three genes of particular interest, *matn1*, *klf2a* and *mxra5b*, emerged based either on their force-dependent regulation in other biological contexts, and/or regulation by TGF- $\beta$ , a well-known force-responsive signal. The top-most upregulated gene by p-value was *matn1*, which encodes an ECM protein highly enriched in cartilage. Matn1 enhances chondrogenesis of synovial fibroblasts treated with TGF- $\beta$  (Pei et al., 2008). The transcription factor *klf2a* was also strongly upregulated and Klf proteins such as Klf2 and Klf4 have been implicated in enthesis development in mammalian tendons. Klf proteins repress TGF- $\beta$  signaling in endothelial cells (Boon et al., 2007; H. Li et al., 2021) and *klf2a* expression is mechanosensitive during heart valve development (Steed et al., 2016). A third DEG of particular interest was *mxra5b*, which encodes an ECM protein expressed in both tendons and ligaments during chick development (Robins & Capehart, 2018) and is regulated by TGF- $\beta$  signaling in cultured human kidney epithelial cells (Poveda et al., 2017). Though other potentially mechanosensitive genes may have arisen from our bulk RNAseq dataset, we focused on *matn1*, *klf2a* and *mxra5b* for further analysis for their expression evidence in other cell type contexts.

### ***matn1*, *klf2a* and *mxra5b* are expressed in cranial and trunk tendon subpopulations of muscular contraction in vivo**

To verify specific expression of *matn1*, *klf2a* and *mxra5b* in tenocytes, we performed in situ hybridization (ISH). Conventional chromogenic ISH for *matn1* failed to detect expression at 36 hpf, whereas strong expression was observed at 48 and 60 hpf in developing craniofacial and pectoral fin cartilages (**Fig. 2A-C**). Because of its strong expression in chondrocytes, we hypothesized that differential expression of *matn1* in our dataset could be a result of tenocyte-

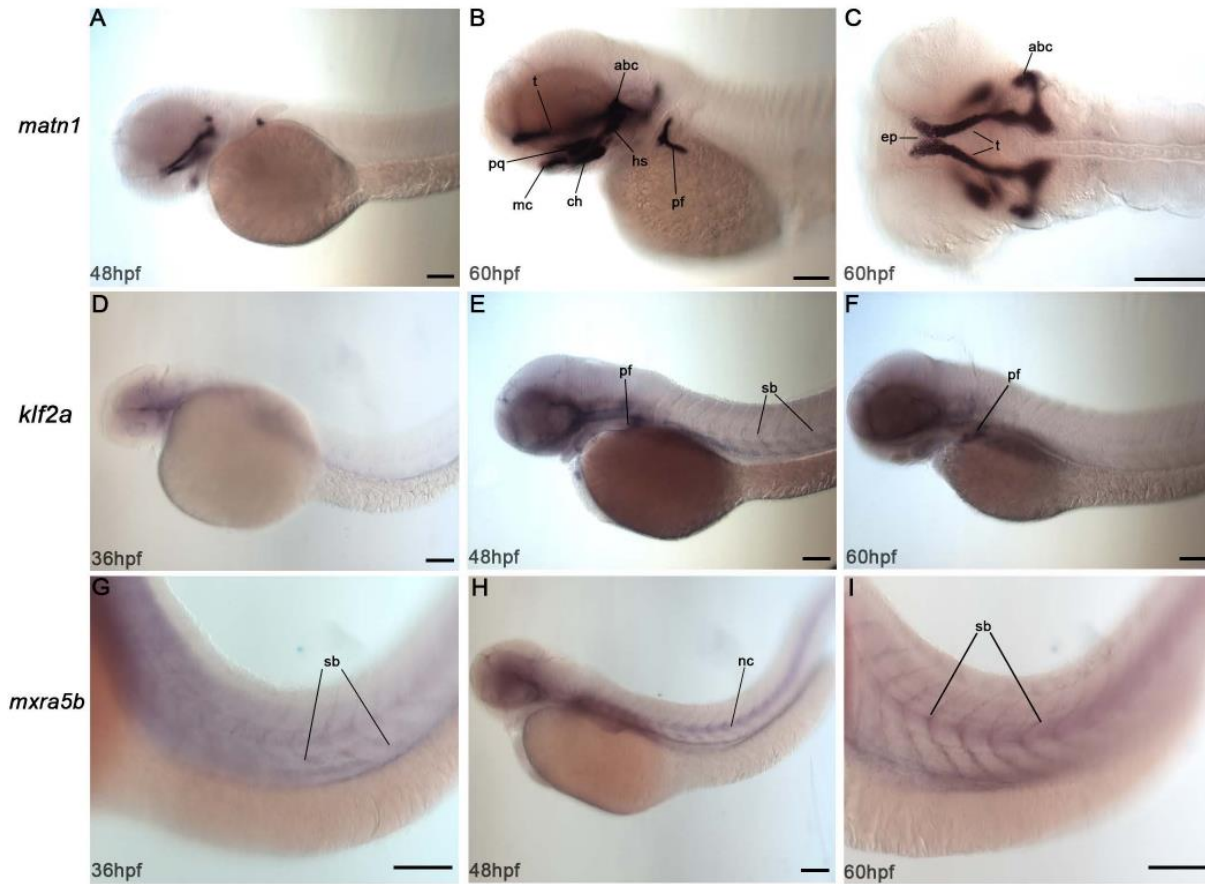


### Figure 2: Embryonic expression of novel tenocyte markers

Expression of *matn1*, *klf2a* and *mxra5b* mRNA detected by whole mount ISH. **(A-C)** *matn1* expression in skeletal progenitors at 48 hpf **(A)** and in pharyngeal, neurocranial and pectoral fin cartilages (and associated tenocytes) at 60 hpf **(B,C)**. **(A,B)** Lateral views. **(C)** Ventral view. **(D-F)** *klf2a* expression in pharyngeal mesenchyme at 36 hpf **(D)**, skeletal progenitors and in tenocytes along somite boundaries (sb) at 48 and 60 hpf **(E,F)**. Lateral views. **(G-I)** *mxra5b* expression in tenocytes along somite boundaries and the notochord at 36, 48 and 60 hpf. Scale bars = 100 $\mu$ m. Abbreviations: abc = anterior basicranial commissure, ch = ceratohyal cartilage, ep = ethmoid plate, hs = hyosymplectic cartilage, mc = meckel's cartilage, nc = notochord, pf = pectoral fin, pq = palatoquadrate cartilage, sb = somite boundaries, t = trabeculae cartilage.

specific expression in developing entheses progenitors closely associated with embryonic cartilages. To this end, we conducted fluorescent in situ Hybridization Chain Reaction (*isHCR*) for *scxa* and *matn1* at 51 hpf, 3 hours older than our RNA-seq samples to allow better visualization of differentiated chondrocytes, and 72 hpf. We found *scxa/matn1* co-expressing cells at the posterior ceratohyal (ch) tendon and sternohyoid (sh) entheses attachment region of the ceratohyal at 72 hpf (**Fig. 3A-E Supplementary Fig. 2A-G**). For *klf2a*, chromogenic ISH

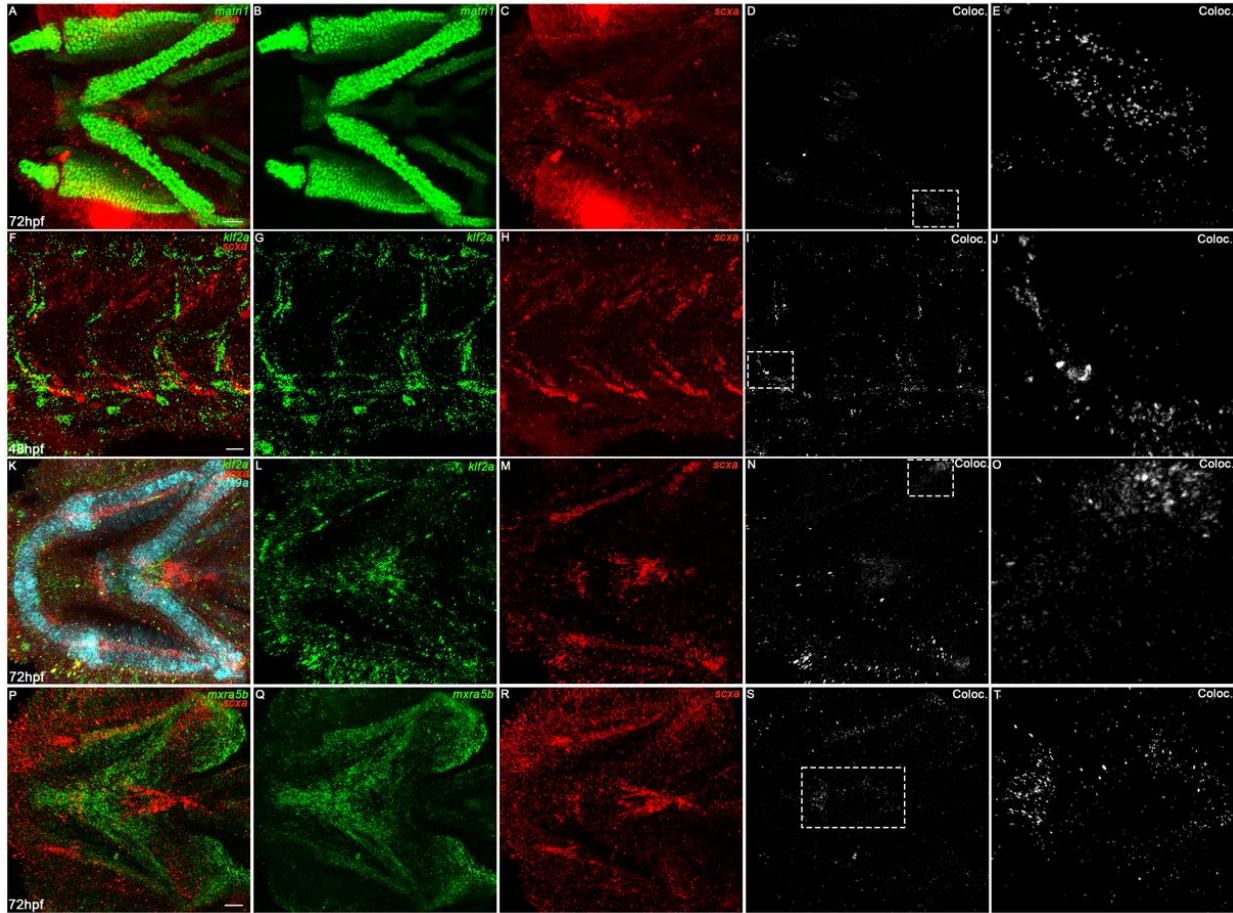


**Figure 3: Co-expression of *matn1*, *klf2a* and *mxra5b* with *scxa* in cranial and trunk tenocytes**

*isHCR* of *matn1*, *klf2a*, and *mxra5b* individually in combination with *scxa*. **(A-C)** *matn1* and *scxa* *isHCR* of 72 hpf embryo head (ventral view). **(D-E)** Colocalization of *matn1* and *scxa*. White dashed box highlights dual expression in posterior enthesis attachment of ch tendon, with magnified view in **(E)**. **(F-H)** *klf2a* and *scxa* *isHCR* of 48 hpf embryo somite boundary (lateral view). **(I-J)** Colocalization of *klf2a* and *scxa* expression. White dashed box highlights dual expression in somite boundary tenocytes, with magnified view in **(J)**. **(K-M)** *klf2a* and *scxa* *isHCR* of 72 hpf embryo head (ventral view). **(N-O)** Colocalization of *klf2a* and *scxa*. White dashed box highlights dual expression in posterior enthesis attachment of ch tendon with magnified view in **(O)**. **(P-R)** *mxra5b* and *scxa* *isHCR* of 72 hpf embryo head (ventral view) **(S-T)** Colocalization of *mxra5b* and *scxa*. White dashed box highlights dual expression in mhj, and sh enthesis attachment, with magnified view in **(T)**.

revealed expression at somite boundaries in the trunk at 48 hpf as well as developing pharyngeal arches and pectoral fins at 48 and 60 hpf (**Fig. 2D-F**). This was confirmed by double *isHCR* of *klf2a* and *scxa* showing overlapping expression in tenocytes at somite boundaries at 48 hpf (**Fig. 3F-J**). More interestingly, we noticed *klf2a* expression in multiple tendons in the

head at 72 hpf most predominantly in the entheses of the sh, posterior ch, intermandibularis tendon (imt), meckel's adductor tendon (mat), but with very little expression at the ceratohyal interhyal attachment, a tendon at the attachment of four different muscles, thus likely primarily containing MTJ tenocyte transcriptional signature (**Supplementary Figure 2D-G**). This provides the first known evidence of *klf2a* as an enthesis marker in the vertebrate cranium, reflecting a similar tissue expression strategy separating the enthesis cells from neighboring chondrocytes and tenocytes seen in mouse limbs (Kult et al., 2021; Lu & Thomopoulos, 2013; Zelzer et al., 2014). *mxra5b* expression was first detected at somite boundaries near the horizontal myoseptum (HMS), which separates dorsal and ventral somites at 36 hpf, as well as in the notochord and head at 48 hpf onwards (**Fig. 2G-H**). Expression increased and extended along

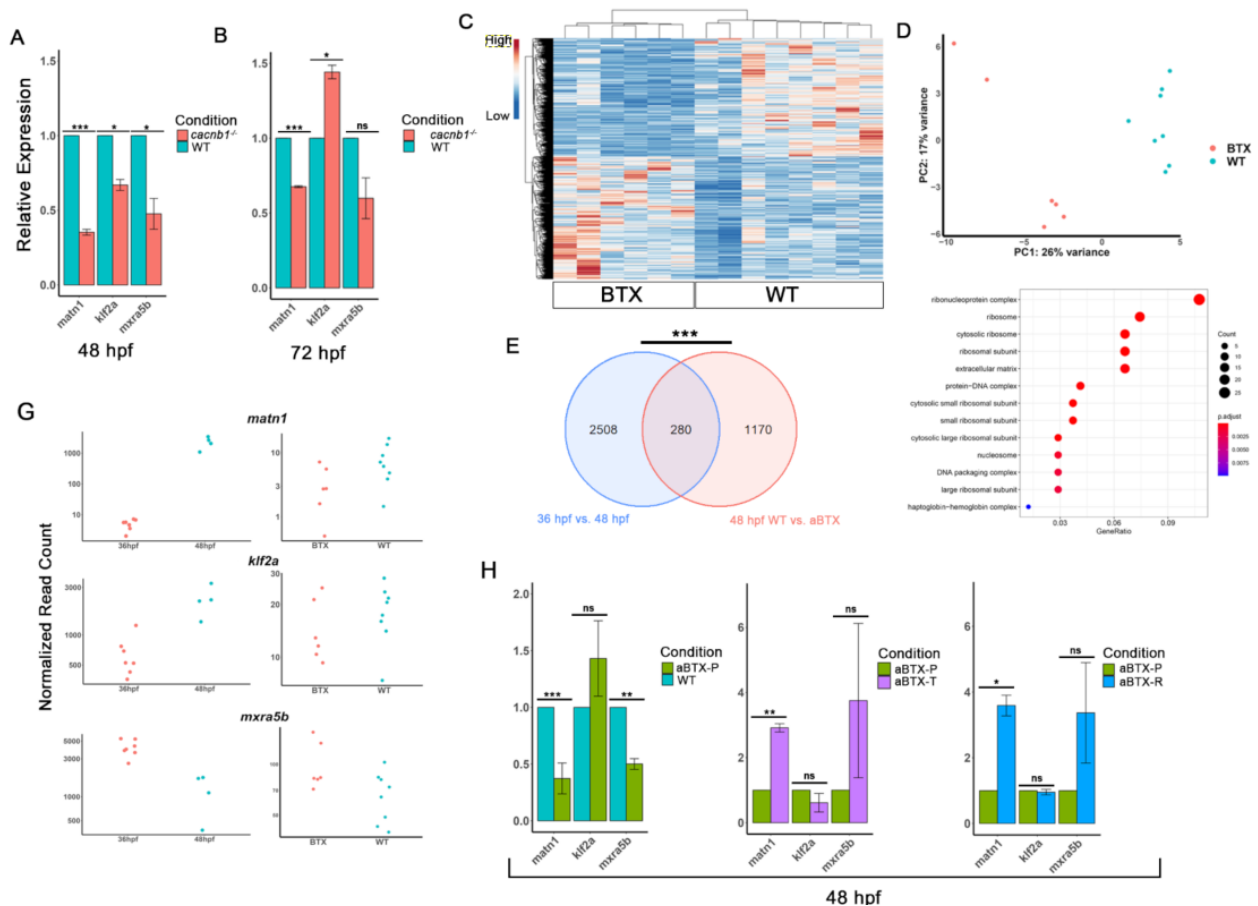


#### Figure 4: Differential gene expression analyses under varied force conditions

**(A)** RT-qPCR of WT vs *cacnb1*<sup>-/-</sup> embryos at 48 hpf for *matn1*, *klf2a*, and *mxra5b*. **(B)** RT-qPCR of WT vs *cacnb1*<sup>-/-</sup> embryos at 72 hpf for *matn1*, *klf2a*, and *mxra5b*. ns = not significant, \* p < 0.05, \*\* p < 0.01, \*\*\* p < 0.001 **(C)** Heatmap of DEGs from bulk RNA-seq between WT and aBTX at 48 hpf showing clear separation of differential expression between conditions. **(D)** PCA of individual replicates from WT vs. aBTX RNA-seq displaying separation by experimental condition. **(E)** Venn diagram showing overlap of genes between RNA-seq experiments. \*\*\* p < 0.001 **(F)** CC GO term analysis of overlapping genes from **(E)**. **(G)** Normalized read counts of *matn1*, *klf2a*, and *mxra5b* in 36 hpf vs. 48 hpf (left) and WT vs. aBTX (right) RNA-seq experiments. **(H)** RT-qPCR of *matn1*, *klf2a*, and *mxra5b* in uninjected WT controls (blue bars) and αBtx-injected paralyzed (green bars) embryos at 48 hpf (left), in αBtx-injected paralyzed (green bars) and αBtx-injected “Twitching” (partially recovered, magenta bars) embryos at 48 hpf (middle), and in WT controls (green bars) and αBtx-injected, “Recovered” (blue bars) embryos at 48 hpf (right). ns = not significant, \* p < 0.05, \*\* p < 0.01, \*\*\* p < 0.001

the somite boundaries by 60 hpf at trunk muscle-tendon attachment sites (**Fig. 2G-I**). Using double isHCR of *scxa* and *mxra5b*, we identified dual expression primarily at the cranial mhj, sh entheses, mhl, and posterior ch entheses in embryos at 72 hpf, marking the first known description of *mxra5a* expression in cranial connective tissue (**Fig. 3P-T**).

#### Tenocyte-specific gene expression of *klf2a*, *mxra5b* and *matn1* is regulated by muscle contraction

Since *matn1*, *klf2a* and *mxra5b* were identified among the top DEGs at the onset of active swimming and persistent muscle activity in zebrafish embryos (**Fig 4A-C**), we hypothesized that mechanical force may regulate their expression. To test this, we performed Real Time Quantitative-PCR (RT-qPCR) in genetically paralyzed embryos. Relative expression of each gene was compared between wild-type (WT) embryos and homozygous mutants for voltage dependent L-type calcium channel subtype beta-1 (*cacnb1*<sup>-/-</sup>), which are paralyzed due to lack of muscle contraction (Subramanian et al., 2018; Zhou et al., 2006). At 48 hpf, we observed significant downregulation of all 3 genes in *cacnb1*<sup>-/-</sup> mutants as compared to WT (**Fig. 4A**). In contrast, at 72 hpf, only *matn1* and *mxra5b* remained downregulated, while *klf2a* expression increased in paralyzed embryos (**Fig. 4B**). To confirm that these, and other gene expression

changes from our original bulk RNA-seq are due to loss of mechanical force, we injected *Tg(scxa:mCherry)* embryos at the 1-cell stage with mRNA encoding full-length alpha-bungarotoxin mRNA (aBTX), which irreversibly binds to acetyl choline receptors at the neuromuscular synapse leading to paralysis and performed bulk RNA-seq on sorted *mCherry+* cells from whole 48 hpf embryos compared with WT uninjected controls (**Fig. 4C**). From this, we observed 1450 DEGs between WT and aBTX paralyzed embryos, and data quality was validated by PCA, in which WT and aBTX replicates neatly separated by experimental condition (**Fig. 4D**). Performing an overlap of significant DEGs between both bulk RNA-seq runs provided a module of 280 genes with potential for muscle-contraction based mechano-responsive gene expression profiles in tenocytes (**Fig. 4E, Supplementary Table 3**). To get an overview of the classes of genes represented in this module, we performed CC GO term analysis and found that genes encoding extracellular matrix proteins were highly enriched (**Fig. 4F**). We then compared expression of *matn1*, *klf2a*, and *mxra5b* between both RNA-seq experiments, and found that although expression of all 3 genes did not differ to the same degree of fold change in the aBTX RNA-seq between aBTX and WT as compared to the 36 hpf vs 48 hpf RNA-seq, the trend of differential expression was similar, suggesting that the expression changes seen in the 36 hpf vs. 48 hpf RNA-seq are partially due to tenocyte responsiveness to muscle contraction force (**Fig. 4G**). Further, comparing the 48 hpf WT vs *cacnb1<sup>-/-</sup>* mutant RT-qPCR with both bulk RNAseq experiments, *matn1* and *mxra5b* expression both had downregulation upon all paralysis conditions in all experiments, whereas *klf2a* expression was variable across experiments (**Fig. 4A, 4G**) perhaps suggesting that *klf2a* expression changes with cell-type specific biological context.

Having shown consistent changes in their expression between the RT-qPCR and bulk RNA-seq results, we next asked if variable recovery of muscle contractile forces rescues changes in *matn1*, *klf2a*, and *mxra5b* expression caused by paralysis. To test this, we used

90ng/ul of full-length  $\alpha$ BTX mRNA, a concentration optimized to paralyze embryos only for the first two days of embryogenesis after which they gradually recover movement. Nearly all  $\alpha$ BTX-injected embryos regained muscle contractions at 48 hpf after such an injection and we performed RT-qPCR on cDNA derived from these and compared them to  $\alpha$ BTX paralyzed ( $\alpha$ BTX-P) and uninjected controls. We separated 48 hpf recovered embryos into two subgroups based on the extent of muscle contraction: 1) partially recovered (Twitching or  $\alpha$ BTX-T), in which embryos showed sporadic contractions of the trunk and pectoral fin muscles, similar to embryos at 36 hpf and 2) fully recovered (Recovered, or  $\alpha$ BTX-R), in which embryos swam freely. At 48 hpf, RT-qPCR revealed significant downregulation of *matn1* and *mxra5b* in  $\alpha$ BTX paralyzed embryos compared to WT uninjected siblings, similar to the relative expression we observed in *cacnb1*<sup>-/-</sup> mutant embryos (**Fig. 4H**). *matn1* and *mxra5b* were upregulated in twitching and recovered embryos, though these results were not statistically significant for *mxra5b* (**Fig. 4H**). In contrast, *klf2a* was upregulated, though this increase was also not statistically significant, in paralyzed embryos versus WT embryos (**Fig. 4F**). These results, combined with our RNA-seq findings, suggest that *matn1*, *klf2a*, and *mxra5b* transcription are regulated by the mechanical forces of muscle contraction.

Since RT-qPCR was performed on cDNA isolated from whole embryos rather than on tenocytes alone, the expression differences we observed for *matn1*, *klf2a*, and *mxra5b* may have reflected changes in expression in cell types other than tenocytes (e.g. *matn1* in cartilage). Therefore, to confirm force-responsiveness in tenocytes, we examined expression of *matn1*, *klf2a*, and *mxra5b* in *scxa*-positive cells at 48 hpf at by *isHCR*, using our  $\alpha$ BTX paralysis-recovery experimental protocol (**Fig. 5A-C**). For *matn1*, we quantified expression by measuring its fluorescence intensity in individual attachment cells at the ch-ih and ch-hh attachment sites of the distal end of the ch cartilage (**Supplementary Fig. 2**) (Subramanian et al., 2023). Individual attachment cells were carefully selected for quantification only if they satisfied the following

criteria: 1) they were located at these muscle attachment sites, 2) they co-expressed both *matn1* and *scxa* and 3) they were spatially adjacent to both chondrocytes expressing high levels of *matn1* alone and tenocytes expressing high levels of *scxa* alone. Individual cell quantification revealed no significant difference in *matn1* expression between WT and paralyzed embryos, but a drastic increase in expression in partially recovered, twitching embryos, followed by a return to WT levels in fully recovered embryos (**Fig. 4I**). For *mxra5b* quantification, we examined its fluorescence intensity in *scxa/mxra5b* double positive tenocytes located at somite boundaries at 48 hpf. Individual cells were selected for analysis only if they were located along ventral somite boundaries or HMS regions and co-expressed *scxa* and *mxra5b*. Similarly, for *klf2a*, we quantified expression by measuring its fluorescence intensity in *scxa/klf2a* double positive

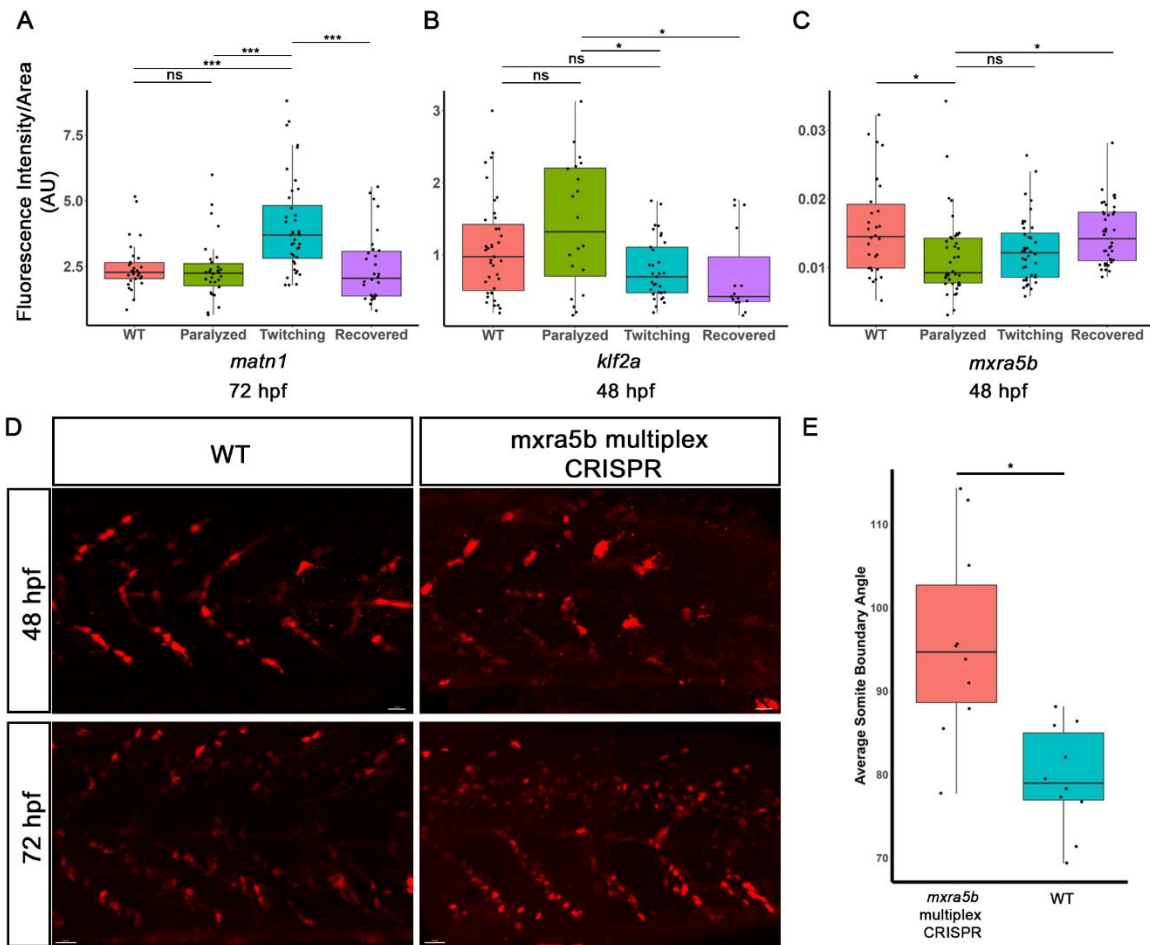


**Figure 5: Tenocyte subpopulation specific gene expression of *matn1*, *klf2a*, *mxra5b*, across varied force frequencies and phenotypic effects of *mxra5b* multiplex CRISPR knockout.**

**(A-C)** Box plots of fluorescence intensity/area measurements from individual cell confocal substacks labeled for *matn1/scxa* **(A)**, *klf2a/scxa* **(B)** and *mxra5b/scxa* **(C)** RNA with *isHCR* in WT controls (red),  $\alpha$ Btx-injected, paralyzed (green), twitching (blue) and recovered (magenta) embryos at 72hpf. By gene and condition, the sample numbers are as follows: for *matn1*, WT: n = 3 embryos, 30 cells; Paralyzed: n= 4 embryos, 30 cells; Twitching: n = 5 embryos, 40 cells; Recovered: 3 embryos, 30 cells; For *klf2a*, WT: n = 5 embryos, 39 cells; Paralyzed: n= 6 embryos, 20 cells; Twitching: n = 5 embryos, 33 cells; Recovered: 3 embryos, 15 cells; For *mxra5b*, WT: n = 3 embryos, 30 cells; Paralyzed: n= 4 embryos, 40 cells; Twitching: n = 4 embryos, 40 cells; Recovered: 4 embryos, 40 cells. ns = not significant, \* p < 0.05, \*\* p < 0.01, \*\*\* p < 0.001. **(D)** Somite boundaries of *Tg(scxa:mCherry)* embryos at 48 hpf and 72 hpf comparing WT uninjected embryos with *mxra5b* multiplex CRISPR injected embryos. **(E)** Quantification of somite boundary angle of 48 hpf embryos, either WT or *mxra5b* multiplex CRISPR injected.

tenocytes at the somite boundaries, primarily at the HMS. We observed increased expression of *klf2a* in paralyzed embryos compared to WT, then a return to WT levels upon full recovery (**Fig. 4J**). Conversely, we observed decreased expression of *mxra5b* in paralyzed embryos compared to WT, followed by a return to WT levels in twitching and recovered groups (**Fig. 4K**). Together, these results suggest that mechanical force initiated by the onset of muscle contraction regulates the transcriptional dynamics of *matn1* in cartilage attachment cells of craniofacial tendons, in developing enthesis progenitors (Subramanian et al., 2023), as well as *klf2a* and *mxra5b* in tenocytes associated with axial trunk muscle attachments.

Lastly, to address functions of these genes in tenocytes we have used multiplex CRISPR/Cas9 mutagenesis (R. S. Wu et al., 2018) to generate F0 crispants for *matn1*, *klf2a* and *mxra5b*. We have not observed any obvious phenotypic defects in *matn1* and *klf2a* crispants, possibly due to genetic redundancy with other similar proteins. *Tg(scx:mCherry)* embryos injected with *mxra5b* multiplex CRISPR gRNAs, displayed a slight loss of trunk tenocytes when compared to uninjected controls (**Fig. 5D**). Additionally, trunk somite boundaries in CRISPR injected embryos displayed a wider somite boundary angle (**Fig. 5E**), although this may be a side effect of notochord deviation, as *mxra5b* expression was located

also located in the notochord (**Fig. 2H-I**) and embryos displaying this phenotype also tended to have mild scoliosis and/or shortened body length along the anterior-posterior axis.

## Discussion

Understanding how cells respond to mechanical forces and translate these signals into biochemical pathways is a fundamental question in biology, with far-reaching implications for tissue development and maintenance. Mechanotransduction is a complex process, and its role in developmental tendon biology, particularly at the transcriptional level, remains poorly explored. In this study we provide a comprehensive genome-wide analysis of differential tenocyte gene expression during the onset of embryonic muscle contraction and in response to paralysis in zebrafish. Our findings highlight the force-responsive nature of three specific genes: *matn1* and *mxra5b*, both encoding ECM proteins, and *klf2a*, a transcription factor. *matn1* and *mxra5b*, both encoding ECM proteins, and *klf2a*, a transcription factor, show that perturbing muscle contraction alters their mRNA levels specifically in tenocytes. Notably, *matn1* exhibits specific expression in enthesal tenocytes, particularly at cranial muscle attachments involved in jaw movements, while *mxra5b* and *klf2a* are predominantly expressed in tenocytes associated with myotendinous junctions in the trunk axial musculature responsible for swimming (Fig. 6). These results are consistent with a model in which tenocytes continuously sense force

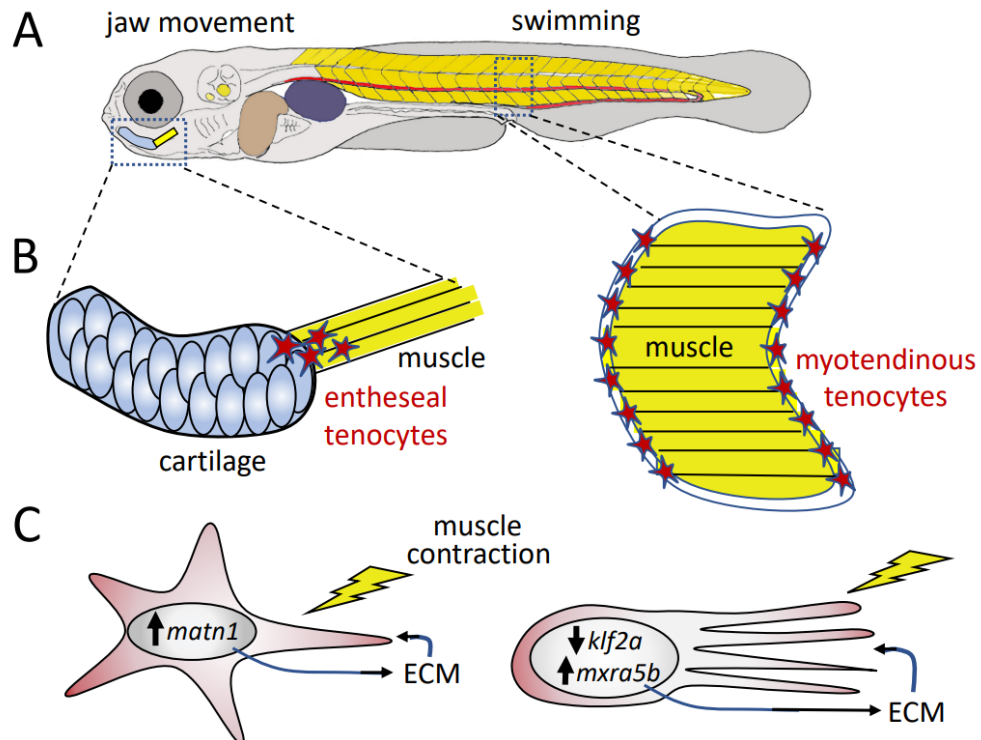


**Figure 6: Proposed model for context-specific expression patterns of *matn1*, *klf2a*, and *mxra5b* across distinct tendon attachment regions.**

**A-B)** Tendons from spatially separate regions must undergo unique force conditions. Whereas cranial jaw enthesal tenocytes may experience more acute forces from jaw contractions, tenocytes of the MTJ may experience both acute and continuous forces from activities such as swimming and posture maintenance respectively. **C)** Acute muscle contraction conditions cause upregulation of *matn1* in enthesal tenocytes, whereas trunk MTJ tenocytes downregulate *klf2a* expression in acute and continuous contraction conditions, while only upregulating *mxra5b* in continuous force conditions.

and respond by altering transcription of genes involved in fine tuning the surrounding ECM (Subramanian et al., 2018; Subramanian & Schilling, 2015). Most tendon mechanotransduction studies have been performed with mature tendons in in vitro/ex vivo conditions e.g. explanted into collagen matrices and exposed to cyclical strain or other forces. Our results demonstrate transcriptional changes in developing tenocytes in response to force in vivo in embryonic tendons as they first form and identify novel components of tenogenesis. They also highlight the close relationship between genes implicated in cartilage (i.e. *matn1*) and fibrocartilage (i.e. *KLF* transcription factors) associated with tendon entheses with tenocytes and their coordinated responses to mechanical force.

Though typically thought of as cartilage-specific ECM proteins, expression of matrilin genes, including *Matn1*, has been reported in single-cell RNA-seq (scRNA-seq) analyses of differentiating tenocytes and fibrocartilage (Kaji et al., 2021). Our results confirm *matn1* expression in zebrafish tenocytes in embryonic entheses (Subramanian et al., 2023), and show that expression is rapidly upregulated at the onset of muscle contractions. Consistent with this force-responsiveness, paralysis transiently reduces *matn1* expression in tenocytes, but it rapidly rebounds as the embryo recovers from paralysis. In mammals, *Matn1* is essential for ECM organization in cartilage; chondrocytes and their surrounding ECM are disorganized in *Matn1*<sup>-/-</sup> mutant mice, and normal organization returns when mechanical load is restored during recovery from medial meniscus destabilization surgery (Y. Chen et al., 2016). Ours are the first studies implicating *Matn1* in tendon/fibrocartilage mechanotransduction. Similarities in

mechanosensitive expression in chondrocytes and tenocytes associated with muscle attachments suggest that *Matn1* may function in establishment/organization of the ECM stiffness gradient between stiffer cartilage and more flexible tendon at the enthesis.

*Mxra5* (also known as *adlican*) encodes a secreted proteoglycan implicated in cell-cell adhesion and/or ECM remodeling as shown in the pathological context of cancer (He et al., 2015; G. H. Wang et al., 2013). We show that, unlike *matn1*, *mxra5* expression in zebrafish is rapidly downregulated in axial tenocytes at the onset of embryonic muscle contraction but upregulated in response to recovery of force following paralysis. *MXRA5* expression has been reported in tendons and connective tissues of developing chick embryos (Robins & Capehart, 2018), but its functions remain unclear. Human *MXRA5* is also expressed in fibroblasts (Chondrogianni et al., 2004), upregulated along with other ECM-associated genes in response to injury (Gabrielsen et al., 2007), and downregulated in response to TGF- $\beta$ 1 (Poveda et al., 2017). Our results provide some of the first evidence that *mxra5* is a mechanosensitive gene, possibly regulated by TGF- $\beta$ . However, while our RT-qPCR results suggest that *mxra5* is downregulated upon muscle contraction, *isHCR* results alone show *mxra5* upregulation upon recovery from paralysis under only fully recovered conditions (**Fig. 5C**). This apparent discrepancy may reflect differences in the cell populations sampled (e.g. whole embryos versus tenocytes), or other developmental regulators of *mxra5b* acting in parallel to mechanotransduction in tenocytes. Further studies will be required to delineate functional roles for *Mxra5* in vertebrate tenocytes.

Recent research in mice showed roles for KLF2, as well as KLF4, in cell differentiation at tendon-bone entheses (Kult et al., 2021), but did not explore their responses to force. We show that *klf2a* in zebrafish axial tenocytes is mechanoresponsive. While aBTX-injected embryos showed no significant changes in *klf2a* expression with paralysis in bulk RNAseq data, it was significantly downregulated in tenocytes upon recovery in *isHCR* fluorescent quantification data

of dual-expressing trunk tenocytes (**Fig. 4G, 5B**). In contrast our RNA-seq of developmental timepoint data showed *klf2a* upregulation with onset of muscle contraction (**Fig. 4G**). Like *mxra5*, these apparent discrepancies may reflect distinct cell populations sampled, as mCherry+ cells were sorted from whole embryos for both RNAseq experiments whereas isHCR quantification analysis sampled solely trunk tenocytes, or separate parallel pathways that regulate *klf2a*. As *klf2a*+ tenocytes sampled in the trunk are MTJ specific whereas *klf2a*+ tenocytes in the head are primarily entheses, this lends evidence to the idea that force-dependent *klf2a* expression may be tuned to individual cell populations and tenocyte sub-types. As *Klf2* binding motifs have been identified upstream of ECM genes such as *Col4V*, it is possible that this cell subtype specific force-response tunes ECM expression to accommodate individual tendon ECM compositions (Kult et al., 2021). *Klf2* is regulated by force in other contexts, such as fluid-force dependent upregulation in endocardial cells leading to fibronectin synthesis (Boselli et al., 2015; J. S. Lee et al., 2006; Steed et al., 2016), suggesting (in combination with our results) that cell-type specific, force-dependent *klf2a* expression is critical for ECM remodeling in a context specific manner.

Our analyses of *matn1*, *mxra5a* and *klf2a* also hint at specific roles in different subpopulations of tenocytes subjected to different forces. While *matn1* is expressed in enthesal tenocytes associated with cartilage, *mxr5a* and *klf2a* expression localizes to tenocytes in the MTJs of axial muscles. We therefore propose a model in which expression of tenocyte marker genes respond distinctly to varying muscle contraction force conditions (**Fig. 6A-6C**). In the developing jaw entheses tenocytes increase *matn1* expression acutely upon sensing of intermittent/acute contraction force (i.e sporadic jaw contraction during cranial tendon development) (**Fig. 6B**). Conversely, the tenocytes of developing trunk MTJs bear the stress of two different contraction conditions: intermittent sporadic trunk contraction forces such as those observed during 36 hpf embryos or during “Twitching” recovery of muscle contraction from  $\alpha$ Btx-

injection induced paralysis, and continuous contractions, such as those required during maintenance of posture along the anteroposterior axis. As individual tendons are likely exposed to varying levels of force according to their specific attachment site, an attractive hypothesis remains that tenocytes transcriptionally maintain distinct ECM structures at each tendon based on the physiological nature, temporal force characteristics, and load-capacity of the specific attachment site (i.e. cartilage, bone, muscle, or soft-tissue). Trunk MTJ tenocytes downregulate *klf2a* expression in both intermittent and continuous force conditions, whereas *mxra5b* expression is increased in only continuous force conditions (**Fig. 6A, 6C**). These contextual differences in force-response may reflect the intricate nature of fine-tuning spatially and mechanically distinct tendon ECM structures during diverse biological processes like development, maintenance and repair.

Whereas bulk RNA sequencing strategies such as those performed here provide deeper read depth for identification of sparsely expressed genes, they may miss critical cell types and specific expression patterns necessary to interpret complex processes occurring in tendons during morphogenesis. Single-cell approaches (e.g. scRNA-seq) at different developmental stages and in the presence or absence of force, will provide a clearer understanding of how individual cells and cell populations respond to force in development. Integrating such knowledge of the basic biology of tenocytes at multiple scales will be essential for developing a nuanced model of tenocyte-ECM interactions at individual tendons, paving the path to advance personalized translational therapies for tendon injuries.

## Methods

### Zebrafish embryos, transgenics and mutants

AB strain wild type, *TgBAC(scxa:mCherry)<sup>fb301</sup>* referred to in this paper as *Tg(scxa:mCherry)*, or *cacnb1<sup>ir1092/ir109</sup>;fb301Tg* (referred to in this paper as *cacnb1<sup>-/-</sup>* transgenic zebrafish embryos were collected in natural matings, raised in embryo medium at 28.5°C (Westerfield, 2000) and staged as described (Kimmel et al., 1995a). Craniofacial musculoskeletal structures were identified as described (Schilling & Kimmel, 1997). All protocols performed on embryos and adult zebrafish in this study had prior IACUC approval.

### In situ hybridization (ISH)

Antisense RNA probes for *matn1*, *klf2a*, and *mxra5b* were generated using T7 sequence-tagged primers (**Supplementary Table 4**) to amplify from cDNA, reverse transcribed using the ProtoScript II First Strand cDNA Synthesis Kit (NEB E6560), from 72 hpf WT embryos and synthesized using T7 RNA polymerase (Roche, 10881767001) and DIG RNA labelling mix (Roche, 11277073910). Whole-mount ISH was performed with anti-DIG-AP fragments (Roche, 11093274910) at 1:2000 dilution, as described in Thisse et al., 1993.

### In situ hybridization chain reaction (*isHCR*) and immunohistochemistry

*isHCR* probes were designed by Molecular Technologies (Los Angeles, CA) and whole mount *isHCR* was performed with amplifiers/probes obtained from Molecular Instruments according to the *isHCR* v3.0 protocol as described (H. M. T. Choi et al., 2014). Probes/amplifier combinations used were: *matn1* (NCBI ref. # 403023) and *mxra5b* (NCBI ref. # 795448) in B1 with B1 Alexa Fluor 488, *scxa* (NCBI ref. # 100034489) in B2 with B2 Alexa Fluor 546, *klf2a* (NCBI ref. # 117508) in B3 with B3 Alexa Fluor 647. Whole embryo immunohistochemistry was performed as described in Subramanian et al., 2018. Primary antibodies used: rat monoclonal anti-mCherry (Molecular Probes – 1:500 dilution, M11217), chicken anti-GFP (Abcam – 1:1000

dilution, ab13970), mouse anti-myosin heavy chain (MHC) (Developmental Hybridoma - 1:250, A1025). Secondary antibodies used: Alexa Fluor 594 conjugated donkey anti-rat IgG (Jackson ImmunoResearch – 1:1000 dilution, 712-586-153), Alexa Fluor 488 conjugated donkey anti-chicken IgY (Jackson ImmunoResearch, 1:1000 dilution, 703-486-155), Alexa Fluor 647 conjugated donkey anti-mouse IgG (Jackson ImmunoResearch, 1:1000 dilution, 715-606-151).

### **Collagenase dissociation and FACS sorting**

36 hpf vs. 48 hpf bulk RNA-seq

Transgenic *Tg(scxa:mCherry)* zebrafish embryos were dissociated using collagenase IV (Roche, 17104019) at a concentration of 6.25 mg/ml without trypsin addition at a temperature of 28C for roughly 40 minutes, homogenizing every 5 min using a P1000 pipette. Cells were then filtered through a 40µm filter (Pluriselect-usa, 43-10040-50). Dissociated cell suspensions were sorted on a Bio-Rad FACS Aria II cell sorter. mCherry-positive cells were gated and sorted for those expressing at high levels.

48 hpf WT vs. aBTX bulk RNA-seq

Transgenic 48 hpf *Tg(scxa:mCherry)* zebrafish embryos were dissociated using Subtilisin A cold-active protease in a stock solution consisting of: 5ul of 1M CaCl<sub>2</sub>, 100ul of protease stock solution (100mg of *Bacillus licheniformis* protease (Sigma P5380) solubilized in 1ml of Ca and Mg free PBS), 889ul of PBS, 1ul of 0.5M EDTA and 5ul of DNase I stock (25U/ul in PBS, stored at -80C). Embryos were triturated once every 2 minutes for 15 seconds using a wide bore 1ml pipette. Every 15 minutes, tissue solution as checked under dissecting scope to verify dissociation. Full dissociation took ~30 minutes per samples, and samples were subsequently run through a 40 micron filter to separate dissociated cells from clumps of aggregate undissociated tissue/ECM and washed with 10ml of PBS/BSA (0.01% BSA in PBS, made fresh on day of dissociation) and transferred to a 15ml conical tube. Cells were

centrifuged at 600g for 5 minutes at 4C, supernatant is discarded, and cells are resuspended in 1ml of ice-cold PBS/BSA before being placed on ice. High expressing mCherry+ cells were gated and sorted on a Bio-Rad FACS Aria II cell sorter.

### **Bulk RNA-seq library preparation and sequencing**

#### 36 hpf vs. 48 hpf bulk RNA-seq

An RNEasy Micro Kit (Qiagen, 74004) was used for RNA extraction of cell lysates from FAC-sorted cells. RNA quality was checked at the UC Irvine Genomics High Throughput Facility (GHTF) using a Bioanalyzer 2100 Instrument (Agilent). The Smart-seq2 protocol was utilized for cDNA library construction (Picelli et al., 2013). Libraries were sequenced at the GHTF using a HiSeq 4000 sequencer (Illumina) at a read depth of ~35M reads per replicate.

#### 48 hpf WT vs. aBTX bulk RNA-seq

Library preparations were performed by the UCI GHTF. Libraries were sequenced at GHTF on a NextSeq 550 sequencer (Illumina) at a read depth of ~35M reads per replicate

### **Bulk RNA-seq data analysis**

Reads were mapped to zebrafish genome version GRCz10 and quantified using STAR v2.5.2a (Dobin et al., 2013) and RSEM v1.2.31 (B. Li & Dewey, 2011). Differential gene expression analysis and PCA were performed using R package DESeq2 v1.30.1. Pairwise comparisons were performed between 36 hpf and 48 hpf sorted tenocytes, and a Benjamini-Hochberg FDR adjusted p-value < 0.05 was used as a threshold for considering significant differences in gene expression levels. PCA was performed on normalized count data which underwent variance-stabilization-transformation using DESeq2. Heatmaps were generated using ClustVis (Metsalu & Vilo, 2015). GO term enrichment analysis was performed using the ClusterProfiler R package (T. Wu et al., 2021a). In GO term plots, Gene Ratios are described as

$k/n$  where  $k$  is the number of genes from the input list of DEGs mapping to the given GO term and  $n$  is the total number of input genes mapping to any GO term.

### **$\alpha$ BTX injections**

$\alpha$ BTX mRNA was synthesized from the *Pmtb-t7-alpha-bungarotoxin* vector (Megason lab, Addgene, 69542) as described in (Swinburne et al., 2015) and injected into embryos at the 1-cell stage at a volume of 500 picoliters per embryo.  $\alpha$ BTX mRNA was injected at a concentration of 90 ng/ $\mu$ l to paralyze embryos that were collected at 48 hpf and 150 ng/ $\mu$ l to paralyze embryos that were collected at 72 hpf.

### **RT-qPCR**

Wild type, *cacnb1*<sup>-/-</sup>,  $\alpha$ Btx-paralyzed, twitching, and recovered embryos were collected at respective timepoints, homogenized in Trizol with prefilled tube kits using high impact zirconium beads (Benchmark Scientific, D1032-10) using a BeadBug 3 Microtube Homogenizer D1030 (Benchmark Scientific), and RNA was extracted using Trizol according to the standard protocol (Invitrogen 15596018). cDNA synthesis was carried out with a standard oligo-dT primer protocol using the ProtoScript II First Strand cDNA Synthesis Kit (NEB E6560). RNA concentrations were normalized between samples prior to reverse transcription. cDNA was diluted 1:25 in water and used as template for RT-qPCR using the Luna Universal qPCR master mix (NEB M3003S). Primers used are listed in **Supplementary Table 4**. Primer efficiencies were calculated with the formula  $\text{PCR-efficiency} = 10^{(-1/\text{slope})}$  from a linear regression of  $\text{Cp}/\ln(\text{DNA})$  using a serial dilution of each primer with 72 hpf embryo cDNA as described in Pfaffl, 2001. PCR reactions were performed on a LightCycler 480 II Real Time PCR Instrument (Roche) and analyzed using LightCycler 480 Software. Each RT-qPCR experiment was repeated in triplicate for each biological replicate, and at least two biological replicates were used for each analysis. P-values were calculated using a two-tailed Student's T-test with  $\alpha = 0.05$  in Microsoft Excel.

Bar charts in **Figure 4** present mean +/- standard error. Venn diagram was created using the VennDiagram v1.7.3 R package with the gene list overlap tested with the Fishers exact test from the GeneOverlap v1.26.0 R package.

### **Automated literature screen**

A python script was written to obtain mouse, rat, and human orthologs for a list of zebrafish gene ENSEMBL IDs by obtaining ortholog information relative to each species from BioMart (Smedley et al., 2009) and using these downloaded lists as a local database. Once the orthologs were placed in a separate Excel file adjacent to the zebrafish genes, the script obtained GenBank gene names/symbols for all genes and orthologs. Lastly, the script identified the number of PubMed articles containing both the GenBank gene name and keyword input search term by sending GET requests to the NCBI Entrez E-utilities API. In our literature screen, the DEG list of 1,123 genes with FDR adj.  $p < 0.05$  was used as input with keyword search terms “TGF beta”, “Retinoic Acid”, “YAP TAZ”, and “Piezo”. This code has been deposited on GitHub and is publicly available. The URL for the GitHub repository is provided here:

**[https://github.com/tschilling-lab/Litscreen\\_Nayak\\_2022](https://github.com/tschilling-lab/Litscreen_Nayak_2022)**

### **Imaging and *isHCR* quantification**

Whole embryos imaged for ISH were mounted on slides in 80% glycerol and imaged using a Zeiss Axioplan 2 compound microscope utilizing an AxioCam 305 Color Micropublisher 5.0 RTV camera with Zeiss Zen 3.1 (blue edition) software. Embryos imaged for *isHCR* were embedded in 1% low melting point agarose/5x SSC and imaged on a Leica SP8 confocal microscope using the PL APO CS2 40X/1.10 W objective. *isHCR* single cell quantification was performed in ImageJ 1.52p using DAPI as a nuclear marker. Embryo imaging for a single experiment was performed with identical parameters across conditions. A substack was created from the top and bottom z-slices of each individual cell displaying co-expression of genes of

interest, and a maximum intensity Z-projection was created using the substack for each measurement. A ROI of the DAPI-stained nucleus from each Z-projection was traced and pixel-intensity/area was measured. *matn1/scxa* co-expressing cells measured were located at the ch-ih and ch-hh attachment sites, at the posterior edge of the ch cartilage. *klf2a/scxa* and *mxra5b/scxa* co-expressing cells measured were located at the boundaries (myosepta) of somites 16-20. *klf2a/scxa* co-expression was measured primarily in tenocytes near the horizontal myoseptum (HMS) whereas *mxra5b/scxa* co-expression was measured primarily from tenocytes in the ventral half of the vertical myoseptum. All experimental condition data pertaining to each embryo image were kept in a separate document, cell measurements on images were performed, and condition identities were matched to images after measurements. All p-values were calculated using one way ANOVA with  $\alpha = 0.05$  and Tukey-Kramer post-hoc tests for pairwise analyses in Microsoft Excel (ns = not significant, \*  $p < 0.05$ , \*\*  $p < 0.01$ , \*\*\*  $p < 0.001$ ). Box plots in **Fig. 5** present median and interquartile range (IQR) with “whiskers” representing largest/smallest value within  $1.5 \times \text{IQR}$  and individual points beyond “whiskers” representing outliers (default R ggplot2 geom\_boxplot parameters).

## Chapter III

### Cranial tenocyte diversity and roles for Wnt signaling in embryonic tendon patterning

#### Introduction

A fundamental question in developmental biology is how cell-ECM units across tissue types send and receive signals such as force, and dynamically modulate each other to direct tissue and organism level changes. This is particularly useful to understand in tendon development, as tendons are defined collectively as extracellular matrix (ECM) rich connective tissues that attach muscles to the skeleton and aid in the transmission of contractile force from muscle activity. Tendon fibroblasts (tenocytes) interspersed within tendon ECM secrete the structural ECM proteins (primarily collagens) that make up the bulk of tendon tissue. Being constantly exposed to passive forces such as ECM stiffness, and active forces such as muscle contraction, tenocytes are known to differentially modify their morphology and transcriptional signatures in response during development (Bobzin et al., 2021; Subramanian & Schilling, 2015). However, how heterogeneous tenocyte populations inhabiting spatially distinct tendons and tendon subregions fine-tune their gene expression to functionally modulate their local ECM is not fully understood.

Though a few studies have profiled heterogeneity in tenocyte transcriptomes and proteomes, they have primarily focused on single tendons, or cells within one region of the tendon such as the enthesis (tendon-bone attachment interface). For example, tenocytes at the enthesis co-express the transcription factors *Scx/Sox9a+* as well as *Col2* both in tenocytes and chondrocytes, whereas tenocytes at the myotendinous junction (muscle-tendon attachment interface, MTJ) express *Thbs4b* in their ECM (Karlsen et al. 2022; Kult et al. 2021; Subramanian and Schilling 2014). However, individual tendons vary by their specific types of attachments, such as to bone, cartilage, muscle, or other soft tissues such as skin. Force-requirements of individual tendons differ widely depending on these attachments. This raises the question of

whether tenocytes differ transcriptionally in terms of their gene expression and subsequent ECM production depending on the unique microenvironment and load-bearing requirements of individual attachment zones. The craniofacial tendons provide an excellent model for studying inter-tendon and intra-tendon signatures as they contain a wide variety of musculoskeletal interfaces and attachment types. Although cranial tenocytes largely originate from cranial neural crest cells (unlike trunk and limb tenocytes which originate primarily from mesoderm), they express most of the same key transcriptional markers such as *Scx*, *Mkx*, *Thbs4b*, and *Tnmd*, suggesting a very similar differentiation trajectory (Bobzin et al., 2021; Nödl et al., 2022; Subramanian & Schilling, 2015).

In this study, we have analyzed transcriptional heterogeneity in cranial tenocytes of embryonic and larval zebrafish using scRNA-seq with FAC-sorted *scx*-expressing cells. We show that a cold-active protease protocol improves tenocyte health during tendon dissociation. We find that individual cranial tenocytes cluster not only by transcriptional signatures that reflect region-specific patterning but also unique ECM expression profiles (e.g. fibrillar, basement membrane, or FACIT collagens) that correlate closely with the physiological nature of their specific attachments (enthesis, mid-substance, or MTJ). We confirm the spatial specificity of many of these tenocyte markers in vivo in embryos or larvae using in situ hybridization chain reaction (*isHCR*). Lastly, our scRNAs-seq data identify a novel population of Wnt-responsive cranial tenocytes and we show that both genetic or pharmacological disruptions of Wnt signaling cause tendon patterning defects and formation of ectopic MTJs, uncovering a new role for Wnt signaling in tendon development.

## Results

### Cold protease tenocyte dissociation reduces stress responses and preserves tenocyte identity

Since tenocytes are embedded in ECM and very sensitive to environmental cues, we hypothesized that a cold 4°C protease protocol would reduce transcriptomic cellular stress artifacts as compared to traditional dissociation methods using collagenases at 28-37°C, as has been shown in mammalian tumor and kidney cells (Adam et al., 2017; O’Flanagan et al., 2019). To test this, we dissociated 50 heads (to maximize mCherry+ cells received from FACS) dissected from embryonic *Tg(scx:mCherry)* transgenic zebrafish at 72 hours post fertilization

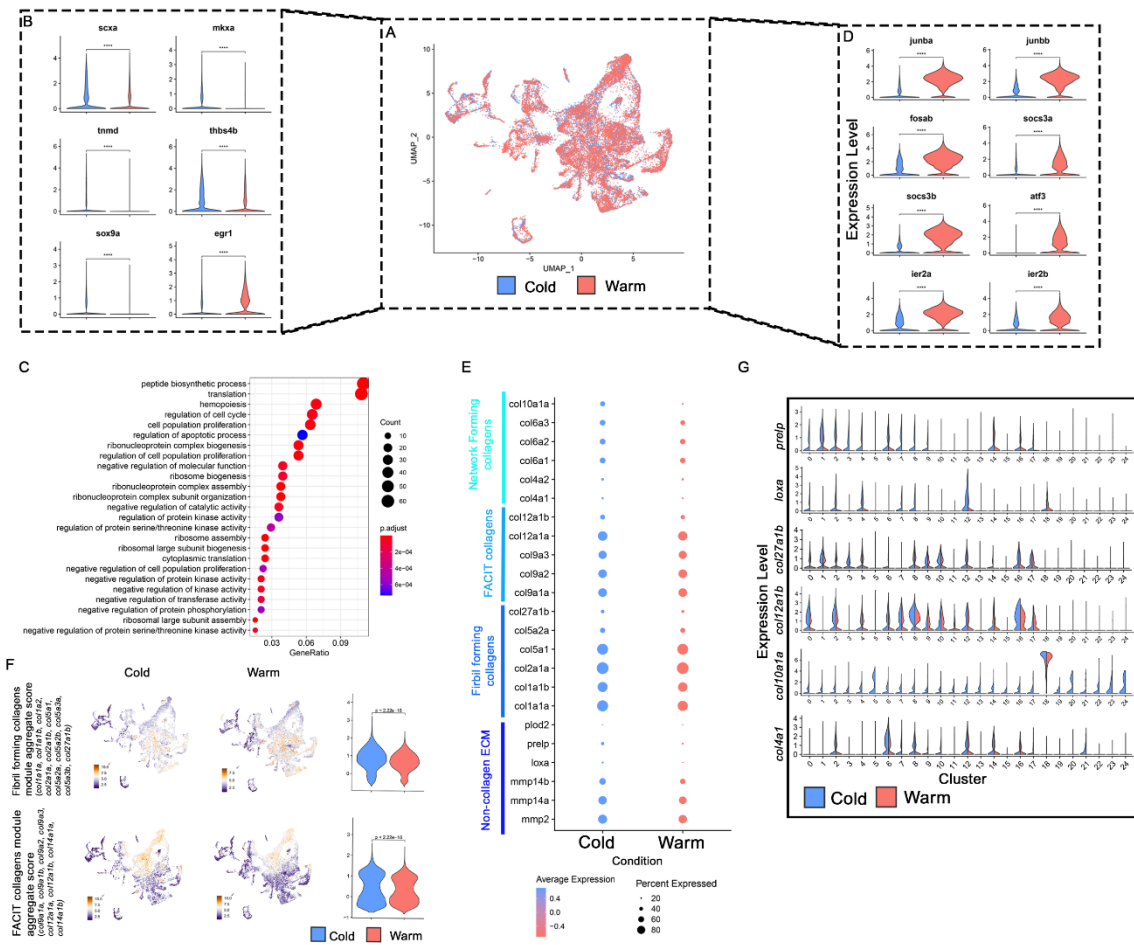


**Figure 1: Analysis of generalized and tenocyte-specific gene expression responses to temperature associated cell dissociation stress**

**A)** UMAP Dimensionality reduction, unsupervised clustering, and pseudo-bulk differential expression analysis of integrated cold and warm datasets. **B)** Violin plots of tenocyte marker genes *scxa*, *mkxa*, *tnmd*, *thbs4b*, *sox9a* all show significant downregulation whereas *egr1* displays upregulation in warm dissociation conditions **C)** Gene Ontology (GO) term analysis for Biological Process (BP) terms of all significant warm upregulated genes display terms enriched for apoptosis related processes. **D)** Violin plots of cell stress associated genes *junba*, *junbb*, *fosab*, *socs3a*, *socs3b*, *atf3*, *ier2a*, *ier2b* all show significant upregulation in warm dissociation conditions. **E)** Dot plot of selected tendon ECM component genes compared between dissociation conditions, organized into broad functional categories: Non-collagen ECM, Fibrillar Collagens, FACIT Collagens, and Network Forming Collagens. All are downregulated in warm-dissociation conditions. **F)** Comparative analysis of gene modules between dissociation conditions for FACIT collagens and Fibril forming collagens. **G)** Split violin plots of selected ECM genes from each functional category in **E** displaying diverse cluster-specific expression patterns in response to dissociation conditions.

(hpf) using either cold protease (Subtilisin A) derived from *B. licheniformis* at  $\sim 4^{\circ}\text{C}$  or a standard collagenase IV at  $\sim 28\text{-}30^{\circ}\text{C}$ , henceforth referred to as “cold” and “warm” conditions, respectively (**See Methods**). At this stage, embryonic cranial muscles have attached to cartilages and jaw movements have begun, allowing for effective assessment of both tenocyte dissociation efficiency and efficacy from within an established tendon ECM. Full dissociation (as indicated by a lack of cell clumps or remnants of stiffer cartilage) took approximately 35 minutes with cold protease versus 60 minutes with warm collagenase. Following FACS sorting with strict gating for mCherry+ cells, 10X single cell sequencing, and read mapping via CellRanger we obtained  $\sim 14,500$  cells with 37,963 mean reads per cell and 1,960 median genes per cell in cold conditions and  $\sim 21,700$  cells with 28,890 mean reads per cell and 1,623 median genes per cell in warm conditions (**Fig. 1A**) (**See Methods**) (Zheng et al., 2017).

After performing quality control, integration, and UMAP dimensionality reduction using Seurat, we examined expression differences in hallmark marker genes crucial for proper tendon development and maturation between cold and warm conditions (Hao et al., 2021). Analysis of pseudo-bulk differential expression found significant increases in expression of *scxa*, *mkxa*, *tnmd*, *thbs4b*, and *sox9a* with cold dissociation, while the zinc-finger transcription factor *egr1*

was upregulated with warm dissociation (**Fig. 1B**). In mouse tendons, *Egr1* plays critical roles in tendon development and injury-repair as well as mediating expression of TGF $\beta$  signaling components such as *Tgf $\beta$ 2*, *Tgf $\beta$ r2*, and *Smad7* (Guerquin et al., 2013). *Egr1* upregulation has, however, also been implicated in TGF $\beta$ -dependent apoptosis, inflammation, fibrosis, and cell stress in disease contexts such as scleroderma, pulmonary fibrosis, and muscle injury, perhaps suggesting that cells undergoing heat exposure during collagenase dissociation may enter a more stressed, TGF $\beta$  dependent pro-inflammatory/pro-fibrotic state (Lee et al., 2004; Warren et al., 2007; Bhattacharyya et al., 2008; M. Wu et al., 2009).

To further investigate the effects of collagenase dissociation on the tenocyte transcriptome, we analyzed genes either upregulated in warm conditions (downregulated in cold) or cold conditions (downregulated in warm) during pseudo-bulk differential expression analysis. Overall, 716 genes were upregulated in warm conditions and 2,142 genes upregulated in cold conditions with adjusted p-values < 0.05. Gene ontology (GO) analyses of the warm list for biological process (BP) terms using clusterProfiler, identified genes highly enriched in terms such as “regulation of apoptotic process”, “regulation of cell cycle” and “translation elongation” suggesting that warm-dissociation disrupts tendon cell and tissue homeostasis (i.e. cell division, transcription/translation, etc.) prior to sequencing, which may interfere with many cellular functions including transcription (**Fig. 1C**) (T. Wu et al., 2021b). Parsing through the top differentially expressed genes (DEG) sorted by log<sub>2</sub> fold change, we found many known to have a strong warm collagenase cell stress response such as *junba*, *junbb*, *fosab*, *socs3a*, *socs3b*, *atf3*, *ier2a*, and *ier2b* (**Fig. 1D**) (O’Flanagan et al., 2019). Upregulation of *Fos*, *Socs3*, and *Jun* expression indicate elevated stress in mouse skeletal muscle satellite cells after injury and in zebrafish fin osteoblasts in response to tissue dissociation (Van Den Brink et al., 2017; Warren et al., 2007). By comparing genes from the DEG list upregulated in warm conditions with existing datasets for stress/dissociation expression responses we found significant overlaps,

e.g. ~18.3% overlap with collagenase stress responses from human patient tumor cells (**See Methods**)(O’Flanagan et al., 2019). From a mouse dataset of muscle satellite cells (dissociated at 37°C) and another of zebrafish osteoblasts (dissociated at 30°C) describing stress response, we observed significant overlaps of DEGs of ~50.9% and ~61%, respectively (**Supplementary Fig. 1A,1C,1D**) (Van Den Brink et al. 2017). Conversely, when comparing cold-upregulated genes with these same datasets, only ~9-13% of genes overlapped (**Supplementary Fig. 1B,1E-F**)(O’Flanagan et al., 2019.; Van Den Brink et al., 2017). KEGG pathway analyses of the DEG list upregulated in cells subjected to warm dissociation revealed similar GO terms to those identified by the pathway analysis of core stress DEGs in tumor cells including “Apoptosis”, “p53 signaling pathway” and “Notch signaling pathway” (**Supplementary Fig. 1G**) (O’Flanagan et al., 2019). These results suggest that usage of warm temperature collagenase dissociation on tenocytes likely recapitulates a global tissue-agnostic stress response which is minimized in a cold temperature dissociation condition.

Given these differences in cellular stress between warm and cold dissociation, we next examined if cold-protease dissociation of tenocytes helps preserve their known in-vivo gene expression patterns both globally and at a subpopulation-specific level, given their distinct functions and microenvironments (e.g. skeletal entheses vs MTJs). We focused on the unique ECM-producing functions of tenocytes. Among the top DEGs upregulated in the cold dissociation conditions were not only known tendon/connective tissue markers such as *scxa*, *tnmd* and *osr1*, but also various collagens (**Supplementary Fig. 1H**). GO term analysis enriched for BP terms including “skeletal system development”, “cartilage development”, and “connective tissue development” (**Fig. 1D**). To test the hypothesis that warm dissociation dysregulates/inhibits expression of critical ECM genes we examined differential expression of a broad range of ECM components upregulated in cold (downregulated in warm) dissociation conditions. As the bulk of the tendon ECM is composed of collagens secreted by tenocytes, we

first identified global collagen expression differences, broadly classified into types based on cellular function, using pseudo-bulk data between warm and cold conditions (Kannus, 2000). These included fibrillar collagens, including Col1, Col2, Col3, Col5, Col11, Col24, and Col27; Fibril-Associated Collagens with Interrupted Triple Helices (FACIT) collagens including Col9, Col12, and Col14; and network-forming collagens including Col4, Col6, Col8, Col10, and Col13 among others (Birk & Brückner, 2011). Of these, a subset of fibrillar collagens *col1a1a*, *col1a1b*, *col2a1a*, *col5a1*, *col5a2a*, and *col27a1b*, FACIT collagens *col9a1a*, *col9a2*, *col9a3*, and *col12a1a*, and network forming collagens *col4a1*, *col4a2*, *col6a1*, *col6a2*, *col6a3*, and *col10a1a* were all downregulation in the warm dissociation conditions (**Fig. 1E**). Both fibrillar and FACIT collagens were significantly downregulated in these conditions (**Fig. 1F**). In addition, many genes encoding non-collagen ECM proteins were downregulated in the warm condition, such as matrix metalloproteinases (MMPs), lysyl oxidases and hydroxylases, and leucine-rich repeat proteins, involved in various aspects of tendon development and maintenance, such as collagen crosslinking, stabilization, remodeling, and degradation (**Fig 1E**) (de Almeida et al., 2022; Eekhoff et al., 2018 Cai et al., 2017; Qi & Xu, 2018; Bengtsson et al., 2002; Ellingson et al., 2022).

Finally, to examine if these expression differences in ECM components with warm versus cold dissociation are specific to distinct tenocyte subpopulations we performed unsupervised clustering with default Seurat resolution parameters (resulting in 25 clusters) and analyzed their relative expression from each broad functional category on a per-cluster basis, split by condition (**Fig. 1G**). Without definitive characterization of subclusters yet, we wanted to investigate if dissociation conditions variably affect expression of putative tenocyte subtype-specific ECM effects of variable dissociation conditions exist. This analysis revealed dramatic differences across functional categories (**Fig. 1G**). For example, within the network-forming collagens, *col4a1* and *col10a1a* showed little relative expression in the warm dissociation

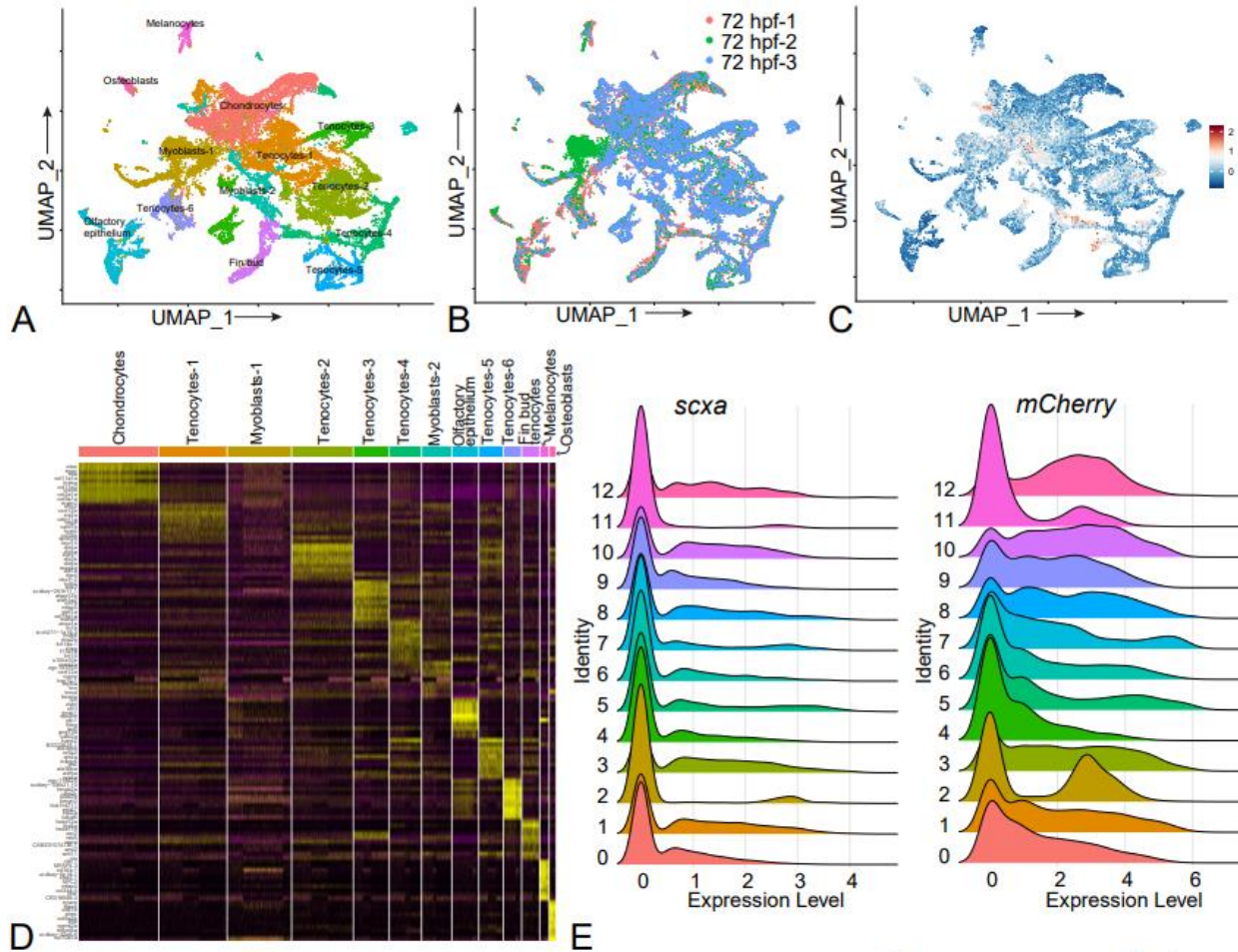


**Figure 2: Unsupervised clustering and quality control of 72 hpf sorted mCherry+ cells from severed zebrafish heads**

**A)** Unsupervised clustering and dimensionality reduction UMAP of 3 biological replicates of sorted mCherry+ cells. **B)** UMAP separated by condition **C)** ModuleScore analysis of tenocyte markers *scxa*, *mkxa*, *loxa*, *col1a1a*, *tnmd*, *thbs4a*, *thbs4b*, *tno*. **D)** Heatmap of cluster markers for each cluster revealing 7 separate tenocyte populations. **E)** Ridge plots of expression of *scxa* and *mCherry* displaying expression across all clusters.

condition compared to cold dissociation in some subclusters. This was particularly striking for *col10a1a*, expression of which was depleted in all clusters except cluster 18 in the warm dissociation conditions (**Fig. 1G**). Of the fibril-forming collagens, *col12a1b* and *col27a1b* were more consistently upregulated in the cold versus warm dissociation conditions across clusters (**Fig. 1G**). Of the non-collagen ECM components, *loxa* and *prelp* showed cluster specific effects with clusters 0, 7, and 8 showing higher expression of *loxa* and clusters 3, 4, 7, 8, 9, and 17 for

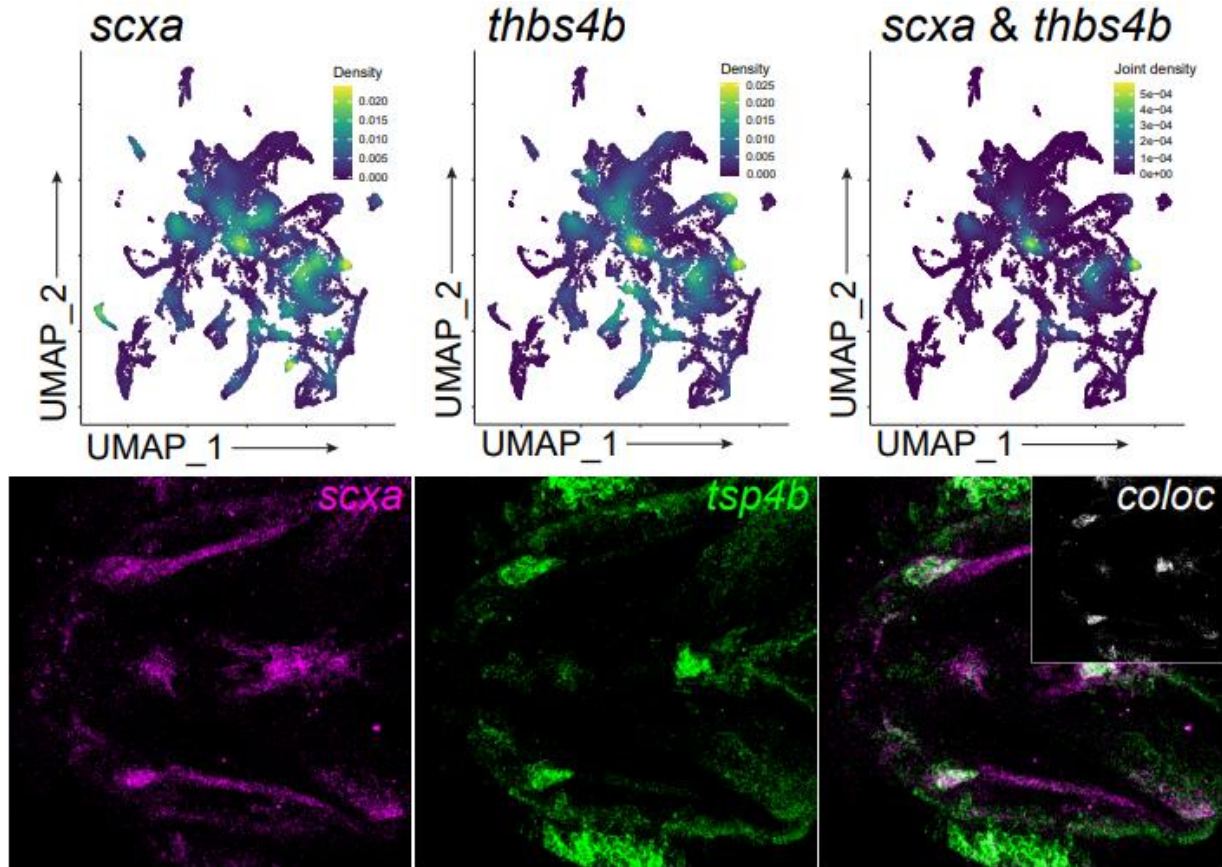


**Figure 3: Co-expression of tenocyte markers *scxa* and *thbs4b* in 72 hpf cranial tendons**

(Top row) Nebulosa plots of *scxa* and *thbs4b* expression individually and joint density plots. (Bottom row) *isHCR* of *scxa* and *thbs4b* individually and co-localization. (inset) Imaris co-localization in z-plane.

*prelp* in the cold dissociation conditions (**Fig. 1G**). Thus traditional warm dissociation with collagenase results in reduced transcription of a large variety of ECM components in tenocytes, both globally and in subpopulations, likely disrupting cellular functions and thereby skewing interpretations of cell states.

### Single cell sequencing of embryonic cranial tenocytes reveals distinct populations marked by established tenocyte genes

Having higher confidence in the optimization of our tissue dissociation protocol for stress gene reduction, we used this methodology to carry out further sequencing of *scx*-mCherry+ cranial tenocytes from 72 hpf zebrafish embryos using scRNAseq with two more biological

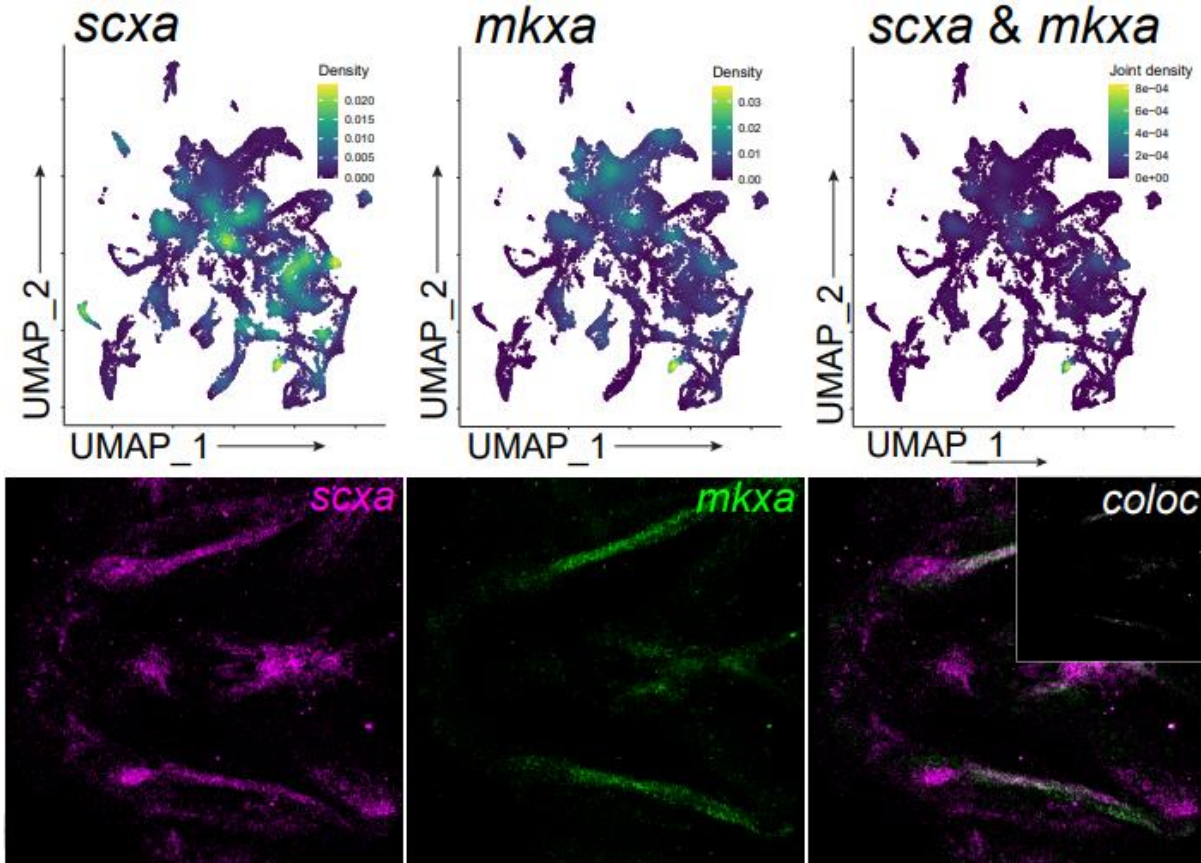


**Figure 4: Co-expression of tenocyte markers *scxa* and *mkxa* in 72 hpf cranial tendons**

(Top row) Nebulosa plots of *scxa* and *mkxa* expression individually and joint density plots. (Bottom row) *isHCR* of *scxa* and *mkxa* individually and co-localization. (inset) Imaris co-localization in z-plane.

replicates to significantly enrich for tenocyte sub populations and begin characterizing transcriptional signatures. Using Seurat to integrate our three datasets together and reperform unsupervised clustering, we obtained 13 distinct sub-clusters. These were distinguished by several highly-expressed genes per cluster, validating the uniqueness of each cluster in gene expression space (**Fig. 2 A-D**). Overlaying all 3 replicates upon the UMAP, cells occupying these sub-clusters were largely overlapping suggesting that even distributions of cell

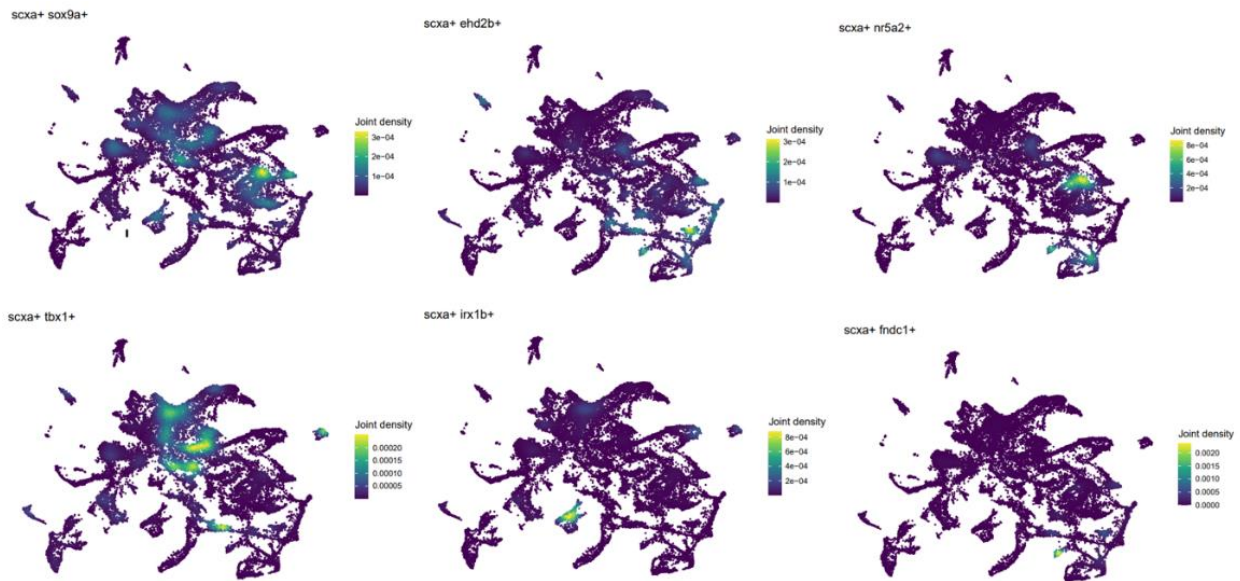


**Figure 5: Nebulosa expression overlap plots of *scxa* with individual cluster markers**

Cluster markers with overlapping expression with *scxa* provides expression patterns of spatially distinct tendons.

populations were captured across all replicates (**Fig. 2B**). To understand whether tenocytes with expression of canonical tenocyte marker genes were captured within individual clusters or across multiple clusters, we performed a module scoring analysis in Seurat using a core module of tenocyte markers. We observed that the tenocyte module had expression across many clusters (**Fig. 2C**). Indeed, cluster markers across unsupervised assigned clusters suggested that, though some other cell types besides tenocytes were present such as chondrocytes and epithelial cells, sorted cells were largely tenocytes (**Fig. 2D**). This was further confirmed by plotting expression of *scxa* and *mCherry* across all clusters, which showed distributions of both in each cluster (**Fig. 2E**).

We next asked how these tenocyte subpopulations were uniquely spatially marked by expression of established tenocyte marker genes. We used Nebulosa to overlap gene expression between marker genes such as *thbs4b* and *scxa* and confirmed separations in

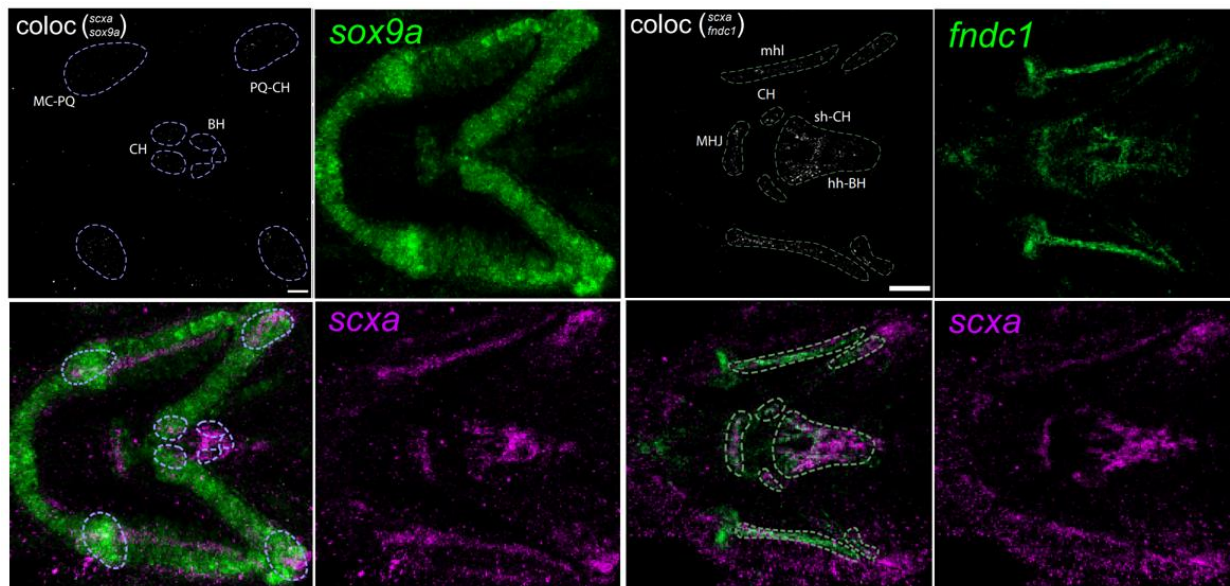


**Figure 6: *isHCRs* and colocalization of *scxa*, *sox9a* and *fndc1* expression**

*isHCRs* show spatially distinct entheses and joints in *scxa* and *sox9a* co-localization, and strong *mhl* overlap in *scxa* and *fndc1* with anterior joint overlap in *fndc1* alone. MC-PQ = meckels-palatoquadrate joint. BH = basihyal, CH = ceratohyal, Sh=sternohyoideus, hh = hyohyal

spatial expression using in situ hybridization chain reaction (*isHCR*). Whereas *thbs4b* primarily marked tenocytes at MTJ regions across all tendons in the head, with particularly strong expression in the sternohyoideus base region where the hyohyal muscle attaches, and very little expression in thinner projections attaching anteriorly, as well the MHL. Additionally, the eye tendon attaching the inferior oblique and inferior rectus musculature appeared to contain stronger *thbs4b* mRNA signal than *scxa*. *mkxa* was primarily localized to the ligament, and specific anterior projections of the sternohyoideus tendon (**Fig. 3, Fig. 4**). The differing tenocyte populations of existing markers across different tendons and ligaments led us to question whether clustering of our dataset tended towards spatially distinct tendons.

### Tenocyte populations cluster by spatially distinct tendons and functional inter-tendon regions

We continued *isHCR* of markers for each cluster along with *scx* and mapped these back to *nebulosa* expression plots on the UMAP (**Fig. 5**). Using this strategy, we were able to identify

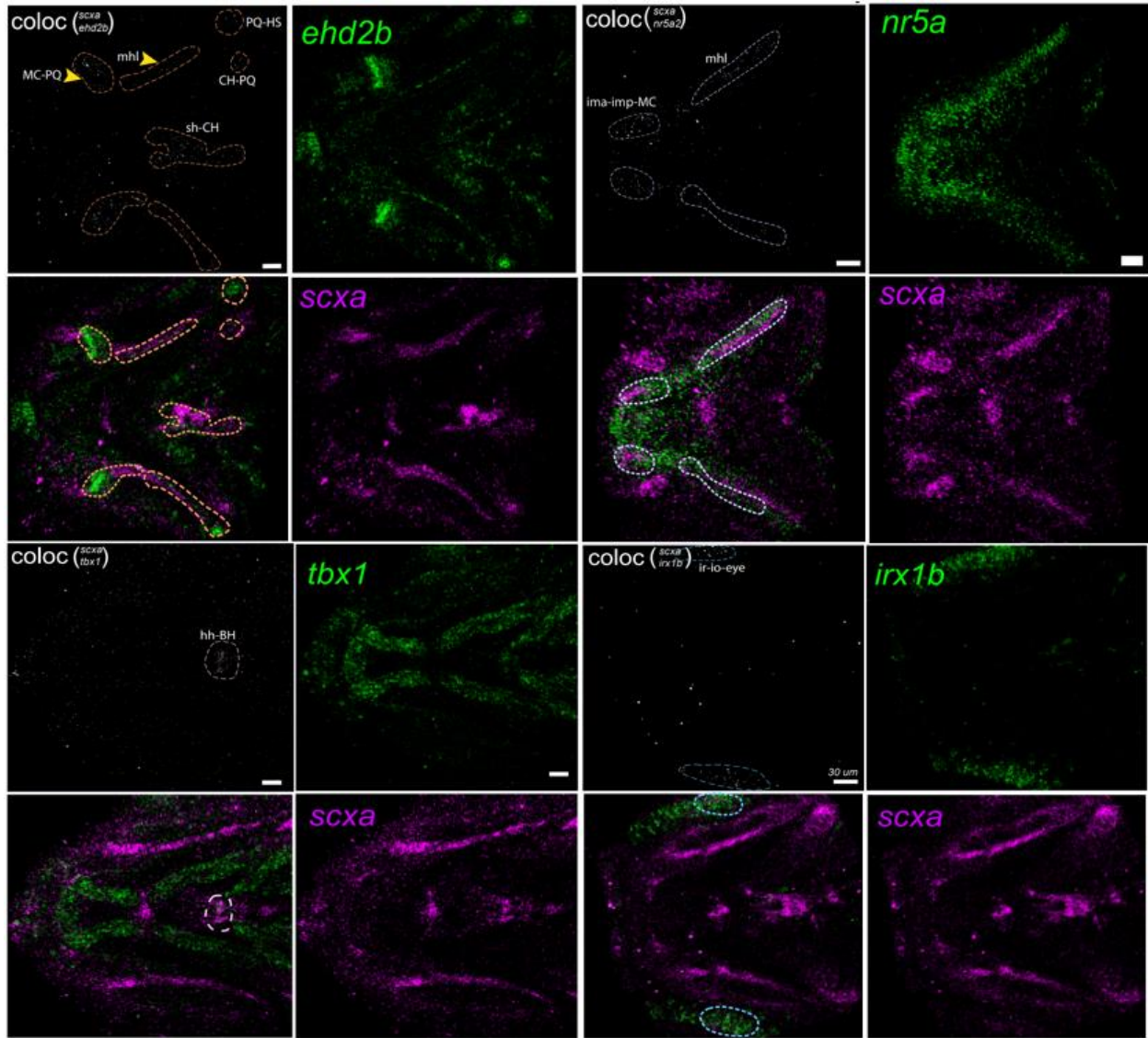


**Figure 7: *is*HCRs and colocalization of *scxa*, *ehd2b*, *nr5a2*, *tbx1*, and *irx1b* expression**

*is*HCRs show all joints in *scxa* and *sox9a* co-localization, overlap of intermandibularis anterior in *scxa* and *nr5a2* co-localization, sternohyodeus base tendon in *scxa* and *tbx1* overlap, and eye tendons alone in *scxa* and *irx1b* overlap.

individual spatially distinct tendons by gene expression overlap. For example, *scxa* and *sox9a* overlap labeled most cranial tendon entheses, and *fndc1* strongly labeled the mhl and all tendons except the ima (**Fig. 6**).

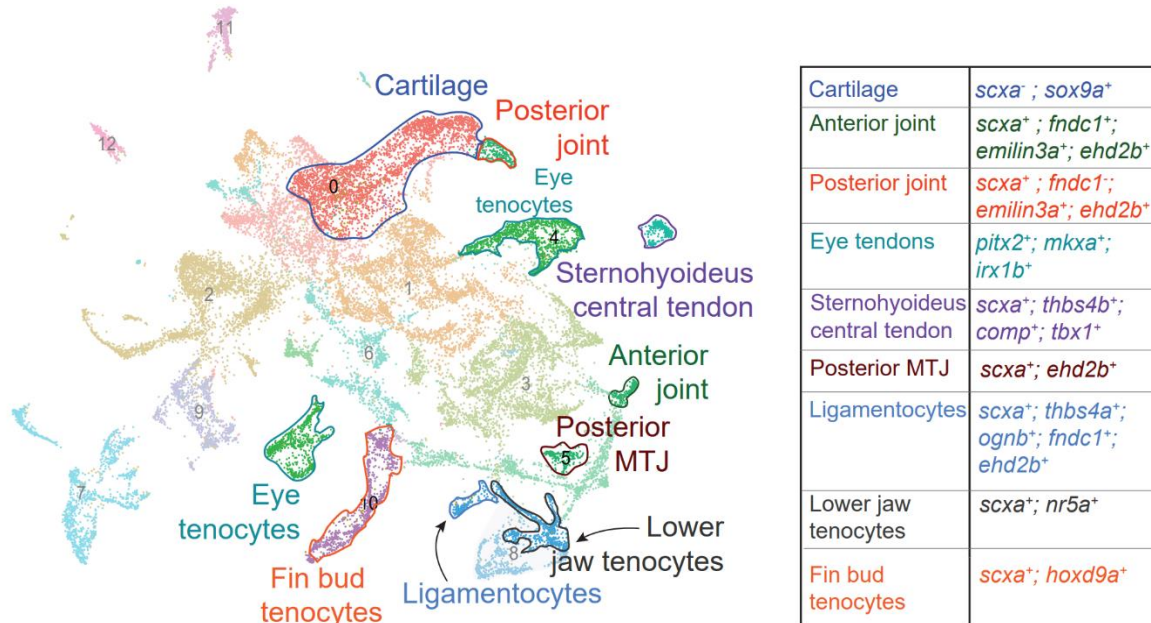


### Figure 8: Labelling of spatially distinct tendon and cartilage regions on scRNAseq UMAP

Combinations of *isHCR* with UMAP overlap labeling allows for labeling of individual tenocytes group by their respective tendon.

Similarly, *ehd2b* and *emilin3a* labeled all joints in the head and mhl ligaments (**Fig. 7, Supplementary Fig. 2**). *scxa* co-localizations with *nr5a2*, *tbx1*, and *irx1b* almost exclusively labeled the intermandibularis anterior tendon, sternohyoid base of the hyohyal-basihyal attachment, and eye tendons respectively (**Fig. 7**). Thus, a portion of the clustering overlaid upon the UMAP were tenocytes of spatially distinct tendons (**Fig. 8, Supplementary Fig. 2**). Other regions of the UMAP seemed, however, to separate based on intra-tendon functionality. Based on expression and *isHCRs* analysis, we dissected intra-tendinous regions across multiple clusters. Using *scx*<sup>+</sup>/*sox9a*<sup>+</sup> expression in **Fig. 5** and *scxa*<sup>+</sup>/*thbs4b*<sup>+</sup> expression in **Fig. 3** we narrowed down regions of the UMAP which labeled enthesis and MTJ within clusters 1, 3, and 5, and putative mid-substance tenocytes, functionally distinct as mature tenocytes with expression of *tnmd* and proliferating tenocytes with high g2/m marker gene expression (using modulescore analysis), in clusters 0 and 9 respectively (**Fig. 9**). Additionally, *isHCR* of *col4a5* displayed expression in peritendinous and periligamentous regions, corresponding with

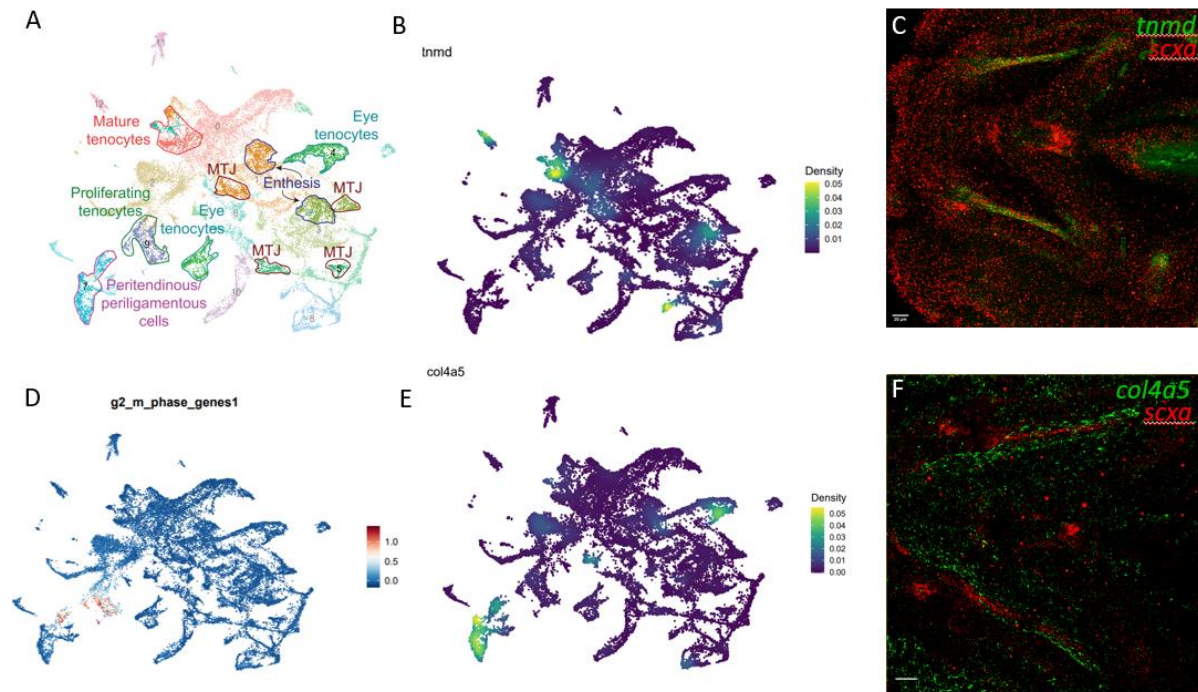


**Figure 9: UMAP regions of tenocytes from functionally distinct intra-tendinous zones**

**A)** Regions of tenocytes from intra-tendon zones of different tendons. Four MTJ and 2 enthesis zones were mapped by expression and *isHCR*. **B)** Nebulosa plot of *tnmd* expression displaying region of mature tenocytes overlaid on UMAP **C)** *isHCR* of *tnmd* and *scxa* **D)** Modulescore analysis of g2/m phase genes displaying cells primarily in clusters 7 and 9. **E)** *col4a5* expression on UMAP displaying predominant expression in cluster 7. **F)** *col4a5 isHCR* with *scxa* marking periligamentous and peritendinous cells.

expression in most of the cells of cluster 7 (**Fig. 9A-F**). *comp* expression also seemed to denote a novel MTJ tenocyte population and an exclusive tendon marker labeling only tendons without labeling ligaments such as the mhl (**Fig. 10A-D**). *klf2a* expression, being an enthesis marker (**See Chapter 2**), also labeled attachment zones for eye tendons, suggesting that the *klf2a* expression region in cluster 4 consisted of tenocytes in the eye attachment region of the eye tendon (**Fig. 10E-H**). Intra-tendon tenocytes existing across different clusters in the UMAP led us to hypothesize that intra-tendon tenocytes have unique ECM compositions which are influenced by differences in inter-tendon structure. To understand this, we performed modulescore analysis of ECM genes by category and observed the distribution of cells

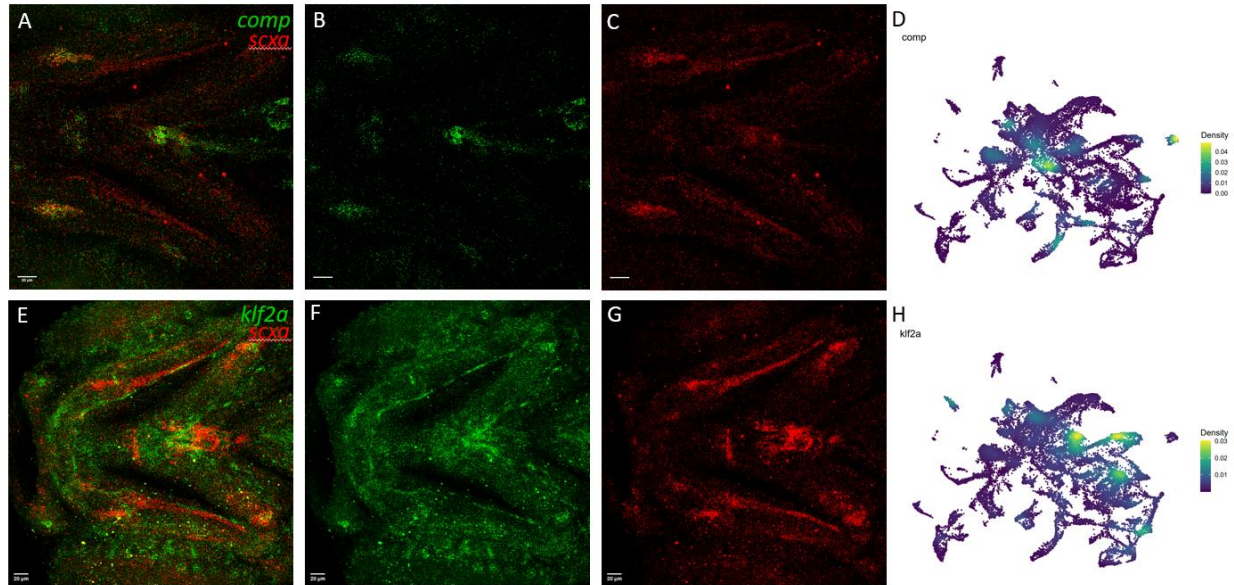


**Figure 10: *isHCRS comp* and *klf2a* mark cranial MTJ and enthesis inter-tendon regions respectively**

**A-C)** *isHCR* of *comp* marks MTJs of all cranial tendons, without marking ligaments **D)** Nebulosa plot of *comp* aligns with MTJ regions of UMAP displayed in **Fig. 9A**. **E-G)** *isHCR* of *klf2a* marks ligaments and entheses of all cranial tendons. **H)** Nebulosa plot of *klf2a* aligns with enthesis regions of UMAP displayed in **Fig. 9A**.

expressing each category across inter-tendon regions. Starting with fibril collagens, which include *col1a1*, *col1a2*, *col2a1*, *col5a1*, *col5a2*, *col5a3*, and *col27a1*, and are responsible for primary structural integrity of tendon ECM, we noticed that the module had high expression across all inter-tendon regions except for the *klf2a* high expressing region in cluster 4 (**Fig. 11**, **Fig. 10H**). Conversely, module expression of basement membrane collagens (*col4a1*, *col4a2*, *col4a3*, *col4a4*, *col4a5*, *col4a6*) and laminins was higher in this region (**Fig. 11B-C**). As an eye tendon “enthesis” attachment region, it follows that this zone would contain a different ECM composition than that of a cartilage or bone enthesis, as the muscle must make an effective attachment to a soft tissue with different load capacity and the tensional strength of the attaching eye muscle would likely be lower than that of a muscle moving the jaw or trunk. The region of cluster 6 denoting the sternohyoideus central tendon depicted in **Fig. 5** and **Fig. 7** also

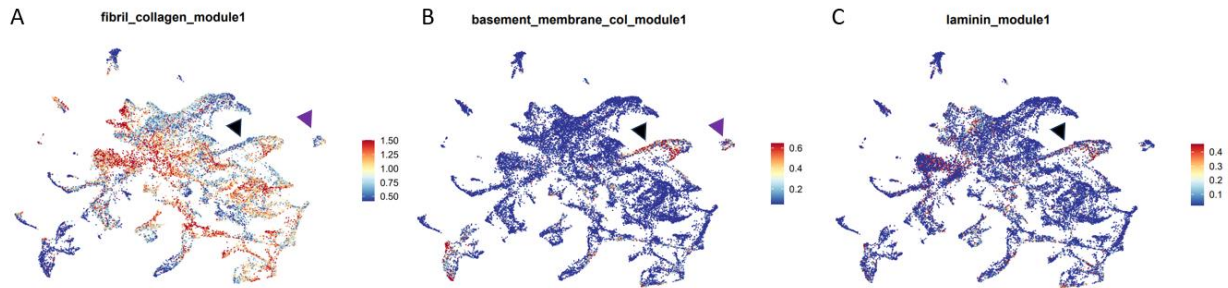


**Figure 11: Modulescore plots of fibril collagens, basement membrane collagens, and laminins**

**A)** Scoring of fibril collagen module, which includes *col1a1*, *col1a2*, *col2a1*, *col5a1*, *col5a2*, *col5a3*, and *col27a1* displays module expression across all MTJ and enthesis regions.

Expression is dramatically reduced in region with high *klf2a* expression (See **Fig. 10H**), denoted by black arrowhead. Expression is also present in *tbx1+/scxa+* sternohyoideus central tendon high expressing region (See **Fig. 5** and **Fig. 7**) denoted by purple arrowhead

**B)** Scoring of basement membrane collagen module, which includes *col4a1*, *col4a2*, *col4a3*, *col4a4*, *col4a5*, *col4a6*, displays module expression primarily in UMAP region with high *klf2a* expression, denoted by black arrowhead. Expression is present in sternohyoid central tendon region denoted by purple arrowhead. **C)** Scoring of laminin module displaying module expression in UMAP region with high *klf2a* expression, denoted by black arrowhead.

has high expression of basement membrane collagens *col4a1*, *col4a2*, *col4a3*, *col4a4*, *col4a5*, and *col4a6* while simultaneously having high fibril collagen expression (**Fig. 11A-B**). This tendon may be unique in its tenocyte population expression of both collagen types, likely having a different ECM protein composition than other cranial tendons due to the multitude of muscle, tendon, and cartilage attachment points. We also looked at FACIT and FACIT-like collagens module expression and noticed that though FACIT collagens were primarily expressed at enthesis regions, FACIT-like collagens were expressed almost exclusively at MTJ regions on the UMAP (**Fig. 12A-B**). Additionally, we noticed little to no expression of FACIT or FACIT-like collagens in ligamentocytes or lower jaw tenocytes (**Fig. 12A-B**). Interestingly, presumptive eye MTJ tenocytes had high expression of FACIT, FACIT-like and fibril collagens, but low expression of basement membranes and laminins, differing from the eye enthesis in the same cluster (**Fig. 12B**, **Fig 10D**, **Fig. 11A-C**). The ligamentocyte cells of cluster 8 also had high expression of lysyl oxidase, *loxa*, a collagen crosslinking protein (**Fig. 12C**). These results

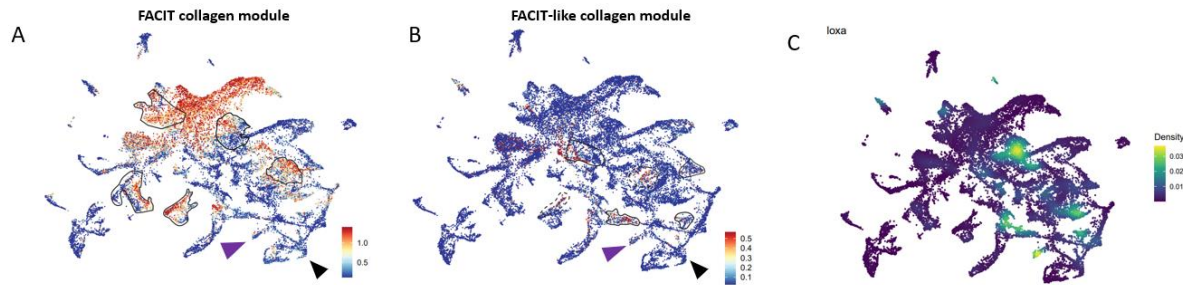


**Figure 12: Modulescore plots of FACIT and FACIT-like collagens and *loxa* expression**

**A)** Scoring of FACIT collagen module which includes *col9a1a*, *col9a1b*, *col9a2*, *col9a3*, *col12a1a*, *col12a1b*, *col14a1a*, and *col14a1b*. Black outlines label enthesis, mid-substance, proliferating tenocytes and eye tenocytes. **B)** Scoring of FACIT-like collagen module which includes *col16a1*, *col19a1*, *col21a1*, and *col22a1*. In both plots, purple arrows indicates lack of expression in ligamentocytes. Black arrow indicates lack of expression in lower jaw tenocytes (intermandibularis anterior), see **Fig. 8A** for labels. Dashed outline in **B** indicates eye MTJ attachment site, with high expression of *thbs4b*, *comp*, and *pitx2*. **C)** Nebulosa plot showing expression of *loxa* primarily in enthesis and ligament UMAP regions.

suggest that tenocytes at inter-tendon regions differ in their ECM transcriptional signature in accordance with the spatially specific tendon they inhabit.

### Pathway analysis shows active WNT signaling in specific cranial tenocyte populations

We next sought to identify genetic mechanisms involved in cranial tendon development and patterning, as they have been less well studied than tendons of the trunk and limbs. We performed KEGG pathway analyses of our dataset cluster markers and found genes associated with TGF $\beta$  signaling significantly enriched in clusters 3, 4, 5, 8, and 12, which plays well-established roles in tendon development (**Fig. 13A**). In addition, genes involved in Wnt signaling were significantly enriched in clusters 1, 3, and **8** (**Fig. 13A**). While Wnt signaling has been implicated in the development of various cranial tissues, specific roles in cranial tendon development have not been reported. To confirm the presence and locations of tenocytes responding to Wnt signaling, we crossed *Tg(scx:mCherry)* zebrafish to a canonical Wnt signaling reporter line *Tg(7XTCF:GFP)* and obtained double transgenic embryos. Starting at 48 hpf, GFP-positive cells, indicating high Wnt signaling, localized to 2 developing clusters in the

ventral mandibular arch and further posteriorly in the ventral hyoid arch (**Fig. 13B-G**), by 53 hpf a medial subset of these cells co-expressed mCherry (**Fig. 13H-M**). By 72 hpf, after cartilage and muscle differentiation, *isHCR* for *sox9a* to mark cartilage and immunostaining for Myosin Heavy Chain (MHC) to mark developing muscles of *Tg(scx:mCherry;7XTCF:GFP)* embryos revealed that high Wnt signalling responses were largely localized to developing MTJs (**Fig. 13N-W**). Medial GFP+ tenocytes localized to the anterior edge of the developing joint at the midline of Meckel's cartilage, as to the sternohyoideus tendon, with additional GFP+ cells

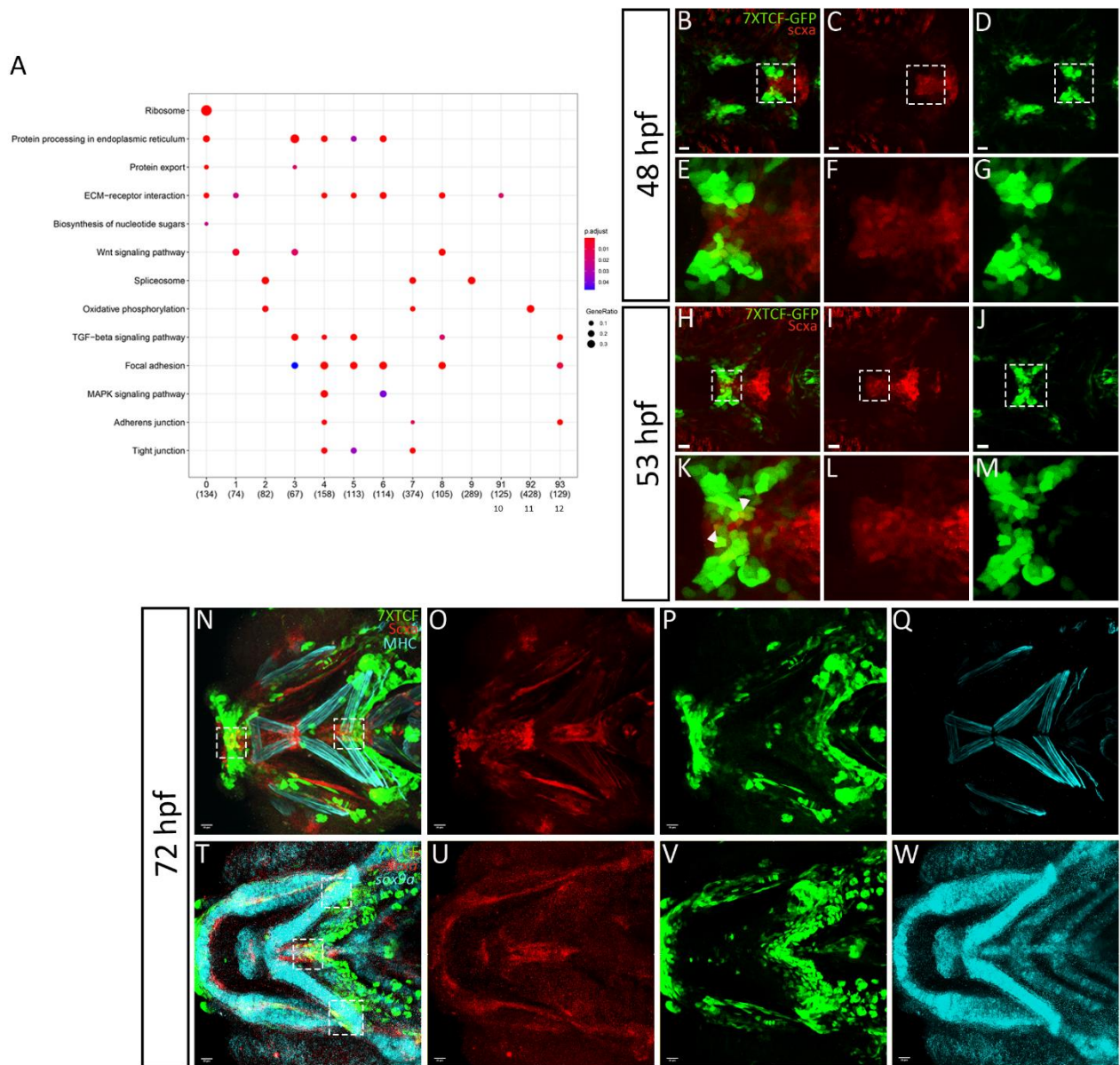


**Figure 13: Identification of a novel population of tenocytes highly responsive to canonical Wnt signaling**

**A)** KEGG pathway analysis of the single-cell dataset revealed WNT signaling as a pathway involved in cranial tenocyte development **B-D)** Images captured of 48 hpf embryos from time lapse of 48-60hpf *Tg(scxa:mCherry;7XTCF:GFP)* embryos showing double-positive cells at the developing meckel's joint. **E-G)** Close-up view of double-positive tenocytes from dashed boxes in **B-D**. Arrowheads point to individual double-positive cells at the developing meckels joint. **H-J)** images captured of 53 hpf embryos from timelapse of 48-60 hpf *Tg(scxa:mCherry;7XTCF:GFP)* embryos showing increasing GFP expression in double-positive cells at developing meckel's joint. **K-M)** Close-up view of double-positive tenocytes from dashed boxes in **H-J**. **N-Q)** 72 hpf embryos fixed and immunostained with GFP, mCherry, and MHC reveal double positive populations at sternohyoideus MTJ, and individual ligamentocytes within the mandibulohyoid ligament. **T-W)** combined GFP immunostaining with HCR of *Scxa*, *Sox9a* in 72hpf *Tg(scx:mCherry;7XTCF:GFP)* embryos show WNT-positive tenocytes at ceratohyal enthesis and sternohyoideus MTJ.

localized to tenocytes at the posterior Hh-Ch tendon attachment region, and in scattered cells within the mandibulohyoid ligaments (**Fig. 13N-W**). Time-lapsed imaging during cranial tendon formation showed dynamic Wnt responses in subsets of tenocytes, which increased in intensity between at 72 hpf as additional cranial muscle attachments migrate (**Fig. 13B-M**).

**Temporally controlled genetic Wnt signaling perturbations disrupt cranial tenocyte patterning and muscle attachments**

Based on the high levels of Wnt signaling observed in tenocytes during critical timepoints of cranial musculoskeletal development we hypothesized a role for Wnt signaling in tendon patterning. To address this possibility we crossed a heat shock inducible dominant-negative TCF-GFP (*Tg(hsp70l:dnTCF-GFP)*) with *Tg(scx:mCherry)* and obtained double-positive (*Tg(scx:mCherry; hsp70l: dnTCF-GFP)*) embryos. These embryos were heat-shocked at 48 hpf at 39°C for 30 minutes and imaged at various stages from 48 hpf to 60 hpf (**Fig. 14A**). At 48 hpf progenitors of cranial cartilages, muscles and tendons are still migrating and differentiating within the pharyngeal arches. Strikingly, tenocytes associated with the developing Meckel's cartilage of heat-shocked *Tg(scx:mCherry; hsp70l: dnTCF-GFP)* embryos were dispersed as compared with those of both control wild type *Tg(scx:mCherry;7XTCF:GFP)* and

negative control *Tg(scx:mCherry)* heat-shocked embryos (**Fig. 14B-E, I-L**). Heat-shocked *Tg(scxa:mCherry; hsp70l: dnTCF-GFP)* embryos often displayed reduced Meckel's cartilages, consistent with a role for Wnt signaling in D-V arch patterning (Alexander et al., 2014). A failure to condense was also observed in tenocytes of the more posterior developing SH-CH tendon. For independent confirmation that this defect in tenocyte condensation was due to disruption of Wnt signaling, we intercrossed a heat shock inducible *dkk1b-GFP* (*Tg(hsp70l:dkk1b-GFP)*) with *Tg(scx:mCherry)*. Secreted Dkk competitively binds to Frizzled co-receptors LRP 5/6 and acts as a Wnt antagonist (Bao et al., 2012). After a 30 minute 39°C heat shock at 48 hpf, the double-positive *Tg(scx:mCherry; hsp70l:dkk1b-GFP)* embryos displayed a similar tenocyte condensation defect, though less severe than seen in the heat-shocked *Tg(scx:mCherry; hsp70l: dnTCF-GFP)* embryos (**Fig. 14E-H, M-P**). MHC/GFP/mCherry antibody staining at 72 hpf in both heat-shocked *Tg(scx:mCherry; hsp70l: dnTCF-GFP)* and *Tg(scxa:mCherry; hsp70l:dkk1b-GFP)* embryos revealed tendon/muscle attachment defects correlated with a failure of tenocyte condensation (**Fig. 15A-U**). *Tg(scxa:mCherry; hsp70l:dnTCF-GFP)* heat-shocked embryos showed severe fraying and ectopic muscle attachment sites at multiple tendons (**Fig. 15G-K**). Interestingly, heat-shocked *Tg(scxa:mCherry; hsp70l:dkk1b-GFP)* embryos tended to show many individual myofibers attached either to ectopic tenocytes, or to other regions besides their normal attachment zone (**Fig. 15L-P**).

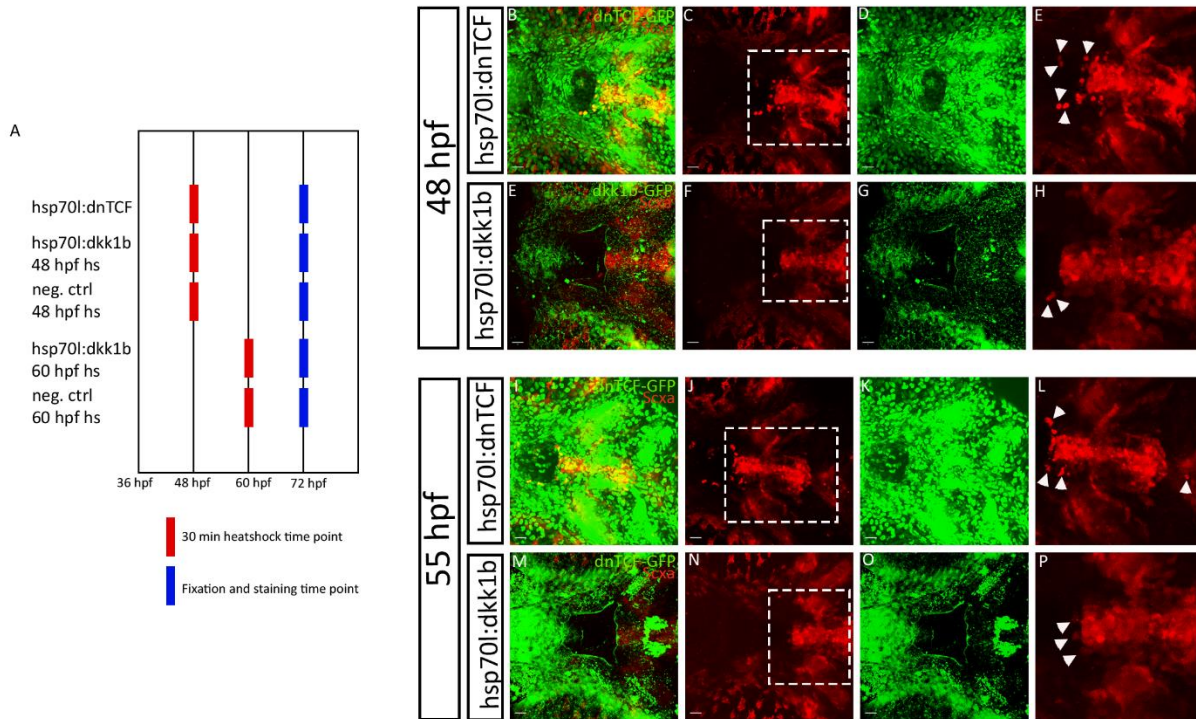
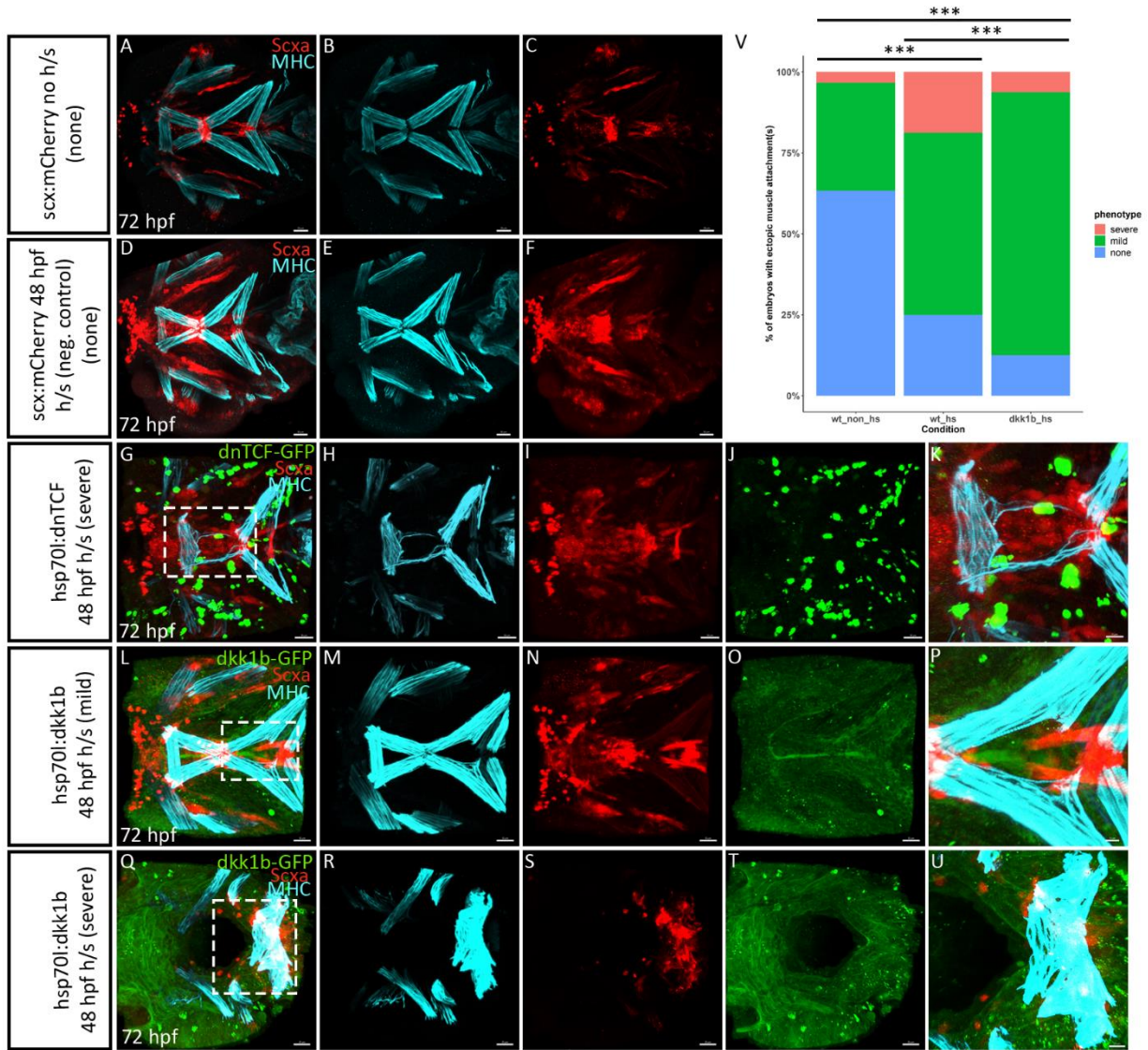


**Figure 14: Live imaging of heatshocked *Tg(scx:mCherry; hsp70l: dnTCF-GFP)* and *Tg(scx:mCherry; hsp70l:dkk1b-GFP)* embryos**

**A)** Experimental design of heatshocks performed on *Tg(scx:mCherry; hsp70l: dnTCF-GFP)* and *Tg(scx:mCherry; hsp70l: dkk1b-GFP)* embryos **B-D)** Live imaging stills of heatshocked 48 hpf *Tg(scx:mCherry; hsp70l: dnTCF-GFP)* embryos. **E)** Close-up of dashed box in **C** with white arrowheads depicting tenocytes which have detached from tendon condensate. **E-G)** Live imaging stills of heatshocked 48 hpf *Tg(scx:mCherry; hsp70l: dkk1b-GFP)* embryos. **H)** Close-up of dashed box in **F** with white arrowheads depicting tenocytes which have detached from tendon condensate. **I-K)** Live imaging stills of heatshocked (at 48hpf) 53hpf *Tg(scx:mCherry; hsp70l: dnTCF-GFP)* embryos. **L)** Close-up of dashed box in **J** with white arrowheads depicting detaching tenocytes. **M-O)** Live imaging stills of heatshocked (at 48 hpf) 53 hpf *Tg(scx:mCherry; hsp70l: dkk1b-GFP)* embryos. **P)** Close-up of dashed box in **N** with white arrowheads depicting tenocytes which have detached from tendon condensate.

We quantified the observed ectopic muscle attachment phenotypes in heat-shocked *Tg(scxa:mCherry; hsp70l:dkk1b-GFP)* against non-heat-shocked *Tg(scxa:mCherry)* and heat-shocked *Tg(scxa:mCherry)* negative control embryos and found a significant increase (**Fig. 15V**). Embryos categorized as having “mild” phenotypes showed normal cartilage development



but ectopic muscle attachments associated with the HH, IH, IMA or IMP muscles (**Fig. 15L-P**). Ectopic muscle attachments included muscle fibers attaching either to one or more ectopic tenocytes (**Fig. 15 L-P**). Embryos with “severe” phenotypes displayed globally disrupted craniofacial morphogenesis, usually with some cartilage reductions, and tenocyte aggregates with several ectopic muscle attachments (**Fig. 15Q-U**). Heat-shocked embryos with ectopic tenocytes but no associated muscle defects were frequently observed but excluded from quantification (**Fig. 16A-J**).

**Figure 15: Antibody staining and quantifications of control, (at 48 hpf) heatshocked *Tg(scx:mCherry; hsp70l: dnTCF-GFP)* and heatshocked *Tg(scx:mCherry; hsp70l:dkk1b-GFP)* 72 hpf embryos**

**A-C)** (Ventral view) Heads of control 72 hpf WT *Tg(scxa:mCherry)* embryo heads without heatshock stained for MHC and mCherry displaying no discernable ectopic muscle attachments **D-F)** (Ventral view) Heads of control WT *Tg(scxa:mCherry)* 48 hpf heatshocked embryo heads fixed and stained for MHC and mCherry displaying no discernable ectopic muscle attachments. **G-K)** (Ventral view) Heads of *Tg(scxa:mCherry; hsp70l:dnTCF-GFP)* 72 hpf embryo heads heatshocked at 48 hpf display severe disruption of muscles and muscle attachments, characterized by thinner intermandibularis posterior muscle fibers and disorganization of the intermandibularis anterior muscle fibers. **K** represents a zoom-in of the dashed white box region displayed in **G**. **L-P)** (Ventral view) Heads of *Tg(scxa:mCherry; hsp70l:dkk1b-GFP)* of 72 hpf embryos heatshocked at 48 hpf display mild disruption of muscles, in particular ectopic attachments of the interhyal muscles. **P** represents a zoom-in of the dashed white box region displayed in **L**. **Q-U)** *Tg(scxa:mCherry; hsp70l:dkk1b-GFP)* 72 hpf embryo heads displaying severe disruption of all cranial jaw muscles characterized by dramatically shortened muscle fibers, reduced tenocyte quantity, and disorganization of muscle fiber attachments. **U** represents a zoom-in of the dashed white box region displayed in **Q**. **V)** Quantification of number of embryos with ectopic muscle attachments between WT *Tg(scxa:mCherry)* non-heatshocked, *Tg(scxa:mCherry)* heatshocked at 48 hpf, and *Tg(scxa:mCherry; hsp70l:dkk1b-GFP)* heatshocked at 48 hpf. ns = not significant, \*  $p < 0.05$ , \*\*  $p < 0.01$ , \*\*\*  $p < 0.001$ .

As cranial tenocytes disperse and reaggregate at embryonic cranial muscle attachments in zebrafish between 48-60 hpf, we hypothesized that Wnt signaling may influence tendon patterning via tenocyte migration. If this is the case we might expect that perturbing Wnt signaling after dispersion/aggregation would not alter the cranial muscle attachment pattern. To address this, we heat-shocked *Tg(scxa:mCherry; hsp70l:dkk1b-GFP)* embryos at 60 hpf at 39°C for 30 min and stained embryos with MHC/mCherry/GFP antibodies at 72 hpf. Unexpectedly, a significant number of embryos displayed ectopic muscle attachments between heat-shocked *Tg(scx:mCherry; hsp70l:dkk1b-GFP)* and control embryos (**Fig. 17**), suggesting that requirements for Wnt signaling persist beyond these migratory stages.

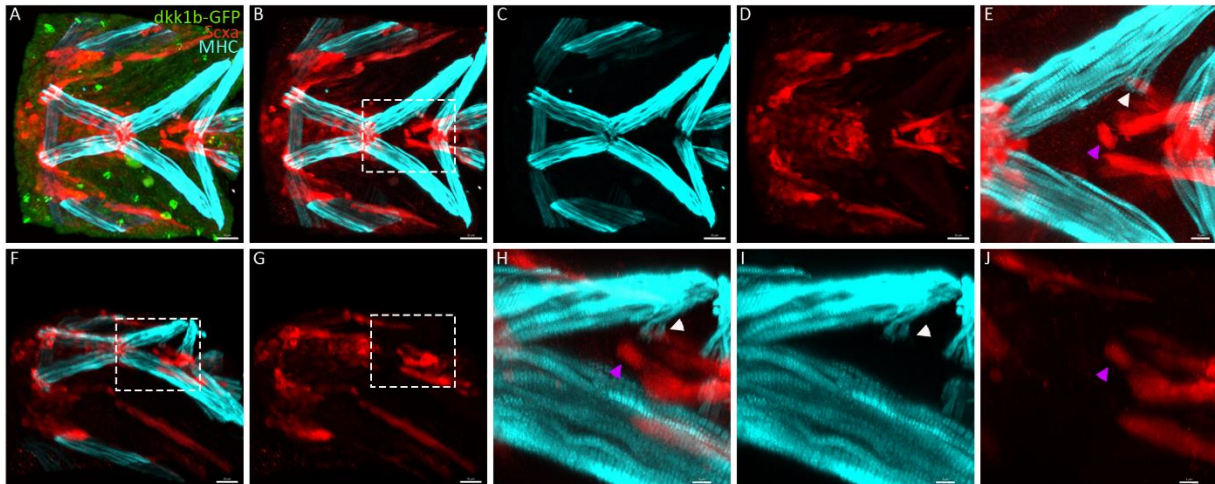


**Figure 16: Ectopic tenocytes and muscle attachments seen in heatshocked *Tg(scx:mCherry; hsp70l:dkk1b-GFP)* at 72 hpf**

**A-D)** (Ventral view) Ectopic muscle attachments and ectopic tenocytes seen after 30 minute heatshocks of *Tg(scx:mCherry; hsp70l:dkk1b-GFP)* **E)** Close-up of dashed box in **B**. White arrowhead marks ectopic muscle attachment to a single ectopic tenocyte. Purple arrowhead marks ectopic tenocyte with no muscle attachment. **F-G)** Lateral angled view of **B** and **D** respectively. **H-J)** Close-up views of dashed boxes in **F** and **G**. White arrowhead marks ectopic muscle attachment to ectopic tenocyte, purple arrowhead marks ectopic tenocyte with no muscle attachment.

Given that disrupting Wnt signaling causes both ectopic tenocytes and muscle attachments we next asked if ectopic tenocyte-muscle attachments show protein expression signatures of specific intra-tendon regions, such as MTJs. We performed heatshocks on *Tg(scx:mCherry; hsp70l:dkk1b-GFP)* embryos at 48 hpf and antibody stained with MTJ marker

Thbs4b and MHC and found that Thbs4b localized to an ectopic attachment, suggesting that ectopic muscle attachments are MTJs (Fig. 18).

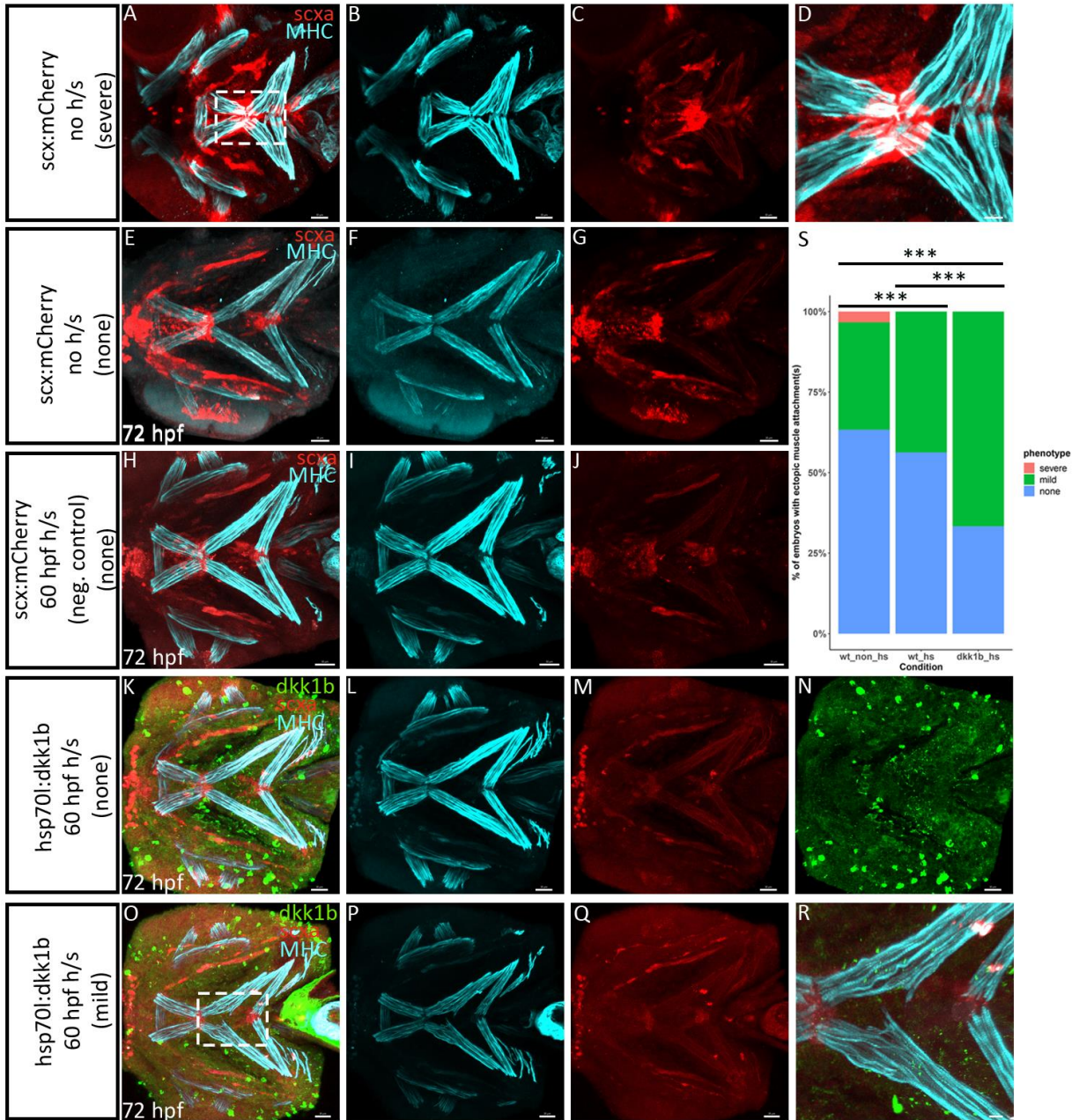


**Figure 17: Antibody staining and quantifications of heatshocked (at 60 hpf) control, *Tg(scx:mCherry; hsp70l:dkk1b-GFP)* 72 hpf embryos**

**A-C)** (Ventral view) Head of control 72 hpf WT *Tg(scxa:mCherry)* embryo heads without heatshock stained for MHC and mCherry displaying a severe ectopic muscle attachment phenotype with shortened jaw **D)** Close-up of dashed box in **A**. **E-G)** Heads of control WT *Tg(scxa:mCherry)* heatshocked embryo fixed and stained for MHC and mCherry displaying no discernable ectopic muscle attachments. **H-J)** Head of *Tg(scxa:mCherry)* 72 hpf embryo heatshocked at 60 hpf displaying no discernable ectopic muscle attachments. **K-N)** Head of *Tg(scxa:mCherry; hsp70l:dkk1b-GFP)* of 72 hpf embryos heatshocked at 60 hpf displaying no discernable ectopic muscle attachments. **O-R)** *Tg(scxa:mCherry; hsp70l:dkk1b-GFP)* 72 hpf embryo heads displaying mild disruption of ceratohyal muscle resulting in ectopic muscle attachments **R** represents a zoom-in of the dashed white box region displayed in **O**. **S)** Quantification of number of embryos with ectopic muscle attachments between WT *Tg(scxa:mCherry)* non-heatshocked, *Tg(scxa:mCherry)* heatshocked at 60 hpf, and *Tg(scxa:mCherry; hsp70l:dkk1b-GFP)* heatshocked at 60 hpf. ns = not significant, \*  $p < 0.05$ , \*\*  $p < 0.01$ , \*\*\*  $p < 0.001$ .

**Temporally controlled pharmacological Wnt signaling perturbations disrupt cranial tenocyte patterning and muscle attachments**

Since heat-shock stimuli alone can modulate a variety of signaling pathways, we wanted to rule out the possibility that ectopic muscle attachments reflect these confounding variables.

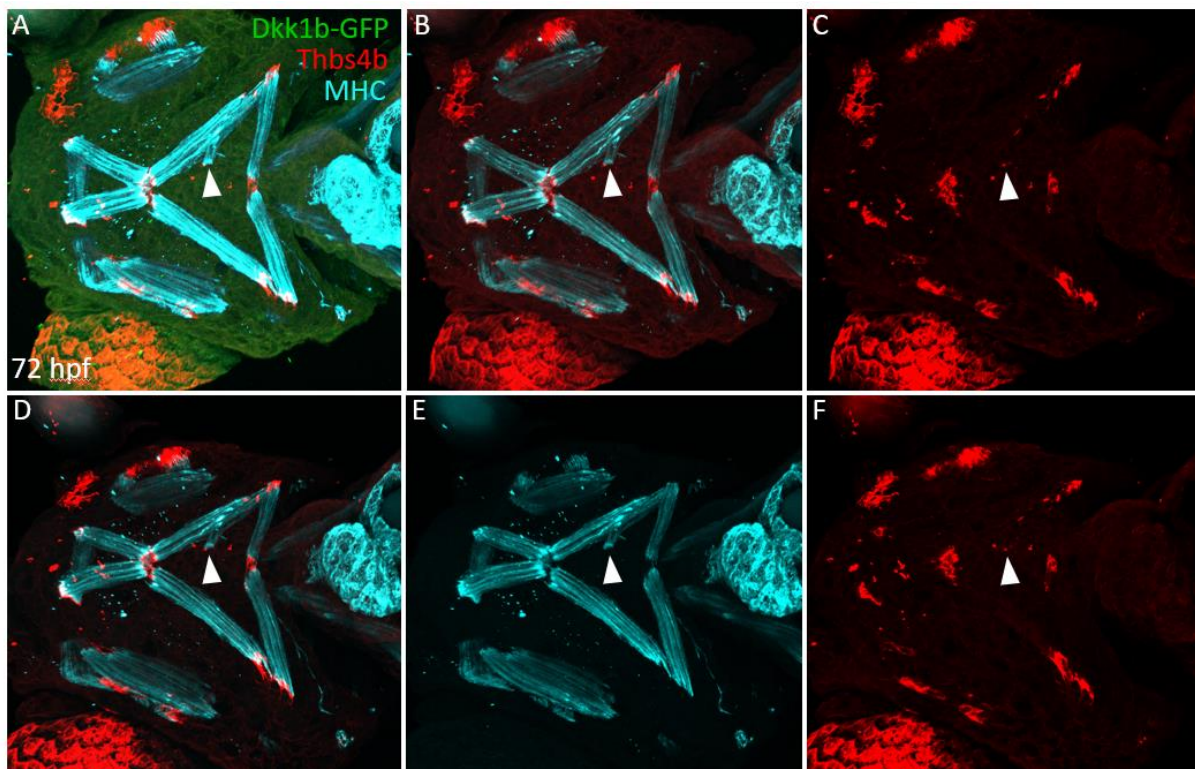


**Figure 18: Thbs4b/MHC staining of *Tg(scx:mCherry; hsp70l:dkk1b-GFP)* and visualization of ectopic MTJ**

**A-C)** (Ventral view) Head of 48 hpf heatshocked *Tg(scx:mCherry; hsp70l:dkk1b-GFP)* embryo stained with Thbs4b and MHC displaying ectopic muscle attachment with Thbs4b protein localized to the ectopic attachment region. White arrow denotes ectopic attachment  
**D-E)** Laterally tilted view of embryo in **A-C**.

To this end, we performed independent drug treatments with two canonical Wnt antagonists, XAV939 and IWR-1 (B. Chen et al., 2009; S. M. A. Huang et al., 2009). We also upregulated Wnt signaling in 48 hpf embryos via addition of a canonical Wnt signaling agonist, 6-bromoindirubin-3'-oxime, also known as BIO (Meijer et al., 2003). Drug treatments were performed in *Tg(scx:mCherry;7XTCF:GFP)* embryos at various concentrations based on previous studies in which they were used in zebrafish (REFs), and compared to 1% DMSO controls to observe morphological effects in tenocytes as well as global 7XTCF-GFP expression

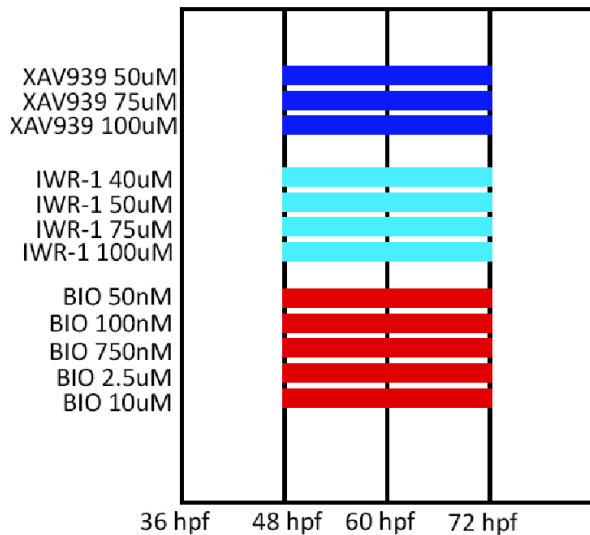
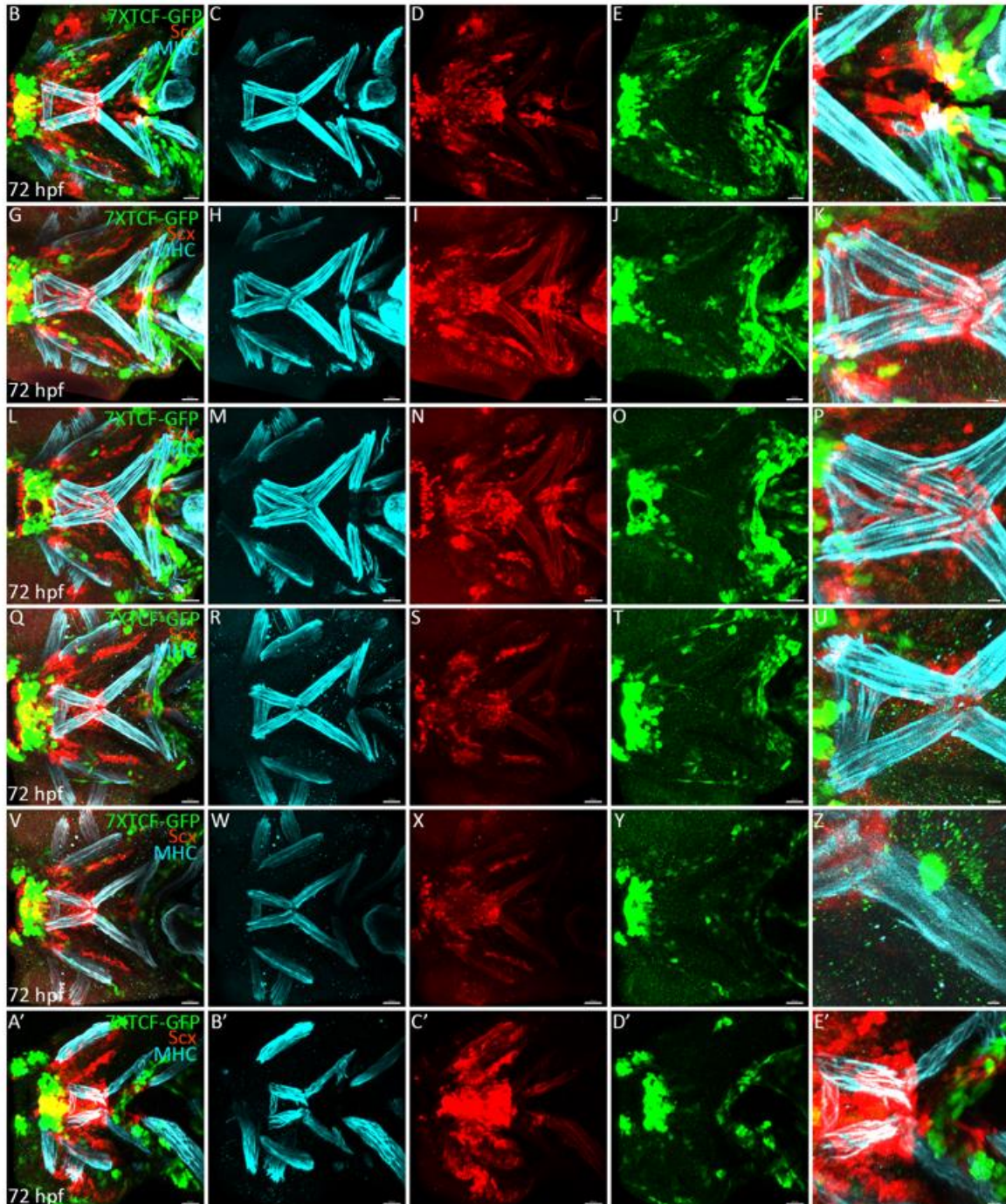


**Figure 19: Experimental strategy for Wnt antagonist/agonist treatments**

**A)** Depiction of 24 hour treatments of varying concentrations of IWR-1 and XAV939 (Wnt antagonists) and BIO (Wnt agonist) on 48 hpf embryos.

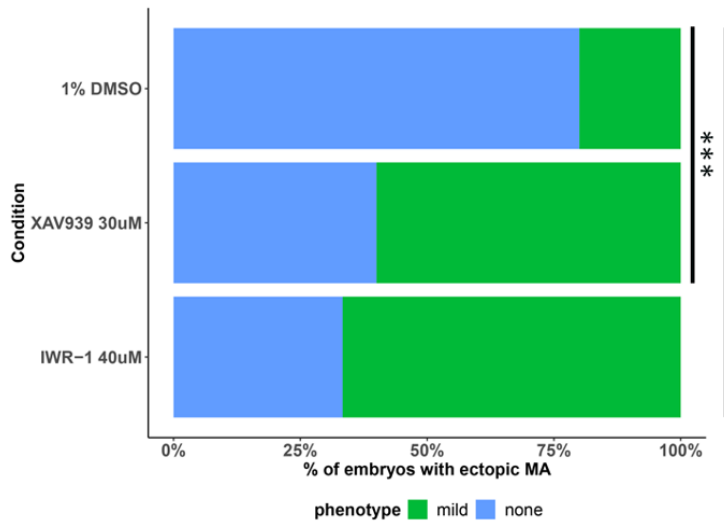


as a readout of Wnt signaling (**Fig. 19**). While XAV939 treated embryos showed normal craniofacial morphology at concentrations up to 100  $\mu$ M, higher concentrations grossly disrupted cartilage, muscle and tenocyte morphology. IWR-1 treatments began showing similar non-specific musculoskeletal defects at concentrations greater than 50  $\mu$ M (**Fig. 20**). Neither antagonist treatment caused observable differences in 7XTCF-GFP expression levels.

**Figure 20: Dose-dependent cranial muscle-attachment defects in Wnt antagonist (IWR-1 and XAV939) treated *Tg(scxa:mCherry;7XTCF:GFP)* embryos**

**B-E)** 24 hour 30 uM XAV939 treatments on 48 hpf embryos. **E** is close-up of ceratohyal and hyohyal muscles in **B**. **G-K)** 24 hour 75 uM XAV939 treatments on 48 hpf embryos. **K** is close-up of intermandibularis anterior/posterior muscles in **G**. **L-P)** 24 hour 100 uM XAV939 treatments on 48 hpf embryos. **P** is close-up of intermandibularis anterior/posterior muscles in **L**. **Q-U)** 24 hour 40 uM IWR-1 treatments on 48 hpf embryos. **U** is close-up of intermandibularis anterior/posterior muscles in **Q**. **V-Z)** 24 hour 50 uM IWR-1 treatments on 48 hpf embryos. **Z** is close-up of ceratohyal muscle displaying ectopic muscle attachment with no attaching tenocyte. **A'-E')** 24 hour 75 uM IWR-1 treatments on 48 hpf embryos. **U** is close-up of intermandibularis anterior/posterior and ceratohyal muscles in **E'**.

However, both drugs have been shown to reduce *axin2* expression in 48 hpf zebrafish embryos (Westphal et al., 2022). Consistent with reduced Wnt signaling, we observed increases in the



number of embryos displaying ectopic muscle attachments

between 1% DMSO and both antagonist treatments (**Fig. 21**).

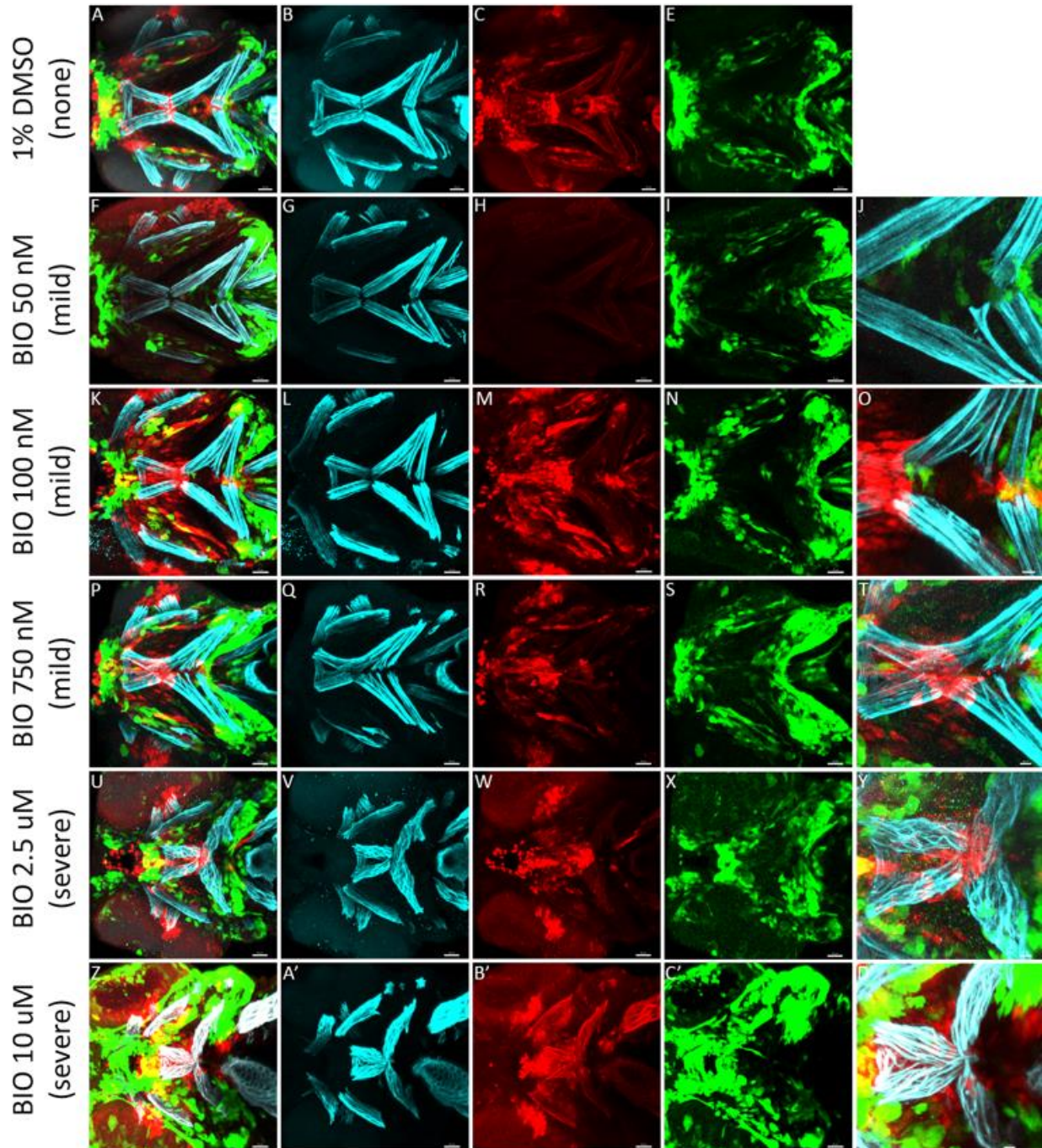
Conversely, BIO-treated embryos displayed increased 7XTCF-GFP expression in a dose dependent manner in cells throughout the developing head and displayed

**Figure 21: Quantification of selected concentrations of 24 hour Wnt antagonist treatments**

Bar plot of 24 hour treatments of varying concentrations of IWR-1 and XAV939 (Wnt antagonists) and BIO (Wnt agonist) on 48 hpf embryos.

morphologically similar ectopic muscle attachments as those seen with antagonist, heatshock *Tg(scxa:mCherry; hsp70l:dkk1b-GFP)* and heatshock

*Tg(scxa:mCherry; hsp70l:dnTCF-GFP)* (**Fig. 22A-Z, A'-D'**). In addition, the numbers of embryos displaying ectopic muscle attachments increased significantly in 750 nM BIO treated embryos,



as compared to 1% DMSO controls (**BIO WNT agonist treatment 72hpf figure E'**). Similarities in muscle attachment defects with Wnt agonist and antagonist treatments suggest that a proper balance of canonical Wnt signaling is necessary for cranial muscle attachments and patterning of MTJs.

**Figure 22: Dose-dependent cranial muscle-attachment defects in Wnt agonist (BIO) treated *Tg(scxa:mCherry;7XTCF:GFP)* embryos**

**A-E)** 24 hour control 1% DMSO treatments on 48 hpf embryos. **F-J)** 24 hour 50 nM BIO treatments on 48 hpf embryos. **J** is a close-up of ectopic muscle attachments in ceratohyal muscles in **F**. **K-O)** 24 hour 100 nM BIO treatments on 48 hpf embryos. **O** is close-up of ectopic muscle attachments in ceratohyal muscles in **K**. **P-T)** 24 hour 750 nM BIO treatments on 48 hpf embryos. **T** is close-up of ectopic muscle attachments at the intermandibularis anterior/posterior and ceratohyal/hyo-hyal muscles in **P**. **U-Y)** 24 hour 2.5  $\mu$ M BIO treatments on 48 hpf embryos. **Y** is a close-up of intermandibularis anterior/posterior muscles and ceratohyal displaying severe ectopic muscle attachment phenotype with shortened jaw seen in **U**. **A'-D')** 24 hour 10  $\mu$ M BIO treatments on 48 hpf embryos. **D'** of intermandibularis anterior/posterior muscles and ceratohyal displaying severe ectopic muscle attachment phenotype with shortened jaw seen in **Z**.

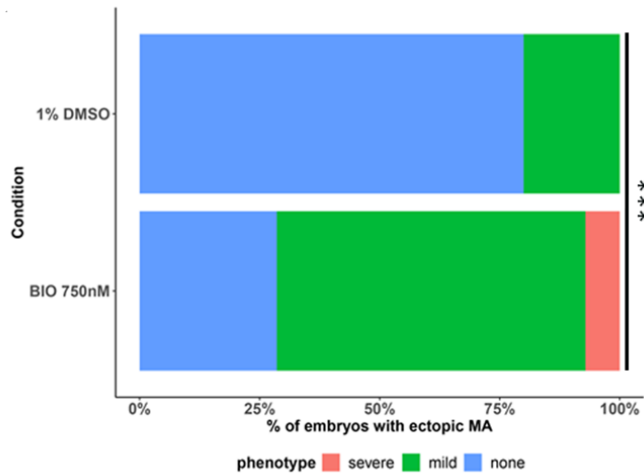


**Figure 23: Quantification of selected concentrations of 24 hour Wnt agonist treatments**

**A)** Bar plot of 24 hour treatments of varying concentrations of IWR-1 and XAV939 (Wnt antagonists) and BIO (Wnt agonist) on 48 hpf embryos.

**Computational cell-cell communication inference suggests epithelial, peritendinous, and osteoblast cells as a source for WNT signaling ligands to cranial tenocytes**

To gain a better understanding of the cell types expressing Wnt ligands and receptors in our dataset, we utilized the cell-cell communication inference software CellChat (Jin et al., 2021). CellChat utilizes computational modeling based upon a database of known signaling interactions of ligands, receptors, and co-factors to make predictions of cell communication in single-cell gene expression datasets. Using CellChat to infer predominant sender and receiver cell types for WNT signaling, clusters 7 and 12 emerged as primary outgoing signaling cell-

types (senders), and all other clusters (with the exception of 2 and 11) were primarily cell-types involved in receiving WNT signals (**Fig. 24A-B**).

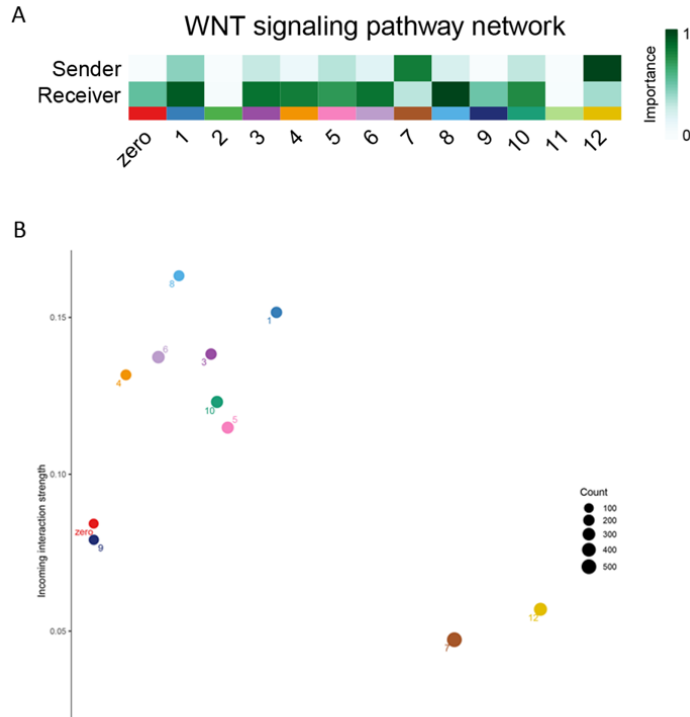
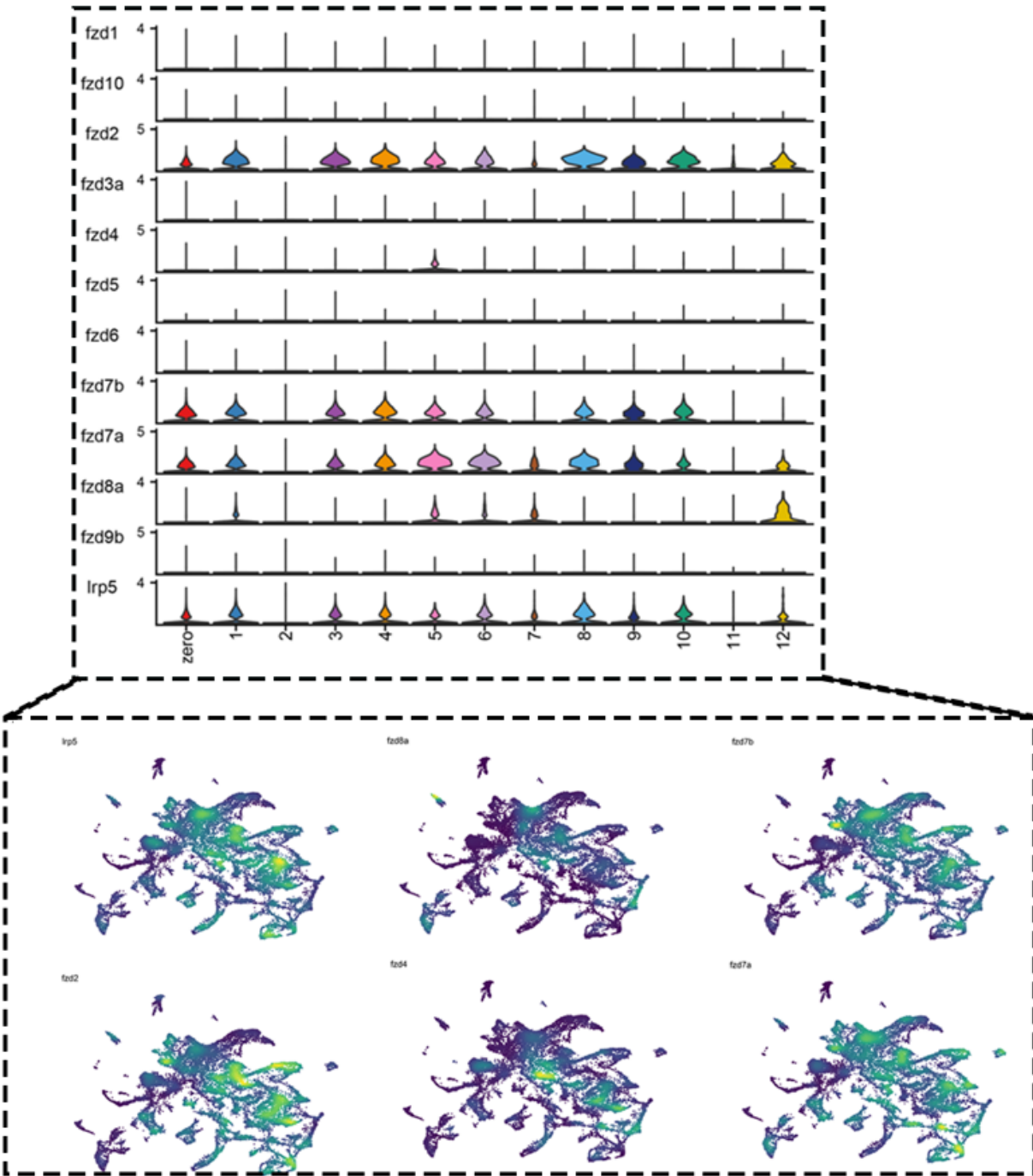


**Figure 24: Ligand-receptor analyses of Wnt signaling in 72 hpf cranial tenocyte scRNAseq using CellChat**  
**A)** Heatmap displaying clusters 7 and 12 (peritendinous/periligamentous/epithelial and osteoblasts respectively) as predominant senders of Wnt signal **B)** Scatterplot of interaction strength (by number of inferred interactions) per cluster

Cluster 7, having high expression of *epcam* and *col4a5* likely contains primarily epithelial cells and peritendinous/periligamentous cells, and cluster 12, having high expression of *ifitm5*, contains predominantly osteoblasts (Patoine et al., 2017). When we looked at expression of canonical WNT signaling receptors across clusters, various *fzd* receptors emerged as having distinct expression patterns across different tenocyte subpopulation domains (e.g. *fzd4* has stronger expression in MTJ domains, whereas *fzd2*, *fzd7a*, and *fzd7b* expression was more spread across MTJ and Enthesis domains) (**Fig. 25,**

**Fig. 9A**). Conversely, the *Lrp5* co-receptor seemed to be globally expressed across almost all cell types in the dataset (**Fig. 25**). We next inferred the specific WNT ligand-receptor



interactions between clusters 7, 12, and all other clusters using CellChat, and found that both clusters 7 and 12 had high communication probabilities with other clusters utilizing *wnt9a* ligand expression, and cluster 12 had high communication probabilities with *wnt10a* expression. Once again, *lrp5* appeared to be utilized as a primary co-receptor for all inferred signaling interactions,

**Figure 25: Wnt receptors with high expression in CellChat ligand-receptor analysis**

**(Top)** Violin plots of Wnt receptors highly expressed in clusters with high incoming interaction strength shown in **Fig. 24**. **(Bottom)** Nebulosa plots of expression of Wnt receptors *lrp5*, *fzd8a*, *fzd7b*, *fzd2*, *fzd4*, *fzd7a* across clusters on UMAP.

with various *fzd* receptor combinations expressed across clusters (**Fig. 26**). This, along with our perturbation studies, may suggest that spatial control of tenocyte and muscle attachment patterning is dictated by combinatorial WNT ligand-receptor interactions with peritendinous/epithelial and osteoblast signaling sources.

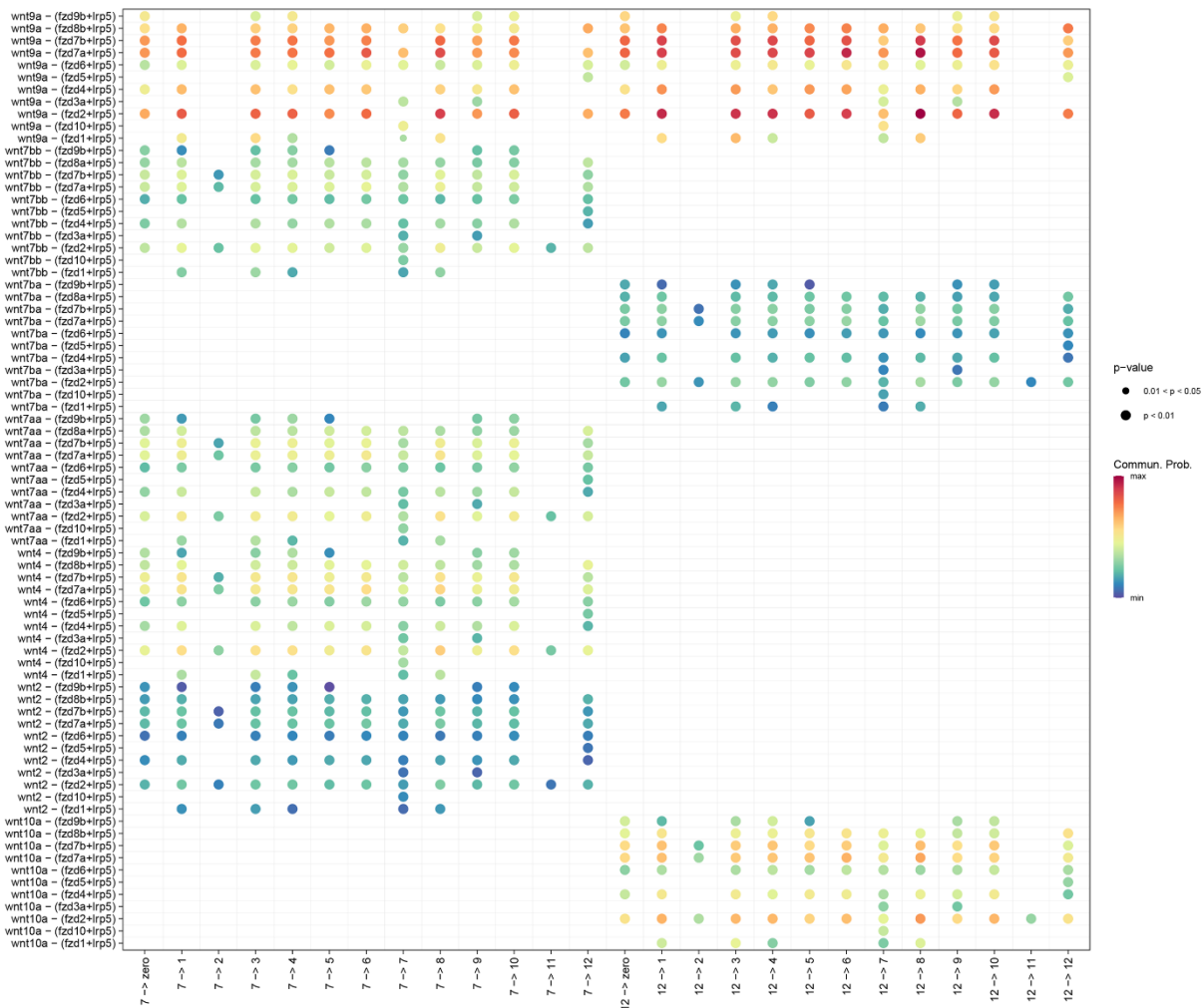


**Figure 26: Wnt ligand-receptor interactions with high confidence in CellChat ligand-receptor analysis**

Inferred outgoing Wnt ligand-receptor communication for clusters 7 and 12.

## Discussion

Though single-cell sequencing and proteomics research has approached tenocyte cell diversity from the perspective of intra-tendon differences, how the physiological differences of distinct tendons play into transcriptomic heterogeneity of intra-tendon attachment zones remains uncovered. In this study, we adapt a cold protease dissociation protocol to provide a high-quality dataset of cranial tenocytes with minimized global cell stress responses with optimally preserved tenocyte identity (defined by maintenance of tenocyte marker expression). Using analyses of this dataset, we show that tenocytes in our dataset effectively cluster by spatially distinct tendons and ligaments, and that transcriptomic differences in tenocytes between these structures is not only unique by conventional patterning genes but by ECM genes. This suggests that the tenocytes in an individual tendon attachment zone are transcriptionally adjusted to suit the attachment zone of a specific tendon. We confirm that well-studied trunk and limb tenocyte developmental and regulatory signaling pathways are active in cranial tenocytes, discover a novel population of Wnt-responsive tenocytes, and suggest a functional role for Wnt signaling in the development and patterning of the cranial MTJs. Compared to previous single-cell studies on sorted tenocytes, our analyses reveal unexpected functional heterogeneity that correlates with attachment type, such as soft vs. hard attachments (e.g. eye enthesis vs. cartilage enthesis), as well as tendon subregion (e.g. enthesis vs. MTJ). Our results begin to dissect cranial tenocyte diversity at a higher resolution than previously studied by unravelling transcriptional differences both within and across spatially separate tendons.

Early studies of cold temperature effects on cellular metabolism have shown drastic slowing of transcription/translation and cessation of RNA degradation mechanisms (Al-Fageeh & Smales, 2006; Fujita, 1999; Sonna et al., 2002). Tissue dissociation methods utilizing common proteases at higher temperatures cause various cell-stress artifacts (M. Kim et al.,

2020; O’Flanagan et al., 2019; Van Den Brink et al., 2017). However, few studies have delved into how specific cell-types modulate their expression patterns in response to different dissociation methods. Here, we show that a cold protease, subtilisin A dissociation method minimizes cell stress artifacts in embryonic zebrafish tendons. Our results also support the notion that tenocytes are highly sensitive to their ECM environment, and that cold dissociation broadly preserves their expression of tenocyte-specific transcription factors, receptors, and ECM components compared with a more traditional high temperature dissociation protocol. We find similar cell stress signatures in our dissociated tenocyte datasets in embryonic zebrafish to existing datasets published using high temperature dissociation of various other cell types **(Supplementary Fig. 1A-F)**. These similarities likely reflect general changes in cellular metabolism that may skew interpretation of cell-type specific changes in gene expression. In addition, surprisingly, our cold protease, subtilisin A dissociation method dissociates zebrafish tenocytes substantially faster than warm dissociation with collagenase. This has several advantages including: 1) Better control over “cellular age” when trying to analyze and compare samples from developing tissues in which cells differentiate rapidly. 2) Improved preservation of “cell state” since, for example, the ECM environment has been shown to affect tenocyte specification, proliferation, differentiation, and ECM production (E. Maeda et al., 2010, 2013; T. Maeda et al., 2011b; Subramanian & Schilling, 2015; J. Zhang & Wang, 2010, 2013, 2015). 3) Improved cell survival, since we find substantially more upregulated genes enriched for apoptosis-related terms in both GO and KEGG enrichment analysis with warm dissociation conditions **(Fig. 1C, Supplementary Fig. 1G)**.

Importantly for cells like tenocytes that produce large amounts of ECM, cold dissociation also appears to preserve their expression of ECM components compared with warm dissociation. These include both collagens (Fibrillar, FACIT, Network Forming) and non-collagen ECM proteins **(Fig. 1E)**, with a broad range of functions in connective tissue structure and

function (Bella & Hulmes, 2017; Birk & Bruckner, 2011; Mienaltowski & Birk, 2014; Ricard-Blum, 2011; Van Der Rest & Garrone, 1991). In addition to global expression differences in tenocytes in these ECM components between cold and warm dissociation conditions, we find cluster-specific expression differences in specific ECM genes from all three categories, such as *col10a1a*, *col4a1*, *col12a1b*, *col27a1b*, *loxa*, and *prelp*, including collagens such as collagen IV and collagen X that are not traditionally thought of as tendon-specific collagens (**Fig. 1E**). Col4 networks are found in tendons that have an exterior sheath of keratinized epithelium and basement membrane (Taylor et al., 2011). Col X is highly expressed in hypertrophic chondrocytes and its expression in tenocytes may reflect a role in fibrocartilage at the tendon-bone interface (enthesis) (Blitz et al., 2013). Expression of Collagen XII has been shown to be spatially localized to various tendons, connective tissue and fascia (Bader et al., 2009). Being a FACIT collagen, Collagen XII is thought to regulate ECM and fibrillar collagen assembly, tissue stabilization, and tendon response to mechanical stimuli, as *Col12a1*<sup>-/-</sup> mutant mice have displayed aberrant tendon fibril packing and decreased/absent tenocyte projections (Izu et al., 2021; Sun et al., 2010). Tenocyte projections are thought to act as force-sensors for maintaining ECM homeostasis, and the expression reduction of *col12a1b* along with other hallmark tendon markers in the warm dissociation dataset may suggest that, since cell transcription machinery has not been frozen, dissociated tenocytes are sensing the lack of tissue-force feedback and responding in a transcriptionally aberrant fashion (Subramanian et al., 2018). In contrast to collagen XII, collagen XVII has been studied and has shown more spatiotemporal expression in cartilage, thought to play a structural and scaffolding role for endochondral ossification, and chondrocyte pericellular organization during skeletogenesis (Christiansen et al., 2009; Hjorten et al., 2007; Plumb et al., 2011). Additionally, collagen XVII contains enhancer elements binding to SOX9, a transcription factor important for cartilage differentiation and regulation of enthesis establishment (Jenkins et al., 2005). As our data shows the first known expression of collagen

XVII in tendons, it may implicate, along with prior research in cartilage, a role for collagen XVII in development/establishment of the enthesis via selective gene expression in entheseal tenocytes which have double expression of *Scx* and *Sox9* (Blitz et al., 2013; Zelzer et al., 2014).

ECM components such as LOX and PLOD are involved more in ECM crosslinking within tendons and are implicated in tendon mechanical adaptations to muscle-contraction force in development, as well regulation of different stages of the tendon injury repair process including inflammation and remodeling of the ECM (Cai et al., 2017b; Pan et al., 2018). Indeed, exogenous LOX treatment has been shown to improve tensile properties of tendon and inhibition of LOX decreases tensile properties in in vivo, ex vivo, and in vitro contexts, further suggesting that the decreased expression of *loxa* and *plod2* we notice in tenocyte subpopulation manner in the warm condition is more reflective of a tendon in a more destabilized state (**Figure 1E,G**) (Makris et al., 2014; Marturano et al., 2013). As tenocyte subpopulations in vertebrates have not been fully characterized, the cluster-specific changes in ECM gene expression changes observed in warm-dissociation conditions may dramatically change the interpretation of single cell sequencing datasets, particularly if experimental conditions of future experiments involve studied variables including ECM-tenocyte/tenocyte communication and signaling or force-related expression responsivity. Though conventionally high temperature dissociation of tendons has been deemed acceptable due to the assumption that tenocytes have a low basal metabolic rate, our data show that even a ~40-minute dissociation at high temperature upregulates genes associated with generalized stress and inflammation as well as downregulating genes involved in tenocyte development and homeostasis (Ackerman et al., 2021). This suggests that the metabolic rate of tenocytes may be more active than previously imagined, and that experimental design planning of tendon research should be careful to minimize potentially unforeseen consequences of these assumptions. Given the emerging interest in the application of both bulk and single-cell sequencing studies on tenocytes,

evidenced by the increasing number of sequencing related publications, it is imperative that there is a thorough early understanding of the implications of conventional tissue and cell sample preparation methodologies for proper downstream data quality and interpretation (De Micheli et al., 2020; Fabian et al., 2022; Kaji et al., 2021; Kult et al., 2021; Yoshimoto et al., 2022).

Through a combination of *isHCR*, cluster marker expression, and literature comparisons, we identified markers of expression for tenocyte populations from distinct tendons and demonstrated that each tendon contains a unique ECM signature. The eye tendon contained the most easily distinguishable markers with higher expression of fibrillar collagens, FACIT, and FACIT-like collagens at the MTJ end, and basement membrane and laminins at the eye attachment end (eye enthesis, (Hertle et al., 2002) ) (**Fig.8, 9A, 10E-H, 11A-C, 12A-B**). The eye enthesis is unique in its attachment site to soft tissue, as tendons of other tissues either attach directly to muscle, cartilage, or bone in later stages. The unique tissue type of the underlying corneal epithelial layer, developmental origin, and the lower muscular forces required to move the eye (versus, for example, those of the jaw) would likely contribute to the basement membrane-rich transcriptional signature of the tenocytes of this attachment zone (Comai et al., 2020; H. Guo et al., 2016; Saikia et al., 2018). Indeed, basement membranes provide tissue elasticity and damage protection through extensive Laminin and Collagen IV networks, which would aid in optimal force transfer from the delicate ocular musculature, compared to the fibrocartilage-rich ECM in more well-studied entheses such as the limb (Lu & Thomopoulos, 2013; Sekiguchi & Yamada, 2018).

Markers of the tenocytes residing within the sternohyoideus central tendon (hyohyal-basihyal attachment region) included *comp* and *tbx1*. Further dissection of the ECM marker genes through subcluster and modulescore analysis revealed that this tendon was rich in tenocytes with basement membrane collagen (*col4a1, col4a2, col4a3, col4a4, col4a5, col4a6*),

and fibrillar collagen (*col1a1*, *col1a2*, *col2a1*, *col5a1*, *col5a2*, *col5a3*, and *col27a1*) expression (**Fig. 9A, 10A-D, 11A-B**). Additionally, tenocytes within this tendon had low expression of laminins, and FACIT and FACIT-like collagens. It is possible that the high expression of basement membrane collagens in these tenocytes serves a developmental role in the cylindrical shape of the central tendon, as basement membrane specific Collagen IV is thought to facilitate constrictive forces in tissue-shape morphogenesis in other models (Isabella & Horne-Badovinac, 2016). Interestingly, the covalent bonds formed in basement membrane via collagen IV is thought to give tissue mechanical stress resistance (Khoshnoodi et al., 2008; Vanacore et al., 2009). This could especially be advantageous for the sternohyoideus central tendon, as it centers at the attachment of two hyohyal muscles, two sternohyoid muscles, and the basihyal cartilage, thereby being exposed to constant mechanical stress across all these tissues. Perhaps the basement membrane integrated with tissue strength of fibrillar collagens would confer increased resistance and stability to this tissue (**Fig. 11A-B**). The ECM expression profiles of both ligamentocytes and the tenocytes of the lower jaw tendons (intermandibularis anterior tendons) appeared low in all collagens (including basement membrane collagens) types except fibril collagens such as collagen I (**Fig. 8, 11A-C, 12A-B**). As the intermandibularis anterior tendons only attach to one muscle each, both the directionality and intensity of muscle contraction force would require the ECM composition to be less reinforced than that of the sternohyoideus central tendon, thus not requiring high expression of basement membrane collagens. Lastly, ligamentocytes (compared to sternohyoideus central tendon and intermandibularis anterior) were unique in their expression of *loxa*, which hints at the unique ECM mechanical properties of ligaments themselves, as low-intensity mechanical stretching upregulates LOX in periodontal ligaments but not higher-intensity stretching forces (**Fig. 12C**) (Y. J. Chen et al., 2013). As the ligaments of the zebrafish mandible are not under the tensional forces of any craniofacial musculature, the expression of *loxa* suggest the adaptation of

ligaments to a stabilization role. However, *loxa* expression was also seen in the enthesis, and multiple MTJ populations, but not high in expression in the tenocytes of the intermandibularis anterior or sternohyoideus central tendon, suggesting that the mechanical properties at each end of individual tendons require the stabilization qualities conferred by *loxa* induced collagen crosslinking, but the ECM at the mid-substance region require force-transmissional mechanical properties (Laczko & Csiszar, 2020). Additionally, enthesis tissue is estimated to bear tensile forces up to four times more than that of the midsubstance, which may explain increased expression of *loxa* in these populations (McGonagle et al., 2003). These findings hint at the functional roles of transcriptional diversity of tenocytes and ligamentocytes within individual tendons and between tendon regions from a developmental and force-responsive context.

KEGG pathway analysis revealed Wnt as a signaling pathway involved in cranial muscle-tendon attachment development. Here, we present evidence of a previously unseen population of Wnt responsive tenocytes in the developing zebrafish cranium. Research on Wnt signaling in tenocytes has shown its inhibitory role in expression of traditional tenocyte markers such as *Scx* and *Mkx* (García-Lee et al., 2021; Kishimoto et al., 2017). In our imaging of *Tg(scx:mCherry;7XTCF:GFP)* embryos, we observed restriction of GFP+/mCherry+ cells to the sternohyoideus core, ceratohyal enthesis, mandibulohyoid ligament, and meckel's joint, suggesting that these double-positive lineages deviate from those of other cranial tendons, as Wnt signaling is necessary for development of the synovial joint, for example (**Fig. 13**) (X. Guo et al., 2004). Our heatshock *Tg(scxa:mCherry; hsp70l:dkk1b-GFP)* and *Tg(scxa:mCherry; hsp70l:dnTCF-GFP)* perturbations led to numerous tenocytes leaving expected condensations and migrating to ectopic locations. This is partially expected, as canonical Wnt signaling plays an important role in migration of neural crest cells (Dickinson et al., 1995). However, this defect may be in larger part due to loss of tenocyte progenitor cell adhesion, as ectopic tenocytes and higher frequencies of ectopic muscle attachments occur even in 60 hpf heatshocked

*Tg(scxa:mCherry; hsp70l:dkk1b-GFP)* embryos, a stage at which tenocytes have already migrated to their final locations. Even once tenocytes have migrated to their final positions, disruption of WNT signaling can increase the likelihood of a tendon and muscle to “detach” from established locations, perhaps due to either tenocytes and muscle attachments being still having some migratory capability, or the lack of full tendon ECM development to reduce tenocyte/muscle spatial maneuverability at this timepoint. Interestingly, both WT 60 hpf heatshocked and *Tg(scxa:mCherry; hsp70l:dkk1b-GFP)* 60 hpf heatshocked embryos displayed no “severe” phenotypes such as those seen in the *Tg(scx:mCherry; hsp70l:dkk1b-GFP)* 48 hpf heatshocked embryos, suggesting that Wnt signaling is likely more crucial to global tissue patterning at earlier craniofacial developmental stages (**Fig. 15V, Fig 17S**). However, in both 48 hpf and 60 hpf heat-shocked conditions, we noticed an increased frequency of embryos displaying ectopic muscle attachment(s) when comparing heatshocked WT embryos with non-heatshocked WT embryos (**Fig. 15V, Fig 17S**). It is likely that the heatshock stimulus at these critical timepoints activates signaling pathways which increase the likelihood of muscle-tendon attachment patterning disruptions as, for example, heat stimuli alone have been shown to influence Wnt signaling in myoblasts (Risha et al., 2021). Wnt antagonist (IWR-1 and XAV939) treatments were an attempt to control for these confounding variables and we noticed that ectopic MTJs still occurred at a frequency higher than control 1% DMSO treatments (**Fig. 19-21**). Additionally, Wnt agonist (BIO) treatments led to a similar phenotype, suggesting that the proper balance of Wnt signaling is required for proper patterning of cranial MTJs. One caveat of the study is that all Wnt disruptions (heatshock and drug treatments) were global which does not provide information as to the mechanism of how Wnt signaling is occurring from a cell-communication standpoint. Using CellChat communication inference analysis to identify ligand-receptor interactions in the scRNAseq data however, hints at peritendinous/epithelial cell and osteoblast sources of Wnt ligand and all other cell types as primary expressors of Wnt receptors (**Fig. 24-26**). Strikingly, expression of different *fzd* receptors varied across tenocyte clusters,

with *fzd8a* and *fzd4* had expression that was more restricted to MTJ and myoblast regions on the UMAP, giving potential avenues for future functional studies (**Fig. 25**). However, as Wnt signaling is heavily involved in many processes in early embryonic development, temporal canonical Wnt disruption studies should be performed. Both muscle cells/myoblasts and tenocytes have disrupted migration patterns in our study, but we do not know whether control of Wnt upon migrating myoblasts/muscle or tenocytes drive the patterning of the MTJ attachment. In fact, Wnt disruptions are known to interfere with myoblast migration in mouse limb (X. Zhu et al., 2012). Additionally, a similar phenotype was seen in zebrafish *cyp26b1* (a retinoic acid (RA) metabolizing enzyme) mutants, suggesting that a complex interplay of Wnt, RA signaling, and other pathways may be involved in the global developmental patterning of the jaw muscle-tendon attachment system (McGurk et al., 2017).

Collectively, our results provide a high-quality single-cell resolution perspective of cranial tendons during development, highlighting the ECM transcriptional differences of tenocytes both within and between individual tendons. They suggest that tenocytes inhabiting intra-tendon regions in different tendons influence the structural, and therefore force-bearing, ECM properties of a tendon for its individual physiological requirements. Additionally, the mapping of a novel Wnt responsive tenocyte population and roles for Wnt signaling in cranial MTJ patterning allude to the intricate balance of signaling pathways involved in patterning specific individual tendons. Deeper understanding of these tissues on a single-cell level at multiple developmental stages and under force-conditions will lead to a clearer map of differentiation trajectories of tenocytes populations between different tendons. This will in turn better inform personalized therapies for improved patient outcomes for tendon trauma.

## Methods

### Zebrafish embryos, transgenics and mutants

AB strain wild type, *TgBAC(scxa:mCherry)<sup>fb301</sup>*, *Tg(7xTCF-Xla.Siam:GFP)<sup>ia4</sup>*, *Tg(hsp70l:dkk1b-GFP)<sup>w32</sup>*, *Tg(hsp70l:pcf711a-GFP)<sup>w26</sup>* (referred to in the text as *Tg(scxa:mCherry)*, *Tg(7XTCF:GFP)*, *Tg(hsp70l:dkk1b-GFP)*, and *Tg(hsp70l:dnTCF)* respectfully), were collected in natural matings, raised in embryo medium (EM) at 28.5°C (Westerfield, 2007) and staged as described (Kimmel et al., 1995b).

### scRNAseq sequencing

Dissociated cell suspensions from cold and warm conditions were sorted on a Bio-Rad FACS Aria Fusion cell sorter located at the UCI Institute for Immunology Flow Cytometry Facility. Sorted mCherry+ cell suspensions were provided to the UCI Genomics High Throughput Facility (GHTF) for 10X library preparation using 3' v3 chemistry and sequenced.

### Processing of raw reads

FASTQ reads for all conditions obtained from GHTF were mapped to zebrafish genome version GRCz11 using CellRanger (version 3.1.0) (Zheng et al., 2017) after modifying the genome and GTF annotations with the addition of the mCherry nucleotide sequence (708 nucleotides). Web summary metrics post-alignment were:

Cold condition:

Estimated number of cells: 14,531, Mean reads per cell: 37,963, Median genes per cell: 1,960, Number of reads: 551,646,943, Valid Barcodes: 97.8%, Valid UMIs: 100%, Sequencing saturation: 54.2%, Reads mapped to genome: 93.1%, Reads mapped confidently to genome: 78.6%, Reads mapped confidently to transcriptome: 61.9%

Warm condition:

Estimated number of cells: 21,755, Mean reads per cell: 28,890, Median genes per cell: 1,623, Number of reads: 628,508,698, Valid Barcodes: 97.8%, Valid UMIs: 100%, Sequencing saturation: 45.4%, Reads mapped to genome: 93.7%, Reads mapped confidently to genome: 78.3%, Reads mapped confidently to transcriptome: 61.3%

Two additional 72 hpf WT samples:

Sample 1:

Estimated number of cells: 11,109, Mean reads per cell: 60,734, Median genes per cell: 1,786, Number of reads: 674,692,117, Valid Barcodes: 97.3%, Valid UMIs: 100%, Sequencing saturation: 73.6%, Reads mapped to genome: 93.6%, Reads mapped confidently to genome: 85.6%, Reads mapped confidently to transcriptome: 69.1%

Sample 2:

Estimated number of cells: 11,040, Mean reads per cell: 93,951, Median genes per cell: 2,277, Number of reads: 1,037,216,198, Valid Barcodes: 96.1%, Valid UMIs: 100%, Sequencing saturation: 79.0%, Reads mapped to genome: 95.5%, Reads mapped confidently to genome: 87.8%, Reads mapped confidently to transcriptome: 66.0%

### **scRNAseq QC and analysis in Seurat for cold protease analysis**

Filtered count matrices for each condition were converted into Seurat objects (version 4.0.5, R version 4.0.2) (Hao et al., 2021). mCherry+ cells were kept for downstream analysis if they met the quality control criteria of  $200 > \text{genes/cell}$  ( $n\text{Features}$ )  $> 4000$  and mitochondrial gene expression  $< 5\%$ . For anchoring/sample integration, individual Seurat objects were merged together with the *merge* function and data were Normalized using *NormalizeData* function with default parameters (*normalization.method* = "LogNormalize", *scale.factor* = 10000). Feature selection was carried out with the *FindVariableFeatures()* function with default

parameters (*selection.method* = "vst", *nfeatures* = 2000). Data was scaled with *ScaleData()* function, PCA was performed with *RunPCA* function with *npcs* = 30. All 30 PCs were used for UMAP reduction using *RunUMAP()* and nearest neighbor graph construction using *FindNeighbors()*. Unsupervised clustering was performed with the *FindClusters()* function using a resolution parameter of *resolution* = 0.5. Pseudo-bulk differential expression between warm and cold conditions was performed by switching identities of the integrated cold/warm dataset to the sample identities (*Idents(Seurat\_object) <- "orig.ident"*), and using the *FindMarkers()* function with parameters *min.pct* = 0.1 and *logfc.threshold* = 0.1, with the default hypothesis test method using Wilcoxon Rank Sum test and Bonferroni correction for multiple hypothesis tests. Gene module aggregate scoring was performed by using the Seurat *AddModuleScore()* function with the default settings (*nbin*=24 and *ctrl* = 100) on the integrated/anchored dataset. Gene lists for the fibrillar collagen module included *col1a1a*, *col1a1b*, *col1a2*, *col2a1a*, *col2a1b*, *col5a1*, *col5a2a*, *col5a2b*, *col5a3a*, *col5a3b*, *col27a1b* and FACIT collagen module included *col9a1a*, *col9a1b*, *col9a2*, *col9a3*, *col12a1a*, *col12a1b*, *col14a1a*, *col14a1b*. Statistical testing for expression differences displayed on all violin plots were performed with the *stat\_compare\_means()* function utilizing the default Wilcoxon rank sum test from the *ggpubr* package (version 0.4.0). The Volcano plot was produced using the *EnhancedVolcano* package (version 1.8.0) with p-value line drawn at 0.05 *pCutoff* = 0.05 and fold change line drawn with *FCcutoff* = 0.5.

### **scRNAseq QC and analysis in Seurat for 72 hpf heterogeneity study**

Filtered count matrices for each condition were converted into Seurat objects (version 4.0.5, R version 4.0.2) (Hao et al., 2021). mCherry+ cells were kept for downstream analysis if they met the quality control criteria of  $200 > nFeatures > 3000$  and mitochondrial gene expression  $< 5\%$  for two samples and integrated with the cold protease condition sample described above. For anchoring/sample integration, individual Seurat objects were merged

together with the *merge* function and data were Normalized using *NormalizeData()* function with default parameters (*normalization.method* = "LogNormalize", *scale.factor* = 10000). Feature selection was carried out with the *FindVariableFeatures* function with default parameters (*selection.method* = "vst" , *nfeatures* = 2000). Data was scaled with *ScaleData()* function, PCA was performed with *RunPCA* function with *npcs* = 20. All 20 PCs were used for UMAP reduction using *RunUMAP()* and nearest neighbor graph construction using *FindNeighbors()*. Unsupervised clustering was performed with the *FindClusters()* function using a resolution parameter of *resolution* = 0.125. Gene Ontology (GO) analysis was performed using the *enrichGO()* function from clusterProfiler package (version 4.4.4) (T. Wu et al., 2021b) with zebrafish genome annotations provided by the org.Dr.eg.db package (version 3.12.0), Biological Process (BP) GO category annotation, *pvalueCutoff* = 0.01 and *qvalueCutoff* = 0.05, and Benjamini-Hochberg correction using *pAdjustMethod*= "BH". KEGG pathway analysis was performed with the *enrichKEGG()* function, with default values for p-value, Benjamini-Hochberg test correction, and q-value (*pvalueCutoff* = 0.05, *pAdjustMethod* = "BH", and *qvalueCutoff* = 0.2). In GO term/KEGG plots, Gene Ratios are described as *k/n* where *k* is the number of genes from the differential expression gene list mapping to the plotted GO or KEGG term, and *n* is the total number of input genes mapping to any GO or KEGG term.

Stress gene comparisons of cold/warm datasets with existing published datasets was performed using (if comparing with a non-zebrafish organism dataset) the *getLDS()* function from the biomaRt package (version 2.46.3) to obtain orthologous genes for Human and Mouse from our zebrafish differentially expressed genes (DEG) lists. Genes from the DEG list from cold/warm were then compared against the stress gene sets published by O'Flanagan et al., n.d. and (Van Den Brink et al., 2017) using the VennDiagram package (version 1.7.3) (H. Chen & Boutros, 2011) and overlap testing was performed with the Fisher's exact test using the GeneOverlap (version 1.26.0) (Shen, 2016) package with number of coding genes for each

genome placed in the *genome.size* argument as 25,525 for zebrafish (assembly GRCz11), 19,804 for Human (assembly GRCh38.p13), and 22,213 for mouse (assembly GRCm39).

CellChat cell-cell communication analysis was performed using CellChat R package (version 1.1.3) with average gene expression per cluster calculated with 5% truncated mean.

## **HCR and Immunohistochemistry**

*isHCR* probes were designed by Molecular Technologies (Los Angeles, CA) and whole mount *isHCR* was performed with amplifiers/probes obtained from Molecular Instruments according to the *isHCR* v3.0 protocol as described (**Choi et al., 2014**). Probes/amplifier combinations used are provided in (**Supplemental table 1**)

## **Cold Protease (Subtilisin A) Embryo Dissociation Protocol and Single-cell Isolation for 10X Sequencing**

A silicone petri dish was created by pouring silicone elastomer with curing agent (Dow SYLGARD 184) into a 60x15mm petri dish (Falcon #351007). 72 hpf embryos were anesthetized in Tricaine and transferred to the silicone plate with Ringer's solution on an ice bath. Per sample, 25 heads were dissected using a pair of fresh 21G beveled edge needles. The heads were placed in a single well in a 24 well multidish (Thermo Scientific, 930186) in 1 ml of ice-cold ringer's solution. The ringer's solution was then replaced with fresh protease digestion solution, consisting of: 5ul of 1M CaCl<sub>2</sub>, 100ul of protease stock solution (100mg of *Bacillus licheniformis* protease (Sigma P5380) solubilized in 1ml of Ca and Mg free PBS), 889ul of PBS, 1ul of 0.5M EDTA and 5ul of DNase I stock (25U/ul in PBS, stored at -80C). The tissue heads were then triturated once every 2 minutes for 15 seconds using a wide bore 1ml pipette. Every 15 min, tissue solution was checked under dissecting scope to verify dissociation. Full dissociation of cells took roughly 30-40 minutes per sample, and samples were subsequently run through a 40 micron filter to separate dissociated cells from clumps of aggregate

undissociated tissue/ECM and washed with 10ml of PBS/BSA (0.01% BSA in PBS, made fresh on day of dissociation) and transferred to a 15ml conical tube. Cells were centrifuged at 600g for 5 minutes at 4C, supernatant is discarded, and cells are resuspended in 1ml of ice-cold PBS/BSA before being placed on ice. High expressing mCherry+ cells were gated and sorted.

### **Wnt Signaling Heat Shock Treatments**

*Tg(scxa:mCherry)* fish were crossed with *Tg(hsp70l:dkk1b-GFP)* and *Tg(hsp70l:dnTCF)* lines to obtain *Tg(scxa:mCherry; hsp70l:dkk1b-GFP)* and *Tg(scxa:mCherry; hsp70l:dnTCF)* lines respectively. Embryos were placed individually in 0.2ml 8-strip PCR tubes (USA Scientific 1402-2500) in 100ul EM with an air-bubble placed at the bottom of each tube and heated at 39C for 30 minutes in a thermocycler (Bio-Rad S1000). 20 minutes after heat shock, GFP positive embryos were screened, fixed, antibody stained, mounted in 1% low melt agarose in PBS in a Glass Bottom Slide dish (MatTek Corporation P35G-1.5-14-C) at 48 hpf and 60 hpf along *Tg(scxa:mCherry)* and *Tg(scxa:mCherry)* heatshocked controls at the same stages, and imaged.

### **Wnt Signaling Drug Treatments**

*Tg(scxa:mCherry)* were crossed with *Tg(7XTCF:GFP)* to obtain *Tg(scxa:mCherry;7XTCF:GFP)* double positive embryos. 10mM stocks of IWR-1 (Sigma #I0161), XAV939 (Sigma, #575545), and BIO (Sigma, #B1686) were created by dissolving in DMSO (99.9+%, Alfa Aesar, #42780). For experiments, 10mM stocks were diluted in 3 ml EM to create working concentrations and added to ~15 embryos in a 35x10mm petri dish (Falcon, #351008) per condition. Dishes with 48 hpf embryos were incubated at 28.5C for 24 hours, fixed, antibody/HCR stained, mounted in 1% low melt agarose in PBS in a Glass Bottom Slide dish (MatTek Corporation P35G-1.5-14-C) and imaged.

### **Live Imaging**

For *Tg(scxa:mCherry)*, *Tg(scxa:mCherry;7XTCF:GFP)*, *Tg(scxa:mCherry; hsp70l:dnTCF)*, and *Tg(scxa:mCherry; hsp70l:dkk1b-GFP)* live imaging, 2-4 embryos of the appropriate condition were mounted in 1% low melt agarose in EM in a Glass Bottom Slide dish (MatTek Corporation P35G-1.5-14-C) , and EM with 4.2% tricaine was added to the dish after the agarose had solidified. This was repeated for Wnt drug treatment live imaging, except that the appropriate working concentration of Wnt agonist/antagonist was added to EM with 4.2% tricaine. A small rectangular cut was made in the agarose plug in front of the embryo heads extending back to the anterior segment of the yoke, and this section was removed from the dish. This allowed for the posterior half of each embryo to be mounted in place by the gel, but for the head to grow and develop without restriction. Imaging was conducted on a Leica SP8 Confocal Microscope using the PL APO CS2 40X/1.10 W objective.

### **Wnt perturbation Heat Shock and Drug Treatment Statistical Analysis**

Embryos with ectopic muscle attachments in Wnt signaling perturbation studies were categorized qualitatively as "none", "mild", or "severe" phenotype accordingly: "none" had no discernable ectopic muscle attachments, normal craniofacial cartilage structure development, jaw muscle length, and no noticeable ectopic muscle attachments in the jaw muscles. "mild" phenotypes had normal craniofacial cartilage structure development, jaw muscle length, and attachment region with at least one ectopic muscle attachments branching off from primary cranial muscles whereas "severe" phenotypes had dramatically shortened cartilage structure, jaw muscle length with multiple ectopic muscle attachments attaching to ectopic tenocytes, tendons other than their wild-type attachment region, or to unlabeled cells. Quantification involved comparing embryos with "none" phenotype against embryos with "mild" or "severe" phenotype as one category. Absolute quantities of embryos with each category were counted for each condition and compared using the chi square test of independence in Excel with ns = not significant, \*  $p < 0.05$ , \*\*  $p < 0.01$ , \*\*\*  $p < 0.001$ .

## Chapter IV

### Identification of novel protein-protein interactions with tenocyte fate regulator Scleraxis

#### Introduction

A key question in developmental biology is how small-scale cell and protein interactions translate to tissue and system level morphological changes. One of many strategies cells employ to this end is mechanotransduction, in which cells sense mechanical force cues and activate signaling cascades to adapt cell behavior and modulate the extracellular microenvironment. Complex cell communication strategies such as mechanotransduction are effectively employed in vertebrate embryonic development of tendon tissue, which requires an interplay of signaling pathways such as Sonic hedgehog (Shh), FGF, and TGF- $\beta$  to control transcriptional upregulation of specific fate determination markers such as bHLH transcription factor Scleraxis (SCX) in mesenchymal stem cells (MSCs) to initiate a tendon progenitor cell (TPC) transcriptional program. Force dependent signaling leading to pSmad3 further upregulation of SCX, EGR1, EGR2, and TALE family transcription factor (TF) MKX, dictates TPC differentiation into tenocytes, as well as maintenance via downregulation of skeletal markers (Subramanian & Schilling, 2015). However, initial transcriptional activation of tenocyte fate determining genes is not sufficient to maintain tenocyte cell fate stability; consistent expression must be maintained via microenvironmental cues. For example, hallmark tenocyte marker genes *Scx*, *Tnmd*, and *Col1a* are significantly downregulated in tenocytes cultured on plastic dish surfaces versus embedded in collagen gels, and conditional *ScxCre;Tgfb2* deletion in mice leads to tenocyte de-differentiation to a more progenitor-cell like state (Shimada et al., 2014; Tan et al., 2020). To gain a clearer understanding of the entire signaling cascade by which MSCs differentiation into tenocytes and fate stability is maintained, importance must be placed upon a greater understanding of the tenocyte transcriptional program at the protein level. TFs such as SCX and MKX drive primary differentiation of tenocytes, but other proteins which

interact with these TFs to execute the tenocyte differentiation and maintenance programs are not clearly mapped.

In this study, we perform tandem affinity purification with mass-spectrometry (TAP-MS) on human SCX and MKX fusion proteins expressed in HEK293 cells to understand stably binding protein-protein interactions (PPIs) biochemically involved in the tenocyte transcriptional program. We uncover a multitude of binding targets to both proteins using MS analysis. Further, we utilize Co-immunoprecipitation and immunofluorescence to confirm known binding partner E47 (also known as E-box protein TCF3) as well as novel related E proteins E2-2 and HEB (also known as TCF4 and TCF12 respectively) with SCX and provide potential functions for these binding interactions (Carlberg et al., 2000). Knowledge of these binding partners would provide a better platform for optimizing tenocyte differentiation protocols in-vitro, which could lead to understanding mechanisms for tendon development and regeneration.

## Results

### Tandem Affinity Purification-Mass Spectrometry identifies multiple binding partners to Scleraxis and Mohawk

To understand novel PPIs to human MKX and SCX, we utilized TAP-MS (X. Li et al., 2015). Briefly, the protocol involves expression of “bait” fusion protein SCX-SFB (S-protein/FLAG-tag/Streptavidin-binding peptide) at the C-terminal end in HEK293 cells, followed by cell lysing and two-part washing steps with streptavidin-agarose beads and S protein-agarose beads respectively to eliminate transient binding interactions. Using SAINT scoring to filter for high confidence binding interactions, the resultant PPIs totaled 7 unique proteins binding with Mxk and 78 binding with SCX (**Table 1 and 2**) (**Supplementary Data 1**) (H. Choi et al., 2011). As Mxk PPIs did not provide many interactions with high confidence via SAINT, we only continued studies with SCX PPIs. Strikingly, these PPIs included transcription factor bHLH E-box proteins TCF3, TCF4, and TCF12 with the highest total peptide fragments identified. E-

Unique Peptide No.	Total Peptide No	Gene Symbol	MWT (kDa)	Annotation	Coverage	SAINT Score
4	6	A2M	163.19	Alpha-2-macroglobulin	53	1
1	2	DBF4B	67.2	Protein DBF4 homolog B	10	0.5
2	2	TBL1R	55.56	F-box-like/WD repeat-containing protein	25	0.17
15	37	MYH9	226.39	Myosin-9	235	0.05
2	2	EIF4A2	46.37	Eukaryotic initiation factor 4A-II	23	0.04
4	5	HBB	15.99	Hemoglobin subunit beta	51	0.02
2	3	CAT	59.72	Catalase	28	0.02

**Table 1:** PPIs detected from MS analysis of TAP human MKX transfected in HEK293 cells

proteins have been known to heterodimerize with other tissue specific bHLH proteins to regulate differentiation such as transcription factor MyoD in vertebrate muscle development (L.-H. Wang & Baker, 2000). To confirm biochemical binding of proteins from MS results, we conducted Co-

immunoprecipitation assays with SCX and putative PPIs in HEK293 cells. Upon expression of

Unique Peptide No.	Total Peptide No.	Gene Symbol	MWT (kDa)	Annotation	Coverage	SAINT Score
17	181	TCF3	67.56	Transcription factor 3	174	1
26	128	TCF12	72.92	Transcription factor 12	316	1
17	89	TCF4	71.26	Transcription factor 4	237	1
23	49	UBE20	141.21	(E3-independent) E2 ubiquitin-conjugating enzyme	288	1
18	25	COPA	138.26	Coatomer subunit alpha	205	1
13	15	COPB2	102.42	Coatomer subunit beta-2	144	1
11	14	COPG1	97.66	Coatomer subunit gamma-1	139	1
11	11	RAD50	153.8	DNA repair protein RAD50	139	1
5	10	ARCN1	57.17	Coatomer subunit delta	53	1
10	10	COPB1	107.07	Coatomer subunit beta-1	133	1
1	1	ANKHD1	73.26	Ankyrin repeat and KH domain-containing protein 1 (Fragment)	10	1
5	5	MRE11	80.54	Double-strand break repair protein MRE11	55	1
5	5	ANKRD17	274.09	Ankyrin repeat domain-containing protein 17	74	1
3	4	LSM14B	42.05	Protein LSM14 homolog B	56	1
2	4	MRPL42	16.65	39S ribosomal protein L42, mitochondrial	19	1
3	4	COPZ1	20.19	Coatomer subunit zeta-1	40	1
2	4	MRPL20	17.43	39S ribosomal protein L20, mitochondrial	19	1
2	3	SRSF6	39.56	Serine/arginine-rich splicing factor 6	18	1

**Table 2:** PPIs detected from MS analysis of TAP human SCX transfected in HEK293 cells

Myc tagged SCX fusion protein (Myc-SCX) along with individually SFB-tagged putative PPIs, SFB-TCF3, SFB-TCF4, and SFB-TCF12 were shown to bind Myc-SCX and show fluorescent co-localization, while UBE20, COPB1, and COPB2 did not bind or show fluorescent co-localization thus serving as negative controls (**Figure 1 and 2**). Individual expression of SFB-TCF3/4/12 in HEK293 cells showed nuclear localization, and individual overexpression of Myc-

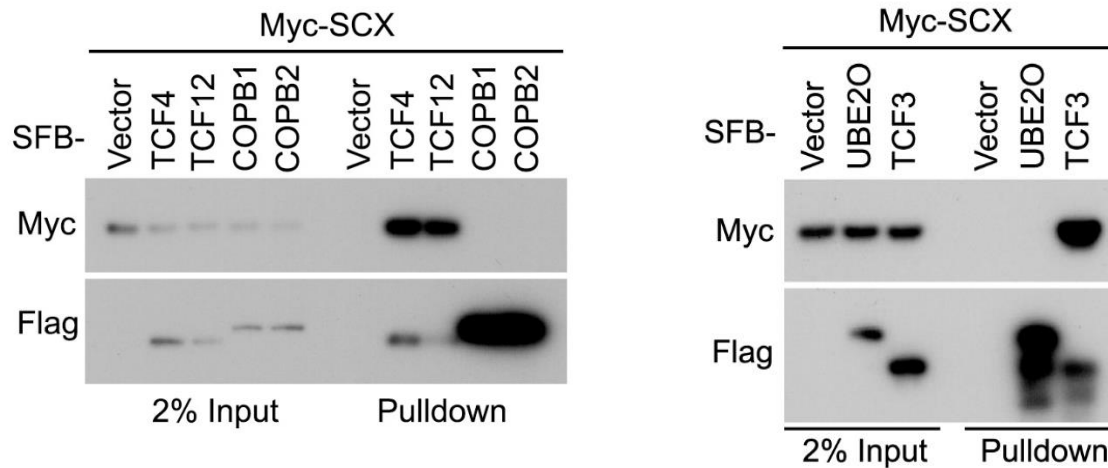


**Figure 1:** Western blot of Co-immunoprecipitation of Myc-Scx and SFB-TCF3/4/12, SFB-COPB1, SFB-COPB2, and SFB-UBE20

Scx displayed cytoplasmic localization uncharacteristic of its role as a transcription factor.

Interestingly co-expression of SFB-TCF3/4/12 and Myc-SCX together exhibited a fluorescent nuclear co-localization suggesting a role for TCF3/4/12 in SCX binding and nuclear transportation.

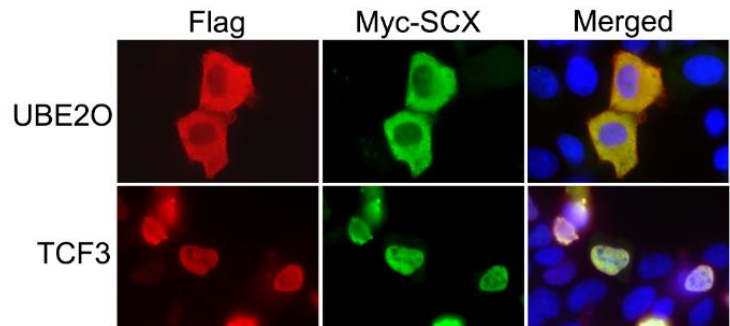
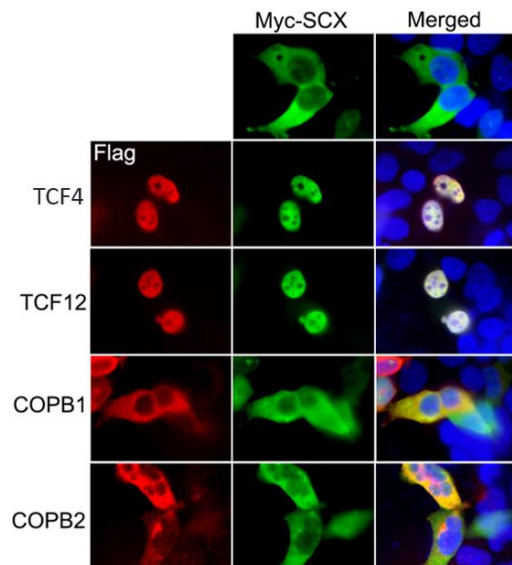


**Figure 2:** Immunofluorescence of Myc-Scx with SFB-TCF3 (above) and SFB-TCF4/12 (left). Individual expression of Myc-SCX displays cytoplasmic localization, whereas addition of SFB-TCF3/4/12 leads to nuclear translocation of Myc-Scx.

## Discussion

Though binding partners of other skeletal differentiation transcription factors such as SOX9 and RUNX2 have been studied (X. Li et al., 2010; Ming et al., 2022), a map of binding partners of tenocyte differentiation markers such as SCX and MKX are unknown. Here, we provide a list of putative binding partners for human MKX and SCX via TAP-MS analysis in HEK293 cells. We further confirm E-box proteins TCF3/4/12 as stably binding heterodimers with SCX and show that they are individually sufficient to drive nuclear translocation.

E-box proteins have known, often context-dependent, roles in differentiation of various cell types such as B-cells (Singh et al., 2005), neural subtypes (Powell & Jarman, 2008), and muscle cells (Lassar, et al., 1991). Given these roles, our data may suggest a mechanism by which SCX can drive MSC to TPC/tenocyte downstream differentiation transcriptional programs. The observation of Myc-SCX having baseline protein localization in the cytoplasm is novel, given the normal function of SCX as a transcription factor. Two caveats of this observation and its applicability to understanding tenocyte differentiation are: 1) that it is possible that the cell type used in our study (HEK293) would confer a different default localization of SCX than what would be observed in an MSC/TPC line and 2) creating and expressing a fusion Myc-SCX protein possibly changes the default SCX protein localization. However, confirmation of these binding partners to SCX is advantageous to guiding future work on tenocyte differentiation. If endogenous cytoplasmic SCX protein localization is confirmed in MSC cell lines or in-vivo, transient (e.g. siRNA) knockdown studies of TCF3/4/12 could better elucidate the nuclear translocation mechanism and individual roles for each TCF protein on tenocyte differentiation. Given that TCFs often direct differentiation in a context dependent manner, it would be useful to understand individual and combinations of expression of TCFs on downstream MSC differentiation. As MSCs are a multipotent progenitor population, one hypothesis is that individual TCF protein heterodimerization with SCX drives differentiation into tenocyte subpopulations, such as enthesis/MTJ/mid-substance of specific tendons and could be tested

via expression analysis of intra-tendon markers. Such studies remain to be performed but would help inform the differentiation trajectories of tenocyte populations in different spatially distinct tendons.

## **Methods**

### **TAP-MS**

HEK293 cells were transfected into 6cm dishes using lentivirus transfection of SFB-SCX or SFB-MKX with polyethylenimine at 60% confluence, and GFP fluorescence checked for transfection confirmation. After 80% confluence, cells were then transferred using trypsin to 10cm dishes with puromycin selection at a concentration of 1 ug/mL, with a control untransfected dish. After death of control cells in ~2 days, cells are transferred to 10 cm dishes. After ~2 weeks, the cells are transferred in single colonies to 24 well plates. When wells are confluent, individual cell samples are collected for western blot (WB) with Flag antibody. Positive colonies by WB are transferred into 6 well plates, then 6cm dish, then 10cm dish, each after 60-70% confluence. Lastly the cells are expanded to twenty 10cm dishes. These cells are then pipetted and moved to 50 mL tubes, and washed with PBS, and spun at 1000 rpm for 5 min. Pellet is resuspended in cold NETN buffer and lysed on a platform shaker at 4C for 30 min. Cell lysate is transferred to 1.5mL centrifuge tubes and spun at 13,000rpm for 15 min. Supernatant is transferred to a 15ml tube on ice and 100ul agarose-streptavidin beads are added, with platform shaking for 4 hours at 4C. Lysate is eluted with biotin elution buffer (biotin in NETN), then S protein-agarose beads are added to the tube, and again platform shaking resumes for 4 hours at 4C. S protein beads are washed with NETN buffer and samples are run on a 10% SDS-PAGE gel. Bands from gel are cut and sent to the Harvard Taplin MS facility for analysis. Resultant protein interactions are run through SAINT for high confidence interactions (H. Choi et al., 2011).

### **Co-Immunoprecipitation**

After transfection, cells in 10cm dish are washed with 4C PBS and then with NETN buffer, then scraped into 1.5mL centrifuge tube. The tube is left shaking for 30 min at 4C and then spun at 13,000rpm for 10 min. Supernatant is transferred to a new tube and then boiled for 10 minutes. Myc or Flag antibodies are added with protein A/G agarose beads overnight. The

beads are then washed in 4C NETN buffer and boiled again for 10 min, spun down, and western blot is performed.

### **Immunofluorescence**

A 12mm glass cover is placed in a 6 well dish and cells are added on the glass cover. After 1 day, the cells are fixed in 4% paraformaldehyde and washed with PBS, then with TBST 3x. primary antibody is added in 1% BSA and added to glass cover, incubated for 1 hour, then secondary antibody in 1xTBST is added and incubated for 1 hour at room temp. cells are washed in TBS 5x and then imaged under fluorescence.

## Chapter V

### Conclusions and Future Directions

Understanding biology at the level of tissues, organs, and whole organisms requires an understanding of systems at the smallest scales, such as how cells receive signaling cues from their microenvironment and modulate their own behavior and microenvironment in response. Since the early studies of cell mechanotransduction and cell-ECM feedback mechanisms in the late 20<sup>th</sup> century, we have come to recognize the cell-ECM unit as an inseparable dynamic system, where modifications in one component have dramatic effects on the other. Tightly regulated feedback loops in these micro systems have huge influences upon tissue level dynamics when performed at scale, orchestrating biological processes from tissue homeostasis to development and disease. Tendons, as ECM-rich tissues constantly subjected to mechanical forces of muscle contraction, have provided an ideal model to investigate cell-ECM feedback mechanisms. Emerging research in the field of tendon biology has elucidated the highly dynamic nature of tendon tissues at resolutions previously never imagined. Since the discovery of key transcription factors responsible for tenocyte specification, differentiation, and maintenance, the field has evolved towards a functional understanding of tenocyte subpopulations across developmental and disease contexts. Discerning the inherent force-transmitting and load-bearing characteristics of tendons has led to a better comprehension of tenocyte force-responsive pathways and resulting tendon ECM composition, though in vivo translation of prior in vitro findings remains ongoing. Further, how tenocytes at spatially distinct tendons with tissue-specific attachment sites uniquely modulate ECM gene expression and tune their microenvironment is still not fully understood.

In my work, I dissect vertebrate tendon development from the perspective of tenocyte mechanotransduction, from how varied muscle contraction force contexts affect gene expression of common force-responsive genes in vivo, to how specific sub-populations of individual tendons transcriptionally fine-tune ECM composition to adapt a tendon to attachment-

specific physical forces, to the key tenocyte transcriptional complexes active downstream of muscle contractile force sensing. Interpreting the mechanisms of tendon biology at these different scales and across distinct tendons is a necessary step forward to not only deepening generalizable understandings of tissue development and morphogenesis but developing optimized context-specific treatments for tendon injuries in the future.

### **A deeper examination of tenocyte mechanotransduction during varied muscle-contraction force contexts**

During vertebrate embryonic development, tenocyte mechanical-force sensing processes directly influence cell differentiation and maintenance (Subramanian et al., 2018; Subramanian & Schilling, 2015). In Chapter II of my thesis, I used RNA sequencing to probe genes responding to muscle contraction force in development and confirmed their mechano-responsive expression patterns using muscle-paralysis perturbation assays. I provided a module of genes likely to respond directly to muscle contraction force during development and showed through GO analysis that a number of these are ECM related. As many ECM proteins are beginning to be understood as force-induced mediators for cell signaling, these genes provide direction for further mechanistic studies. Though *ex vivo* studies have long confirmed differences in load-bearing capabilities between tendons, few studies have compared individual gene expression patterns between other tissues and individual tendons across varied temporal force-dynamic conditions *in vivo*, especially during development. In zebrafish cranial tendons, we confirmed previously unseen dual expressing populations of *matn1+/scxa+*, *klf2a+/scxa+*, and *mxra5b+/scxa+* tenocytes, with all three having expression in enthesal tenocytes. Interestingly, *klf2a* served as a novel enthesis marker for most cranial tendons, likely an extension of the role seen in transcriptional maintenance of a dual tenocyte/chondrocyte expression pattern in mouse limb (Kult et al., 2021). Using two independent muscle-paralysis perturbation assays and gene expression analyses in both whole embryos and sorted

tenocytes, we confirmed that differential expression of these genes is in fact due to muscle-contraction forces, and not purely developmental regulatory processes. We also gained an understanding into gene expression dynamics of *matn1*, *mxra5b*, and *klf2a* across varied force conditions, showing that individual tendons may transcriptionally control ECM gene expression to adapt tendon tissue to specific force-types, such as stabilization versus active contraction involved in organism movement, forces which are present in different stages of embryo development. The effects of tendon ECM mechanical properties resulting from these expression changes, as well as subsequent tenocyte mechanotransduction responses to these properties is a future avenue of study. Additionally, how individual tendon ECM is adaptively and globally remodeled in response to variations in force remains to be seen.

Studies modulating force amplitude and duration in vitro have begun to address these questions. In a tissue engineered tendon construct, shorter duration and lower frequency stimulation seemed to increase cell proliferation, and longer force duration significantly downregulated expression of ECM protein Decorin while increased stimulation frequency decreased tenocyte marker *Tnmd* expression (Engebretson et al., 2018). Decorin expression, for example, has been thought to modulate changes in age-related tendon structural and mechanical properties, which perhaps suggests that longer term contractile forces can have anti-aging effects on tendons themselves (Dunkman et al., 2013). Tissue tensile strength remained the same across all force intensities and durations, however (Engebretson et al., 2018). Higher intensity mechanical stretching force has also been shown to cause cultured tendon stem cells to upregulate chondrogenic, adipogenic, and osteogenic differentiation lineage markers versus tenogenic markers at lower strain intensities, which could suggest that during development the correct force conditions from muscle contraction and pre-tendon ECM has a role in tuning the correct cell fate and preventing dedifferentiation of TPCs (Subramanian & Schilling, 2015; J. Zhang & Wang, 2010). This work provides a platform for studying tenocyte force requirements in vivo in development and adds a new layer of complexity to tenocyte-ECM

dynamics, though future studies will be required to map gene expression and protein level changes at the scales of individual tenocyte populations across distinct tendons, force intensities, and temporal frequency and duration to fully characterize tissue level adaptations in various biological contexts. This is important to understand within specific tendons and would deepen the understanding of context specific cell-ECM feedback mechanisms, given the role of tenocytes as a force-sensitive cell type, and since tissue strength and mechanical properties vary dramatically between tendons and across subject age (Johnson et al., 1994; Maganaris & Paul, 2002).

### **Understanding cranial tenocyte heterogeneity and how inter-tendon physiological diversity influences intra-tendon ECM composition**

Though tenocyte populations at tendons of the trunk and limb are now much more well-characterized, populations at cranial tendons have been given less attention. In Chapter III I used single-cell RNA sequencing to investigate cranial tenocyte diversity and showed that not only do tenocytes of spatially distinct tendons transcriptionally cluster together, but ECM gene expression of attachment zones also differ between tendons, likely due to differences in both developmental expression patterns and the unique physiological characteristics of the specific tendon. Through *isHCRs* and computational analysis, I mapped out unique transcriptional markers of extraocular tendons, intermandibularis anterior tendons, ligaments, fin bud tendons, and the sternohyoideus central tendon. Further, through expression analysis, I showed that these tendons and ligaments likely have unique ECM compositions that fit the context of the function of their attaching tissue type and forces experienced, for example, high expression of basement membrane collagens in the extraocular and sternohyoideus central tendons, and low expression of FACIT collagens in ligaments and intermandibularis anterior tendons. Lastly, I described a novel population of canonical Wnt responsive tenocytes that inhabit ligaments and multiple cranial tendons. I show through five (two heatshock-inducible antagonist lines, two drug

antagonists, and one drug agonist) independent canonical Wnt perturbation methods, that a proper balance of Wnt signaling has a primary role in patterning of jaw MTJs. Recent research has suggested that Wnt signaling acts as an inhibitory signal to *Scx* expression, and that repression of Wnt in combination with activation of TGF- $\beta$  signaling combinatorially promotes *Scx* gene expression in the chick limb, suggesting a mechanism of control for Wnt in tenocyte differentiation (Garcia-Lee et al., 2021). Through computational cell-communication inference analysis, I provide putative source and sink cell populations by which canonical Wnt signaling may occur and address putative ligand and receptor targets for further mechanistic studies.

Though -omics technology has in recent years revolutionized the understanding of intra-tendon heterogeneity in disease contexts, the unique force and tissue microenvironment of different tendons has remained elusive. This work furthers understanding of comparative tenocyte diversity across tissues, for example the expression differences between cranial ligamentocytes and tenocytes, but future work will be required to characterize and validate functional roles for ECM gene expression diversity at these individual tendons. How signaling interactions changes from the varied load-bearing characteristics of these distinct tendons and how these feedback on these distinct differentiated tenocyte populations, respective tenocyte lineage trajectories, and the resulting ECM remodeling response is an avenue of continued research.

### **Further examining the transcriptional machinery driving tenocyte differentiation and fate maintenance**

Though the field of tendon biology has vastly improved interpretations of tenocyte diversity and lineage trajectories, the fundamental mechanism by which tenocyte specification occurs at the molecular level is not fully clear. Key transcription factors such as *Scx*, *Mkx*, *Egr1* and *Egr2* are well known to drive upregulation of tendon ECM structural genes, but the mechanism at the level of transcriptional control and subcellular localization is not clear. In

Chapter IV, we used TAP-MS to globally screen for putative binding factors to human SCX and MKX and found a multitude of potential protein interactors with each. Subsequent Co-immunoprecipitations and immunofluorescence assays confirmed E-box proteins TCF3, TCF4, and TCF12 as not only binding with SCX, but individually sufficient to cause subcellular translocation of the SCX complex from the cytoplasm to the nucleus of HEK293 cells. Though binding of E-box proteins to HLH transcription factors such as SCX have been previously verified and TCF3 has been confirmed to biochemically interact with SCX in other cell types, the discovery of TCF4 and TCF12 as binding partners and the nuclear translocation mechanism remains novel (Carlberg et al., 2000; Furumatsu et al., 2010). Future work will be required to address remaining questions: Is this mechanism viable in the MSC to TPC specification trajectory, and does endogenous SCX expression localize to the cytoplasm in MSCs? Does the binding of different E-box proteins to SCX serve a functional role beyond genetic redundancy for pathway robustness, such as TPC/tenocyte subpopulation lineage specification? This seems possible, as E proteins have been found to preferentially direct differentiation in other cell types, such as in neural progenitors, activating neural ASCL1/ATOH1 to differentiate progenitors to more specialized neurons while repressing neural NEUROG1/2 progenitors to fine tune neuronal population quantities (Le Dréau et al., 2018). In-vitro MSC/TPC knockdowns and conditional in-vivo knockouts at tenocyte developmental stages will pave the way for a more complete elucidation of the gene regulatory network controlling TPC specification and tenocyte differentiation and maintenance.

In conclusion, the exploration of tendon biology has undergone a remarkable transformation in recent years, revealing the dynamic nature of tendons at levels of detail previously unimaginable. The integration of -omics technologies, advanced imaging techniques, and in particular, in vivo functional validation, has enabled the dissection of tenocyte subpopulations, uncovering their unique responses to mechanical forces and distinct contributions to tissue composition. By examining the heterogeneity of cranial tenocyte

populations across distinct tendons and understanding the interplay between force dynamics and tenocyte gene expression, my thesis has contributed to the field's effort to paint a comprehensive picture of tendon diversity and adaptation across development and disease. Additionally, the investigation into transcriptional complexes guiding tenocyte specification, differentiation, and maintenance has provided novel insights into regulatory mechanisms underpinning tendon development. Collectively, these findings span from the scales of subcellular protein-protein interactions resulting from cell-ECM interactions up to multi-tissue morphogenesis, showing how mechanisms at each scale can feedback upon each other to constantly respond to changing internal and external conditions. Though focused on a developmental scale, these foundational insights extend beyond basic science. A better grasp of tenocyte diversity, mechanotransduction and tissue adaptation, and transcriptional regulation opens the door to optimizing context-specific therapeutic interventions long term. The journey towards comprehending the complexity of tendon biology is ongoing, but each advancement moves the field closer to understanding generalizable tissue morphogenesis principles and creating transformative clinical solutions for the future of tendon health and rehabilitation.

## References

- Ackerman, J. E., Best, K. T., Muscat, S. N., & Loiselle, A. E. (2021). Metabolic Regulation of Tendon Inflammation and Healing Following Injury. In *Current Rheumatology Reports* (Vol. 23, Issue 3). Springer. <https://doi.org/10.1007/s11926-021-00981-4>
- Adam, M., Potter, A. S., & Potter, S. S. (2017). Psychrophilic proteases dramatically reduce single-cell RNA-seq artifacts: a molecular atlas of kidney development. *Development (Cambridge, England)*, *144*(19), 3625. <https://doi.org/10.1242/DEV.151142>
- Alexander, C., Piloto, S., Le Pabic, P., & Schilling, T. F. (2014). Wnt Signaling Interacts with Bmp and Edn1 to Regulate Dorsal-Ventral Patterning and Growth of the Craniofacial Skeleton. *PLoS Genetics*, *10*(7). <https://doi.org/10.1371/journal.pgen.1004479>
- Al-Fageeh, M. B., & Smales, C. M. (2006). Control and regulation of the cellular responses to cold shock: The responses in yeast and mammalian systems. In *Biochemical Journal* (Vol. 397, Issue 2, pp. 247–259). <https://doi.org/10.1042/BJ20060166>
- Anderson, D. M., George, R., Noyes, M. B., Rowton, M., Liu, W., Jiang, R., Wolfe, S. A., Wilson-Rawls, J., & Rawls, A. (2012). *Characterization of the DNA-binding Properties of the Mohawk Homeobox Transcription Factor \* □ S*. <https://doi.org/10.1074/jbc.M112.399386>
- Bader, H. L., Keene, D. R., Charvet, B., Veit, G., Driever, W., Koch, M., & Ruggiero, F. (2009). Zebrafish collagen XII is present in embryonic connective tissue sheaths (fascia) and basement membranes. *Matrix Biology*, *28*(1), 32–43. <https://doi.org/10.1016/j.matbio.2008.09.580>
- Baneyx, G., Baugh, L., & Vogel, V. (2002). Fibronectin extension and unfolding within cell matrix fibrils controlled by cytoskeletal tension. *Proceedings of the National Academy of Sciences*, *99*(8), 5139–5143. <https://doi.org/10.1073/pnas.072650799>

- Bao, J., Zheng, J. J., & Wu, D. (2012). The Structural Basis of DKK-Mediated Inhibition of Wnt/LRP Signaling. *Science Signaling*, 5(224), pe22. <https://doi.org/10.1126/SCISIGNAL.2003028>
- Barakat, A. I. (1999). Responsiveness of vascular endothelium to shear stress: potential role of ion channels and cellular cytoskeleton (review). *International Journal of Molecular Medicine*. <https://doi.org/10.3892/ijmm.4.4.323>
- Barriga, E. H., Franze, K., Charras, G., & Mayor, R. (2018). Tissue stiffening coordinates morphogenesis by triggering collective cell migration in vivo. *Nature*, 554(7693), 523–527. <https://doi.org/10.1038/nature25742>
- Bella, J., & Hulmes, D. J. S. (2017). Fibrillar Collagens. In *Fibrous Proteins: Structure and Mechanisms* (pp. 457–490). <http://www.springer.com/series/6515>
- Bengtsson, E., Mörgelin, M., Sasaki, T., Timpl, R., Heinegård, D., & Aspberg, A. (2002). The Leucine-rich Repeat Protein PRELP Binds Perlecan and Collagens and May Function as a Basement Membrane Anchor. *Journal of Biological Chemistry*, 277(17), 15061–15068. <https://doi.org/10.1074/JBC.M108285200>
- Berthet, E., Chen, C., Butcher, K., Schneider, R. A., Alliston, T., & Amirtharajah, M. (2013). Smad3 binds Scleraxis and Mohawk and regulates tendon matrix organization. *Journal of Orthopaedic Research*, 31(9), 1475–1483. <https://doi.org/10.1002/JOR.22382>
- Bhattacharya, A., & Baker, N. E. (2011). A Network of Broadly Expressed HLH Genes Regulates Tissue-Specific Cell Fates. *Cell*, 147(4), 881–892. <https://doi.org/10.1016/j.cell.2011.08.055>
- Bhattacharyya, S., Chen, S. J., Wu, M., Warner-Blankenship, M., Ning, H., Lakos, G., Mori, Y., Chang, E., Nihijima, C., Takehara, K., Feghali-Bostwick, C., & Varga, J. (2008). Smad-Independent Transforming Growth Factor- $\beta$  Regulation of Early Growth Response-1 and

- Sustained Expression in Fibrosis: Implications for Scleroderma. *The American Journal of Pathology*, 173(4), 1085–1099. <https://doi.org/10.2353/AJPATH.2008.080382>
- Birk, D. E., & Brückner, P. (2011). Collagens, Suprastructures, and Collagen Fibril Assembly. *The Extracellular Matrix: An Overview*, 77–115. [https://doi.org/10.1007/978-3-642-16555-9\\_3](https://doi.org/10.1007/978-3-642-16555-9_3)
- Birk, D. E., & Bruckner, P. (2011). Collagens, Suprastructures, and Collagen Fibril Assembly. In *The Extracellular Matrix: An Overview* (pp. 77–115). [www.springer.com/series/8422](http://www.springer.com/series/8422)
- Bisell, M. J., & Barcellos-Hoff, M. H. (1987). The Influence of Extracellular Matrix on Gene Expression: Is Structure the Message? *Journal of Cell Science*, 1987(Supplement\_8), 327–343. [https://doi.org/10.1242/jcs.1987.Supplement\\_8.18](https://doi.org/10.1242/jcs.1987.Supplement_8.18)
- Bissell, M., & Glennhall, H. (1982). How Does the Extracellular Matrix Direct Gene Expression? In *J. theor. Biol* (Vol. 99).
- Blitz, E., Sharir, A., Akiyama, H., & Zelzer, E. (2013). Tendon-bone attachment unit is formed modularly by a distinct pool of Scx-and Sox9-positive progenitors. *Development (Cambridge)*, 140(13), 2680–2690. <https://doi.org/10.1242/dev.093906>
- Bobzin, L., Roberts, R. R., Chen, H.-J., Crump, J. G., & Merrill, A. E. (2021). *Development and maintenance of tendons and ligaments*. <https://doi.org/10.1242/dev.186916>
- Boon, R. A., Fledderus, J. O., Volger, O. L., Van Wanrooij, E. J. A., Pardali, E., Weesie, F., Kuiper, J., Pannekoek, H., Ten Dijke, P., & Horrevoets, A. J. G. (2007). *KLF2 Suppresses TGF-Signaling in Endothelium Through Induction of Smad7 and Inhibition of AP-1*. <https://doi.org/10.1161/01.ATV.0000256466.65450.ce>
- Borges, R., & García, A. G. (2021). One hundred years from Otto Loewi experiment, a dream that revolutionized our view of neurotransmission. *Pflugers Archiv European Journal of Physiology*, 473(6), 977–981. <https://doi.org/10.1007/s00424-021-02580-9>

- Boselli, F., Freund, J. B., & Julien Vermot, •. (2015). Blood flow mechanics in cardiovascular development. *Cellular and Molecular Life Sciences*, 72. <https://doi.org/10.1007/s00018-015-1885-3>
- Cai, L., Xiong, X., Kong, X., & Xie, J. (2017a). The Role of the Lysyl Oxidases in Tissue Repair and Remodeling: A Concise Review. *Tissue Engineering and Regenerative Medicine*, 14(1), 15. <https://doi.org/10.1007/S13770-016-0007-0>
- Cai, L., Xiong, X., Kong, X., & Xie, J. (2017b). The Role of the Lysyl Oxidases in Tissue Repair and Remodeling: A Concise Review. In *Tissue Engineering and Regenerative Medicine* (Vol. 14, Issue 1, pp. 15–30). Kluwer Academic Publishers. <https://doi.org/10.1007/s13770-016-0007-0>
- Caplan, A. I. (2017). Mesenchymal Stem Cells: Time to Change the Name! *Stem Cells Translational Medicine*, 6(6), 1445–1451. <https://doi.org/10.1002/sctm.17-0051>
- Carlberg, A. L., Tuan, R. S., & Hall, D. J. (2000). *Regulation of Scleraxis Function by Interaction with the bHLH Protein E47*. <https://doi.org/10.1006/mcbr.2000.0195>
- Chappell, D. C., Varner, S. E., Nerem, R. M., Medford, R. M., & Alexander, R. W. (1998). Oscillatory Shear Stress Stimulates Adhesion Molecule Expression in Cultured Human Endothelium. *Circulation Research*, 82(5), 532–539. <https://doi.org/10.1161/01.RES.82.5.532>
- Chen, B., Dodge, M. E., Tang, W., Lu, J., Ma, Z., Fan, C. W., Wei, S., Hao, W., Kilgore, J., Williams, N. S., Roth, M. G., Amatruda, J. F., Chen, C., & Lum, L. (2009). Small molecule–mediated disruption of Wnt-dependent signaling in tissue regeneration and cancer. *Nature Chemical Biology* 2009 5:2, 5(2), 100–107. <https://doi.org/10.1038/nchembio.137>
- Chen, H., & Boutros, P. C. (2011). *VennDiagram: a package for the generation of highly-customizable Venn and Euler diagrams in R*. <https://doi.org/10.1186/1471-2105-12-35>

- Chen, Y., Cossman, J., Jayasuriya, C. T., Li, X., Guan, Y., & Fonseca, V. (2016). Deficient Mechanical Activation of Anabolic Transcripts and Post-Traumatic Cartilage Degeneration in Matrilin-1 Knockout Mice. *PLoS ONE*, *11*(6), 156676.  
<https://doi.org/10.1371/journal.pone.0156676>
- Chen, Y. J., Jeng, J. H., Chang, H. H., Huang, M. Y., Tsai, F. F., & Jane Yao, C. C. (2013). Differential regulation of collagen, lysyl oxidase and MMP-2 in human periodontal ligament cells by low- and high-level mechanical stretching. *Journal of Periodontal Research*, *48*(4), 466–474.  
<https://doi.org/10.1111/jre.12028>
- Choi, H., Larsen, B., Lin, Z. Y., Breikreutz, A., Mellacheruvu, D., Fermin, D., Qin, Z. S., Tyers, M., Gingras, A. C., & Nesvizhskii, A. I. (2011). SAINT: Probabilistic scoring of affinity purification-mass spectrometry data. *Nature Methods*, *8*(1), 70–73. <https://doi.org/10.1038/nmeth.1541>
- Choi, H. M. T., Beck, V. A., & Pierce, N. A. (2014). *Next-Generation in Situ Hybridization Chain Reaction: Higher Gain, Lower Cost, Greater Durability*. <https://doi.org/10.1021/nn405717p>
- Chondrogianni, N., De, D., Simoes, C. M., Franceschi, C., & Gonos, E. S. (2004). Cloning of differentially expressed genes in skin fibroblasts from centenarians. *Biogerontology*.  
<https://doi.org/10.1007/s10522-004-3188-1>
- Christiansen, H. E., Lang, M. R., Pace, J. M., & Parichy, D. M. (2009). Critical early roles for col27a1a and col27a1b in zebrafish notochord morphogenesis, vertebral mineralization and post-embryonic axial growth. *PLoS ONE*, *4*(12). <https://doi.org/10.1371/journal.pone.0008481>
- Chuang, H. N., Hsiao, K. M., Chang, H. Y., Wu, C. C., & Pan, H. (2014). The homeobox transcription factor *Irx11* negatively regulates *MyoD* expression and myoblast differentiation. *FEBS Journal*, *281*(13), 2990–3003. <https://doi.org/10.1111/FEBS.12837>

- Comai, G. E., Tesařová, M., Dupé, V., Rhinn, M., Vallecillo-García, P., da Silva, F., Feret, B., Exelby, K., Dollé, P., Carlsson, L., Pryce, B., Spitz, F., Stricker, S., Zikmund, T., Kaiser, J., Briscoe, J., Schedl, A., Ghyselinck, N. B., Schweitzer, R., & Tajbakhsh, S. (2020). Local retinoic acid signaling directs emergence of the extraocular muscle functional unit. *PLoS Biology*, *18*(11). <https://doi.org/10.1371/journal.pbio.3000902>
- Cserjesi, P., Brown, D., Ligon, K. L., Lyons, G. E., Copeland, N. G., Gilbert, D. J., Jenkins, N. A., & Olson, E. N. (1995). Scleraxis: a basic helix-loop-helix protein that prefigures skeletal formation during mouse embryogenesis. *Development*, *121*, 1099–1110.
- D'Angelo, F., Tiribuzi, R., Armentano, I., Kenny, J. M., Martino, S., & Orlacchio, A. (2011). Mechanotransduction: Tuning Stem Cells Fate. *Journal of Functional Biomaterials*, *2*(2), 67–87. <https://doi.org/10.3390/jfb2020067>
- Davies, P. F. (2009). Hemodynamic shear stress and the endothelium in cardiovascular pathophysiology. *Nature Clinical Practice Cardiovascular Medicine*, *6*(1), 16–26. <https://doi.org/10.1038/ncpcardio1397>
- De Micheli, A. J., Swanson, J. B., Disser, N. P., Martinez, L. M., Walker, N. R., Oliver, D. J., Cosgrove, B. D., Christopher, X., & Mendias, L. (2020). Single-cell transcriptomic analysis identifies extensive heterogeneity in the cellular composition of mouse Achilles tendons. *Am J Physiol Cell Physiol*, *319*, 885–894. <https://doi.org/10.1152/ajpcell.00372.2020>.-Tendon
- Dickinson, M. E., Selleck, M. A. J., McMahon, A. P., & Bronner-Fraser, M. (1995). Dorsalization of the neural tube by the non-neural ectoderm. *Development*, *121*, 2099–2106.
- Discher, D. E., Janmey, P., & Wang, Y. (2005). Tissue Cells Feel and Respond to the Stiffness of Their Substrate. *Science*, *310*(5751), 1139–1143. <https://doi.org/10.1126/science.1116995>

- Dobin, A., Davis, C. A., Schlesinger, F., Drenkow, J., Zaleski, C., Jha, S., Batut, P., Chaisson, M., & Gingeras, T. R. (2013). *Sequence analysis STAR: ultrafast universal RNA-seq aligner*. *29*(1), 15–21. <https://doi.org/10.1093/bioinformatics/bts635>
- Dunkman, A. A., Buckley, M. R., Mienaltowski, M. J., Adams, S. M., Thomas, S. J., Satchell, L., Kumar, A., Pathmanathan, L., Beason, D. P., Iozzo, R. V., Birk, D. E., & Soslowky, L. J. (2013). Decorin expression is important for age-related changes in tendon structure and mechanical properties. *Matrix Biology*, *32*(1), 3–13. <https://doi.org/10.1016/j.matbio.2012.11.005>
- Ellingson, A. J., Pancheri, N. M., & Schiele, N. R. (2022). REGULATORS OF COLLAGEN CROSSLINKING IN DEVELOPING AND ADULT TENDONS. *European Cells & Materials*, *43*, 130. <https://doi.org/10.22203/ECM.V043A11>
- Engebretson, B., Mussett, Z. R., & Sikavitsas, V. I. (2018). The effects of varying frequency and duration of mechanical stimulation on a tissue-engineered tendon construct. *Connective Tissue Research*, *59*(2), 167–177. <https://doi.org/10.1080/03008207.2017.1324431>
- Espira, L., Lamoureux, L., Jones, S. C., Gerard, R. D., Dixon, I. M. C., & Czubryt, M. P. (2009). The basic helix-loop-helix transcription factor scleraxis regulates fibroblast collagen synthesis. *Journal of Molecular and Cellular Cardiology*, *47*(2), 188–195. <https://doi.org/10.1016/j.yjmcc.2009.03.024>
- Fabian, P., Tseng, K. C., Thirupathy, M., Arata, C., Chen, H. J., Smeeton, J., Nelson, N., & Crump, J. G. (2022). Lifelong single-cell profiling of cranial neural crest diversification in zebrafish. *Nature Communications*, *13*(1). <https://doi.org/10.1038/s41467-021-27594-w>
- Fang, F., Xiao, Y., Zelzer, E., Leong, K. W., & Thomopoulos, S. (2022). A mineralizing pool of Gli1-expressing progenitors builds the tendon enthesis and demonstrates therapeutic potential. *Cell Stem Cell*, *29*(12), 1669-1684.e6. <https://doi.org/10.1016/j.stem.2022.11.007>

- Folkman, J., & Moscona, A. (1978). Role of cell shape in growth control. In *Nature* (Vol. 273, Issue 1).
- Fujita, J. (1999). Cold shock response in mammalian cells. In *Article in Journal of Molecular Microbiology and Biotechnology*. <https://www.researchgate.net/publication/12376344>
- Furumatsu, T., Shukunami, C., Amemiya-Kudo, M., Shimano, H., & Ozaki, T. (2010). Scleraxis and E47 cooperatively regulate the Sox9-dependent transcription. *The International Journal of Biochemistry & Cell Biology*, 42, 148–156. <https://doi.org/10.1016/j.biocel.2009.10.003>
- Gabrielsen, A., Lawler, P. R., Yongzhong, W., Steinbrüchel, D., Blagoja, D., Paulsson-Berne, G., Kastrup, J., & Hansson, G. K. (2007). *Gene expression signals involved in ischemic injury, extracellular matrix composition and fibrosis defined by global mRNA profiling of the human left ventricular myocardium*. <https://doi.org/10.1016/j.yjmcc.2006.12.016>
- García-Lee, V., Díaz-Hernandez, M. E., & Chimal-Monroy, J. (2021). Inhibition of WNT/b-catenin is necessary and sufficient to induce scx expression in developing tendons of chicken limb. *International Journal of Developmental Biology*, 65(5–6), 395–401. <https://doi.org/10.1387/ijdb.200166jc>
- Garcia-Lee, V., Díaz-Hernandez, M. E., & Chimal-Monroy, J. (2021). Inhibition of WNT/ $\beta$ -catenin is necessary and sufficient to induce Scx expression in developing tendons of chicken limb. *The International Journal of Developmental Biology*, 65(4-5–6), 395–401. <https://doi.org/10.1387/ijdb.200166jc>
- Gomez, M. A., Amiel, D., Bitter, M. A., Gelberman, R. H., & Akeson, W. H. (1981). The Effects of Exercise on the Biomechanical and Biochemical Properties of Swine Digital Flexor Tendons. *Journal of Biomechanical Engineering*, 103, 51–56. [http://asmedigitalcollection.asme.org/biomechanical/article-pdf/103/1/51/5647918/51\\_1.pdf](http://asmedigitalcollection.asme.org/biomechanical/article-pdf/103/1/51/5647918/51_1.pdf)

- Gospodarowicz, D., Greenburg, G., & Birdwell, C. R. (1978). Determination of Cellular Shape by the Extracellular Matrix and Its Correlation with the Control of Cellular Growth<sup>1</sup>. *Cancer Research*, 38, 4155–4171. [http://aacrjournals.org/cancerres/article-pdf/38/11\\_Part\\_2/4155/2401143/cr03811p24155.pdf](http://aacrjournals.org/cancerres/article-pdf/38/11_Part_2/4155/2401143/cr03811p24155.pdf)
- Guerquin, M. J., Charvet, B., Nourissat, G., Havis, E., Ronsin, O., Bonnin, M. A., Ruggiu, M., Olivera-Martinez, I., Robert, N., Lu, Y., Kadler, K. E., Baumberger, T., Doursounian, L., Berenbaum, F., & Duprez, D. (2013). Transcription factor EGR1 directs tendon differentiation and promotes tendon repair. *The Journal of Clinical Investigation*, 123(8), 3564–3576. <https://doi.org/10.1172/JCI67521>
- Guo, H., Gao, Z., & Chen, W. (2016). Contractile Force of Human Extraocular Muscle: A Theoretical Analysis. *Applied Bionics and Biomechanics*, 2016. <https://doi.org/10.1155/2016/4091824>
- Guo, X., Day, T. F., Jiang, X., Garrett-Beal, L., Topol, L., & Yang, Y. (2004). Wnt/ $\beta$ -catenin signaling is sufficient and necessary for synovial joint formation. *Genes and Development*, 18(19), 2404–2417. <https://doi.org/10.1101/gad.1230704>
- Hall, M. S., Alisafaei, F., Ban, E., Feng, X., Hui, C. Y., Shenoy, V. B., & Wu, M. (2016). Fibrous nonlinear elasticity enables positive Mechanical feedback between cells and ECMs. *Proceedings of the National Academy of Sciences of the United States of America*, 113(49), 14043–14048. <https://doi.org/10.1073/pnas.1613058113>
- Hamada, H. (2015). Role of physical forces in embryonic development. *Seminars in Cell & Developmental Biology*, 47, 88–91. <https://doi.org/10.1016/j.semcd.2015.10.011>
- Hao, Y., Hao, S., Andersen-Nissen, E., Mauck, W. M., Zheng, S., Butler, A., Lee, M. J., Wilk, A. J., Darby, C., Zager, M., Hoffman, P., Stoeckius, M., Papalex, E., Mimitou, E. P., Jain, J., Srivastava, A., Stuart, T., Fleming, L. M., Yeung, B., ... Satija, R. (2021). Integrated analysis of

multimodal single-cell data. *Cell*, 184(13), 3573-3587.e29.

<https://doi.org/10.1016/J.CELL.2021.04.048>

Harvey, T., Flamenco, S., & Fan, C. M. (2019). A Tpp3 + Pdgfra + tendon stem cell population contributes to regeneration and reveals a shared role for PDGF signalling in regeneration and fibrosis. *Nature Cell Biology*, 21(12), 1490–1503. <https://doi.org/10.1038/s41556-019-0417-z>

Havis, E., Bonnin, M. A., Olivera-Martinez, I., Nazaret, N., Ruggiu, M., Weibel, J., Durand, C., Guerquin, M. J., Bonod-Bidaud, C., Ruggiero, F., Schweitzer, R., & Duprez, D. (2014). Transcriptomic analysis of mouse limb tendon cells during development. *Development (Cambridge)*, 141(19), 3683–3696. <https://doi.org/10.1242/dev.108654>

He, Y., Chen, X., Liu, H., Xiao, H., Kwapong, W. R., & Mei, J. (2015). Matrix-remodeling associated 5 as a novel tissue biomarker predicts poor prognosis in non-small cell lung cancers. *Cancer Biomarkers*, 15(5), 645–651. <https://doi.org/10.3233/CBM-150504>

Herchenhan, A., Bayer, M. L., Svensson, R. B., Magnusson, S. P., & Kjaer, M. (2013). In vitro tendon tissue development from human fibroblasts demonstrates collagen fibril diameter growth associated with a rise in mechanical strength. *Developmental Dynamics*, 242(1), 2–8. <https://doi.org/10.1002/dvdy.23896>

Hertle, R. W., Chan, C. C., Galita, D. A., Maybodi, M., & Crawford, M. A. (2002). Neuroanatomy of the extraocular muscle tendon enthesis in macaque, normal human, and patients with congenital nystagmus. *Journal of AAPOS*, 6(5), 319–327. <https://doi.org/10.1067/mpa.2002.127116>

Hjorten, R., Hansen, U., Underwood, R. A., Telfer, H. E., Fernandes, R. J., Krakow, D., Sebald, E., Wachsmann-Hogiu, S., Bruckner, P., Jacquet, R., Landis, W. J., Byers, P. H., & Pace, J. M. (2007). Type XXVII collagen at the transition of cartilage to bone during skeletogenesis. *Bone*, 41(4), 535–542. <https://doi.org/10.1016/j.bone.2007.06.024>

- Huang, D. W., Sherman, B. T., & Lempicki, R. A. (2008). *Systematic and integrative analysis of large gene lists using DAVID bioinformatics resources*. <https://doi.org/10.1038/nprot.2008.211>
- Huang, R.-P., Fan, Y., Peng, A., Zeng, Z.-L., Reed, J. C., Adamson, E. D., & Boynton, A. L. (1998). Suppression of human fibrosarcoma cell growth by transcription factor, Egr-1, involves down-regulation of Bcl-2. *International Journal of Cancer*, *77*(6), 880–886.  
[https://doi.org/10.1002/\(SICI\)1097-0215\(19980911\)77:6<880::AID-IJC14>3.0.CO;2-5](https://doi.org/10.1002/(SICI)1097-0215(19980911)77:6<880::AID-IJC14>3.0.CO;2-5)
- Huang, S. M. A., Mishina, Y. M., Liu, S., Cheung, A., Stegmeier, F., Michaud, G. A., Charlat, O., Wiellette, E., Zhang, Y., Wiessner, S., Hild, M., Shi, X., Wilson, C. J., Mickanin, C., Myer, V., Fazal, A., Tomlinson, R., Serluca, F., Shao, W., ... Cong, F. (2009). Tankyrase inhibition stabilizes axin and antagonizes Wnt signalling. *Nature* *2009* *461*:7264, *461*(7264), 614–620.  
<https://doi.org/10.1038/nature08356>
- Huang, Z., Yin, Z., Xu, J., Fei, Y., Heng, B. C., Jiang, X., Chen, W., & Shen, W. (2021). Tendon Stem/Progenitor Cell Subpopulations and Their Implications in Tendon Biology. *Frontiers in Cell and Developmental Biology*, *9*. <https://doi.org/10.3389/fcell.2021.631272>
- Hynes, R. O., & Yamada, K. M. (1982). Fibronectins: Multifunctional Modular Glycoproteins. *Journal of Cell Biology*, *95*(2), 369–377. <http://rupress.org/jcb/article-pdf/95/2/369/1641134/369.pdf>
- Ireland, D., Harrall, R., Curry, V., Holloway, G., Hackney, R., Hazleman, B., & Riley, G. (2001). Multiple changes in gene expression in chronic human Achilles tendinopathy. *Matrix Biology*, *20*, 159169.
- Isabella, A. J., & Horne-Badovinac, S. (2016). Rab10-Mediated Secretion Synergizes with Tissue Movement to Build a Polarized Basement Membrane Architecture for Organ Morphogenesis In Brief. *Developmental Cell*, *38*, 47–60. <https://doi.org/10.1016/j.devcel.2016.06.009>

- Izu, Y., Adams, S. M., Connizzo, B. K., Beason, D. P., Soslowsky, L. J., Koch, M., & Birk, D. E. (2021). Collagen XII mediated cellular and extracellular mechanisms regulate establishment of tendon structure and function. *Matrix Biology*, *95*, 52–67.  
<https://doi.org/10.1016/j.matbio.2020.10.004>
- Jain, N., Mahendran, R., Philp, R., Guy, G. R., Tan, Y. H., & Cao, X. (1996). Casein Kinase II Associates with Egr-1 and Acts as a Negative Modulator of Its DNA Binding and Transcription Activities in NIH 3T3 Cells. *Journal of Biological Chemistry*, *271*(23), 13530–13536.  
<https://doi.org/10.1074/jbc.271.23.13530>
- Jenkins, E., Moss, J. B., Pace, J. M., & Bridgewater, L. C. (2005). The new collagen gene COL27A1 contains SOX9-responsive enhancer elements. *Matrix Biology*, *24*(3), 177–184.  
<https://doi.org/10.1016/j.matbio.2005.02.004>
- Jeon, H., Tsui, J. H., Jang, S. I., Lee, J. H., Park, S., Mun, K., Boo, Y. C., & Kim, D.-H. (2015). Combined Effects of Substrate Topography and Stiffness on Endothelial Cytokine and Chemokine Secretion. *ACS Applied Materials & Interfaces*, *7*(8), 4525–4532.  
<https://doi.org/10.1021/acsami.5b00554>
- Jin, S., Guerrero-Juarez, C. F., Zhang, L., Chang, I., Ramos, R., Kuan, C. H., Myung, P., Plikus, M. V., & Nie, Q. (2021). Inference and analysis of cell-cell communication using CellChat. *Nature Communications* *2021 12:1*, *12*(1), 1–20. <https://doi.org/10.1038/s41467-021-21246-9>
- Johnson, G. A., Tramaglino, D. M., Levine, R. E., Ohno, K., Choi, N.-Y., & L-Y. Woo, S. (1994). Tensile and viscoelastic properties of human patellar tendon. *Journal of Orthopaedic Research*, *12*(6), 796–803. <https://doi.org/10.1002/jor.1100120607>
- Kaji, D. A., Montero, A. M., Patel, R., & Huang, A. H. (2021). *Transcriptional profiling of mESC-derived tendon and fibrocartilage cell fate switch*. <https://doi.org/10.1038/s41467-021-24535-5>

- Kang, J. S., Alliston, T., Delston, R., & Derynck, R. (2005). Repression of Runx2 function by TGF- $\beta$  through recruitment of class II histone deacetylases by Smad3. *EMBO Journal*, 24(14), 2543–2555. <https://doi.org/10.1038/SJ.EMBOJ.7600729>
- Kannus, P. (2000). Structure of the tendon connective tissue. *Scandinavian Journal of Medicine & Science in Sports*, 10(6), 312–320. <https://doi.org/10.1034/J.1600-0838.2000.010006312.X>
- Katsumi, A., Orr, A. W., Tzima, E., & Schwartz, M. A. (2004). Integrins in Mechanotransduction. *Journal of Biological Chemistry*, 279(13), 12001–12004. <https://doi.org/10.1074/jbc.R300038200>
- Karlsen, A., Gonzalez-Franquesa, A., Jakobsen, J. R., Krogsgaard, M. R., Koch, M., Kjaer, M., Schiaffino, S., Mackey, A. L., & Deshmukh, A. S. (2022). The proteomic profile of the human myotendinous junction. *iScience*, 25(2). <https://doi.org/10.1016/j.isci.2022.103836>
- Keller, R., Shook, D., & Skoglund, P. (2008). The forces that shape embryos: Physical aspects of convergent extension by cell intercalation. In *Physical Biology* (Vol. 5, Issue 1). Institute of Physics Publishing. <https://doi.org/10.1088/1478-3975/5/1/015007>
- Khoshnoodi, J., Pedchenko, V., & Hudson, B. G. (2008). Mammalian collagen IV. In *Microscopy Research and Technique* (Vol. 71, Issue 5, pp. 357–370). <https://doi.org/10.1002/jemt.20564>
- Kim, M., Franke, V., Brandt, B., Lowenstein, E. D., Schöwel, V., Spuler, S., Akalin, A., & Birchmeier, C. (2020). Single-nucleus transcriptomics reveals functional compartmentalization in syncytial skeletal muscle cells. *Nature Communications*, 11(1). <https://doi.org/10.1038/s41467-020-20064-9>
- Kim, S.-G., Akaike, T., Sasagawa, T., Atomi, Y., & Kurosawa, H. (2002). Gene Expression of Type I and Type III Collagen by Mechanical Stretch in Anterior Cruciate Ligament Cells. In *CELL STRUCTURE AND FUNCTION* (Vol. 27). <http://www.ncbi.nih.gov>

- Kimmel, C. B., Ballard, W. W., Kimmel, S. R., Ullmann, B., & Schilling, T. F. (1995a). Stages of embryonic development of the zebrafish. *Developmental Dynamics*, 203(3), 253–310.  
<https://doi.org/10.1002/AJA.1002030302>
- Kimmel, C. B., Ballard, W. W., Kimmel, S. R., Ullmann, B., & Schilling, T. F. (1995b). Stages of embryonic development of the zebrafish. *Developmental Dynamics*, 203(3), 253–310.  
<https://doi.org/10.1002/AJA.1002030302>
- Kimura, W., Machii, M., Xue, X. D., Sultana, N., Hikosaka, K., Sharkar, M. T. K., Uezato, T., Matsuda, M., Koseki, H., & Miura, N. (2011). Irx11 mutant mice show reduced tendon differentiation and no patterning defects in musculoskeletal system development. In *Genesis* (Vol. 49, Issue 1, pp. 2–9). <https://doi.org/10.1002/dvg.20688>
- Kishimoto, Y., Ohkawara, B., Sakai, T., Ito, M., Masuda, A., Ishiguro, N., Shukunami, C., Docheva, D., & Ohno, K. (2017). Wnt/ $\beta$ -catenin signaling suppresses expressions of Scx, Mxk, and Tnmd in tendon-derived cells. *PLoS ONE*, 12(7). <https://doi.org/10.1371/journal.pone.0182051>
- Kishore, V., Bullock, W., Sun, X., Van Dyke, W. S., & Akkus, O. (2012). Tenogenic differentiation of human MSCs induced by the topography of electrochemically aligned collagen threads. *Biomaterials*, 33(7), 2137–2144. <https://doi.org/10.1016/j.biomaterials.2011.11.066>
- Krammer, A., Craig, D., Thomas, W. E., Schulten, K., & Vogel, V. (2002). A structural model for force regulated integrin binding to fibronectin's RGD-synergy site. *Matrix Biology*, 21(2), 139–147.  
[https://doi.org/10.1016/S0945-053X\(01\)00197-4](https://doi.org/10.1016/S0945-053X(01)00197-4)
- Kolahi, K. S., & Mofrad, M. R. K. (2010). Mechanotransduction: a major regulator of homeostasis and development. *WIREs Systems Biology and Medicine*, 2(6), 625–639.  
<https://doi.org/10.1002/wsbm.79>

- Kult, S., Olender, T., Osterwalder, M., Markman, S., Leshkowitz, D., Krief, S., Blecher-Gonen, R., Ben-Moshe, S., Farack, L., Keren-Shaul, H., Salame, T.-M., Capellini, T. D., Itzkovitz, S., Amit, I., Visel, A., & Zelzer, E. (2021). Bi-fated tendon-to-bone attachment cells are regulated by shared enhancers and KLF transcription factors. *ELife*. <https://doi.org/10.7554/eLife.55361>
- Laczko, R., & Csiszar, K. (2020). Lysyl oxidase (Lox): Functional contributions to signaling pathways. In *Biomolecules* (Vol. 10, Issue 8, pp. 1–16). MDPI AG. <https://doi.org/10.3390/biom10081093>
- Lamberti, P. M., & Wezeman, F. H. (2002). Biologic Behavior of an In Vitro Hydrated Collagen Gel-Human Tenocyte Tendon Model. *Clinical Orthopaedics and Related Research*, 397, 414–423. <https://doi.org/10.1097/00003086-200204000-00049>
- Lassar, A. B., Davis, R. L., Wright, W. E., Kadesch, T., Murre, C., Voronova, A., Baltimore, D., & Weintraub, H. (1991). *Functional Activity of Myogenic HLH Proteins Requires Hetero-Oligomerization with E12/E47-like Proteins In Vivo* (Vol. 66).
- Le Dréau, G., Escalona, R., Fueyo, R., Herrera, A., Martínez, J. D., Usieto, S., Menendez, A., Pons, S., Martínez-Balbas, M. A., & Martí, E. (2018). E proteins sharpen neurogenesis by modulating proneural bHLH transcription factors' activity in an E-box-dependent manner. *ELife*, 7. <https://doi.org/10.7554/eLife.37267>
- Lee, C. G., Cho, S. J., Kang, M. J., Chapoval, S. P., Lee, P. J., Noble, P. W., Yehualaeshet, T., Lu, B., Flavell, R. A., Milbrandt, J., Homer, R. J., & Elias, J. A. (2004). Early Growth Response Gene 1-mediated Apoptosis Is Essential for Transforming Growth Factor  $\beta$ 1-induced Pulmonary Fibrosis. *The Journal of Experimental Medicine*, 200(3), 377. <https://doi.org/10.1084/JEM.20040104>
- Lee, G. M., & Loeser, R. F. (1999). Cell Surface Receptors Transmit Sufficient Force to Bend Collagen Fibrils. *Experimental Cell Research*, 248(1), 294–305. <https://doi.org/10.1006/excr.1999.4418>

- Lee, J. S., Yu, Q., Shin, J. T., Sebzda, E., Bertozzi, C., Chen, M., Mericko, P., Stadtfeld, M., Zhou, D., Cheng, L., Graf, T., MacRae, C. A., Lepore, J. J., Lo, C. W., & Kahn, M. L. (2006). Klf2 Is an Essential Regulator of Vascular Hemodynamic Forces In Vivo. *Developmental Cell*, 11(6), 845–857. <https://doi.org/10.1016/j.devcel.2006.09.006>
- Lejard, V., Blais, F., Guerquin, M. J., Bonnet, A., Bonnin, M. A., Havis, E., Malbouyres, M., Bidaud, C. B., Maro, G., Gilardi-Hebenstreit, P., Rossert, J., Ruggiero, F., & Duprez, D. (2011). EGR1 and EGR2 involvement in vertebrate tendon differentiation. *Journal of Biological Chemistry*, 286(7), 5855–5867. <https://doi.org/10.1074/jbc.M110.153106>
- Léjard, V., Brideau, G., Blais, F., Salingcarnboriboon, R., Wagner, G., Roehrl, M. H. A., Noda, M., Duprez, D., Houillier, P., & Rossert, J. (2007). Scleraxis and NFATc regulate the expression of the pro- $\alpha$ 1(I) collagen gene in tendon fibroblasts. *Journal of Biological Chemistry*, 282(24), 17665–17675. <https://doi.org/10.1074/jbc.M610113200>
- Li, B., & Dewey, C. N. (2011). RSEM: accurate transcript quantification from RNA-Seq data with or without a reference genome. *BMC Bioinformatics*, 12, 323. <https://doi.org/10.1186/1471-2105-12-323>
- Li, H., Wang, Y., Liu, J., Chen, X., Duan, Y., Wang, X., Shen, Y., Kuang, Y., Zhuang, T., Tomlinson, B., Chan, P., Yu, Z., Cheng, Y., Zhang, L., Liu, Z., Zhang, Y., Zhao, Z., Zhang, Q., & Liu, J. (2021). Endothelial Klf2-Foxp1-TGF $\beta$  signal mediates the inhibitory effects of simvastatin on maladaptive cardiac remodeling. 11(4), 4. <https://doi.org/10.7150/thno.48153>
- Li, X., Decker, M., & Westendorf, J. J. (2010). TEThered to Runx: Novel binding partners for runx factors. *Blood Cells, Molecules, and Diseases*, 45(1), 82–85. <https://doi.org/10.1016/j.bcmd.2010.03.002>

- Li, X., Wang, W., & Chen, J. (2015). From pathways to networks: Connecting dots by establishing protein-protein interaction networks in signaling pathways using affinity purification and mass spectrometry. *Proteomics*, *15*, 188–202. <https://doi.org/10.1002/pmic.201400147>
- Liu, D., Black, B. L., & Derynck, R. (2001). *TGF-inhibits muscle differentiation through functional repression of myogenic transcription factors by Smad3*. <https://doi.org/10.1101/gad.925901>
- Liu, H., Xu, J., & Jiang, R. (2019). Mxk-Deficient Mice Exhibit Hedgehog Signaling-Dependent Ectopic Ossification in the Achilles Tendons. *Journal of Bone and Mineral Research*, *34*(3), 557–569. <https://doi.org/10.1002/jbmr.3630>
- Loebel, C., Mauck, R. L., & Burdick, J. A. (2019). Local nascent protein deposition and remodelling guide mesenchymal stromal cell mechanosensing and fate in three-dimensional hydrogels. *Nature Materials*, *18*(8), 883–891. <https://doi.org/10.1038/s41563-019-0307-6>
- Lu, H. H., & Thomopoulos, S. (2013). *Functional Attachment of Soft Tissues to Bone: Development, Healing, and Tissue Engineering*. <https://doi.org/10.1146/annurev-bioeng-071910-124656>
- Maeda, E., Fleischmann, C., Mein, C. A., Shelton, J. C., Bader, D. L., & Lee, D. A. (2010). Functional analysis of tenocytes gene expression in tendon fascicles subjected to cyclic tensile strain. *Connective Tissue Research*, *51*(6), 434–444. <https://doi.org/10.3109/03008201003597056>
- Maeda, E., Sugimoto, M., & Ohashi, T. (2013). Cytoskeletal tension modulates MMP-1 gene expression from tenocytes on micropillar substrates. *Journal of Biomechanics*, *46*(5), 991–997. <https://doi.org/10.1016/j.jbiomech.2012.11.056>
- Maeda, T., Sakabe, T., Sunaga, A., Sakai, K., Rivera, A. L., Keene, D. R., Sasaki, T., Stavnezer, E., Iannotti, J., Schweitzer, R., Ilic, D., Baskaran, H., & Sakai, T. (2011a). Conversion of Mechanical Force into TGF- $\beta$ -Mediated Biochemical Signals. *Current Biology*, *21*, 933–941. <https://doi.org/10.1016/j.cub.2011.04.007>

- Maeda, T., Sakabe, T., Sunaga, A., Sakai, K., Rivera, A. L., Keene, D. R., Sasaki, T., Stavnezer, E., Iannotti, J., Schweitzer, R., Ilic, D., Baskaran, H., & Sakai, T. (2011b). Conversion of mechanical force into TGF- $\beta$ -mediated biochemical signals. *Current Biology*, *21*(11), 933–941. <https://doi.org/10.1016/j.cub.2011.04.007>
- Maganaris, C. N., & Paul, J. P. (2002). Tensile properties of the in vivo human gastrocnemius tendon. *Journal of Biomechanics*, *35*(12), 1639–1646. [https://doi.org/10.1016/S0021-9290\(02\)00240-3](https://doi.org/10.1016/S0021-9290(02)00240-3)
- Makris, E. A., Responde, D. J., Paschos, N. K., Hu, J. C., & Athanasiou, K. A. (2014). Developing functional musculoskeletal tissues through hypoxia and lysyl oxidase-induced collagen cross-linking. *Proceedings of the National Academy of Sciences of the United States of America*, *111*(45), E4832–E4841. <https://doi.org/10.1073/pnas.1414271111>
- Marturano, J. E., Arena, J. D., Schiller, Z. A., Georgakoudi, I., & Kuo, C. K. (2013). Characterization of mechanical and biochemical properties of developing embryonic tendon. *Proceedings of the National Academy of Sciences of the United States of America*, *110*(16), 6370–6375. <https://doi.org/10.1073/pnas.1300135110>
- McGurk, P. D., Swartz, M. E., Chen, J. W., Galloway, J. L., & Eberhart, J. K. (2017). In vivo zebrafish morphogenesis shows Cyp26b1 promotes tendon condensation and musculoskeletal patterning in the embryonic jaw. *PLoS Genetics*, *13*(12). <https://doi.org/10.1371/journal.pgen.1007112>
- Mcneilly, C. M., Banes, A. J., Benjamin' And, M., & Ralphs', J. R. (1996). Tendon cells in vivo form a three dimensional network of cell processes linked by gap junctions. *J. Anat*, *189*, 593–600.
- Meijer, L., Skaltsounis, A. L., Magiatis, P., Polychronopoulos, P., Knockaert, M., Leost, M., Ryan, X. P., Vonica, C. A., Brivanlou, A., Dajani, R., Crovace, C., Tarricone, C., Musacchio, A., Roe, S. M., Pearl, L., & Greengard, P. (2003). GSK-3-Selective Inhibitors Derived from Tyrian Purple

Indirubins. *Chemistry & Biology*, 10(12), 1255–1266.

<https://doi.org/10.1016/J.CHEMBIOL.2003.11.010>

Meng, R., Song, M., & Pan, J. (2015). Rho is involved in periodontal tissue remodelling with experimental tooth movement in rats. *Archives of Oral Biology*, 60(6), 923–931.

<https://doi.org/10.1016/j.archoralbio.2015.01.017>

Merabet, S., & Mann, R. S. (2016). To Be Specific or Not: The Critical Relationship Between Hox And TALE Proteins. *Trends in Genetics*, 32(6), 334–347.

<https://doi.org/10.1016/j.tig.2016.03.004>

Metsalu, T., & Vilo, J. (2015). ClustVis: a web tool for visualizing clustering of multivariate data using Principal Component Analysis and heatmap. *Web Server Issue Published Online*, 43.

<https://doi.org/10.1093/nar/gkv468>

Mi, H., & Thomas, P. (n.d.). *PANTHER Pathway: An Ontology-Based Pathway Database Coupled with Data Analysis Tools*. [https://doi.org/10.1007/978-1-60761-175-2\\_7](https://doi.org/10.1007/978-1-60761-175-2_7)

Mienaltowski, M. J., & Birk, D. E. (2014). Structure, Physiology, and Biochemistry of Collagens. In *Progress in Heritable Soft Connective Tissue Diseases* (pp. 5–29).

<http://www.springer.com/series/5584>

Ming, Z., Vining, B., Bagheri-Fam, S., & Harley, V. (2022). SOX9 in organogenesis: shared and unique transcriptional functions. *Cellular and Molecular Life Sciences*, 79(10).

<https://doi.org/10.1007/s00018-022-04543-4>

Nakagawa, Y., Nishikimi, T., & Kuwahara, K. (2019). Atrial and brain natriuretic peptides: Hormones secreted from the heart. *Peptides*, 111, 18–25. <https://doi.org/10.1016/j.peptides.2018.05.012>

- Nödl, M. T., Tsai, S. L., & Galloway, J. L. (2022). The impact of Drew Noden's work on our understanding of craniofacial musculoskeletal integration. In *Developmental Dynamics* (Vol. 251, Issue 8, pp. 1250–1266). John Wiley and Sons Inc. <https://doi.org/10.1002/dvdy.471>
- O'Flanagan, C. H., Campbell, K. R., Zhang, A. W., Kabeer, F., P Lim, J. L., Biele, J., Eirew, P., Lai, D., McPherson, A., Kong, E., Bates, C., Borkowski, K., Wiens, M., Hewitson, B., Hopkins, J., Pham, J., Ceglia, N., Moore, R., Mungall, A. J., ... Aparicio, S. (2019). Dissociation of solid tumor tissues with cold active protease for single-cell RNA-seq minimizes conserved collagenase-associated stress responses. *Genome Biology*. <https://doi.org/10.1186/s13059-019-1830-0>
- Olivares-Navarrete, R., Lee, E. M., Smith, K., Hyzy, S. L., Doroudi, M., Williams, J. K., Gall, K., Boyan, B. D., & Schwartz, Z. (2017). Substrate Stiffness Controls Osteoblastic and Chondrocytic Differentiation of Mesenchymal Stem Cells without Exogenous Stimuli. *PLOS ONE*, 12(1), e0170312. <https://doi.org/10.1371/journal.pone.0170312>
- Pan, X. S., Li, J., Brown, E. B., & Kuo, C. K. (2018). Embryo movements regulate tendon mechanical property development. *Philosophical Transactions of the Royal Society B: Biological Sciences*, 373(1759). <https://doi.org/10.1098/rstb.2017.0325>
- Patoine, A., Husseini, A., Kasaai, B., Gaumond, M. H., & Moffatt, P. (2017). The osteogenic cell surface marker BRIL/IFITM5 is dispensable for bone development and homeostasis in mice. *PLOS ONE*, 12(9), e0184568. <https://doi.org/10.1371/JOURNAL.PONE.0184568>
- Pei, M., Luo, J., & Chen, Q. (2008). Enhancing and maintaining chondrogenesis of synovial fibroblasts by cartilage extracellular matrix protein matrilins. *Osteoarthritis and Cartilage*, 16(9), 1110–1117. <https://doi.org/10.1016/j.joca.2007.12.011>
- Pfaffl, M. W. (2001). A new mathematical model for relative quantification in real-time RT-PCR. *Nucleic Acids Research*, 29(9), 0.

- Picelli, S., Faridani, O. R., Bj, sa K., Winberg, sta, Sagasser, S., & Sandberg, R. (2013). Full-length RNA-seq from single cells using Smart-seq2. *Nature Protocols*.  
<https://doi.org/10.1038/nprot.2014.006>
- Pingel, J., Lu, Y., Starborg, T., Fredberg, U., Langberg, H., Nedergaard, A., Weis, M., Eyre, D., Kjaer, M., & Kadler, K. E. (2014). 3-D ultrastructure and collagen composition of healthy and overloaded human tendon: Evidence of tenocyte and matrix buckling. *Journal of Anatomy*, 224(5), 548–555. <https://doi.org/10.1111/JOA.12164>
- Plumb, D. A., Ferrara, L., Torbica, T., Knowles, L., Mironov, A., Kadler, K. E., Briggs, M. D., & Boot-Handford, R. P. (2011). Collagen XXVII organises the pericellular matrix in the growth plate. *PLoS ONE*, 6(12). <https://doi.org/10.1371/journal.pone.0029422>
- Poveda, J., Sanz, A. B., Fernandez-Fernandez, B., Carrasco, S., Ruiz-Ortega, M., Cannata-Ortiz, P., Ortiz, A., & Sanchez-Ni ~ No, M. D. (2017). MXRA5 is a TGF-b1-regulated human protein with anti-inflammatory and anti-fibrotic properties. *J. Cell. Mol. Med.*, 21(1), 154–164.  
<https://doi.org/10.1111/jcmm.12953>
- Powell, L. M., & Jarman, A. P. (2008). Context dependence of proneural bHLH proteins. In *Current Opinion in Genetics and Development* (Vol. 18, Issue 5, pp. 411–417).  
<https://doi.org/10.1016/j.gde.2008.07.012>
- Pryce, B. A., Watson, S. S., Murchison, N. D., Staverosky, J. A., Dünker, N., & Schweitzer, R. (2009). Recruitment and maintenance of tendon progenitors by TGFB signaling are essential for tendon formation. *Development*, 136(8), 1351–1361. <https://doi.org/10.1242/dev.027342>
- Qi, Y., & Xu, R. (2018). Roles of PLODs in Collagen Synthesis and Cancer Progression. *Frontiers in Cell and Developmental Biology*, 6(JUN), 66. <https://doi.org/10.3389/FCELL.2018.00066>

- Ricard-Blum, S. (2011). The Collagen Family. *Cold Spring Harbor Perspectives in Biology*, 3(1), 1–19. <https://doi.org/10.1101/cshperspect.a004978>
- Rifkin, D. B. (2005). Latent Transforming Growth Factor- $\beta$  (TGF- $\beta$ ) Binding Proteins: Orchestrators of TGF- $\beta$  Availability. *Journal of Biological Chemistry*, 280(9), 7409–7412. <https://doi.org/10.1074/jbc.R400029200>
- Riley, S. E., Feng, Y., & Hansen, C. G. (2022). Hippo-Yap/Taz signalling in zebrafish regeneration. *Npj Regenerative Medicine*. <https://doi.org/10.1038/s41536-022-00209-8>
- Risha, M. A., Ali, A., Siengdee, P., Trakooljul, N., Haack, F., Dannenberger, D., Wimmers, K., & Ponsuksili, S. (2021). Wnt signaling related transcripts and their relationship to energy metabolism in C2C12 myoblasts under temperature stress. *PeerJ*, 9. <https://doi.org/10.7717/PEERJ.11625/SUPP-3>
- Robins, E. J., & Capehart, A. A. (2018). Matrix remodeling associated 5 expression in trunk and limb during avian development. *International Journal of Developmental Biology*, 62(4–5), 335–340. <https://doi.org/10.1387/ijdb.170225ac>
- Rognoni, E., Pisco, A. O., Hiratsuka, T., Sipilä, K. H., Belmonte, J. M., Mobasser, S. A., Philippeos, C., Dilão, R., & Watt, F. M. (2018). Fibroblast state switching orchestrates dermal maturation and wound healing. *Molecular Systems Biology*, 14(8). <https://doi.org/10.15252/msb.20178174>
- Roovers, K., & Assoian, R. K. (2003). Effects of Rho Kinase and Actin Stress Fibers on Sustained Extracellular Signal-Regulated Kinase Activity and Activation of G 1 Phase Cyclin-Dependent Kinases. *Molecular and Cellular Biology*, 23(12), 4283–4294. <https://doi.org/10.1128/MCB.23.12.4283-4294.2003>

- Rullman, E., Norrbom, J., Strömberg, A., Wågsäter, D., Rundqvist, H., Haas, T., & Gustafsson, T. (2009). Endurance exercise activates matrix metalloproteinases in human skeletal muscle. *J Appl Physiol*, *106*, 804–812. <https://doi.org/10.1152/jappphysiol.90872.2008>.-In
- Saikia, P., Medeiros, C. S., Thangavadivel, S., & Wilson, S. E. (2018). *Basement membranes in the cornea and other organs that commonly develop fibrosis*. <https://doi.org/10.1007/s00441-018-2934-7>
- Saraswathibhatla, A., Indana, D., & Chaudhuri, O. (2023). Cell–extracellular matrix mechanotransduction in 3D. *Nature Reviews Molecular Cell Biology*, *24*(7), 495–516. <https://doi.org/10.1038/s41580-023-00583-1>
- Schilling, T. F., & Kimmel, C. B. (1997). Musculoskeletal patterning in the pharyngeal segments of the zebrafish embryo. *Development*, 2945–2960.
- Schlaepfer, D. D., Hanks, S. K., Hunter, T., & van der Geer, P. (1994). Integrin-mediated signal transduction linked to Ras pathway by GRB2 binding to focal adhesion kinase. *Nature*, *372*, 786–791.
- Schweitzer, R., Chyung, J. H., Murtaugh, L. C., Brent, A. E., Rosen, V., Olson, E. N., Lassar, A., & Tabin, C. J. (2001). Analysis of the tendon cell fate using Scleraxis, a specific marker for tendons and ligaments. *Development*, *128*, 3855–3866.
- Schweitzer, R., Zelzer, E., & Volk, T. (2010). Connecting muscles to tendons: Tendons and musculoskeletal development in flies and vertebrates (Development 137 (2807-2817)). In *Development* (Vol. 137, Issue 19, p. 3347). <https://doi.org/10.1242/dev.057885>
- Sekiguchi, R., & Yamada, K. M. (2018). Basement Membranes in Development and Disease. In *Current Topics in Developmental Biology* (Vol. 130, pp. 143–191). Academic Press Inc. <https://doi.org/10.1016/bs.ctdb.2018.02.005>

- Shen, L. (2016). *GeneOverlap: Test and visualize gene overlaps* (3.17).
- Shimada, A., Wada, S., Inoue, K., Ideno, H., Kamiunten, T., Komatsu, K., Kudo, A., Nakamura, Y., Sato, T., Nakashima, K., & Nifuji, A. (2014). Efficient expansion of mouse primary tenocytes using a novel collagen gel culture method. *Histochem Cell Biol*, *142*, 205–215. <https://doi.org/10.1007/s00418-014-1191-4>
- Singh, H., Medina, K. L., & Pongubala, J. M. R. (2005). Contingent gene regulatory networks and B cell fate specification. *Proceedings of the National Academy of Sciences of the United States of America*, *102*(14), 4949–4953. <https://doi.org/10.1073/PNAS.0500480102>
- Skutek, M., Van Griensven, M., Zeichen, J., Brauer, N., & Bosch, U. (2001). Cyclic mechanical stretching modulates secretion pattern of growth factors in human tendon fibroblasts. *Eur J Appl Physiol*, *2001*, 48–52. <https://doi.org/10.0007/s004210100502>
- Smedley, D., Haider, S., Ballester, B., Holland, R., London, D., Thorisson, G., & Kasprzyk, A. (2009). *BioMart-biological queries made easy*. <https://doi.org/10.1186/1471-2164-10-22>
- Steed, E., Faggianelli, N., Roth, S., Ramsbacher, C., Concordet, J.-P., & Vermot, J. (2016). klf2a couples mechanotransduction and zebrafish valve morphogenesis through fibronectin synthesis. *Nature Communications*, *7*. <https://doi.org/10.1038/ncomms11646>
- Subramanian, A., Kanzaki, L. F., Galloway, J. L., & Schilling, T. F. (2018). *Mechanical force regulates tendon extracellular matrix organization and tenocyte morphogenesis through TGFbeta signaling*. <https://doi.org/10.7554/eLife.38069.001>
- Subramanian, A., Kanzaki, L. F., & Schilling, T. F. (2023). Mechanical force regulates Sox9 expression at the developing enthesis. *Development (Cambridge, England)*, *150*(16). <https://doi.org/10.1242/dev.201141>

- Subramanian, A., & Schilling, T. F. (2014). Thrombospondin-4 controls matrix assembly during development and repair of myotendinous junctions. *ELife*, 2014(3).  
<https://doi.org/10.7554/eLife.02372>
- Subramanian, A., & Schilling, T. F. (2015). Tendon development and musculoskeletal assembly: Emerging roles for the extracellular matrix. In *Development (Cambridge)* (Vol. 142, Issue 24, pp. 4191–4204). Company of Biologists Ltd. <https://doi.org/10.1242/dev.114777>
- Sugimoto, A., Miyazaki, A., Kawarabayashi, K., Shono, M., Akazawa, Y., Hasegawa, T., Ueda-Yamaguchi, K., Kitamura, T., Yoshizaki, K., Fukumoto, S., & Iwamoto, T. (2017). Piezo type mechanosensitive ion channel component 1 functions as a regulator of the cell fate determination of mesenchymal stem cells. *Scientific Reports*, 7(1).  
<https://doi.org/10.1038/s41598-017-18089-0>
- Sun, H. B., Andarawis-Puri, N., Li, Y., Fung, D. T., Lee, J. Y., Wang, V. M., Basta-Pljakic, J., Leong, D. J., Sereysky, J. B., Ros, S. J., Klug, R. A., Braman, J., Schaffler, M. B., Jepsen, K. J., & Flatow, E. L. (2010). Cycle-dependent matrix remodeling gene expression response in fatigue-loaded rat patellar tendons. *Journal of Orthopaedic Research*, 28(10), 1380–1386.  
<https://doi.org/10.1002/jor.21132>
- Smith, M. L., Gourdon, D., Little, W. C., Kubow, K. E., Eguiluz, R. A., Luna-Morris, S., & Vogel, V. (2007). Force-Induced Unfolding of Fibronectin in the Extracellular Matrix of Living Cells. *PLoS Biology*, 5(10), e268. <https://doi.org/10.1371/journal.pbio.0050268>
- Sonna, L. A., Fujita, J., Gaffin, S. L., & Lilly, C. M. (2002). highlighted topics Molecular Biology of Thermoregulation Invited Review: Effects of heat and cold stress on mammalian gene expression. *Molecular Biology of Thermoregulation*, 92, 1725–1742.  
<https://doi.org/10.1152/jappphysiol>

- Swift, J., Ivanovska, I. L., Buxboim, A., Harada, T., Dingal, P. C. D. P., Pinter, J., Pajeroski, D. J., Spinler, K. R., Shin, J.-W., Tewari, M., Rehfeldt, F., Speicher, D. W., & Discher, D. E. (2013). Nuclear Lamin-A Scales with Tissue Stiffness and Enhances Matrix-Directed Differentiation. *Science*, *341*(6149), 965–966. <https://doi.org/10.1126/science.1243643>
- Swinburne, I. A., Mosaliganti, K. R., Green, A. A., & Megason, S. G. (2015). Improved long-term imaging of embryos with genetically encoded  $\alpha$ -bungarotoxin. *PLoS ONE*, *10*(8). <https://doi.org/10.1371/journal.pone.0134005>
- Tan, G. K., Pryce, B. A., Stabio, A., Brigande, J. V., Wang, C., Xia, Z., Tufa, S. F., Keene, D. R., & Schweitzer, R. (2020). TGF $\beta$  signaling is critical for maintenance of the tendon cell fate. *eLife*, *9*. <https://doi.org/10.7554/eLife.52695>
- Taylor, S. H., Al-Youha, S., van Agtmael, T., Lu, Y., Wong, J., McGrouther, D. A., & Kadler, K. E. (2011). Tendon is covered by a basement membrane epithelium that is required for cell retention and the prevention of adhesion formation. *PLoS ONE*, *6*(1). <https://doi.org/10.1371/journal.pone.0016337>
- Torsoni, A. S., Constancio, S. S., Nadruz, W., Hanks, S. K., & Franchini, K. G. (2003). Focal Adhesion Kinase Is Activated and Mediates the Early Hypertrophic Response to Stretch in Cardiac Myocytes. *Circulation Research*, *93*(2), 140–147. <https://doi.org/10.1161/01.RES.0000081595.25297.1B>
- Van Den Brink, S. C., Sage, F., Vértesy, Á., Spanjaard, B., Peterson-Maduro, J., Baron, C. S., Robin, C., & Van Oudenaarden, A. (2017). Single-cell sequencing reveals dissociation-induced gene expression in tissue subpopulations. *Nature Methods* *2017 14:10*, *14*(10), 935–936. <https://doi.org/10.1038/nmeth.4437>
- Van Der Rest, M., & Garrone, R. (1991). Collagen family of proteins. *The FASEB Journal*.

- Vanacore, R., Ham, A. J. L., Voehler, M., Sanders, C. R., Conrads, T. P., Veenstra, T. D., Sharpless, B., Dawson, P. E., & Hudson, B. G. (2009). A Sulfilimine Bond Identified in Collagen IV. *Science*, 325(5945), 1230–1234. <https://doi.org/10.1126/science.1176811>
- Viidik, A. (1969). Tensile strength properties of achilles tendon systems in trained and untrained rabbits. *Acta Orthopaedica*, 40(2), 261–272. <https://doi.org/10.3109/17453676908989506>
- Vogel, V. (2006). Mechanotransduction involving multimodular proteins: converting force into biochemical signals. *Annual Review of Biophysics and Biomolecular Structure*, 35(1), 459–488. <https://doi.org/10.1146/annurev.biophys.35.040405.102013>
- Vogel, V., & Sheetz, M. (2006). Local force and geometry sensing regulate cell functions. *Nature Reviews Molecular Cell Biology*, 7(4), 265–275. <https://doi.org/10.1038/nrm1890>
- Wang, G. H., Yao, L., Xu, H. W., Tang, W. T., Fu, J. H., Hu, X. F., Cui, L., & Xu, X. M. (2013). Identification of MXRA5 as a novel biomarker in colorectal cancer. *Oncology Letters*, 5(2), 544–548. <https://doi.org/10.3892/ol.2012.1038>
- Wang, J. H. C. (2006). Mechanobiology of tendon. In *Journal of Biomechanics* (Vol. 39, Issue 9, pp. 1563–1582). <https://doi.org/10.1016/j.jbiomech.2005.05.011>
- Wang, J. H.-C., Jia, F., Yang, G., Yang, S., Campbell, B. H., Stone, D., & Woo, S. L.-Y. (2003). Cyclic Mechanical Stretching of Human Tendon Fibroblasts Increases the Production of Prostaglandin E<sub>2</sub> and Levels of Cyclooxygenase Expression: A Novel In Vitro Model Study. *Connective Tissue Research*, 44(3–4), 128–133. <https://doi.org/10.1080/03008200390223909>
- Wang, L.-H., & Baker, N. E. (2000). Developmental Cell Review E Proteins and ID Proteins: Helix-Loop-Helix Partners in Development and Disease. *Murre*. <https://doi.org/10.1016/j.devcel.2015.10.019>

- Warren, G. L., Summan, M., Gao, X., Chapman, R., Hulderman, T., & Simeonova, P. P. (2007). Mechanisms of skeletal muscle injury and repair revealed by gene expression studies in mouse models. *The Journal of Physiology*, 582(Pt 2), 825.  
<https://doi.org/10.1113/JPHYSIOL.2007.132373>
- Westerfield, M. (2000). *The zebrafish book. A guide for the laboratory use of zebrafish (Danio rerio)* (5th ed.). University of Oregon Press.
- Westerfield, M. (2007). *The zebrafish book. A guide for the laboratory use of zebrafish (Danio rerio)*. (5th ed.). Univ. of Oregon Press.
- Westphal, M., Panza, P., Kasthuber, E., Wehrle, J., & Driever, W. (2022). Wnt/ $\beta$ -catenin signaling promotes neurogenesis in the diencephalospinal dopaminergic system of embryonic zebrafish. *Scientific Reports* 2022 12:1, 12(1), 1–19. <https://doi.org/10.1038/s41598-022-04833-8>
- Wipff, P.-J., Rifkin, D. B., Meister, J.-J., & Hinz, B. (2007). Myofibroblast contraction activates latent TGF- $\beta$ 1 from the extracellular matrix. *The Journal of Cell Biology*, 179(6), 1311–1323.  
<https://doi.org/10.1083/jcb.200704042>
- Wu, M., Melichian, D. S., De La Garza, M., Gruner, K., Bhattacharyya, S., Barr, L., Nair, A., Shahrara, S., Sporn, P. H. S., Mustoe, T. A., Tourtellotte, W. G., & Varga, J. (2009). Essential Roles for Early Growth Response Transcription Factor Egr-1 in Tissue Fibrosis and Wound Healing. *The American Journal of Pathology*, 175(3), 1041.  
<https://doi.org/10.2353/AJPATH.2009.090241>
- Wu, R. S., Lam, I. I., Clay, H., Duong, D. N., Deo, R. C., & Coughlin Correspondence, S. R. (2018). A Rapid Method for Directed Gene Knockout for Screening in G0 Zebrafish. *Developmental Cell*, 46, 112-125.e4. <https://doi.org/10.1016/j.devcel.2018.06.003>

- Wu, T., Hu, E., Xu, S., Chen, M., Guo, P., Dai, Z., Feng, T., Zhou, L., Tang, W., Zhan, L., Fu, X., Liu, S., Bo, X., & Yu, G. (2021a). clusterProfiler 4.0: A universal enrichment tool for interpreting omics data. *Innovation*, 2(3). <https://doi.org/10.1016/j.xinn.2021.100141>
- Wu, T., Hu, E., Xu, S., Chen, M., Guo, P., Dai, Z., Feng, T., Zhou, L., Tang, W., Zhan, L., Fu, X., Liu, S., Bo, X., & Yu, G. (2021b). clusterProfiler 4.0: A universal enrichment tool for interpreting omics data. *Innovation (Cambridge (Mass.))*, 2(3). <https://doi.org/10.1016/J.XINN.2021.100141>
- Xie, J., Zhou, C., Zhang, D., Cai, L., Du, W., Li, X., & Zhou, X. (2018). Compliant Substratum Changes Osteocyte Functions: The Role of ITGB3/FAK/ $\beta$ -Catenin Signaling Matters. *ACS Applied Bio Materials*, 1(3), 792–801. <https://doi.org/10.1021/acsabm.8b00246>
- Xu, B., Song, G., Ju, Y., Li, X., Song, Y., & Watanabe, S. (2012). RhoA/ROCK, cytoskeletal dynamics, and focal adhesion kinase are required for mechanical stretch-induced tenogenic differentiation of human mesenchymal stem cells. *Journal of Cellular Physiology*, 227(6), 2722–2729. <https://doi.org/10.1002/jcp.23016>
- Yaseen, W., Kraft-Sheleg, O., Zaffryar-Eilot, S., Melamed, S., Sun, C., Millay, D. P., & Hasson, P. (2021). Fibroblast fusion to the muscle fiber regulates myotendinous junction formation. *Nature Communications*, 12(1). <https://doi.org/10.1038/s41467-021-24159-9>
- Yoshimoto, Y., Uezumi, A., Ikemoto-Uezumi, M., Tanaka, K., Yu, X., Kurosawa, T., Yambe, S., Maehara, K., Ohkawa, Y., Sotomaru, Y., & Shukunami, C. (2022). Tenogenic Induction From Induced Pluripotent Stem Cells Unveils the Trajectory Towards Tenocyte Differentiation. *Frontiers in Cell and Developmental Biology*, 10. <https://doi.org/10.3389/fcell.2022.780038>
- Zelzer, E., Blitz, E., Killian, M. L., & Thomopoulos, S. (2014). *Tendon-to-Bone Attachment: From Development to Maturity*. <https://doi.org/10.1002/bdrc.21056>

- Zhang, J., & Wang, J. H. C. (2010). Mechanobiological response of tendon stem cells: Implications of tendon homeostasis and pathogenesis of tendinopathy. *Journal of Orthopaedic Research*, 28(5), 639–643. <https://doi.org/10.1002/jor.21046>
- Zhang, J., & Wang, J. H. C. (2013). The effects of mechanical loading on tendons--an in vivo and in vitro model study. *PloS One*, 8(8). <https://doi.org/10.1371/journal.pone.0071740>
- Zhang, J., & Wang, J. H. C. (2015). Moderate exercise mitigates the detrimental effects of aging on tendon stem cells. *PLoS ONE*, 10(6). <https://doi.org/10.1371/journal.pone.0130454>
- Zhang, M., Meng, N., Wang, X., Chen, W., & Zhang, Q. (2022). TRPV4 and PIEZO Channels Mediate the Mechanosensing of Chondrocytes to the Biomechanical Microenvironment. *Membranes*. <https://doi.org/10.3390/membranes12020237>
- Zheng, G. X. Y., Terry, J. M., Belgrader, P., Ryvkin, P., Bent, Z. W., Wilson, R., Ziraldo, S. B., Wheeler, T. D., Mcdermott, G. P., Zhu, J., Gregory, M. T., Shuga, J., Montesclaros, L., Underwood, J. G., Masquelier, D. A., Nishimura, S. Y., Schnall-Levin, M., Wyatt, P. W., Hindson, C. M., ... Bielas, J. H. (2017). Massively parallel digital transcriptional profiling of single cells. *Nature Communications*. <https://doi.org/10.1038/ncomms14049>
- Zhou, W., Saint-Amant, L., Hirata, H., Cui, W. W., Sprague, S. M., & Kuwada, J. Y. (2006). Non-sense mutations in the dihydropyridine receptor  $\beta 1$  gene, CACNB1, paralyze zebrafish relaxed mutants. *Cell Calcium*, 39(3), 227–236. <https://doi.org/10.1016/j.ceca.2005.10.015>
- Zhu, J., Li, J., Wang, B., Zhang, W. J., Zhou, G., Cao, Y., & Liu, W. (2010). The regulation of phenotype of cultured tenocytes by microgrooved surface structure. *Biomaterials*, 31(27), 6952–6958. <https://doi.org/10.1016/j.biomaterials.2010.05.058>

Zhu, X., Zhu, H., Zhang, L., Huang, S., Cao, J., Ma, G., Feng, G., He, L., Yang, Y., & Guo, X. (2012).

Wls-mediated Wnts differentially regulate distal limb patterning and tissue morphogenesis.

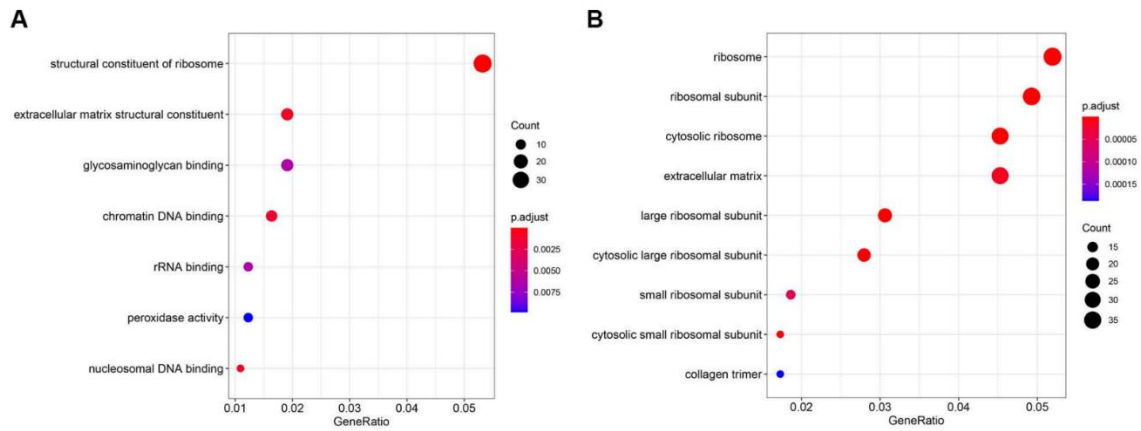
*Developmental Biology*, 365(2), 328–338. <https://doi.org/10.1016/J.YDBIO.2012.02.019>

## Appendix I

### Supplementary Material: Chapter II

#### An in vivo investigation of tenocyte transcriptional responses to muscle contraction force paradigms

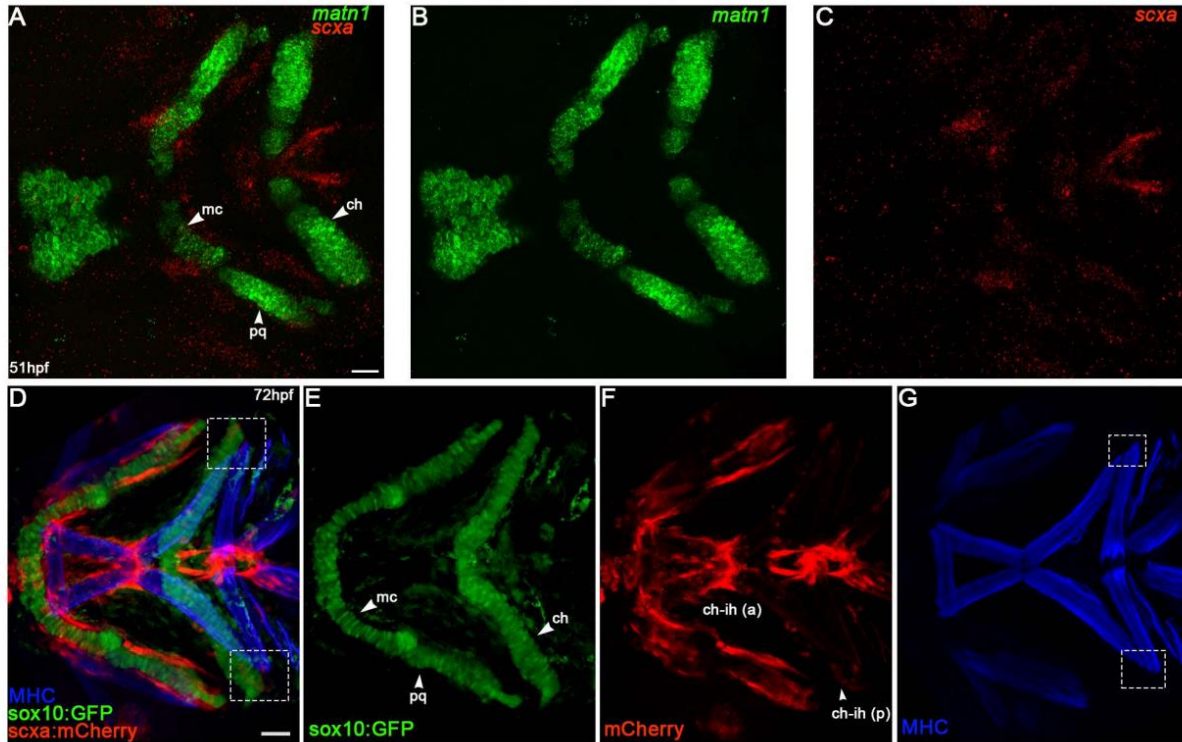
#### Supplementary Figure 1



#### Supplementary Figure 1: RNA-seq GO term analyses for Molecular Function (MF) and Cellular Compartment (CC) GO categories

**A)** MF GO term analysis from DEG list by p-value with  $p < 0.05$ . **B)** CC GO term analysis from DEG list with  $p < 0.05$

## Supplementary Figure 2



### Supplementary Figure 2: *matn1* expression in the embryonic zebrafish craniofacial complex and associated tendons and muscles

(A-C) *isHCR* for *matn1* (green) and *scxa* (red) in 51 hpf zebrafish embryos, ventral views, anterior to the left. (D-G) Immunolabeling for mCherry in *Tg(scxa:mCherry;sox10:GFP)* embryos (red, tendon), GFP (green, cartilage) and Myosin Heavy Chain (blue, muscle) at 72 hpf. White-dashed boxes depict ceratohyal-interhyal and ceratohyal-hyohyal attachment regions measured in *isHCRs* in **Fig. 4I**. Abbreviations: ch = ceratohyal cartilage, ch-ih (a) = anterior ceratohyal-interhyal attachment region, ch-ih (p) = posterior ceratohyal-interhyal attachment region, mc = meckel's cartilage, pq = palatoquadrate cartilage, Scale bars = 20um

# Supplementary Table 1

## PANTHER Bioinformatics Pathway Analysis

PANTHER Pathway	Number of Genes	Genes
Gonadotropin-releasing hormone receptor pathway (P06564)	17	prkg2, prkg, arf2, egr1, fto, tgf3, fob, fob, jun, tuba1c, jund, junb, atf3, foab, atf, cacco1a, nfatc1
CCR signaling map (P06559)	16	prkg, prkg, arf2, egr1, myc, cdrl1b, ppp1r1a, smad3, cdrl1, wrt1a, cdrl1b, fdr, wrt1, act1b, foab, atf, cacco1a, nfatc1
Wnt signaling pathway (P00075)	16	prkg, prkg, arf2, egr1, myc, cdrl1b, ppp1r1a, smad3, cdrl1, wrt1a, cdrl1b, fdr, wrt1, act1b, foab, atf, cacco1a, nfatc1
Apoptosis signaling pathway (P00060)	13	prkg, prkg, arf2, egr1, myc, cdrl1b, ppp1r1a, smad3, cdrl1, wrt1a, cdrl1b, fdr, wrt1, act1b, foab, atf, cacco1a, nfatc1
Integrin signaling pathway (P00034)	13	prkg, prkg, arf2, egr1, myc, cdrl1b, ppp1r1a, smad3, cdrl1, wrt1a, cdrl1b, fdr, wrt1, act1b, foab, atf, cacco1a, nfatc1
Inflammation mediated by chemokine and cytokine signaling pathway (P00031)	12	prkg, prkg, arf2, egr1, myc, cdrl1b, ppp1r1a, smad3, cdrl1, wrt1a, cdrl1b, fdr, wrt1, act1b, foab, atf, cacco1a, nfatc1
TGF-beta signaling pathway (P00052)	10	prkg, prkg, arf2, egr1, myc, cdrl1b, ppp1r1a, smad3, cdrl1, wrt1a, cdrl1b, fdr, wrt1, act1b, foab, atf, cacco1a, nfatc1
PDGF signaling pathway (P00047)	10	prkg, prkg, arf2, egr1, myc, cdrl1b, ppp1r1a, smad3, cdrl1, wrt1a, cdrl1b, fdr, wrt1, act1b, foab, atf, cacco1a, nfatc1
Angiogenesis (P00000)	9	prkg, prkg, arf2, egr1, myc, cdrl1b, ppp1r1a, smad3, cdrl1, wrt1a, cdrl1b, fdr, wrt1, act1b, foab, atf, cacco1a, nfatc1
Hemostasis (P00029)	9	prkg, prkg, arf2, egr1, myc, cdrl1b, ppp1r1a, smad3, cdrl1, wrt1a, cdrl1b, fdr, wrt1, act1b, foab, atf, cacco1a, nfatc1
Cadherin signaling pathway (P00012)	8	prkg, prkg, arf2, egr1, myc, cdrl1b, ppp1r1a, smad3, cdrl1, wrt1a, cdrl1b, fdr, wrt1, act1b, foab, atf, cacco1a, nfatc1
Alzheimer disease-prosolin pathway (P00004)	7	prkg, prkg, arf2, egr1, myc, cdrl1b, ppp1r1a, smad3, cdrl1, wrt1a, cdrl1b, fdr, wrt1, act1b, foab, atf, cacco1a, nfatc1
T cell activation (P00015)	7	prkg, prkg, arf2, egr1, myc, cdrl1b, ppp1r1a, smad3, cdrl1, wrt1a, cdrl1b, fdr, wrt1, act1b, foab, atf, cacco1a, nfatc1
Cytoskeletal regulation by Rho GTPase (P00016)	7	prkg, prkg, arf2, egr1, myc, cdrl1b, ppp1r1a, smad3, cdrl1, wrt1a, cdrl1b, fdr, wrt1, act1b, foab, atf, cacco1a, nfatc1
Parkinson disease (P00049)	6	prkg, prkg, arf2, egr1, myc, cdrl1b, ppp1r1a, smad3, cdrl1, wrt1a, cdrl1b, fdr, wrt1, act1b, foab, atf, cacco1a, nfatc1
Oxidative stress response (P00046)	6	prkg, prkg, arf2, egr1, myc, cdrl1b, ppp1r1a, smad3, cdrl1, wrt1a, cdrl1b, fdr, wrt1, act1b, foab, atf, cacco1a, nfatc1
Nicotinic acetylcholine receptor signaling pathway (P00044)	6	prkg, prkg, arf2, egr1, myc, cdrl1b, ppp1r1a, smad3, cdrl1, wrt1a, cdrl1b, fdr, wrt1, act1b, foab, atf, cacco1a, nfatc1
Interleukin signaling pathway (P00036)	6	prkg, prkg, arf2, egr1, myc, cdrl1b, ppp1r1a, smad3, cdrl1, wrt1a, cdrl1b, fdr, wrt1, act1b, foab, atf, cacco1a, nfatc1
Oxytocin receptor mediated signaling pathway (P04391)	6	prkg, prkg, arf2, egr1, myc, cdrl1b, ppp1r1a, smad3, cdrl1, wrt1a, cdrl1b, fdr, wrt1, act1b, foab, atf, cacco1a, nfatc1
Heterotrimeric G-protein signaling pathway Gq alpha and Gs alpha mediated pathway (P00026)	6	prkg, prkg, arf2, egr1, myc, cdrl1b, ppp1r1a, smad3, cdrl1, wrt1a, cdrl1b, fdr, wrt1, act1b, foab, atf, cacco1a, nfatc1
SH2 tyrosine receptor mediated signaling pathway (P04374)	6	prkg, prkg, arf2, egr1, myc, cdrl1b, ppp1r1a, smad3, cdrl1, wrt1a, cdrl1b, fdr, wrt1, act1b, foab, atf, cacco1a, nfatc1
Alzheimer disease-amyloid precursor pathway (P00001)	5	prkg, prkg, arf2, egr1, myc, cdrl1b, ppp1r1a, smad3, cdrl1, wrt1a, cdrl1b, fdr, wrt1, act1b, foab, atf, cacco1a, nfatc1
Muscarinic acetylcholine receptor 1 and 3 signaling pathway (P00042)	5	prkg, prkg, arf2, egr1, myc, cdrl1b, ppp1r1a, smad3, cdrl1, wrt1a, cdrl1b, fdr, wrt1, act1b, foab, atf, cacco1a, nfatc1
Metabotropic glutamate receptor group II pathway (P00040)	5	prkg, prkg, arf2, egr1, myc, cdrl1b, ppp1r1a, smad3, cdrl1, wrt1a, cdrl1b, fdr, wrt1, act1b, foab, atf, cacco1a, nfatc1
Metabotropic glutamate receptor group I pathway (P00039)	5	prkg, prkg, arf2, egr1, myc, cdrl1b, ppp1r1a, smad3, cdrl1, wrt1a, cdrl1b, fdr, wrt1, act1b, foab, atf, cacco1a, nfatc1
Thyrotropin-releasing hormone receptor signaling pathway (P04394)	5	prkg, prkg, arf2, egr1, myc, cdrl1b, ppp1r1a, smad3, cdrl1, wrt1a, cdrl1b, fdr, wrt1, act1b, foab, atf, cacco1a, nfatc1
FGF receptor signaling pathway (P00018)	5	prkg, prkg, arf2, egr1, myc, cdrl1b, ppp1r1a, smad3, cdrl1, wrt1a, cdrl1b, fdr, wrt1, act1b, foab, atf, cacco1a, nfatc1
Beta1 adrenergic receptor signaling pathway (P04378)	5	prkg, prkg, arf2, egr1, myc, cdrl1b, ppp1r1a, smad3, cdrl1, wrt1a, cdrl1b, fdr, wrt1, act1b, foab, atf, cacco1a, nfatc1
B cell activation (P00010)	5	prkg, prkg, arf2, egr1, myc, cdrl1b, ppp1r1a, smad3, cdrl1, wrt1a, cdrl1b, fdr, wrt1, act1b, foab, atf, cacco1a, nfatc1
Beta1 adrenergic receptor signaling pathway (P04377)	5	prkg, prkg, arf2, egr1, myc, cdrl1b, ppp1r1a, smad3, cdrl1, wrt1a, cdrl1b, fdr, wrt1, act1b, foab, atf, cacco1a, nfatc1
Ubiquitin proteasome pathway (P00005)	4	prkg, prkg, arf2, egr1, myc, cdrl1b, ppp1r1a, smad3, cdrl1, wrt1a, cdrl1b, fdr, wrt1, act1b, foab, atf, cacco1a, nfatc1
Toll receptor signaling pathway (P00054)	4	prkg, prkg, arf2, egr1, myc, cdrl1b, ppp1r1a, smad3, cdrl1, wrt1a, cdrl1b, fdr, wrt1, act1b, foab, atf, cacco1a, nfatc1
Muscarinic acetylcholine receptor 2 and 4 signaling pathway (P00043)	4	prkg, prkg, arf2, egr1, myc, cdrl1b, ppp1r1a, smad3, cdrl1, wrt1a, cdrl1b, fdr, wrt1, act1b, foab, atf, cacco1a, nfatc1
Inulin/GF pathway-mitogen activated protein kinase/RAF kinase cascade (P00032)	4	prkg, prkg, arf2, egr1, myc, cdrl1b, ppp1r1a, smad3, cdrl1, wrt1a, cdrl1b, fdr, wrt1, act1b, foab, atf, cacco1a, nfatc1
Opioid proenkephalin pathway (P05917)	4	prkg, prkg, arf2, egr1, myc, cdrl1b, ppp1r1a, smad3, cdrl1, wrt1a, cdrl1b, fdr, wrt1, act1b, foab, atf, cacco1a, nfatc1
Opioid prodynorphin pathway (P05916)	4	prkg, prkg, arf2, egr1, myc, cdrl1b, ppp1r1a, smad3, cdrl1, wrt1a, cdrl1b, fdr, wrt1, act1b, foab, atf, cacco1a, nfatc1
Interleukin release (P05913)	4	prkg, prkg, arf2, egr1, myc, cdrl1b, ppp1r1a, smad3, cdrl1, wrt1a, cdrl1b, fdr, wrt1, act1b, foab, atf, cacco1a, nfatc1
FGF signaling pathway (P00023)	4	prkg, prkg, arf2, egr1, myc, cdrl1b, ppp1r1a, smad3, cdrl1, wrt1a, cdrl1b, fdr, wrt1, act1b, foab, atf, cacco1a, nfatc1
Histamine H1 receptor mediated signaling pathway (P04385)	4	prkg, prkg, arf2, egr1, myc, cdrl1b, ppp1r1a, smad3, cdrl1, wrt1a, cdrl1b, fdr, wrt1, act1b, foab, atf, cacco1a, nfatc1
Interleukin signaling pathway (P00019)	4	prkg, prkg, arf2, egr1, myc, cdrl1b, ppp1r1a, smad3, cdrl1, wrt1a, cdrl1b, fdr, wrt1, act1b, foab, atf, cacco1a, nfatc1
Beta1 adrenergic receptor signaling pathway (P04379)	4	prkg, prkg, arf2, egr1, myc, cdrl1b, ppp1r1a, smad3, cdrl1, wrt1a, cdrl1b, fdr, wrt1, act1b, foab, atf, cacco1a, nfatc1
SH1 tyrosine receptor mediated signaling pathway (P04373)	4	prkg, prkg, arf2, egr1, myc, cdrl1b, ppp1r1a, smad3, cdrl1, wrt1a, cdrl1b, fdr, wrt1, act1b, foab, atf, cacco1a, nfatc1
Notch signaling pathway (P00045)	3	prkg, prkg, arf2, egr1, myc, cdrl1b, ppp1r1a, smad3, cdrl1, wrt1a, cdrl1b, fdr, wrt1, act1b, foab, atf, cacco1a, nfatc1
Ionotropic glutamate receptor pathway (P00017)	3	prkg, prkg, arf2, egr1, myc, cdrl1b, ppp1r1a, smad3, cdrl1, wrt1a, cdrl1b, fdr, wrt1, act1b, foab, atf, cacco1a, nfatc1
Inulin/GF pathway-protein kinase B signaling cascade (P00033)	3	prkg, prkg, arf2, egr1, myc, cdrl1b, ppp1r1a, smad3, cdrl1, wrt1a, cdrl1b, fdr, wrt1, act1b, foab, atf, cacco1a, nfatc1
p53 pathway feedback loop 2 (P04398)	3	prkg, prkg, arf2, egr1, myc, cdrl1b, ppp1r1a, smad3, cdrl1, wrt1a, cdrl1b, fdr, wrt1, act1b, foab, atf, cacco1a, nfatc1
Ras pathway (P04393)	3	prkg, prkg, arf2, egr1, myc, cdrl1b, ppp1r1a, smad3, cdrl1, wrt1a, cdrl1b, fdr, wrt1, act1b, foab, atf, cacco1a, nfatc1
Heterotrimeric G-protein signaling pathway-ras outer segment phototransduction (P00028)	3	prkg, prkg, arf2, egr1, myc, cdrl1b, ppp1r1a, smad3, cdrl1, wrt1a, cdrl1b, fdr, wrt1, act1b, foab, atf, cacco1a, nfatc1
Heterotrimeric G-protein signaling pathway-Gq alpha and Go alpha mediated pathway (P00027)	3	prkg, prkg, arf2, egr1, myc, cdrl1b, ppp1r1a, smad3, cdrl1, wrt1a, cdrl1b, fdr, wrt1, act1b, foab, atf, cacco1a, nfatc1
Hedgehog signaling pathway (P00015)	3	prkg, prkg, arf2, egr1, myc, cdrl1b, ppp1r1a, smad3, cdrl1, wrt1a, cdrl1b, fdr, wrt1, act1b, foab, atf, cacco1a, nfatc1
Opioid proenkephalin pathway (P05915)	3	prkg, prkg, arf2, egr1, myc, cdrl1b, ppp1r1a, smad3, cdrl1, wrt1a, cdrl1b, fdr, wrt1, act1b, foab, atf, cacco1a, nfatc1
Dopamine receptor mediated signaling pathway (P05912)	3	prkg, prkg, arf2, egr1, myc, cdrl1b, ppp1r1a, smad3, cdrl1, wrt1a, cdrl1b, fdr, wrt1, act1b, foab, atf, cacco1a, nfatc1
Histamine H2 receptor mediated signaling pathway (P04386)	3	prkg, prkg, arf2, egr1, myc, cdrl1b, ppp1r1a, smad3, cdrl1, wrt1a, cdrl1b, fdr, wrt1, act1b, foab, atf, cacco1a, nfatc1
Corticotropin releasing factor receptor signaling pathway (P04380)	3	prkg, prkg, arf2, egr1, myc, cdrl1b, ppp1r1a, smad3, cdrl1, wrt1a, cdrl1b, fdr, wrt1, act1b, foab, atf, cacco1a, nfatc1
DNA replication (P00017)	3	prkg, prkg, arf2, egr1, myc, cdrl1b, ppp1r1a, smad3, cdrl1, wrt1a, cdrl1b, fdr, wrt1, act1b, foab, atf, cacco1a, nfatc1
Blood coagulation (P00011)	3	prkg, prkg, arf2, egr1, myc, cdrl1b, ppp1r1a, smad3, cdrl1, wrt1a, cdrl1b, fdr, wrt1, act1b, foab, atf, cacco1a, nfatc1
SH1 tyrosine receptor mediated signaling pathway (P04376)	3	prkg, prkg, arf2, egr1, myc, cdrl1b, ppp1r1a, smad3, cdrl1, wrt1a, cdrl1b, fdr, wrt1, act1b, foab, atf, cacco1a, nfatc1
Toll pathway-drosophila (P06217)	2	prkg, prkg, arf2, egr1, myc, cdrl1b, ppp1r1a, smad3, cdrl1, wrt1a, cdrl1b, fdr, wrt1, act1b, foab, atf, cacco1a, nfatc1
Kvon guidance mediated by RhoGTPase (P00008)	2	prkg, prkg, arf2, egr1, myc, cdrl1b, ppp1r1a, smad3, cdrl1, wrt1a, cdrl1b, fdr, wrt1, act1b, foab, atf, cacco1a, nfatc1
Alpha adrenergic receptor signaling pathway (P00002)	2	prkg, prkg, arf2, egr1, myc, cdrl1b, ppp1r1a, smad3, cdrl1, wrt1a, cdrl1b, fdr, wrt1, act1b, foab, atf, cacco1a, nfatc1
p53 pathway (P00059)	2	prkg, prkg, arf2, egr1, myc, cdrl1b, ppp1r1a, smad3, cdrl1, wrt1a, cdrl1b, fdr, wrt1, act1b, foab, atf, cacco1a, nfatc1
FGF signaling pathway (P00046)	2	prkg, prkg, arf2, egr1, myc, cdrl1b, ppp1r1a, smad3, cdrl1, wrt1a, cdrl1b, fdr, wrt1, act1b, foab, atf, cacco1a, nfatc1
Transcription regulation by bZIP transcription factor (P00055)	2	prkg, prkg, arf2, egr1, myc, cdrl1b, ppp1r1a, smad3, cdrl1, wrt1a, cdrl1b, fdr, wrt1, act1b, foab, atf, cacco1a, nfatc1
P53 kinase pathway (P00048)	2	prkg, prkg, arf2, egr1, myc, cdrl1b, ppp1r1a, smad3, cdrl1, wrt1a, cdrl1b, fdr, wrt1, act1b, foab, atf, cacco1a, nfatc1
IGFBP-3 receptor II signaling (P05731)	2	prkg, prkg, arf2, egr1, myc, cdrl1b, ppp1r1a, smad3, cdrl1, wrt1a, cdrl1b, fdr, wrt1, act1b, foab, atf, cacco1a, nfatc1
Interferon gamma signaling pathway (P00035)	2	prkg, prkg, arf2, egr1, myc, cdrl1b, ppp1r1a, smad3, cdrl1, wrt1a, cdrl1b, fdr, wrt1, act1b, foab, atf, cacco1a, nfatc1
p53 pathway by glucose deprivation (P04397)	2	prkg, prkg, arf2, egr1, myc, cdrl1b, ppp1r1a, smad3, cdrl1, wrt1a, cdrl1b, fdr, wrt1, act1b, foab, atf, cacco1a, nfatc1
Vitamin D metabolism and pathway (P04396)	2	prkg, prkg, arf2, egr1, myc, cdrl1b, ppp1r1a, smad3, cdrl1, wrt1a, cdrl1b, fdr, wrt1, act1b, foab, atf, cacco1a, nfatc1
Serine glycine biosynthesis (P02746)	2	prkg, prkg, arf2, egr1, myc, cdrl1b, ppp1r1a, smad3, cdrl1, wrt1a, cdrl1b, fdr, wrt1, act1b, foab, atf, cacco1a, nfatc1
FAS signaling pathway (P00020)	2	prkg, prkg, arf2, egr1, myc, cdrl1b, ppp1r1a, smad3, cdrl1, wrt1a, cdrl1b, fdr, wrt1, act1b, foab, atf, cacco1a, nfatc1
Angiotensin II-stimulated signaling through G proteins and beta-arrestin (P05911)	2	prkg, prkg, arf2, egr1, myc, cdrl1b, ppp1r1a, smad3, cdrl1, wrt1a, cdrl1b, fdr, wrt1, act1b, foab, atf, cacco1a, nfatc1
Circadian clock system (P00010)	2	prkg, prkg, arf2, egr1, myc, cdrl1b, ppp1r1a, smad3, cdrl1, wrt1a, cdrl1b, fdr, wrt1, act1b, foab, atf, cacco1a, nfatc1
5-Hydroxytryptamine degradation (P04372)	2	prkg, prkg, arf2, egr1, myc, cdrl1b, ppp1r1a, smad3, cdrl1, wrt1a, cdrl1b, fdr, wrt1, act1b, foab, atf, cacco1a, nfatc1
Pyrimidyl-5-phosphate biosynthesis (P02759)	1	prkg, prkg, arf2, egr1, myc, cdrl1b, ppp1r1a, smad3, cdrl1, wrt1a, cdrl1b, fdr, wrt1, act1b, foab, atf, cacco1a, nfatc1
Oxetane degradation (P02748)	1	prkg, prkg, arf2, egr1, myc, cdrl1b, ppp1r1a, smad3, cdrl1, wrt1a, cdrl1b, fdr, wrt1, act1b, foab, atf, cacco1a, nfatc1
Adrenaline and noradrenaline biosynthesis (P00001)	1	prkg, prkg, arf2, egr1, myc, cdrl1b, ppp1r1a, smad3, cdrl1, wrt1a, cdrl1b, fdr, wrt1, act1b, foab, atf, cacco1a, nfatc1
Glutamine glutamate conversion (P02745)	1	prkg, prkg, arf2, egr1, myc, cdrl1b, ppp1r1a, smad3, cdrl1, wrt1a, cdrl1b, fdr, wrt1, act1b, foab, atf, cacco1a, nfatc1
Formylated hydroxamate biosynthesis (P02743)	1	prkg, prkg, arf2, egr1, myc, cdrl1b, ppp1r1a, smad3, cdrl1, wrt1a, cdrl1b, fdr, wrt1, act1b, foab, atf, cacco1a, nfatc1
Tetrahydrofolate biosynthesis (P02742)	1	prkg, prkg, arf2, egr1, myc, cdrl1b, ppp1r1a, smad3, cdrl1, wrt1a, cdrl1b, fdr, wrt1, act1b, foab, atf, cacco1a, nfatc1
De novo pyrimidine deoxyribonucleotide biosynthesis (P02739)	1	prkg, prkg, arf2, egr1, myc, cdrl1b, ppp1r1a, smad3, cdrl1, wrt1a, cdrl1b, fdr, wrt1, act1b, foab, atf, cacco1a, nfatc1
De novo purine biosynthesis (P02738)	1	prkg, prkg, arf2, egr1, myc, cdrl1b, ppp1r1a, smad3, cdrl1, wrt1a, cdrl1b, fdr, wrt1, act1b, foab, atf, cacco1a, nfatc1
Synaptic vesicle trafficking (P02734)	1	prkg, prkg, arf2, egr1, myc, cdrl1b, ppp1r1a, smad3, cdrl1, wrt1a, cdrl1b, fdr, wrt1, act1b, foab, atf, cacco1a, nfatc1
Endogenous cannabinoid signaling (P02730)	1	prkg, prkg, arf2, egr1, myc, cdrl1b, ppp1r1a, smad3, cdrl1, wrt1a, cdrl1b, fdr, wrt1, act1b, foab, atf, cacco1a, nfatc1
Lanthine and gamma-salvage pathway (P02728)	1	prkg, prkg, arf2, egr1, myc, cdrl1b, ppp1r1a, smad3, cdrl1, wrt1a, cdrl1b, fdr, wrt1, act1b, foab, atf, cacco1a, nfatc1
Adenine and hypoxanthine salvage pathway (P02723)	1	prkg, prkg, arf2, egr1, myc, cdrl1b, ppp1r1a, smad3, cdrl1, wrt1a, cdrl1b, fdr, wrt1, act1b, foab, atf, cacco1a, nfatc1
Vitamin B6 metabolism (P02787)	1	prkg, prkg, arf2, egr1, myc, cdrl1b, ppp1r1a, smad3, cdrl1, wrt1a, cdrl1b, fdr, wrt1, act1b, foab, atf, cacco1a, nfatc1
Hypoxia response via HIF activation (P00030)	1	prkg, prkg, arf2, egr1, myc, cdrl1b, ppp1r1a, smad3, cdrl1, wrt1a, cdrl1b, fdr, wrt1, act1b, foab, atf, cacco1a, nfatc1
Thiamin metabolism (P02780)	1	prkg, prkg, arf2, egr1, myc, cdrl1b, ppp1r1a, smad3, cdrl1, wrt1a, cdrl1b, fdr, wrt1, act1b, foab, atf, cacco1a, nfatc1
p53 pathway feedback loop 1 (P04392)	1	prkg, prkg, arf2, egr1, myc, cdrl1b, ppp1r1a, smad3, cdrl1, wrt1a, cdrl1b, fdr, wrt1, act1b, foab, atf, cacco1a, nfatc1
General transcription regulation (P00021)	1	prkg, prkg, arf2, egr1, myc, cdrl1b, ppp1r1a, smad3, cdrl1, wrt1a, cdrl1b, fdr, wrt1, act1b, foab, atf, cacco1a, nfatc1
General transcription by RNA polymerase I (P00022)	1	prkg, prkg, arf2, egr1, myc, cdrl1b, ppp1r1a, smad3, cdrl1, wrt1a, cdrl1b, fdr, wrt1, act1b, foab, atf, cacco1a, nfatc1
Nicotine pharmacodynamics pathway (P06587)	1	prkg, prkg, arf2, egr1, myc, cdrl1b, ppp1r1a, smad3, cdrl1, wrt1a, cdrl1b, fdr, wrt1, act1b, foab, atf, cacco1a, nfatc1
5-adenosylmethionine biosynthesis (P02773)	1	prkg, prkg, arf2, egr1, myc, cdrl1b, ppp1r1a, smad3, cdrl1, wrt1a, cdrl1b, fdr, wrt1, act1b, foab, atf, cacco1a, nfatc1
Pyruvate metabolism (P02772)	1	prkg, prkg, arf2, egr1, myc, cdrl1b, ppp1r1a, smad3, cdrl1, wrt1a, cdrl1b, fdr, wrt1, act1b, foab, atf, cacco1a, nfatc1
Purine metabolism (P02769)	1	prkg, prkg, arf2, egr1, myc, cdrl1b, ppp1r1a, smad3, cdrl1, wrt1a, cdrl1b, fdr, wrt1, act1b, foab, atf, cacco1a, nfatc1
SH1 tyrosine receptor mediated signaling pathway (P04375)	1	prkg, prkg, arf2, egr1, myc, cdrl1b, ppp1r1a, smad3, cdrl1, wrt1a, cdrl1b, fdr, wrt1, act1b, foab, atf, cacco1a, nfatc1

## Supplementary Table 1: Pathway list from differentially expressed genes using PANTHER

## Supplementary Table 2

DAVID Bioinformatics Pathway Analysis

Kegg Pathway	No. of Genes	P-value	Genes
Ribosome	45	2.20E-24	<i>rpl10</i> <i>rpl10a</i> <i>rpl12</i> <i>rpl13</i> <i>rpl15</i> <i>rpl17</i> <i>rpl19</i> <i>rpl21</i> <i>rpl22</i> <i>rpl23</i> <i>rpl23a</i> <i>rpl24</i> <i>rpl32</i> <i>rpl136a</i> <i>rpl38</i> <i>rpl39</i> <i>rpl14</i> <i>rpl15a</i> <i>rpl7</i> <i>rpl8</i> <i>rpl9</i> <i>rps10</i> <i>rps11</i> <i>rps12</i> <i>rps18</i> <i>rps19</i> <i>rps24</i> <i>rps25</i> <i>rps26l</i> <i>rps29</i> <i>rps3a</i> <i>rps8a</i> <i>rps9</i> <i>rpsa</i> <i>rplp2l</i> <i>rplp0</i> <i>rpl28</i> <i>rpl29</i> <i>rps15a</i> <i>rps16</i> <i>rplp1</i> <i>uba52</i>
Glutathione metabolism	8	2.50E-02	<i>gstp1</i> <i>gsta.1</i> <i>gpx1a</i> <i>gpx8</i> <i>mgst1.2</i> <i>mgst2</i> <i>rrm2</i> <i>rrm2</i>
Retinol metabolism	6	5.40E-02	<i>aldh1a2</i> <i>bco1</i> <i>cyp26c1</i> <i>cyp26b1</i> <i>rdh8a</i> <i>rdh8b</i>
Insulin resistance	12	9.40E-02	<i>cpt1ab</i> <i>mgea5</i> <i>nfkbiab</i> <i>nfkbiab</i> <i>pck1</i> <i>pygma</i> <i>prkcg</i> <i>prkag1</i> <i>ppp1caa</i> <i>ppp1r3b</i> <i>ppp1r3cb</i> <i>socs3b</i>

**Supplementary Table 2: KEGG pathways analyzed from differentially expressed genes using DAVID**

Supplementary Table 3

Overlapping Genes							
1	myh9b	59	EIF3D	117	RPL11	174	MYH9A
2	GULP1A	60	PPM1DB	118	MS4A17A.8	175	ANTXR1C
3	PSMB6	61	NCOA4	119	POSTNA	176	ARID3C
4	EIF5	62	SEC61A1	120	SI:CH211-241J12.3	177	YAP1
5	IDH2	63	GOPC	121	ETF1B	178	SLC16A1B
6	AQP3A	64	CREMA	122	LOXL2A	179	CD151
7	NR1D2A	65	HE1.1	123	FMODA	180	ALDH3A1A.1
8	SIX4A	66	TOP2A	124	SLIT1A	181	IGSF9BB
9	PSEN1	67	SELENBP1	125	AQP8A.1	182	SI:DKKEY-238C7.16
10	RPL28	68	INHBB	126	HBBE2	183	OSTM1
11	TRIOBPB	69	TNN	127	RPS16	184	ZGC:162944
12	DDI2	70	PTGR1	128	ZGC:113263	185	HMGA2
13	MYCN	71	SYNJ1	129	SI:CH211-214J24.10	186	PPAP2D
14	MTA1	72	ARHGAP29A	130	SNAILB	187	KN1
15	RAB31I1	73	RAB5C	131	SI:CH211-113A14.18	188	CHAC1
16	MYL9B	74	BCL2L10	132	RPLP0	189	TMEM45A
17	SLC10A4	75	UROS	133	ISLR2	190	ARID3A
18	VCANB	76	YY1B	134	USH1C	191	DUSP6
19	PDCI	77	TPMT.2	135	IST1	192	ZGC:153675
20	HDLBPA	78	TP53INP1	136	COL4A6	193	RELI2
21	MAPK8B	79	ALDH3A2B	137	COL4A5	194	COL3A1A
22	RPS15A	80	MATN1	138	EIF2S1B	195	THBS2B
23	RPS9	81	NAAL5B	139	RPS11	196	SALL1A
24	DLX4A	82	CCDC80I1	140	RPL23	197	IBTK
25	PTPN11B	83	IRX3B	141	ENTPD5A	198	NRDE2
26	COL1A1A	84	TUBA8I2	142	H1-10	199	H1FA
27	GPIA	85	MYLK2	143	RIPPLY1	200	FRMPD3
28	HOBX5A	86	DAB2	144	KTI12	201	IGDCC3
29	GADD45BB	87	AMPD3B	145	DOTPP1	202	LUZP1
30	CILP2	88	ARL4CB	146	GABPB2B	203	LZTS1
31	SNX13	89	NR2F5	147	TMSB	204	BIRC5A
32	RPS4X	90	PRKAR2AA	148	CXCL12B	205	SHOX2
33	MATN4	91	SELENON	149	RET	206	FTH128
34	ZFP361A	92	RARGA	150	ACTA1B	207	MKRA5B
35	GALCB	93	JPT2	151	RPS8A	208	ZNF451
36	PSAT1	94	CRABP1B	152	CYP26C1	209	CEP70
37	HUWE1	95	CITED4A	153	RCA2.1	210	DUS2
38	FARSB	96	SUMO3B	154	SNAILA	211	ODCA7A
39	PABPC1A	97	COL18A1A	155	RAN	212	IQSEC2B
40	SMARCC1A	98	RPS12	156	SERPINE3	213	XPO1A
41	KLF1	99	TBX18	157	NMT1B	214	ACD
42	ROCK2A	100	ZIC2B	158	PRPF40A	215	CSPG4
43	BGNA	101	PLRG1	159	PLK1	216	AIL8A
44	XROCC3	102	ATP5MF	160	OTUD5A	217	MYO1F
45	RPL35	103	HBBE3	161	PLOD1A	218	ENOX2
46	ZGC:56095	104	TSC22D1	162	METT19	219	TPCN3
47	SLC6A9	105	H1-0	163	LRN1	220	HBAE3
48	FLNCB	106	PLK3	164	NIN	221	EHBP11B
49	RHAG	107	TRAPPC8	165	WASF1	222	TMEM41B
50	SPARC	108	RPS24	166	CBX5	223	SI:DKKEY-71B5.7
51	ZGC:158803	109	SI:CH211-121A2.2	167	SI:DKKEY-44G23.5	224	BRI3
52	SERPINK1B	110	TENT5BA	168	SLC7A3B	225	MTSS1B
53	VCP	111	MCM4	169	CEMP2	226	CEBPD
54	PSMD8	112	ID1	170	AMOTL2A	227	RPL35A
55	CEP85I	113	RAK1	171	CHAF1A	228	SI:DKKEY-30C15.10
56	TNS1B	114	EBF2	172	DIP2CA	229	AND1
57	PTMAA	115	ODCA8	173	CTSF	230	NES
		116	CKBB			231	SI:CH211-14K19.8

232	hapln1a
233	si:ch211-265o23.1
234	ifit1
235	si:dkeyp-115e12.6
236	mki67
237	si:ch211-102c2.7
238	si:dkey-108k21.21
239	oip5
240	si:ch211-197h24.9
241	rflnb
242	fthi31
243	vgll4a
244	si:dkey-121i2.1
245	rhoab
246	si:dkey-217d24.6
247	nrp2a
248	zgc:153405
249	si:ch211-108d22.2
250	ube2a
251	rela
252	suz12b
253	slc25a42
254	cygb1
255	si:dkey-93h22.7
256	pnp5b
257	cnmd
258	utrn
259	eef2b
260	zgc:114200
261	cited4b
262	EIF2A
263	map1lc3b
264	larp1
265	nap1l1
266	pin1
267	bmp1r
268	ece2b
269	syt4
270	hist1h2a2
271	cacna2d2a
272	rpl14
273	si:ch211-262i1.3
274	hoxa11a
275	por58
276	anxa1c
277	si:dkey-112a7.4
278	arf6ip4
279	si:dkey-23a13.17
280	si:ch1073-153i20.5

**Supplementary Table 3: List of overlapping DEGs between 36 vs. 48 hpf and WT vs. BTX 48 hpf bulk RNAseq datasets**

## Supplementary Table 4

Primers for in situ hybridization and RT-qPCR

Name	Sequence	Gene	Usage	Primer Pair Efficiency (for RT-qPCR)
matn1-FP	CACCCGGATCTTCAAGTGC	<i>matrilin 1</i>	in situ hybridization probe synthesis	
matn1-RP-T7	TAATACGACTCACTATAGGGATTACACACCACGTCCCA		in situ hybridization probe synthesis	
kif2a-FP	GCAGCAGCTATATACCGGGG	<i>kruppel like factor 2a</i>	in situ hybridization probe synthesis	
kif2a-RP-T7	TAATACGACTCACTATAGGGAGCCTCCCAACTGCAATGA		in situ hybridization probe synthesis	
mxra5b-FP	TGGCATCTCCAAACAGGTCC	<i>matrix remodeling associated 5b</i>	in situ hybridization probe synthesis	
mxra5b-RP-T7	TAATACGACTCACTATAGGGGCTGGATTAATCCGCCT		in situ hybridization probe synthesis	
rpl13a-FP-qPCR	TCTGGAGGACTGTAAAGAGTATGC	<i>ribosomal protein L13a</i>	RT-qPCR	1.86
rpl13a-RP-qPCR	AGACGCACAATCTTGAGAGCAG		RT-qPCR	
matn1-FP-qPCR	CTATGCATCTTGGGAGCTCAA	<i>matrilin 1</i>	RT-qPCR	1.92
matn1-RP-qPCR	ACTTTAACCTGCTCGAACTCAG		RT-qPCR	
kif2a-FP-qPCR	CAGTTACCGTGCAATTCTGTG	<i>kruppel like factor 2a</i>	RT-qPCR	1.94
kif2a-RP-qPCR	CGTTCTGATGGTAAAAGTGCC		RT-qPCR	
mxra5b-FP-qPCR	AGACGGTGCTTTTCAGGATC	<i>matrix remodeling associated 5b</i>	RT-qPCR	1.91
mxra5b-RP-qPCR	GATGGAGGAGATGTGTTGTG		RT-qPCR	

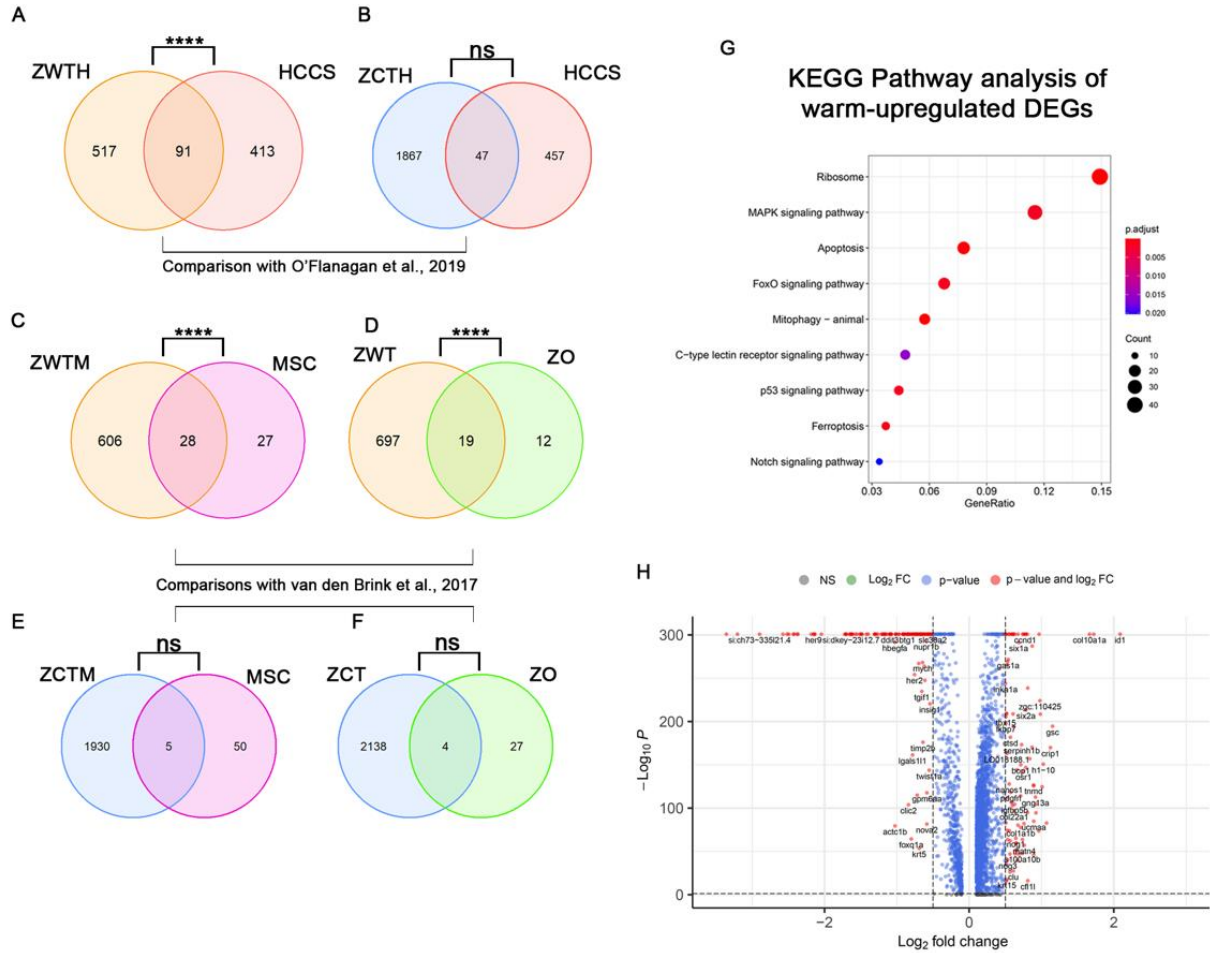
**Supplementary Table 4: Primer sequences (5' -> 3') used for ISH and RT-qPCR**

## Appendix II

### Supplementary Material: Chapter III

#### Cranial tenocyte diversity and roles for Wnt signaling in embryonic tendon patterning

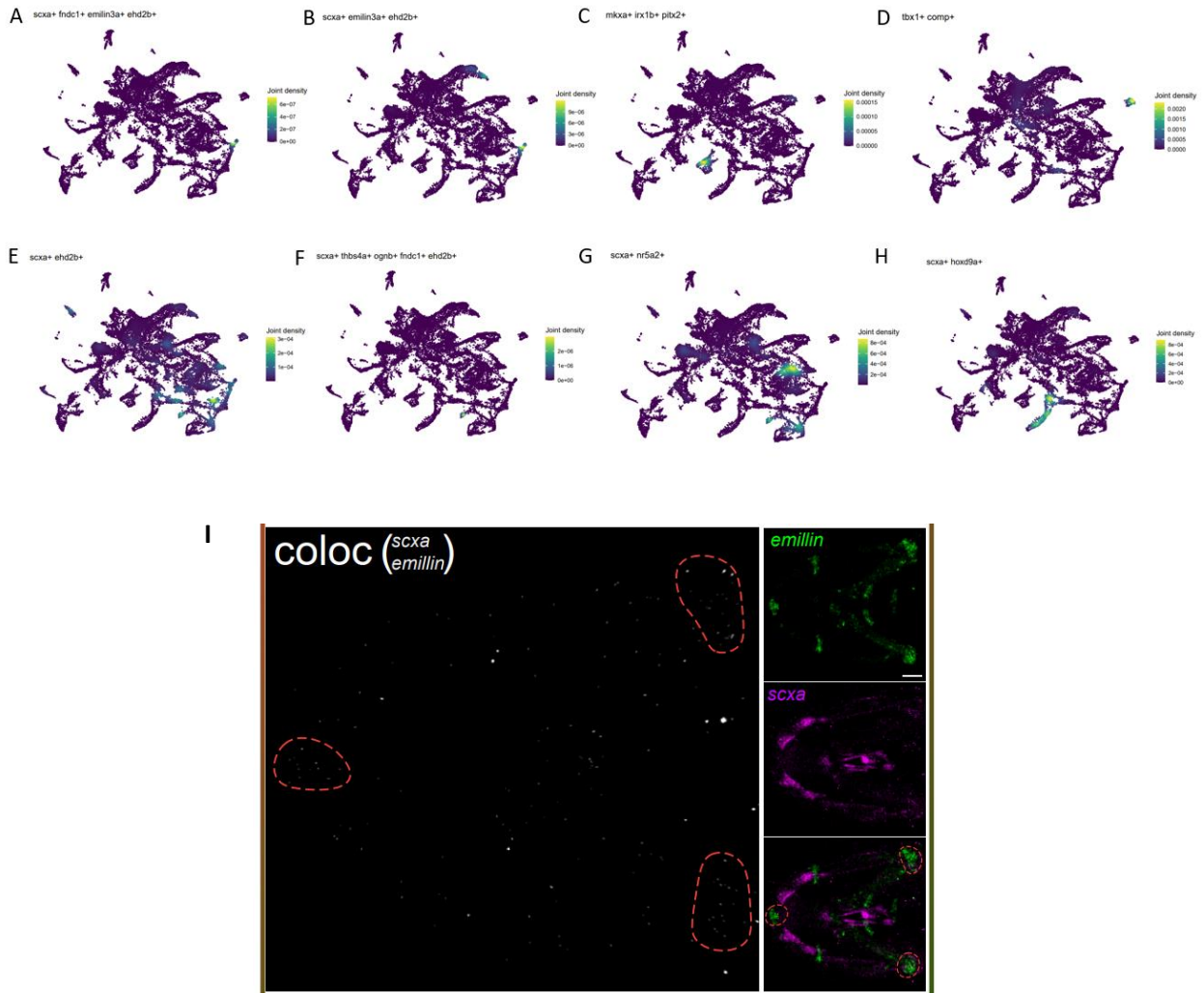
#### Supplementary Figure 1



**Supplemental Figure 1: Gene set overlap analysis, Kegg Pathway analysis, and volcano plot of differentially expressed genes in cold vs. warm dissociation conditions.**

**A)** Gene set overlaps between warm-upregulated genes with published dissociation cell-stress gene set. ZWTH = zebrafish warm-upregulated tenocyte significant differentially expressed genes (DEG) converted to human orthologs, HCCS = Human cancer cell stress core gene set published by O'Flanagan et al. 2019. **B)** Overlap of cold-upregulated genes with published datasets by O'Flanagan et al., 2019. ZCTH = zebrafish cold-upregulated tenocyte significant DEGs converted to human orthologs, HCCS = Human cancer cell stress core gene set published by O'Flanagan et al. 2019. **C-D)** Overlap of warm-upregulated genes with published core gene set from van den Brink et al., 2017. ZWTM = zebrafish warm-upregulated tenocytes DEG converted to mouse orthologs, MSC = mouse muscle satellite cells stress-related gene set published by van den Brink et al., 2017. ZWT = zebrafish warm-upregulated tenocytes, ZO = zebrafish osteoblast cell stress-related gene set published by van den Brink et al., 2017. **E-F)** Overlap of cold-upregulated genes with published core gene set from van den Brink et al., 2017. ZCTM = zebrafish cold-upregulated tenocyte DEG converted to mouse orthologs, MSC = mouse muscle satellite cells stress-related gene set published by van den Brink et al., 2017. ZCT = zebrafish cold-upregulated tenocytes, ZO = zebrafish osteoblast cell stress-related gene set published by van den Brink et al., 2017. ns = not significant, \*  $p < 0.05$ , \*\*  $p < 0.01$ , \*\*\*  $p < 0.001$ , \*\*\*\*  $p < 0.0001$

## Supplementary Figure 2



### Supplementary Figure 2: Gene markers for tenocytes from spatially distinct cranial tendons

**A)** *scxa/fndc1/emilin3a/ehd2b* as markers for anterior joint tenocytes **B)** *scxa/emilin3a/ehd2b* as markers for both anterior and posterior joint tenocytes **C)** *mkxa/irx1b/pitx2* as markers for eye tendons and periorcular mesenchyme **D)** *comp/tbx1* as markers for the sternohyoideus central tendon. **E)** *scxa/ehd2b* as markers for posterior MTJ **F)** *scxa/thbs4b/ognb/fndc1/ehd2b* overlap as marker for ligamentocytes **G)** *scxa/nr5a2* overlap as marker for lower jaw tenocytes/intermandibularis anterior **H)** *scxa/hoxd9a* overlap as marker for fin bud tenocytes. **I)** overlap of *scx/emillin3a* displaying co-expression with all cranial joints, highlighted with dashed orange lines.

## Appendix III

### Supplementary Material: Chapter IV

#### Identification of novel protein-protein interactions with tenocyte fate regulator Scleraxis

Unique Peptide No.	Total Pep	Gene Sym	MWT (kDa)	Annotation	Coverage	SAINT Score
17	181	TCF3	67.56	Transcription factor 3	174	1
26	128	TCF12	72.92	Transcription factor 12	316	1
17	89	TCF4	71.26	Transcription factor 4	237	1
23	49	UBE2O	141.21	(E3-independent) E2 ubiquitin-conjugating enzyme	288	1
18	25	COPA	138.26	Coatomer subunit alpha	205	1
13	15	COPB2	102.42	Coatomer subunit beta-2	144	1
11	14	COPG1	97.66	Coatomer subunit gamma-1	139	1
11	11	RAD50	153.8	DNA repair protein RAD50	139	1
5	10	ARCN1	57.17	Coatomer subunit delta	53	1
10	10	COPB1	107.07	Coatomer subunit beta-1	133	1
1	1	ANKHD1	73.26	Ankyrin repeat and KH domain-containing protein 1 (Fragment)	10	1
5	5	MRE11	80.54	Double-strand break repair protein MRE11	55	1
5	5	ANKRD17	274.09	Ankyrin repeat domain-containing protein 17	74	1
3	4	LSM14B	42.05	Protein LSM14 homolog B	56	1
2	4	MRPL42	16.65	39S ribosomal protein L42, mitochondrial	19	1
3	4	COPZ1	20.19	Coatomer subunit zeta-1	40	1
2	4	MRPL20	17.43	39S ribosomal protein L20, mitochondrial	19	1
2	3	SRSF6	39.56	Serine/arginine-rich splicing factor 6	18	1
3	3	FAM135A	169.73	Protein FAM135A	34	0.99
3	3	NBN	84.91	Nibrin	55	0.99
3	3	PYCR3	28.64	Pyroline-5-carboxylate reductase 3	28	0.99
5	5	PPP6R3	97.61	Serine/threonine-protein phosphatase 6 regulatory subunit 3	77	0.98
6	6	DCTN2	44.2	Dynactin subunit 2 OS=Homo sapiens	86	0.97
2	2	HNRNPCL2	32.05	Heterogeneous nuclear ribonucleoprotein C-like 2 O	21	0.97
2	2	LANCL1	45.25	LanC-like protein 1	25	0.97
3	4	MRPL43	23.42	39S ribosomal protein L43, mitochondrial	29	0.95
2	2	NRDC	131.49	Nardilysin OS=Homo sapiens	21	0.94
2	2	DCAF16	24.18	DDB1- and CUL4-associated factor 16	27	0.94
1	2	HEXIM2	32.4	Protein HEXIM2	11	0.94
5	5	COPE	34.46	Coatomer subunit epsilon	62	0.91
3	4	TBCB	27.31	Tubulin-folding cofactor B	38	0.86
5	6	MRPL44	37.51	39S ribosomal protein L44, mitochondrial	49	0.83
2	2	FBXO22	44.48	F-box only protein 22	35	0.78
3	3	LSG1	75.18	Large subunit GTPase 1 homolog	35	0.77
8	24	CSNK2A2	41.19	Casein kinase II subunit alpha'	104	0.74
4	7	MRPS18B	29.38	28S ribosomal protein S18b, mitochondrial	50	0.73
2	2	WASF2	54.25	Wiskott-Aldrich syndrome protein family member 2	32	0.66
2	2	ABI1	55.05	Abl interactor 1	31	0.66
3	3	USP11	109.75	Ubiquitin carboxyl-terminal hydrolase 11	32	0.61
4	12	CSNK2B	24.93	Casein kinase II subunit beta	48	0.59
4	4	PRKAG1	37.56	5'-AMP-activated protein kinase subunit gamma-1	42	0.58
2	2	PUS1	47.44	tRNA pseudouridine synthase A, mitochondrial	21	0.52
2	2	EARS2	58.65	Probable glutamate--tRNA ligase, mitochondrial	32	0.51
2	2	USP15	112.35	Ubiquitin carboxyl-terminal hydrolase 15	22	0.51
5	5	CYFIP1	145.09	Cytoplasmic FMR1-interacting protein 1	53	0.48
3	4	AZGP1	34.24	Zinc-alpha-2-glycoprotein	39	0.46

4	4	AHCYL1	58.91	S-adenosylhomocysteine hydrolase-like protein 1	38	0.44
2	2	THUMP3	56.97	THUMP domain-containing protein 3	22	0.44
3	3	FXR1	69.68	Fragile X mental retardation syndrome-related protein 1	51	0.42
2	2	TRIM26	62.13	Tripartite motif-containing protein 26	21	0.33
3	4	RPS4Y1	29.44	40S ribosomal protein S4, Y isoform 1	23	0.27
3	3	CDKN2A	16.52	Cyclin-dependent kinase inhibitor 2A	41	0.27
2	2	SNRPD3	13.91	Small nuclear ribonucleoprotein Sm D3	19	0.21
7	10	PRMT1	41.49	Protein arginine N-methyltransferase 1	81	0.2
2	2	RBMX	42.31	RNA-binding motif protein, X chromosome	27	0.2
3	3	PRKAA1	63.97	5'-AMP-activated protein kinase catalytic subunit alpha-1	37	0.17
3	3	FBXO3	54.53	F-box only protein 3 OS=Homo sapiens	51	0.15
8	10	TRIM28	88.49	Transcription intermediary factor 1-beta	123	0.12
3	3	C18orf25	43.3	Uncharacterized protein C18orf25	33	0.12
11	28	CSNK2A1	45.11	Casein kinase II subunit alpha	117	0.1
2	2	POLRMT	138.53	DNA-directed RNA polymerase, mitochondrial	35	0.09
3	4	HBB	15.99	Hemoglobin subunit beta	42	0.07
2	2	PIP	16.56	Prolactin-inducible protein	10	0.07
2	2	PSMA8	28.51	Proteasome subunit alpha type-7-like	25	0.07
1	3	IGKC	11.76	Immunoglobulin kappa constant	18	0.06
2	2	AIMP1	34.33	Aminoacyl tRNA synthase complex-interacting multifunctional protein 1	30	0.06
3	3	RPSA	32.83	40S ribosomal protein SA	38	0.05
13	30	MYH9	226.39	Myosin-9	228	0.04
3	3	NAP1L4	42.8	Nucleosome assembly protein 1-like 4	36	0.03
2	2	UBA1	117.77	Ubiquitin-like modifier-activating enzyme 1	31	0.03
1	6	MYH10	228.86	Myosin-10	21	0.02
3	3	MRPS28	20.83	28S ribosomal protein S28, mitochondrial	29	0.02
2	3	HNRNPC	33.65	Heterogeneous nuclear ribonucleoproteins	27	0.02
3	5	PGAM5	31.98	Serine/threonine-protein phosphatase PGAM5, mitochondrial	34	0.01
3	4	MRPS26	24.2	28S ribosomal protein S26, mitochondrial	37	0.01
2	3	RPL10	24.59	60S ribosomal protein L10	14	0.01
2	2	PPIA	18	Peptidyl-prolyl cis-trans isomerase A	20	0.01

**Supplementary Data 1: All detected PPIs with SCX with SAINT score > 0**